ERRATA

Page

88 line 9 should read. Differentiating 2.6.(3) $r' = R'_2/R_1$...

101 line 1 for ...or... read ...of...

126 line 3 should read $\frac{\mu_{so}\,\mu_n}{\mu_o\,\mu_{sn}\,r_o^2}\prod_1^n$.....

164 Equation 3.4.2.(3). The exponent of e should read $-N_A\rho X\,(\xi_o x_o + \xi_1 x_1)$

175 line 18 should read ...X or R_o.

205 line 20 should read ...was set at channel 32.

219 last line should read ...no significant effect on the count rate when the cadmium cover was used.

240 last line should read ...in a manner which may have depended...

248 line 22 for ...increase in sensitivity... read ...improvement in sensitivity...

255 Equation 4.6.6.(2) should read $T \propto \frac{S}{I_o\,\sigma_d^2}$

228 last line for ...c_∞ ... read ...e_∞ ...

262 Ordinate is R_S not R

279 last line for ...RELEM... read ...RILEM...

280 Pawliw J.... for ...Con... read ...Can...

282 line 18 for T_S read R_S

285 Equation B.4 should read $E_2 = \frac{E_o}{1+\epsilon_o[2-\cos\theta_1-\cos(\theta-\theta_1)]}$

286 line 12 $\frac{d^2E_2}{d\theta_1^2} < 0$

line 13 $\frac{d^2E_2}{d\theta_1^2} > 0$

298 Equation D.(6). First factor of the right hand side should read $\frac{N_{ao}}{\lambda_b-\lambda_a}$ and not $\frac{N_{ao}}{\lambda_b\,\lambda_a}$

THE USE OF RADIOACTIVE ISOTOPES FOR THE NON-DESTRUCTIVE TESTING OF CONCRETE

by

KENNETH PREISS, B.Sc.(Eng.), D.I.C.

A thesis submitted for the degree of
Doctor of Philosophy, in the Faculty of Engineering,
University of London.

Imperial College of Science and Technology,
University of London,
1964.

ABSTRACT

This thesis deals with the use of gamma radiation to measure the density and neutron radiation to measure the water content of concrete.

It is shown for both these methods that by eliminating the effects of certain nuclear processes the reading may be made independent of the chemical composition and therefore the types and proportions of constituents of the concrete. The design and calibration of apparatus in which this was achieved is discussed.

For determining density with gamma radiation, the source and detector were placed on opposite faces of a specimen, in which case predominantly unscattered radiation was detected, or on one face of a specimen so that scattered radiation was detected. Both these methods were analysed, showing how to design and use such apparatus and equations relating count rate and density empirically derived.

Experiments were performed with various geometries, sources and detectors for neutron water content apparatus, and the best arrangement of source and detector chosen on the basis of those results.

LIST OF CONTENTS

	Page
ABSTRACT	2
LIST OF CONTENTS	3
ACKNOWLEDGEMENTS	9
PART 1 GENERAL INTRODUCTION	10
PART 2 THE USE OF GAMMA RADIATION TO MEASURE DENSITY BY BACKSCATTER	16
CHAPTER 2.1 INTRODUCTION	16
CHAPTER 2.2 DESCRIPTION OF THE RELEVANT NUCLEAR PROCESSES	23
CHAPTER 2.3 CONSIDERATION OF VARIOUS BACKSCATTER METHODS	30
CHAPTER 2.4 THE EFFECT OF THE COLLISION PROCESSES ON THE CALIBRATION CURVE	37
CHAPTER 2.5 THE VARIABLE PARAMETER EXPERIMENTS	40
2.5.1 Description of the Apparatus	40
2.5.2 The Experiments	43
2.5.3 The Experimental Results	55
2.5.4 Discussion of the Calibration Curves	55
2.5.5 Discussion of the Effectively Infinite Volume	70

		Page
2.5.6	The Relation Between Count Rate and Distance Source to Detector	73
2.5.7	Conclusions	84
CHAPTER 2.6	DEFINITION OF SENSITIVITY S	85
CHAPTER 2.7	THE DESIGN AND CALIBRATION OF THE BACK-SCATTER DENSITY GAUGES	88
2.7.1	Design of the Mark 1 and Mark 2 Gauges	88
2.7.2	Experimental Calibration	91
2.7.3	The Design and Calibration of the Mark 3 Gauge	104
2.7.4	Conclusions	116
CHAPTER 2.8	REDUCTION OF THE INFLUENCE OF SURFACE ROUGHNESS ON THE COUNT RATE	117
CHAPTER 2.9	THE EQUATION OF THE CALIBRATION CURVE	122
2.9.1	The Theoretical Equation	122
2.9.2	Consideration of the Curves Log R_s vs ρx	127
2.9.3	Application of the Equation	132
2.9.4	Comparison with Other Proposed Equations	133
CHAPTER 2.10	USE OF THE APPARATUS TO LOCATE STEEL IN CONCRETE	135
CHAPTER 2.11	HAZARDS OF GAMMA RAY METHODS	138

		Page
CHAPTER 2.12	CONCLUSIONS	140
PART 3	THE USE OF GAMMA RADIATION TO MEASURE DENSITY BY TRANSMISSION	145
CHAPTER 3.1	INTRODUCTION	145
CHAPTER 3.2	DESIGN OF APPARATUS	150
CHAPTER 3.3	EXPERIMENTAL CALIBRATION OF THE APPARATUS	154
CHAPTER 3.4	ANALYSIS OF THE APPARATUS	158
3.4.1	The Curve $Ln(R_o/R)$ vs ρ	158
3.4.2	Determination of the Relative Intensity of Scattered Radiation	163
3.4.3	Determination of the Spatial Distribution of Radiation Within the Specimen	167
3.4.4	Analysis of Errors	170
CHAPTER 3.5	USES OF THE METHOD	172
3.5.1	To Measure Uniformity of Concrete Specimens	172
3.5.2	To Measure Density of Concrete	176
CHAPTER 3.6	CONCLUSIONS	179
PART 4	THE USE OF NEUTRON RADIATION TO MEASURE THE WATER CONTENT OF CONCRETE	183
CHAPTER 4.1	INTRODUCTION	183

		Page
CHAPTER 4.2	DESCRIPTION OF THE RELEVANT NUCLEAR PROCESSES	191
CHAPTER 4.3	THE INFLUENCE OF THE NUCLEAR PROCESSES ON THE APPARATUS	195
CHAPTER 4.4	THE SERIES I EXPERIMENTS	201
4.4.1	The Source	201
4.4.2	The Detector	201
4.4.3	The Apparatus	205
4.4.4	Establishment of the Calibration Curve	208
4.4.5	Determination of the Effectively Infinite Volume	216
4.4.6	The Effect of Neutron Absorbers	217
4.4.7	Conclusions	220
CHAPTER 4.5	THE BACKSCATTER METHOD WITH A LITHIUM GLASS SCINTILLATOR	220
4.5.1	The Apparatus	221
4.5.2	Establishment of the Calibration Curves	221
4.5.3	Determination of the Effectively Infinite Dimensions	227
4.5.4	The Effect of Neutron Absorbers	237
4.5.5	Investigation of the Count due to Gamma Radiation and Fast Scattered Neutrons	238

Page

4.5.6 Conclusions 240

CHAPTER 4.6 THE BACKSCATTER METHOD USING A BORON TRIFLUORIDE COUNTER 241

4.6.1 The Source, Detector and Apparatus 241

4.6.2 Determination of the Effect of Neutron Absorbers 243

4.6.3 Determination of the Effect of Gamma Radiation and Fast Scattered Neutrons 246

4.6.4 Establishment of the Calibration Curves 247

4.6.5 Assessment of the Results and Comparison with the Lithium Glass Scintillator 248

4.6.6 Some Considerations in the Design of a Practical Instrument 254

4.6.7 Conclusions 258

CHAPTER 4.7 THE EQUATION OF THE GAUGE 259

CHAPTER 4.8 CONCLUSIONS 266

PART 5 GENERAL CONCLUSIONS 272

LIST OF REFERENCES 277

APPENDIX A NOTATION 282

APPENDIX B CALCULATION OF THE FINAL ENERGY OF A PHOTON WHICH HAS SCATTERED TWICE, THROUGH A GIVEN TOTAL ANGLE, IN A PLANE SYSTEM 285

Page

APPENDIX C CALCULATION OF THE RELATIVE COUNT DUE TO ONCE SCATTERED RADIATION IN THE GAMMA RAY TRANSMISSION APPARATUS 289

APPENDIX D ANALYSIS OF THE STATISTICAL ERRORS DUE TO A RHODIUM FOIL DETECTOR IN A CONSTANT BACKGROUND 297

ACKNOWLEDGEMENTS

The author wishes to express his gratitude to the Commonwealth Scholarship Commission for making available the opportunity for postgraduate study and research and to the Central Electricity Generating Board for support to finish the project; to Dr.P.J.Grant of the Nuclear Power Group, Department of Mechanical Engineering, and Professor A.L.L.Baker and Mr.K.Newman of the Concrete Structures and Technology Section, Department of Civil Engineering, for much useful discussion, guidance and support; to the laboratory staffs of both those Departments for able and willing help; and to various colleagues for many hours of informative and enjoyable discussion.

The author wishes to thank Dr.J.R.Butler of the Geochemistry Department for arranging analysis of the sand used in the concrete specimens, Mr. Brown of the Associated Portland Cement Manufacturers Research Laboratory for determining the total water content of the concrete specimens used in Part 4, and Mr.D.J.McConologue of the Department of Mechanical Engineering for making available the minimization routine used in Chapter 2.9.

PART 1 GENERAL INTRODUCTION

The aim of concrete engineering is to provide a structure to perform a given function with the most economic use of material and human resources. The deformation of a structure, due to load, temperature or shrinkage, must be limited and the structure must resist deterioration by the environment.

The concrete in a typical structure may be required to be strong, durable and impermeable, and not exhibit large amounts of thermal expansion, shrinkage due to water movement, thermal or sound conduction or chemical deterioration.

Concrete is made of cement and inert aggregate mixed with water and placed before hardening can occur. The properties of the structure will depend on the properties of the components, their proportions, the adequacy of mixing, the method of placing and the subsequent temperature and relative humidity surrounding the structure.

If a structure in service be found to be unsatisfactory the economic loss to the user may be great and it is necessary to ensure the quality of the structure at the time of construction. For that reason materials are selected, proportioned, mixed and placed with care, but because of the inherent variability of the components and the dependence of the concrete quality on the reliability

of both labour and machines, the finished structure must be tested.

The usual procedure is to take standard small samples of concrete, cure them under specified conditions, and then subject them to tests which are usually standard crushing tests. If a sufficiently large proportion of the samples pass a specified test limit, the concrete in the structure is assumed to be of adequate quality. This procedure cannot be regarded as more than an empirical method of quality control, as the concrete samples are much smaller than the structure and are subjected to a different environment while curing and different conditions of stress under loading. Because of the long delay between placing the concrete and testing the samples, often as much as 28 days, it may be very expensive to remove unsatisfactory concrete.

Although the cube crushing strength is related to other properties of concrete the crushing test is related to the historical development of engineering techniques rather than to the real conditions of forces and stresses within the concrete which determine its behaviour.

There is a need therefore for in situ tests to assess the quality of concrete as soon as possible after placing.

These needs are partially met, on hardened concrete, by the measurement of the elastic rebound, resonant fre-

quency or ultrasonic velocity. These tests derive from mathematical studies of elasticity and are strictly valid only for a homogeneous, isotropic, elastic material. Concrete in fact is made up of inert stone in a cement mortar matrix which is a complex material composed of inert sand, cement at different stages of hydration and water both free and in various states of combination. This mixture is neither uniform nor elastic, and its properties constantly change with applied stress or vapour pressure. The values of pulse velocity and resonant frequency are used to calculate elastic constants of a concrete but this result is related only empirically to the load bearing properties of a structure and requires knowledge of the density of the concrete.

The properties of concrete listed above, strength, durability, impermeability, thermal expansion, shrinkage, insulation and resistance to chemical attack are for given materials all related to the water content and density but no method has been available to measure these accurately on a structure. Even in a laboratory, density is measured by weighing in air and in a fluid such as water or paraffin which may permanently alter the properties of the specimen. Water content of a specimen is calculated, when desired, from the density of the concrete and its constituents, assuming a value for the air voids ratio.

These difficulties can be overcome by the use of radioactive isotopes to determine both density and water content of concrete without making any assumptions as to its elastic properties. These techniques can be used on fresh, unset concrete or hardened concrete, on site or in the laboratory and should open new methods of control of and research into concrete.

Of the types of radioactivity available from radio-isotopes, gamma and neutron radiation are sufficiently penetrating to give information about structural concrete. The use of these radiations falls into two categories; gamma ray methods for determining density and neutron ray methods for determining water content.

As this thesis deals with non-destructive testing, probe type instruments, used usually in soil boreholes but seldom in concrete, were not considered. In practice a source and detector of gamma rays may be placed on one face of a specimen, so that radiation is scattered into the detector, or the source and detector may be placed on opposite sides of a specimen so that predominantly un-scattered radiation is detected. In both cases the count rate will be a function of the specimen density. The arrangement chosen for testing a particular part of a structure will depend upon the shape and accessibility of the member under consideration. A practical site instru-

ment would consist of the source, detector and relevant shielding together with a portable electronic detection system.

When a fast neutron source is placed near concrete the scattered slow neutron intensity is a function primarily of the hydrogen content, and therefore the total water content of the concrete so that the count rate at a slow neutron detector would be a measure of water content. Portable equipment would consist of the source-detector assembly with necessary shielding and the portable electronic detection system.

Both neutron and gamma ray methods have been in use for some years, particularly on soils. The design of apparatus has generally been purely empirical, and the readings appeared to be influenced by undesired factors, such as the chemistry of the tested material. The research reported here shows how the latter effect may be eliminated.

Although possible applications to concrete technology were constantly borne in mind during the conduct of this research, the work has concentrated on analysis of the methods rather than the development of the applications, because a thorough understanding of the principles and problems involved is necessary before these methods may successfully and correctly be applied.

The work reported in this thesis is divided into four parts. Part 2 deals with the determination of density by gamma ray backscatter; Part 3 with the determination by gamma ray transmission; Part 4 with the use of neutron radiation to measure water content; and in Part 5 the conclusions of the different parts are considered together.

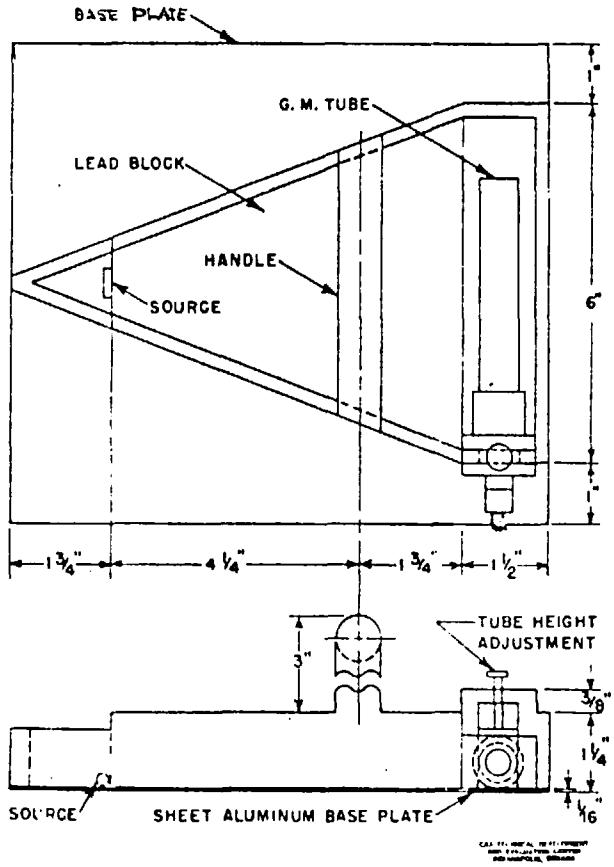
PART 2 THE USE OF GAMMA RADIATION TO MEASURE DENSITY BY BACKSCATTER

CHAPTER 2.1 INTRODUCTION

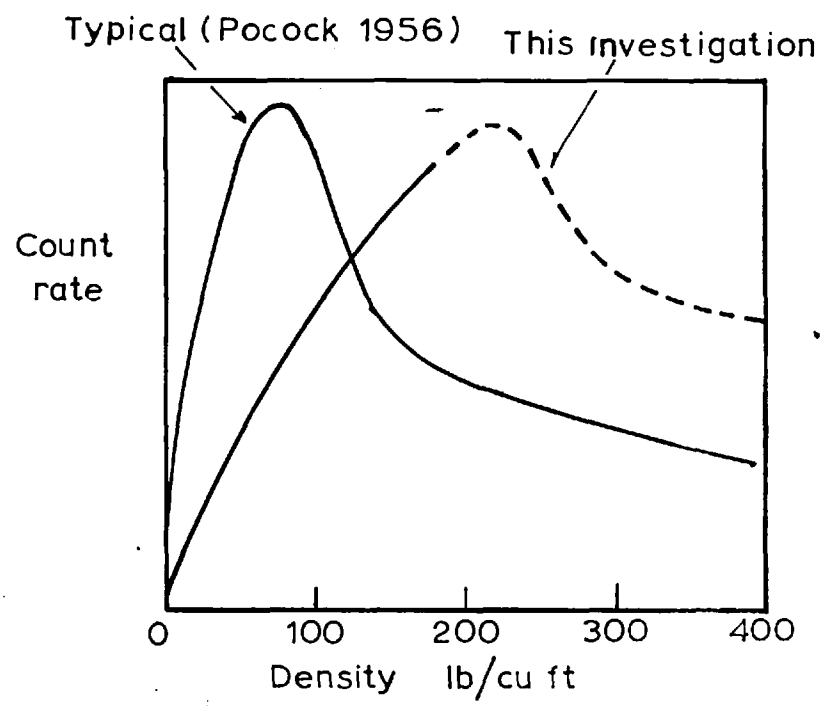
All the work previously reported on this method has been carried out with the aim of using the apparatus on soils, generally for quality control of earth structures. Sources used, of intensity up to 60 millicuries, have been Co 60, Cs 137 or the radium in a radium-beryllium neutron source, in which case the instrument was used for both moisture and density determination (Kuhn 1960). Detectors have usually been Geiger-Muller tubes.

In these density gauges the source was separated from the detector by a thickness of lead. The assembly was placed on the material to be tested and a count taken. A typical assembly is shown in Figure 1 and a typical curve of count rate against density, the calibration curve, shown in Figure 2. In all reported work count rate fell as density was increased in the range above about 100 lb/cu ft, and it has been explicitly stated (Jacquesson 1954) that this must be so in practice. This type of calibration curve can lead to ambiguous readings at low densities.

Some workers (Neville and van Zelst 1960 , Gnaedinger 1960, Mintzer 1960, Kuhn 1964) found that the type of soil affected the calibration curve. Gnaedinger (1960) and



The apparatus of Belcher et al (1952) Fig 1



The calibration curve Fig 2

Carey et al (1960) found that the manufacturer's calibration curve differed from their own, which may have been due to the types of soil used in establishing the curves. Carlton (1960) and Huet (1961) reported that for the soils used no soil type effect was observed. It must be concluded that in general a soil type effect does occur. It is shown in the present work that this must be so with apparatus in which count rate falls as density is increased.

The distance between source and detector affected the shape of the calibration curve and was chosen by each worker to give the most sensitive reading over a particular range of densities. This distance varied from $5\frac{1}{2}$" (Carey and Reynolds 1958) or 6" (Pocock 1956) to 20 cm (Lauchaud 1961) or 30 cm (Brocard 1954). Some instruments (Kuhn 1960) included a mechanism for varying the source detector distance to give best sensitivity for each range of density.

Roughness of the surface upon which the instrument was placed was observed to cause error (Belcher et al 1952, Carey and Reynolds 1958, Kuranz 1959, Carlton 1960, Lauchaud 1961, Kuhn 1964). Carey and Reynolds (1958), Belcher et al (1952) and Kuhn (1964) reported that this error may be reduced by placing the instrument on three legs. Other workers (Kuranz 1959, Neville and van Zelst

1960, Carlton 1960, Lauchaud 1961) relied on bedding the instrument well down on a specially prepared surface.

The depth of effective penetration of the instrument was reported by various authors as shown below.

TABLE 1

Author	Reported depth
Belcher et al (1952)	4"
Brocard (1954)	$\not>$ 4"
Pocock (1956)	$3\frac{1}{2}$" in concrete, 20" in air
Carey and Reynolds (1958)	5" at density 140 lb/cu ft
Carey et al (1960)	6"
Carlton (1960)	3" to 4"
Gnaedinger (1960)	< 8"
Neville and van Zelst (1960)	approx. 6"
Lauchaud (1961)	6"
Huet (1961)	6" at density 125 lb/cu ft

Carey and Reynolds (1958), Carlton (1960) and Neville and van Zelst (1960) stated that if Co 60 were used rather than Cs 137 the depth would increase but that opinion is invalidated by the present work.

The horizontal extent of the zone of influence was usually determined by each worker for his apparatus.

Belcher et al (1952) using the apparatus shown in Figure 1 found that this volume did not extend beyond 2" from the base plate. These dimensions were different for different instruments but a plan area two feet square seemed generally effectively infinite.

Calibration of an instrument offered problems to all workers. Belcher et al (1952), Pocock (1956), Neville and van Zelst (1960) and Carey et al (1960) used blocks of material and measured the overall weight and volume of each block. Differences between the overall density and the local density at the point of observation gave rise to errors. Carey et al (1960), Kuhn (1960) and Huet (1961) used the instrument on site and calibrated it against a standard technique such as a balloon volumeter or a replacement method but these methods themselves were subject to error, particularly on granular soils. Kuhn (1960) did statistical tests on the results of both radiation and sand replacement methods and concluded that the nuclear method gave results at least as accurate as the sand replacement method. Carey et al (1960) tested the instrument by taking 20 observations on a carefully chosen coarse rolled base, containing stone of $1\frac{1}{2}$" maximum size. They obtained the following results.

TABLE 2

Method	Mean lb/cu ft	Standard error lb/cu ft
Nuclear gauge	147.7	0.7
Balloon volumeter	150.3	4.8
Sand cone device	150.5	4.9

The nuclear gauge appeared to give more consistent results but the authors were unsure as to which method gave rise to the difference between the means.

The accuracy attainable with gamma ray backscatter density gauges appears to vary from author to author. Some quoted values are shown below.

TABLE 3

Author	Quoted accuracy	Remarks
Belcher et al (1952)	1½%	
Carlton (1960)	2.8 lb/cu ft	Compared with replacement
Gnaedinger (1960)	"within 5%"	
Carey et al (1960)	4.4 lb/cu ft	Compared with balloon volumeter
Huet (1961)	Std.error=0.01g/cc	

It appears, in general, that whereas reasonable accuracy is obtainable with a good instrument calibrated

for a particular material, the error when used on a different material may be significant. In addition, an unstable electronic system may give rise to errors (Gnaedinger 1960, Carey and Reynolds 1958). The usual procedure was to take a reading on a standard specimen and if this differed from the standard reading an adjustment was made to one or other electronic stage until the error was eliminated. Neville and van Zelst (1960) and Huet (1961) used, instead of count rate, the ratio of count on specimen to count on standard in order to overcome both the drift effect and the effect of source decay.

The background count due to cosmic radiation or other causes may be significant. Carey and Reynolds (1958) found that this was so when the total count rate was about 300 counts per second with a Geiger-Muller tube. The significance of this effect will depend upon the instrument, the location and the time, so that in general the background rate must be considered.

No theoretical expression has been developed to give count rate as a function of density for backscatter gauges. Some functions quoted for the equation of the calibration curve are discussed in Chapter 2.9.4. Carey et al (1960) who obtained experimental curves of density against count rate fitted a first order polynomial, a quadratic and a simple exponential to the experimental curve and found that for the range of densities considered, from 98 lb/cu ft

to 143 lb/cu ft the linear model was sufficiently accurate, but for extension to higher densities a curved function would have been preferred. Neville and van Zelst (1960), Carlton (1960), Lauchaud (1961) and Huet (1961) found that for the range of soils tested count rate fell linearly with density.

CHAPTER 2.2 DESCRIPTION OF THE RELEVANT NUCLEAR PROCESSES

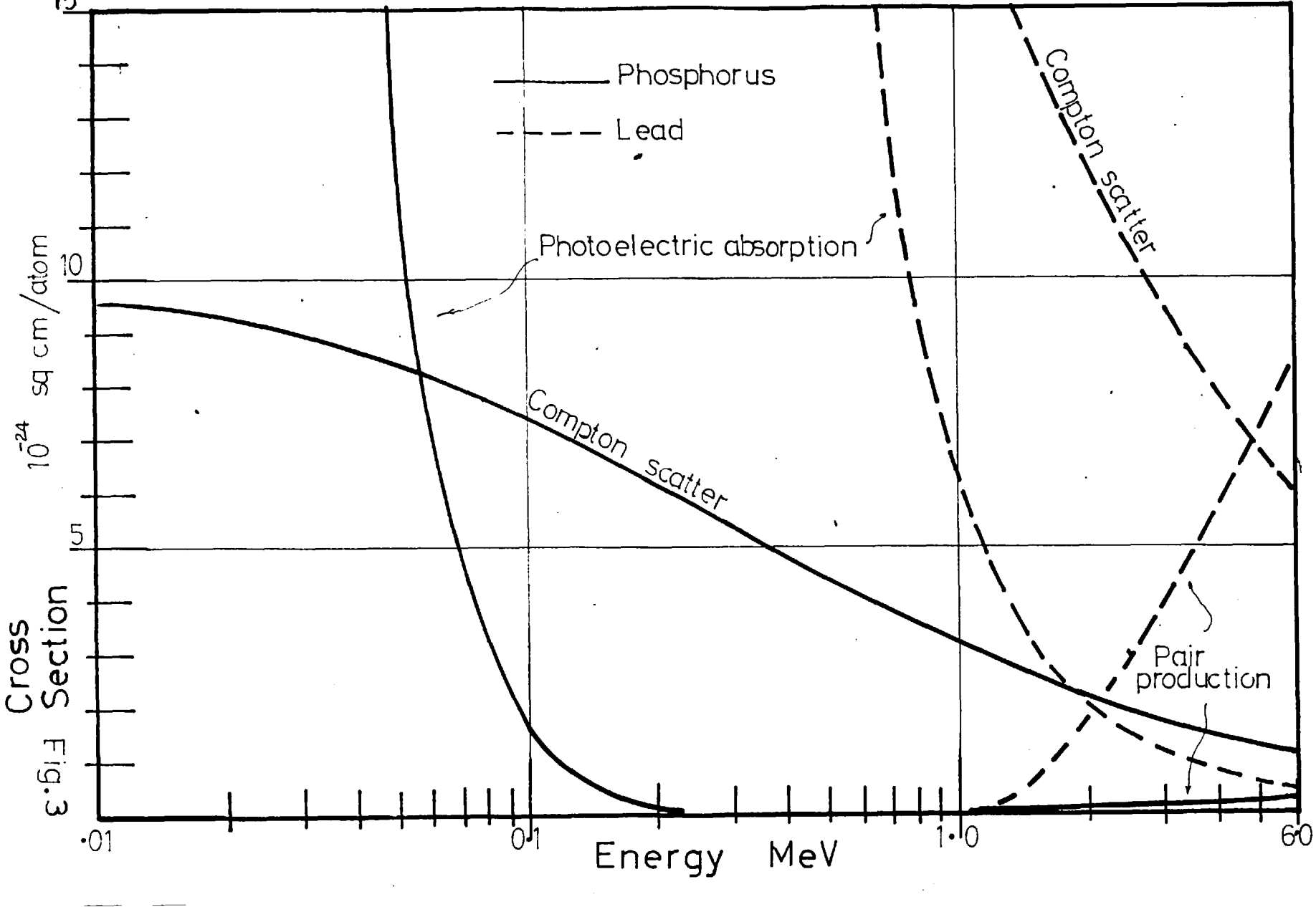
When a beam of gamma photons passes through a material, many reactions may occur between photons and the elemental particles of the material, but the only reactions that need be considered for this method are:-

(a) Pair production.

(b) Compton scattering.

(c) Photoelectric absorption.

(a) Pair Production. In pair production a photon reacts in the presence of matter giving rise to a positron-electron pair. The cross section per atom for this reaction increases with Z^2, where Z is the atomic number. The pair production cross section depends, therefore, on the proportions of elements in the material. As the method should be independent of these proportions, the effects of pair production should be eliminated. Figure 3, which gives the cross sections or reaction probabilities


15
10
5
Phosphorus
Lead
Photoelectric absorption
Compton scatter
Compton scatter
Pair production
10^{-24} sq cm/atom
Cross Section
Fig. 3
·01
0·1
1·0
60
Energy MeV

for the above processes as functions of energy (Grodstein 1957), shows that the cross section is zero below 1.02 MeV and up to 2 MeV is very small in materials of medium atomic weight such as phosphorus or concrete and may be neglected. For this reason the source energy should not be above 2 MeV.

(b) Compton Scattering. Compton scatter is the scatter of a photon by an orbital electron. In this process the energy of the photon is much greater than the binding energy of the electron to the nucleus so that the electron is effectively free. The cross section per electron is given by the Klein Nishina formula (Evans 1955) and is dependent only upon the incident photon energy. If ξ be this cross section per electron and Z the atomic number of the scattering material, then the cross section per atom is $Z\xi$ and the macroscopic cross section is

$$\Sigma = \frac{Z}{A}\rho N_A \xi \qquad 2.2.(1)$$

where A is the atomic weight and ρ the density of the material, and N_A is Avogadro's number.

If the material is composed of n elements, the mass fraction of each being G_i, then the mass of each element per cc is $G_i\rho$ and the macroscopic cross section is given by

$$\Sigma = \sum_n \frac{Z_i G_i \rho N_A \xi}{A_i}$$

$$= \rho N_A \xi \sum_n \frac{G_i Z_i}{A_i} \qquad 2.2.(2)$$

For convenience the quantity $\sum_n \frac{G_i Z_i}{A_i}$ of a concrete will be defined the Compton scattering factor, X.

At each scatter a photon loses energy. If E_o is the incident energy, and θ the angle of scatter, the energy of the scattered photon is given by

$$E = \frac{E_o}{1 + \frac{E_o}{0.511}(1 - \cos\theta)} \qquad 2.2.(3)$$

The maximum energy loss occurs when the photon is scattered back through 180^o.

(c) Photoelectric Absorption. In the photoelectric absorption process all the photon energy is absorbed by a single collision with an orbital electron which is tightly bound to the nucleus. The cross section per atom is given approximately by (Price, Horton and Spinney 1957)

$$\sigma = 1.25 \times 10^{-9} Z^5 E_o^{-7/2}$$

Therefore $\Sigma = K N_A \rho \frac{Z^5}{A}$ where $K = 1.25 \times 10^{-9} E_o^{-7/2}$

For a material comprising n elements as above

$$\Sigma = K N_A \rho \sum_n \frac{G_i Z_i^5}{A_i} \qquad 2.2.(4)$$

It is to be noted that the quantity Z/A is very nearly $\frac{1}{2}$ for all elements except hydrogen, for which it is almost 1. Table 4 shows the quantities $\sum_n \frac{G_i Z_i^5}{A_i}$ and $\sum_n \frac{G_i Z_i}{A_i}$

for a wide range of concretes and phosphorus for comparison, from which it is seen that whereas the former varies from one concrete to another the latter varies hardly at all. Therefore the absorption process is greatly dependent upon the elemental constitution of the material while scattering is not. It is apparent that any technique devised to measure the density of concrete over a large range of mix proportions should be based on Compton scattering processes, the influence of photoelectric absorption and pair production reactions being reduced to a minimum or entirely eliminated.

TABLE 4

Quantities $\sum_{n}\frac{G_i Z_i^5}{A_i}$ and $\sum_{n}\frac{G_i Z_i}{A_i}$ for various concretes and phosphorus for comparison

Proportions			(Trade Grouping) Aggregate Type	$\sum_{n}\frac{G_i Z_i^5}{A_i}$	$\sum_{n}\frac{G_i Z_i}{A_i}$
Water	Portland Cement	Aggregate			
Pure Phosphorus				24,510	.484
.8	1.0	1.5	Granite(a)	26,670	.512
.3	1.0	9.0		27,870	.503
.8	1.0	1.5	Basalt(b)	27,670	.513
.3	1.0	9.0		31,160	.502
.8	1.0	1.5	Granite(c)	28,590	.512
.3	1.0	9.0		32,930	.500
.8	1.0	1.5	Limestone(d)	28,510	.513
.3	1.0	9.0		32,860	.501
.8	1.0	1.5	Hornfels(e)	26,340	.511
.3	1.0	9.0		28,610	.497
Maximum Variation				22.6%	3.2%

Maximum Variation is the difference between the highest and lowest values expressed as a percentage of the mean value.

TABLE 4 (Cont'd)

Chemical analyses of the components were from the following references.

Aggregate	Reference
(a)	H.M.S.O. 1956a rock no.650
(b)	H.M.S.O. 1956a rock no.684
(c)	H.M.S.O. 1956a rock no.652
(d)	H.M.S.O. 1956b rock no.S1 149
(e)	H.M.S.O. 1931 rock no.529

A typical ordinary portland cement analysis, by private communication from the Associated Portland Cement Manufacturers Research Laboratory, was used.
"Trade Grouping" follows H.M.S.O. (1960)
Values of A_i from Etherington (1958).

Figure 3 shows that if the source energy is below about 2 MeV and if photons of energy less than 0.1 MeV are not detected, Compton scatter will be the only relevant process, and the effects of chemical composition on the count rate will then be very small.

None of the processes described above depends upon interatomic, crystalline or other forces. While in general these forces may influence energy quanta, the effect

at this range of energy is negligible. Gamma density methods measure the number of electrons per unit volume without regard to chemical binding forces and effects, and therefore are insensitive to the structure of the concrete.

CHAPTER 2.3 CONSIDERATION OF VARIOUS BACKSCATTER METHODS

In this research programme a sodium iodide scintillation counter was used. A photon entering the NaI scintillator and colliding, either by photoelectric absorption or scatter processes, deposited energy in the crystal. This appeared as a flash of light which was converted into an electronic pulse by a photomultiplier. The intensity of the light flash was proportional to the energy lost by the photon. If the photon was completely absorbed, the light flash and therefore the magnitude or height of the electronic pulse was that corresponding to full absorption of the photon. Some photons scattered within the crystal and then scattered out, depositing less than all their energy. Therefore, for photons of some single energy detected by the scintillator, there was a distribution of pulse heights ranging from zero for one glancing collision to the pulse height corresponding to full absorption of the photon.

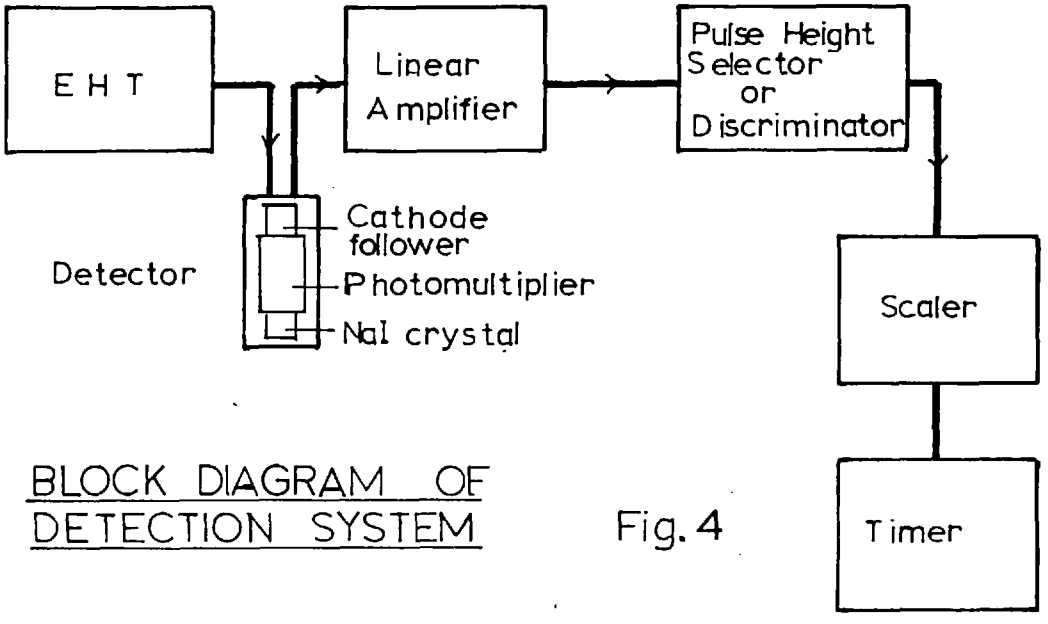
In this project the crystal, 1½ in dia. by 1 in thick, was coupled to the photomultiplier by means of silicone grease. From the photomultiplier the pulses were passed through a cathode follower to a linear amplifier and then to a discriminator, as shown in the block diagram of Figure 4. The discriminator passed only those pulses of amplitude greater than the discriminator voltage level which was set as desired. From the discriminator pulses were passed to a scaler-timer unit for determining the count rate, R.

As pulse height was proportional to photon energy, discriminating at a particular pulse height level was equivalent to discriminating at a particular energy level.

A scintillation counter was preferred in this project because it was more efficient than a Geiger-Muller counter (about 50% compared with 1%) and permitted energy discrimination and selection.

With the exception of the work by Forrester (1960), surface backscatter apparatus has been of the type shown in Figure 1 where the source and detector, separated by a lead shield, were placed on the material to be tested. The use of a scintillation counter with pulse height selector made other geometrical arrangements feasible.

In the first series of experiments the source was attached to the detector and then placed upon the concrete



BLOCK DIAGRAM OF DETECTION SYSTEM

Fig. 4

surface as shown in Figure 5.

The pulse height selector was set to reject pulses of height corresponding to the source energy and to accept the lower pulses due to photons scattered off the concrete. The source photons did, however, produce a large number of pulses of height as low as that due to scattered photons, so that the ratio of scattered to source count was low, as shown in Figure 5.

The next development was to make the apparatus shown in Figure 6a. The scattered count was reduced, compared with the previous arrangement, on account of both the lead shield and the increased distance from concrete to detector. The source count was however reduced by a greater factor, so that an overall improvement in the ratio of scattered to source count was obtained.

The size of concrete block which was effectively infinite to this apparatus was determined by taking readings at the centre of a 4" x 4" x 2" block, a 6" x 6" x 3" block, and so on, the block size being increased by equal increments. The resulting curve of count rate against block size is shown in Figure 6b. The count rate reached a constant value when the 14" x 14" x 7" block was reached, from which it was concluded that that size of concrete of density 140 lb/cu ft was effectively infinite.

The pulse height spectrum, in Figure 6a, showed that

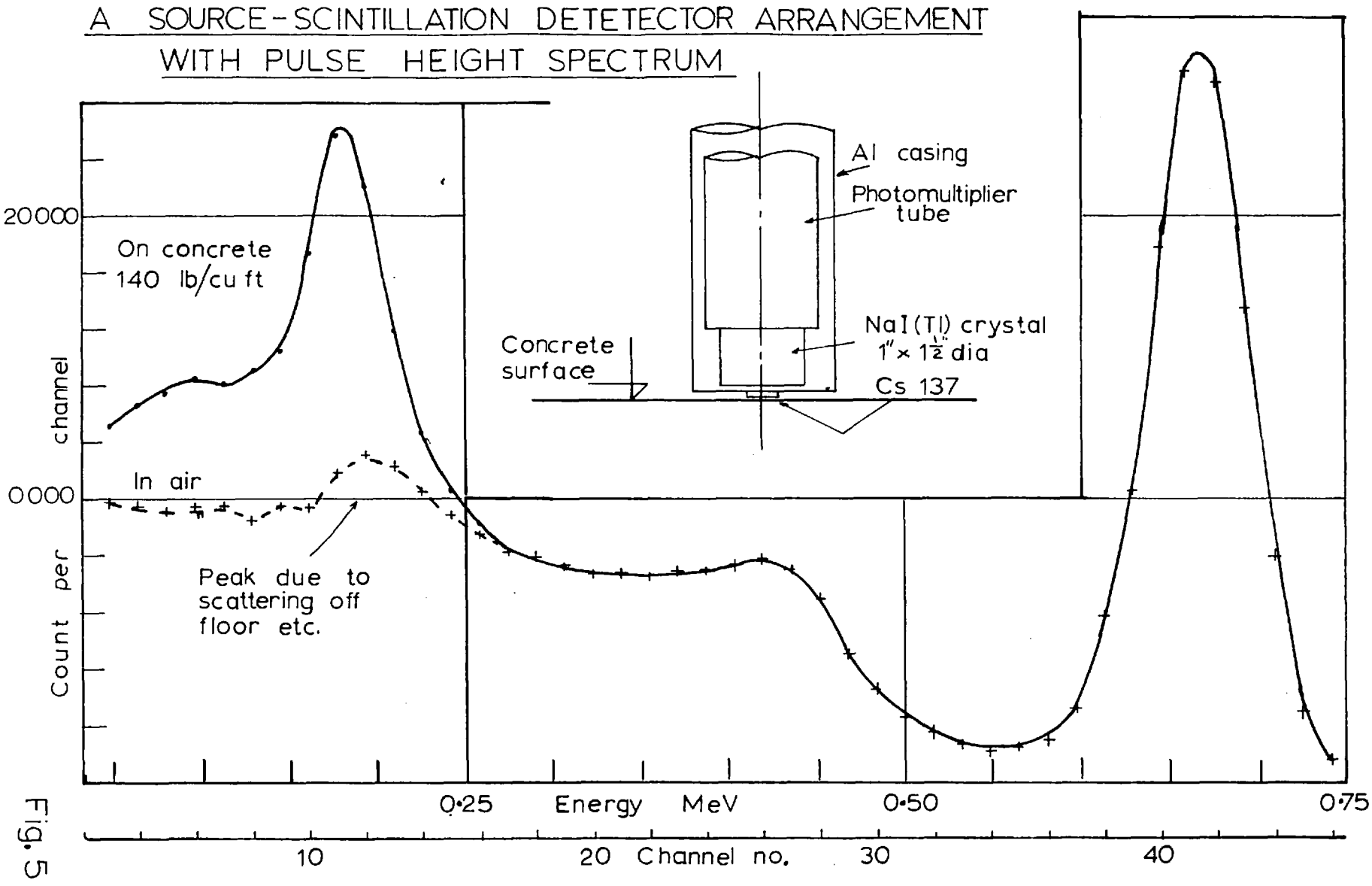

A SOURCE-SCINTILLATION DETETECTOR ARRANGEMENT
WITH PULSE HEIGHT SPECTRUM
Al casing
Photomultiplier tube
NaI(Tl) crystal
1" × 1½" dia
Cs 137
Concrete surface
On concrete
140 lb/cu ft
In air
Peak due to scattering off floor etc.
20000
0000
Count per channel
0·25
Energy MeV
0·50
0·75
10
20
Channel no.
30
40

Fig. 5

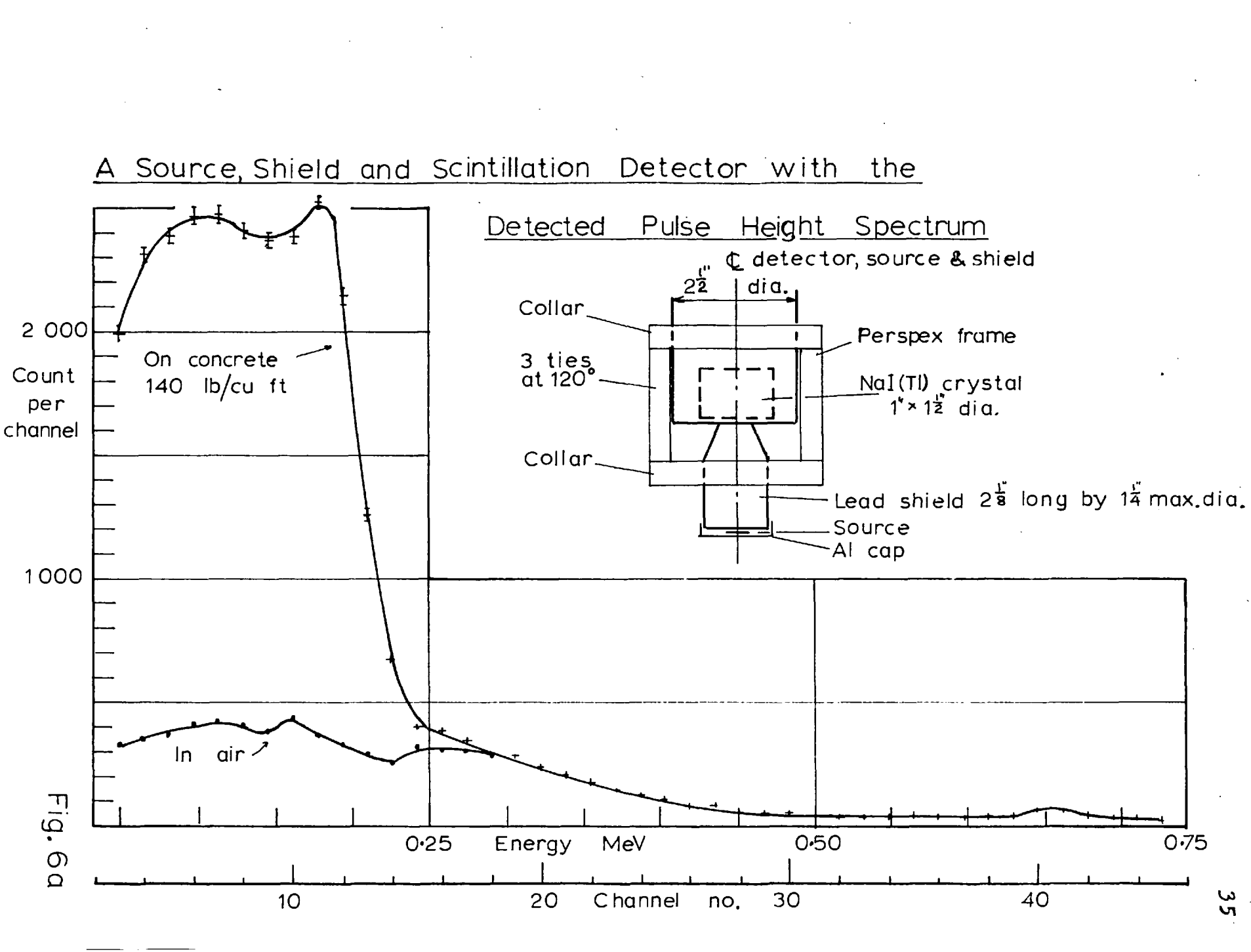

A Source, Shield and Scintillation Detector with the
Detected Pulse Height Spectrum
℄ detector, source & shield
2½" dia.
Collar
Perspex frame
3 ties at 120°
NaI(Tl) crystal 1" × 1½" dia.
Collar
Lead shield 2⅛" long by 1¼" max. dia.
Source
Al cap
2 000
Count per channel
1000
On concrete 140 lb/cu ft
In air
0·25
Energy MeV
0·50
0·75
10
20
Channel no.
30
40

Fig. 6a

Count Rate vs Block Size

Density = 140 lb/cu ft

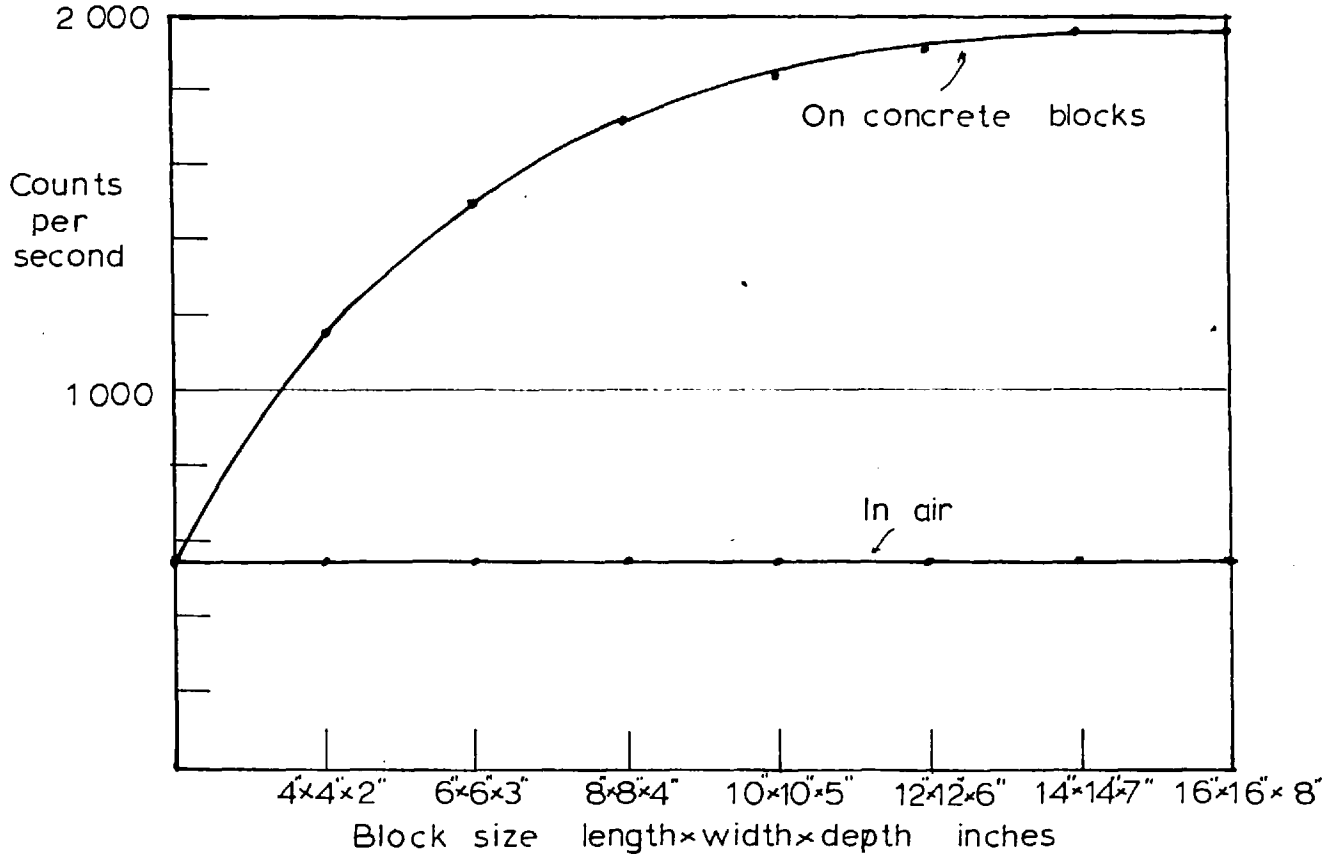


Fig. 6b

the scattered radiation fell in a broad peak between 0.05 MeV and 0.20 MeV, which, as shown in Chapter 2.2, made the count dependent on the chemical composition of the concrete. The results shown are for a Cs 137 source but similar results were obtained using Co 60.

Because the ratio of scattered to source count was low, and because the count was dependent on chemical composition, this method was rejected.

Initial experiments, in which a scintillation counter and source were separated by 6" of lead in an arrangement similar to that shown in Figure 1, indicated that this geometry may give better results. Readings were taken with the source and detector separated by distances of 3" or more, which gave curves of count rate against density with negative slopes for densities over about 120 lb/cu ft. The pulse height spectra showed all the scattered photons to be below 0.1 MeV.

This method then led through the theory discussed in Chapter 2.4 to the apparatus discussed in the chapters following.

CHAPTER 2.4 THE EFFECT OF THE COLLISION PROCESSES ON THE CALIBRATION CURVE

The total count comprised radiation scattered off the concrete R_s, radiation penetrating through the lead shield

from the source R_p, and background radiation due to cosmic and other sources R_b.

$$R_T = R_s + R_p + R_b \qquad 2.4.(1)$$

The background count R_b was always subtracted from the total count to give

$$R_T - R_b = R_s + R_p$$

The nett count rate $R_T - R_b$ was denoted by the symbol R, so that

$$R = R_s + R_p \qquad 2.4.(2)$$

The shape of a typical calibration curve for a back scatter density meter was shown in Figure 2. At zero density no photons were scattered back to the detector, i.e. $R_s = 0$. As the density of the material was increased, two opposing processes occurred. Whereas on the one hand more photons were scattered towards the detector, on the other, photons directed towards the detector were again scattered and moved away from it. At low densities the number of scatters experienced by a detected photon was low, perhaps only one scatter. An increase in density in this range caused an increase in the count rate as the number of once or twice scattered detected photons increased. On the rising portion of the curve, the photons had lost little energy. At some density, the multi-scatter pro-

cess began to predominate and as few once or twice scattered photons survived to detection, the curve fell. As density was further increased, the photons scattered more until their energy was reduced to that region in which absorption probability was high. Thus as $\rho \to \infty$, $R_s \to 0$.

The intensity R_s of the back scattered radiation showed a peak at a density dependent upon the source-detector geometry. Reports of this type of apparatus indicated that for densities above about 1.0 g/cc, R_s was a falling function of ρ. It must be inferred that in those pieces of equipment, the source, shield and detector were situated so that at normal densities the probability of detection of once or few times scattered photons was smaller than the probability of detection of multi-scattered photons.

Carey and Reynolds (1958) assumed that the calibration curve was the product of a polynomial in ρ of positive slope, due to the scattering process, and a negative exponential due to the photoelectric absorption process. Results reported in Chapter 2.5 show that scattering alone may account for the shape of the calibration curve.

The above discussion assumed that the tested concrete was an effectively infinite scatterer for the apparatus. Because photons which penetrated deep into the concrete had low probability of scattering back to the detector, an "effectively infinite volume" was defined as the volume beyond which the material had negligible effect on the

count. It is apparent that, in general, the effectively infinite volume depended on the geometry of the source-detector system, the source energy, the material density, the reaction cross sections for the material and the detector characteristics.

CHAPTER 2.5 THE VARIABLE PARAMETER EXPERIMENTS

Chapter 2.5.1 Description of the Apparatus

The aims of this series of experiments were

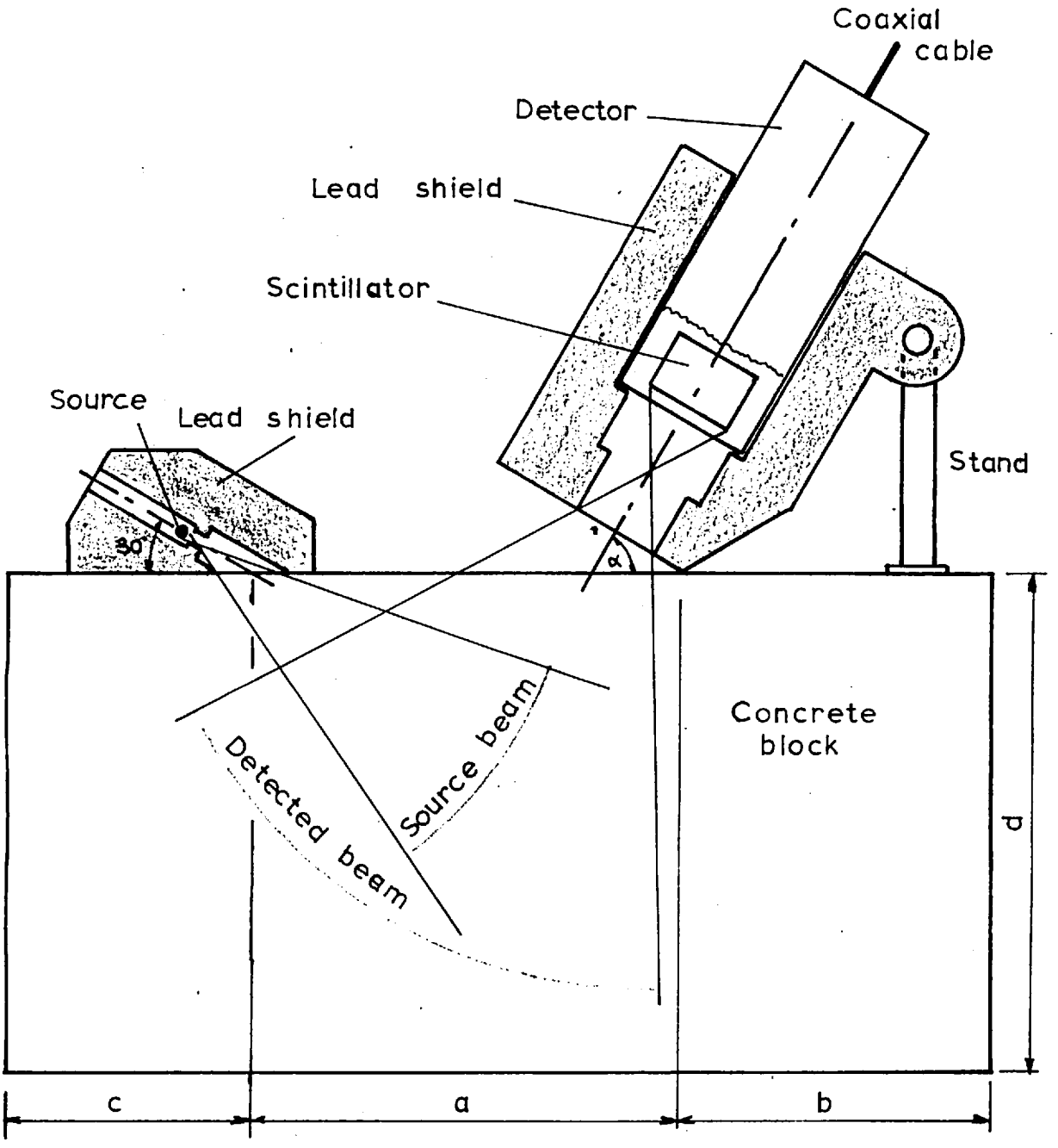
a) To discover whether a calibration curve could be obtained with a peak at a density high enough, so that count rate would give a unique value of density over all practical ranges.

b) To find the size of the effectively infinite volume and how this was affected by the source-detector distance, the total angle of scatter and the source energy.

c) To determine whether it were practical to eliminate all photons of energy less than 0.1 MeV so that a change in the proportions of elements in the concrete would have very small effect on the count rate.

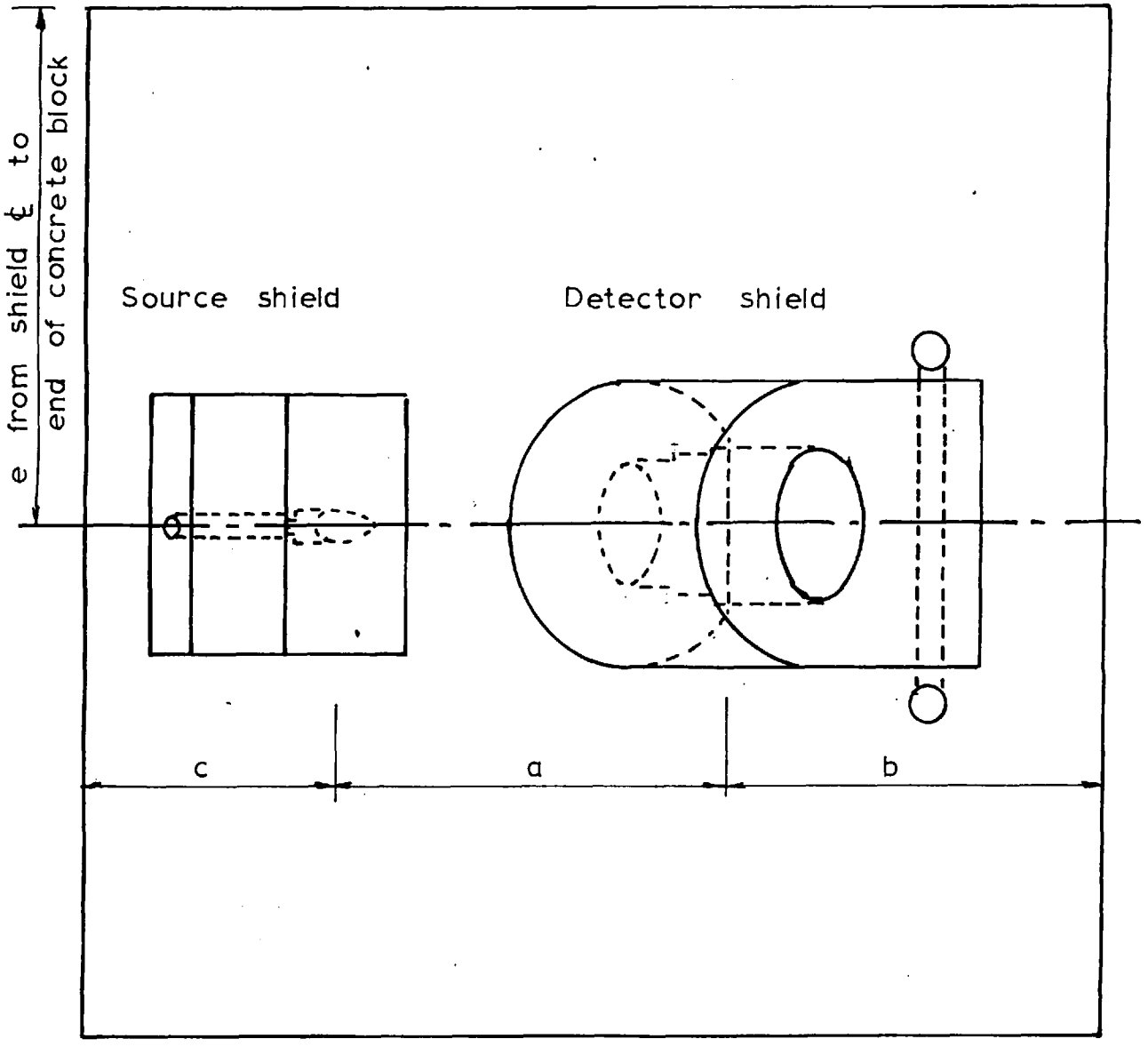
The sources used were 5 millicuries of Cs 137 and 1 millicurie of Co 60.

The detector was the scintillation counter system described in Chapter 2.3.



SECTION SHOWING SOURCE AND DETECTOR COLLIMATING SHIELDS

Fig. 7 a



PLAN ON SHIELDS

Fig. 7 b

Two lead shields were made as shown in Figures 7a and 7b. The source shield absorbed all the photons except those penetrating the inclined hole, providing a directed source beam. The scintillation counter, fitted inside the detector shield, could detect only those photons from within a limited cone. This shield could be inclined at any angle α to the concrete by means of a special stand, and set at any distance 'a' from the source shield.

Chapter 2.5.2 The Experiments

The primary aim of the experiments was to obtain curves of count rate R against density ρ for various configurations of source and detector beams, thereby showing which geometry gave the required calibration curve, as described in Chapter 2.5.1. Before doing this it was necesary to know the size of the effectively infinite volume as a function of the density of the material under test, the source energy and the geometrical parameters.

The first series of experiments was performed therefore in order to determine the size of the effectively infinite volume as a function of these parameters at a concrete density of 140 lb/cu ft. The experiments were then repeated on concrete of 39 lb/cu ft. The distances b, c, d, and e hereafter referred to are shown in Figures 7a and 7b.

The effectively infinite dimensions were obtained as follows. The detector shield, inclined at angle α, with the source shield distance 'a' from it were set up at the edge of the block of concrete and a reading taken. They were then moved some interval of distance along the concrete, the distance between the shields being kept constant. At positions near the edge, photons which would have been scattered back to the detector escaped from the block and the count rate was consequently low. When the source and detector were at the centre of the block, concrete near the edges had negligible effect on the count rate and the count rate against distance curve became horizontal (see Figures 8a to 8g). The distance from the beginning of the straight portion of the curve to the edge of the block was the minimum distance required to give the same count rate as an infinite block. The effectively infinite depth was obtained by using blocks of concrete 1" or 3" thick. The apparatus was placed in the centre of a block in a region where the R vs b, c, and e curves were horizontal, and readings were taken on one block, two blocks, and so on until the count rate reached a steady value. The curves are shown in Figures 8a to 8g, and the dimensions b_∞, c_∞, d_∞, and e_∞ given in Table 5 as functions of source energy, distance 'a' and angle α, for densities of 140 lb/cu ft and 39 lb/cu ft. The suffix ∞ refers to that dimension corresponding to the

DETERMINATION OF b_∞ at DENSITY 140 LB. per CU. FT.

R vs b

Source Co 60

Source Cs 137

$\alpha = 90°$

a = 4·5"

a = 5·5"

a = 6·5"

a = 7·5"

a = 8·5"

a = 9·5"

$\alpha = 60°$

a = 4"

a = 5"

a = 6"

$\alpha = 30°$

a = 4"

a = 5"

a = 6"

R Counts per sec

2 4 6 8 10

b inches

$c = 16 - (a + b)$

Fig. 8a

45

DETERMINATION OF e_∞ at DENSITY 140 LB. per CU. FT.


Fig. 8b

DETERMINATION OF d_∞ at DENSITY 140 LB. per CU.FT.

R vs d

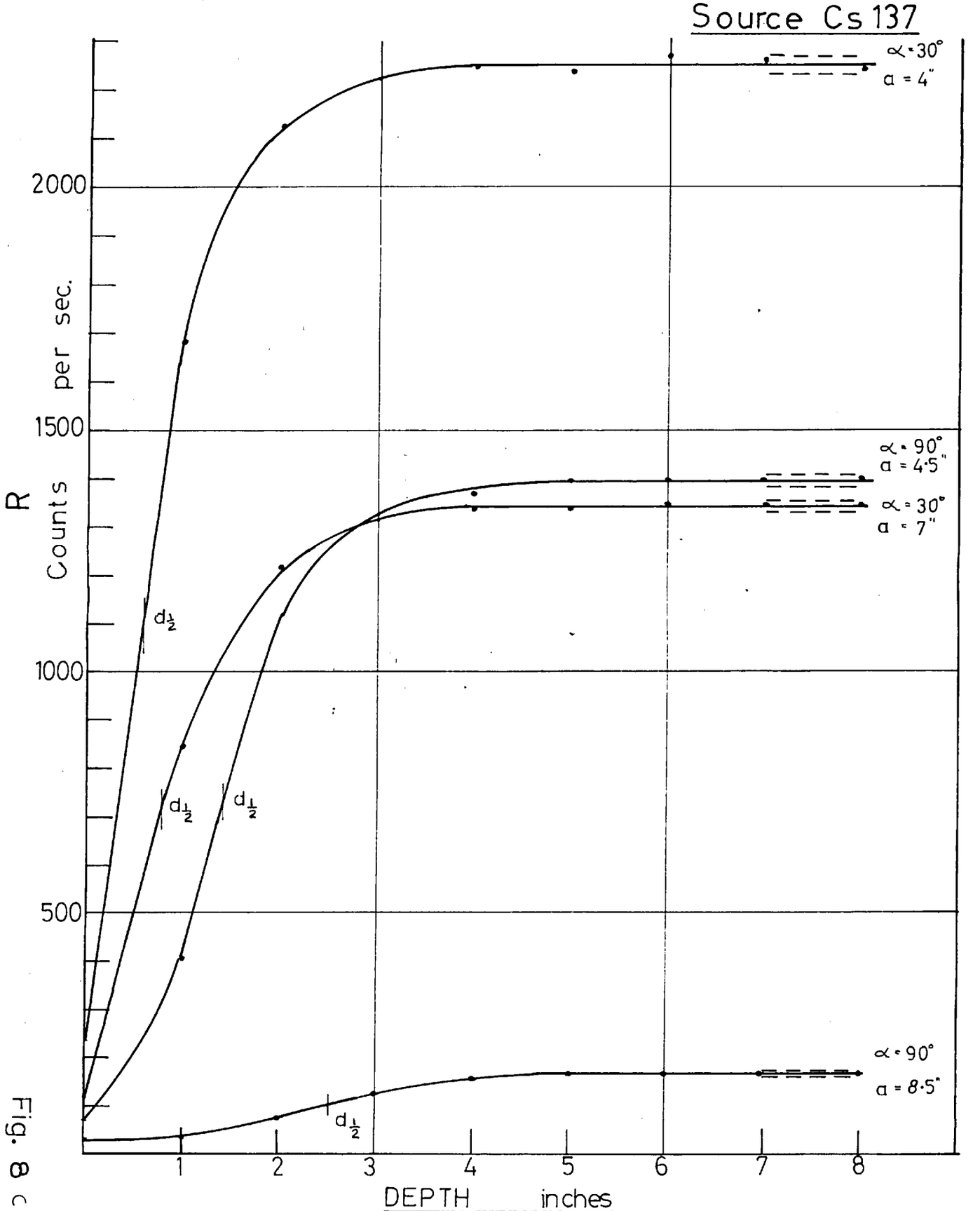


Fig. 8 c

DETERMINATION OF d_∞ at DENSITY 140 LB.per CU.FT.

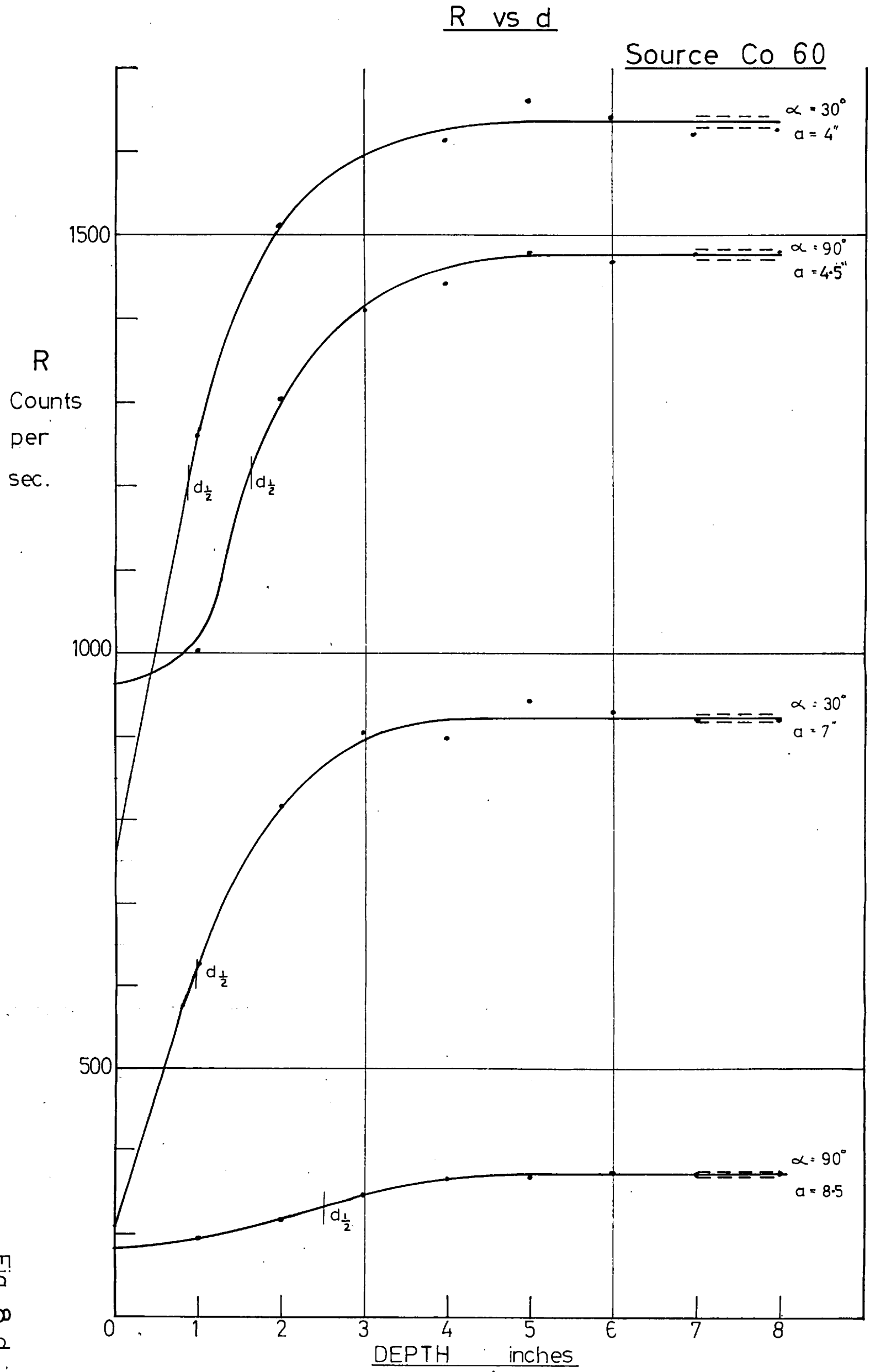


Fig. 8 d

DETERMINATION OF b_∞ at DENSITY 39 LB. per CU. FT.

R vs b

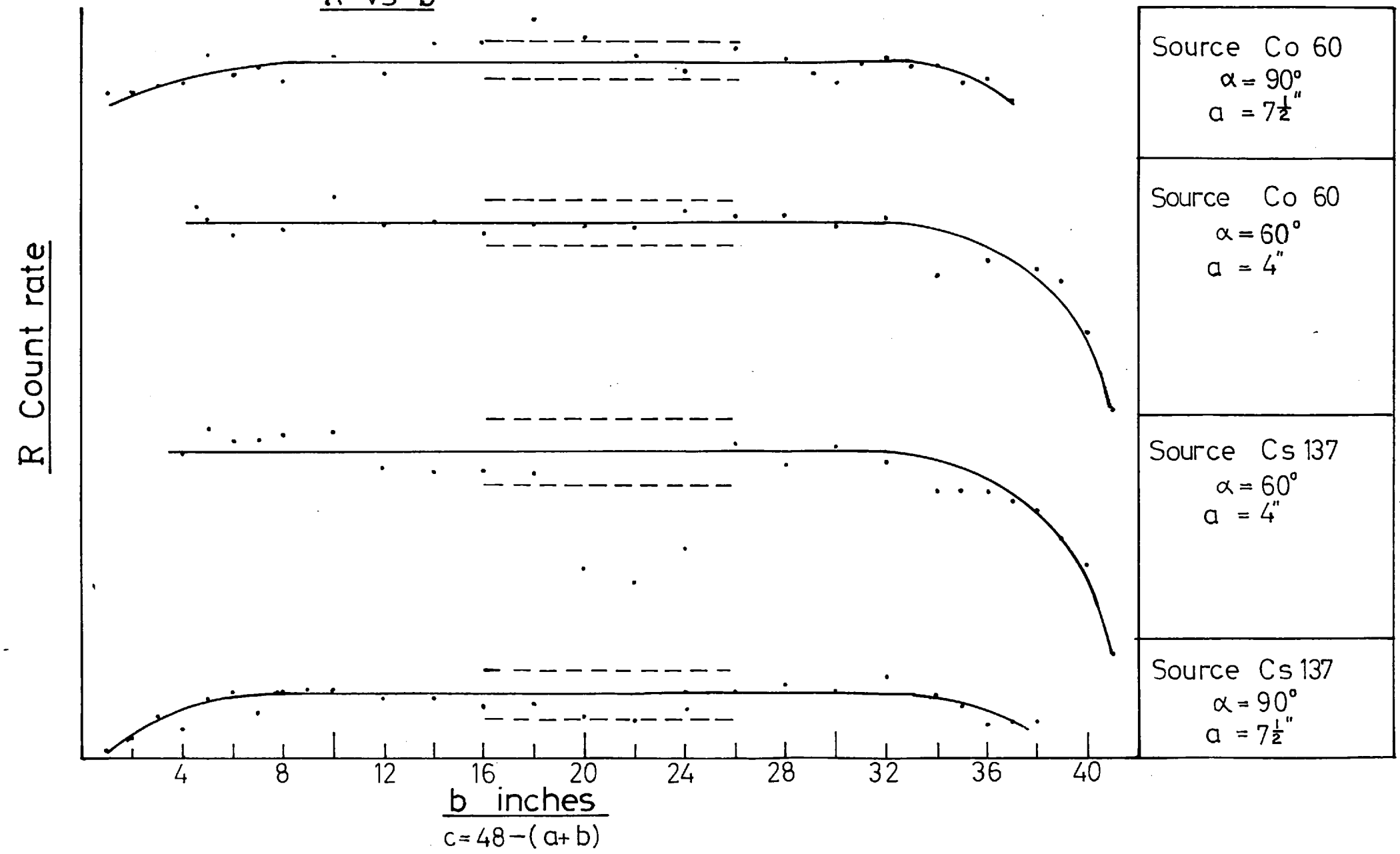


Fig. 8 e

DETERMINATION OF e_∞ at DENSITY 39 LB. per CU. FT.

R vs e

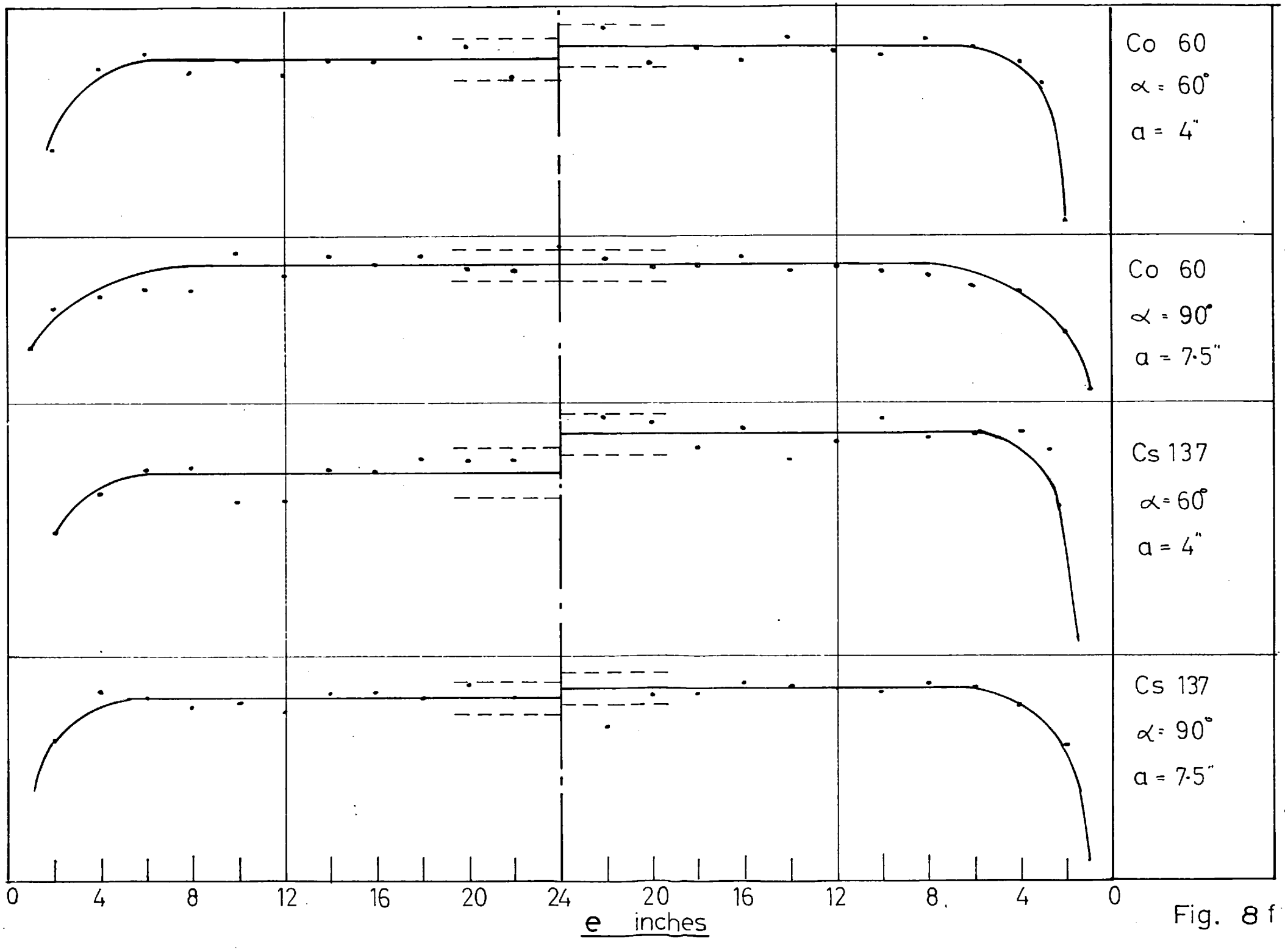


Fig. 8 f

DETERMINATION OF d_∞ at DENSITY 39 LB. per CU.FT.

R vs d

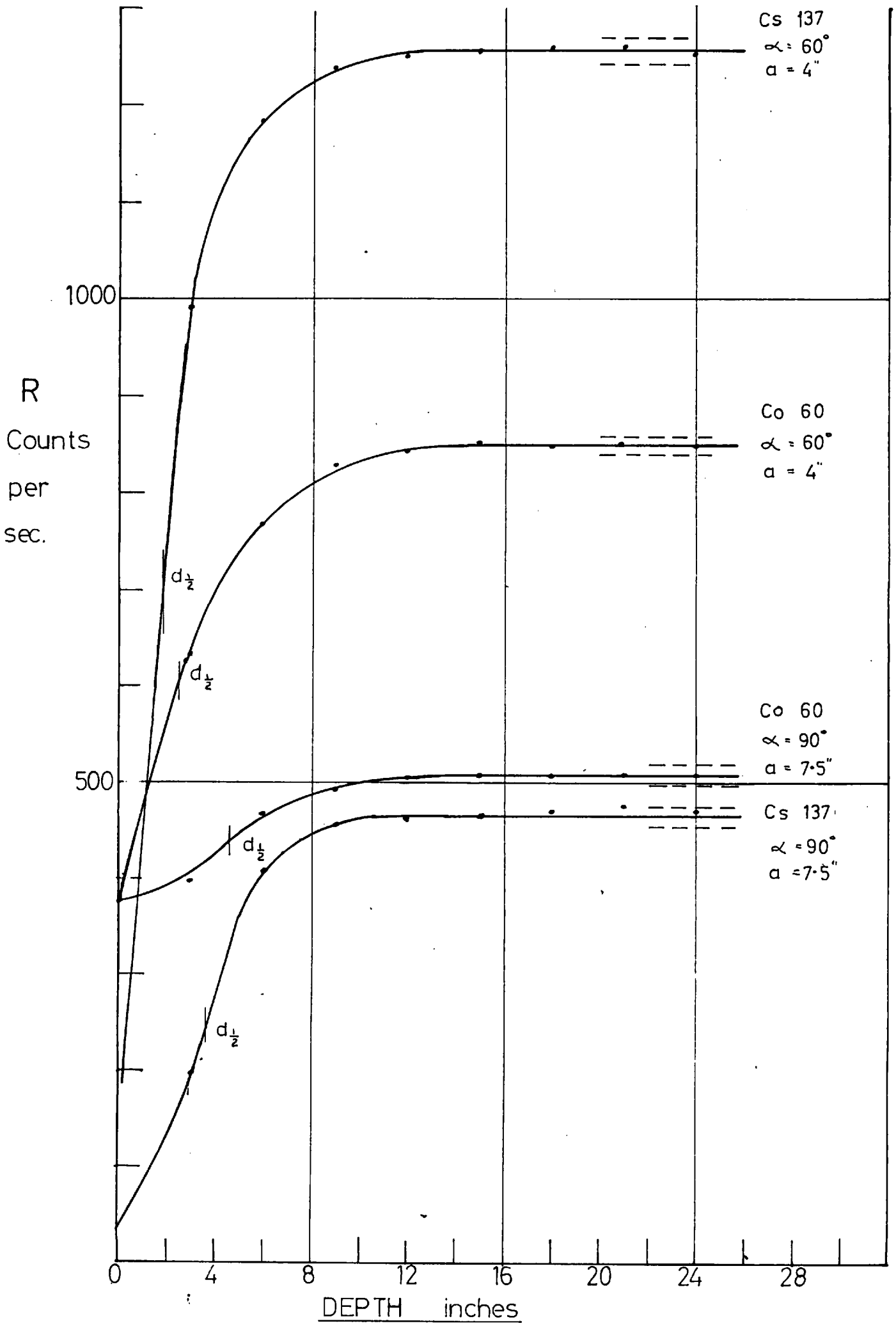


Fig. 8 & 9

infinite size. For example, in the curve of R vs b (Figure 8a) with source Cs 137, $\alpha = 30^{\circ}$ and a = 5", the dimension b giving an effectively infinite reading is seen to be $b_{\infty} = 2"$.

TABLE 5

The Effectively Infinite Dimensions for the Variable Parameter Experiments

ρ	α	a	Source Co 60					Source Cs 137				
			b_{∞}	c_{∞}	e_{∞}	d_{∞}	$d_{\frac{1}{2}}$	b_{∞}	c_{∞}	e_{∞}	d_{∞}	$d_{\frac{1}{2}}$
140	90°	4½"	2"	3½"	3"	5"	1.6"	1"	4"	3"	4½"	1.4"
lb		5½"	1½"	3½"	-	-		1"	4"	-	-	
per		6½"	1½"	2½"	-	-		1"	4"	-	-	
cu		7½"	1"	2½"	-	-		1½"	3"	-	-	
ft		8½"	1½"	<1½"	3"	5"	2.5"	1½"	2½"	3"	4½"	2.5"
		9½"	0"	<1½"	-	-		1"	<1½"	-	-	
	60°	4"	<0"	6"	3"	-		<1"	5"	3"	-	
		5"	<0"	6"	-	-		<1"	5½"	-	-	
		6"	<0"	5"	-	-		<1"	4"	-	-	
		8"	-	-	3"	-		-	-	4"	-	
	30°	4"	<1"	4"	4"	5"	0.8"	2"	4"	3"	4"	0.6"
		5"	<1"	4"	4"	-		2"	3"	3"	-	
		6"	<1"	4"	4"	-		2"	3½"	3"	-	
		7"	-	-	3½"	4"	1"	-	-	3"	4"	0.8"
39 lb per cuft	90°	7½"	8"	7½"	8"	12"	4.6"	7"	7½"	6"	10"	3.7"
	60°	4"	<4"	12"	6"	13"	2.5"	<4"	12"	6"	12"	1.8"

The quantity R_b was always determined by taking a count with the source removed. R_p was obtained by placing the source and detector upon a thin sheet of perspex remote from the floor, walls and laboratory equipment, so that no source photons could be scattered into the detector. The errors in R_b, R_p and R_s were estimated by usual nuclear statistical methods, but this neglected two further causes of error in the count rate.

a) Local variation in density from point to point in the concrete.

b) Errors in positioning the source shield relative to the detector shield.

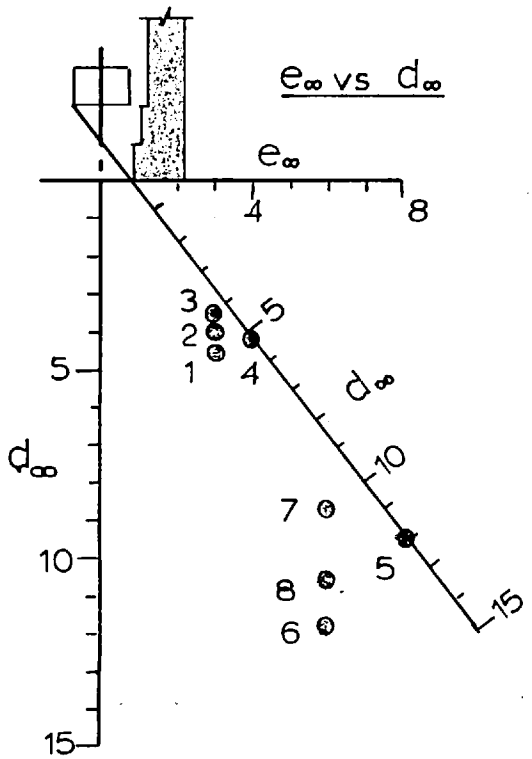
The broken lines in Figures 8 indicate $\pm$ 2 standard deviations calculated from consideration of the nuclear statistics only, so that the actual errors were greater than those indicated.

Figure 9 shows the values of e_∞ and b_∞ plotted against d_∞, where d_∞ was taken to be the last path distance from the edge of the effectively infinite volume. This gives a clearer picture of the shape of that volume and is further discussed in Chapter 2.5.5.

The distances $d_{\frac{1}{2}}$, at which the scattered count rate R_s was equal to half the maximum, are plotted on the curves in Figures 8c and 8d and are shown in Table 5.

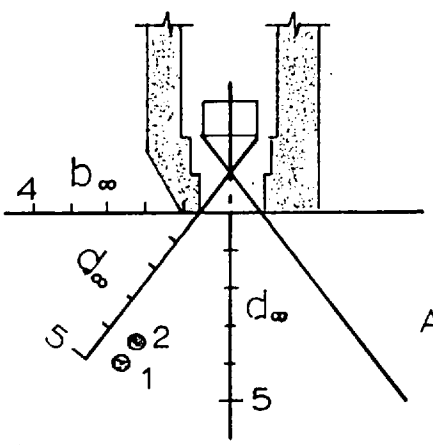
By interpolation using certainly safe assumptions the minimum size of concrete block required at each density

The Variable Parameter Experiments



Code

No	Source	α	ρ	a
1	Co 60	90°	140	4·5" & 8·5"
2	Cs 137	90°	140	4·5" & 8·5"
3	Cs 137	30°	140	4"
4	Co 60	30°	140	4"
5	Co 60	90°	39	7·5"
6	Co 60	60°	39	4"
7	Cs 137	90°	39	4"
8	Cs 137	60°	39	4"



b_∞ vs d_∞
with $\alpha = 90°$, $\rho = 140$ lb/cu ft

All $(a+c_\infty)$ plot outside the cone.

Code

No	Source	a
1	Co 60	4·5", 8·5"
2	Cs 137	4·5", 8·5"

Fig. 9

was calculated. Blocks larger than this minimum size were made at a further five densities, giving a range from 39 lb/cu ft to 156 lb/cu ft. Count rate readings were taken at four values of α, five or six values of 'a', and two values of source energy, giving the curves of Figures 10a to 10h.

Chapter 2.5.3 The Experimental Results

The count at the detector was due to three separate sources, as discussed in Chapter 2.4.

Determination of effectively infinite size (Figures 8a to 8g)

Nett count rate R, which is $(R_T - R_b)$, was plotted against b, e or d as appropriate in order to find b_∞, c_∞, e_∞, and d_∞ for a number of geometries, for two sources and two densities. The discriminator level was 0.05 MeV, which was the minimum operating bias of the discriminator.

The calibration curves (Figures 10a to 10h)

Nett count rate was plotted against density. The discriminator level was again 0.05 MeV.

Chapter 2.5.4 Discussion of the Calibration Curves

From examination of the curves R vs ρ (Figures 10a to 10h) the following conclusions may be drawn.

a) A calibration curve giving a unique value of density over all ranges is obtainable when the

COUNT RATE vs DENSITY

Source Co 60

$\alpha = 90°$

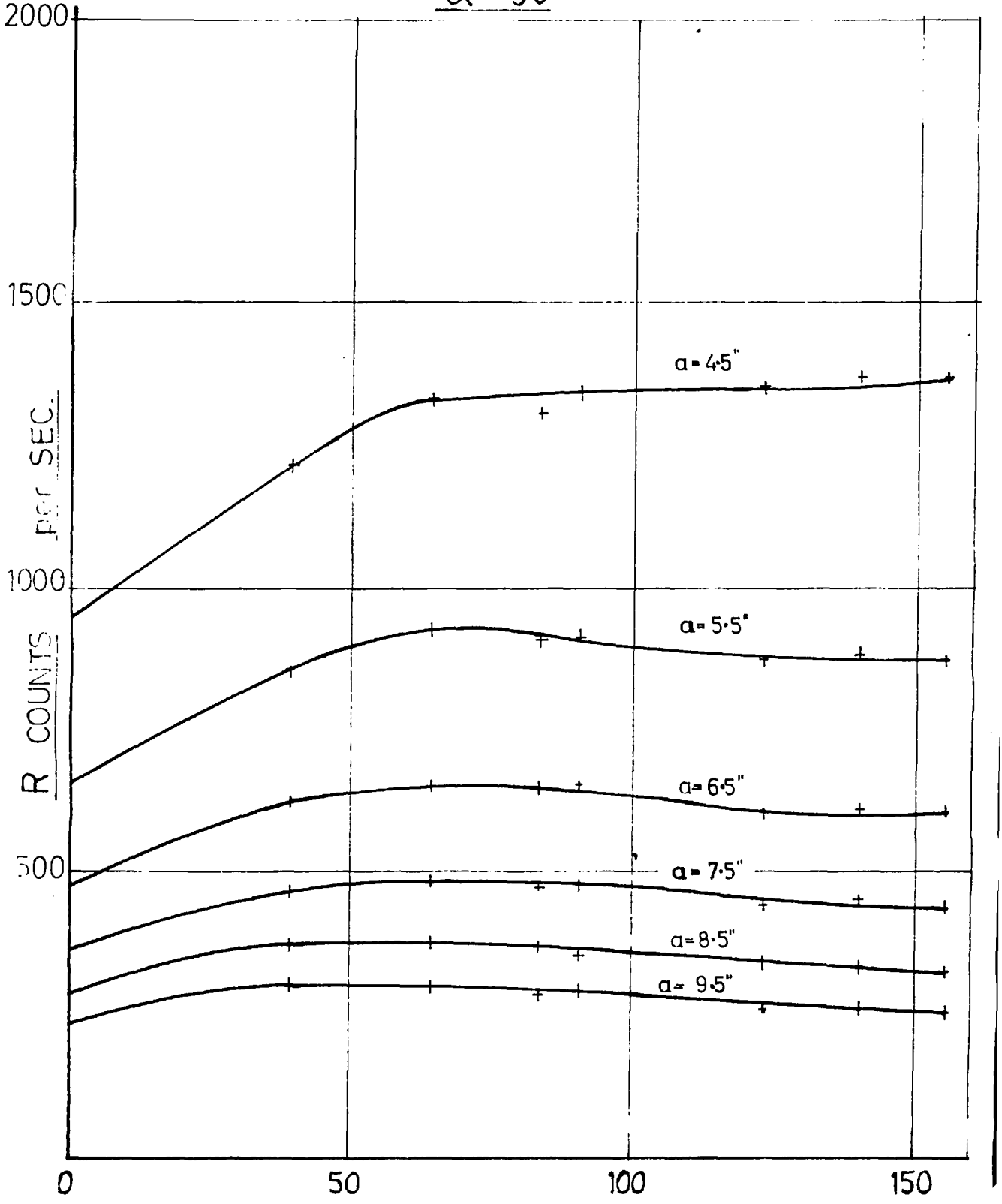


Fig.10 a

COUNT RATE vs DENSITY

Source Cs 137

$\alpha = 90°$

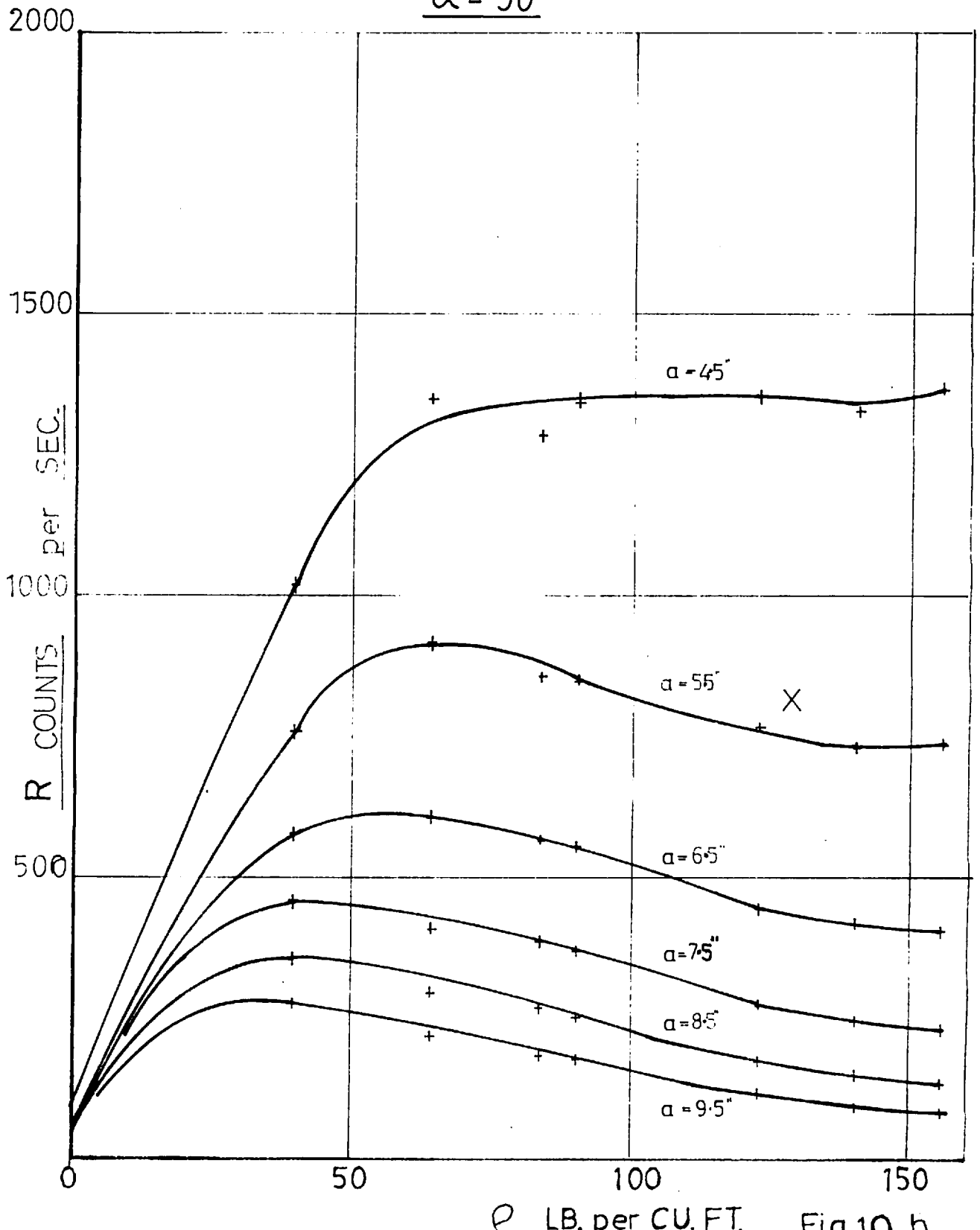


Fig.10 b

COUNT RATE vs DENSITY

Source Co 60

$\alpha = 75°$

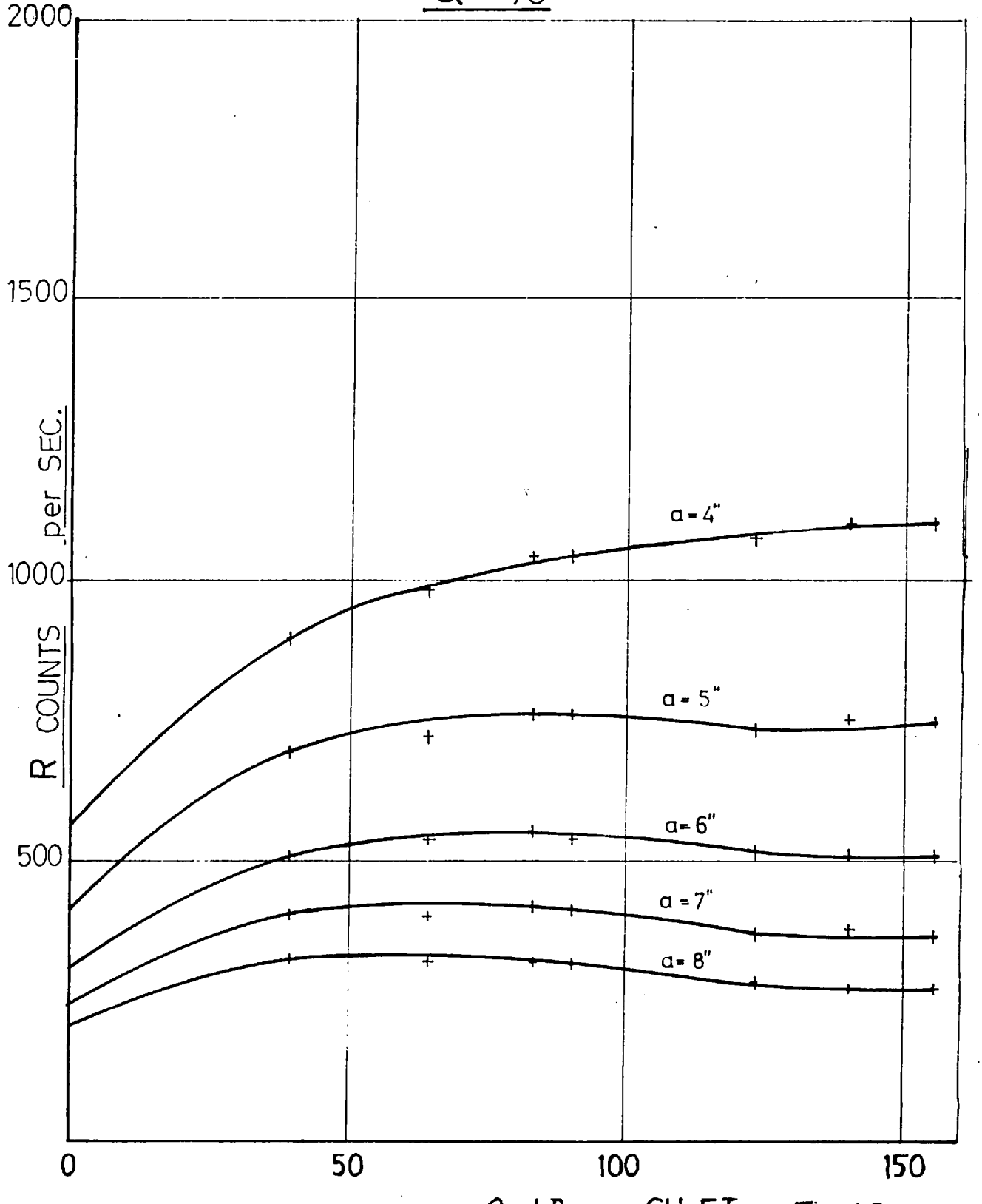


Fig.10 c

COUNT RATE vs DENSITY

Source Cs 137

$\alpha = 75°$

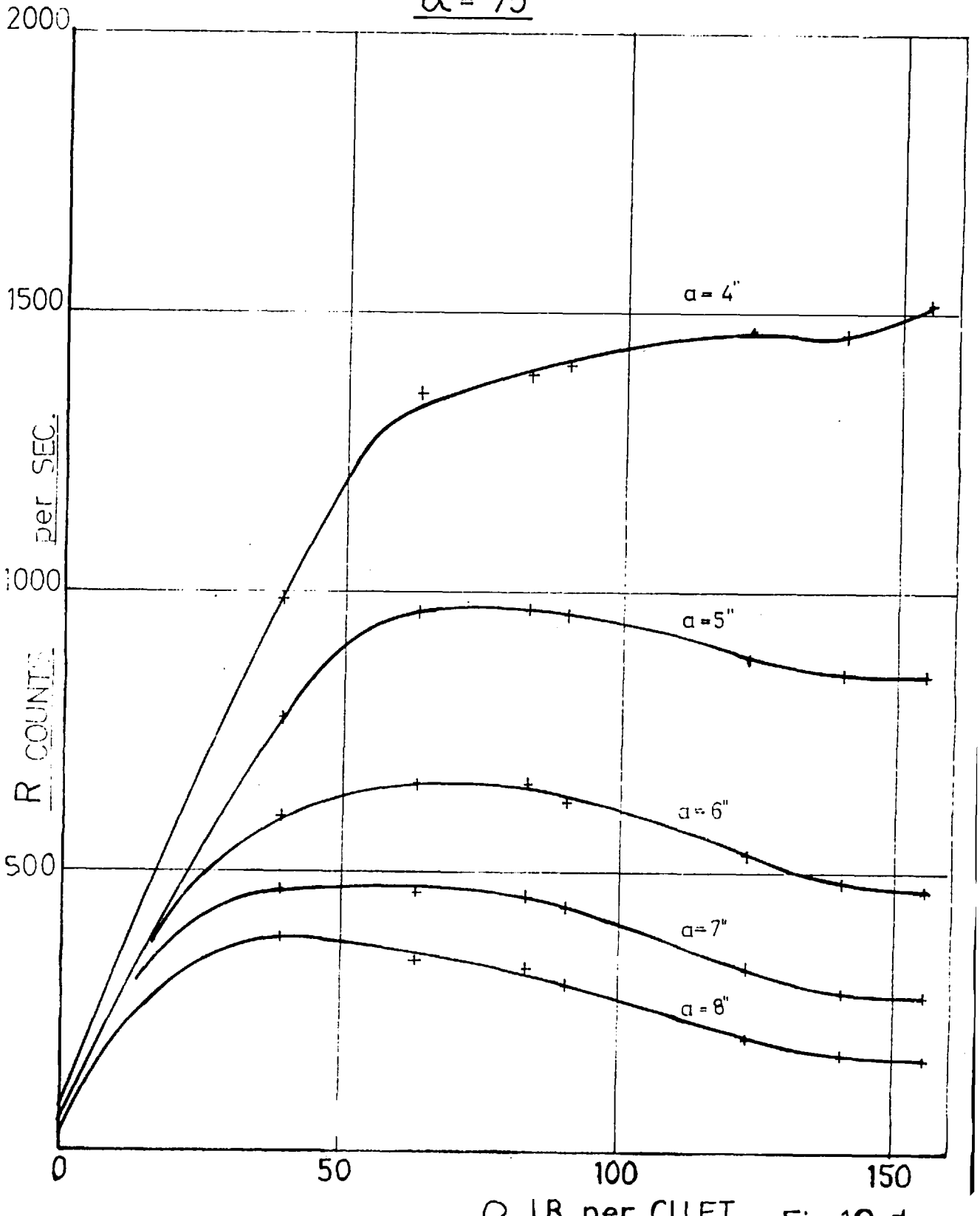


Fig. 10 d

COUNT RATE vs. DENSITY

Source Co 60

$\alpha = 60°$

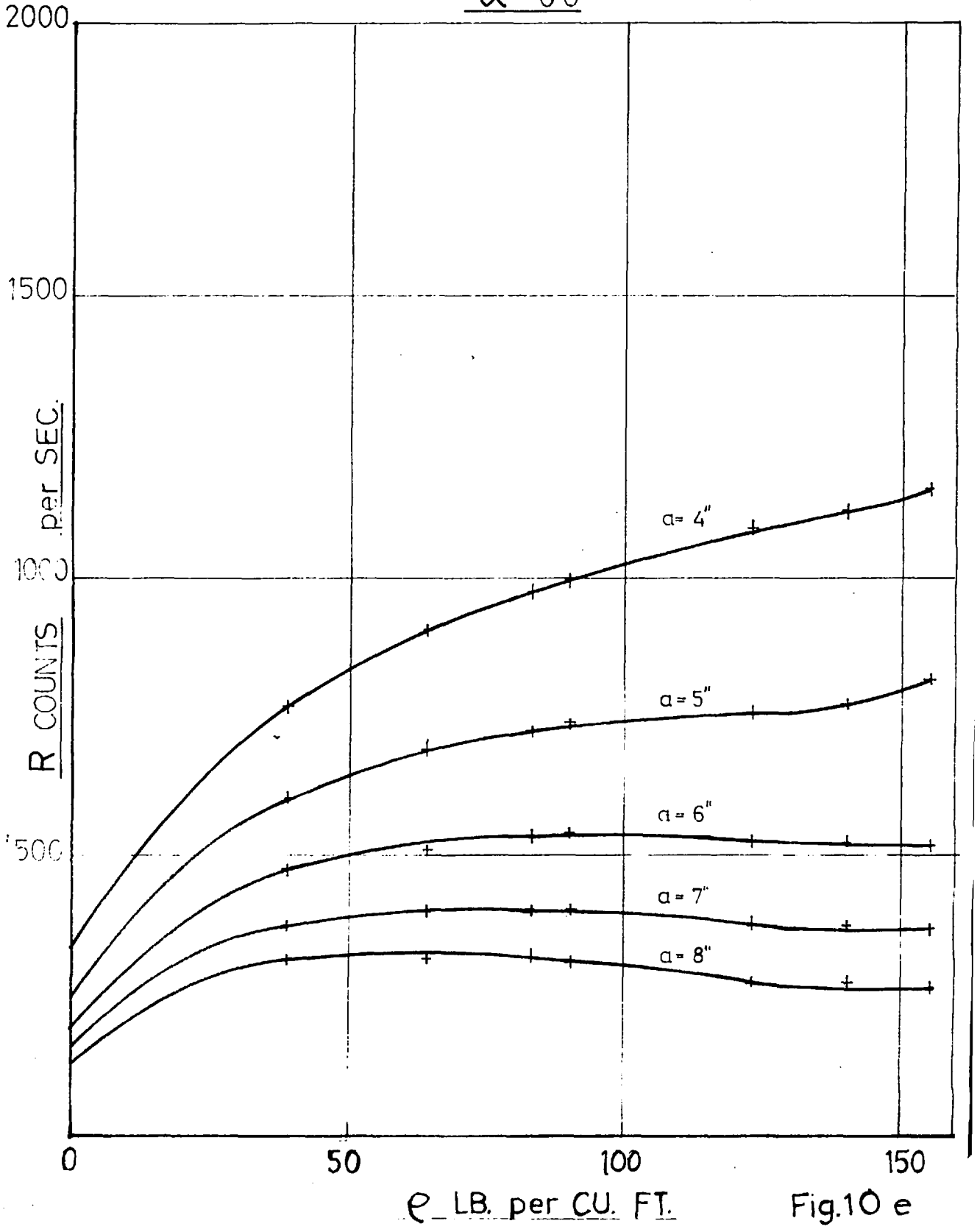


Fig.10 e

COUNT RATE vs DENSITY

Source Cs 137

$\alpha = 60°$

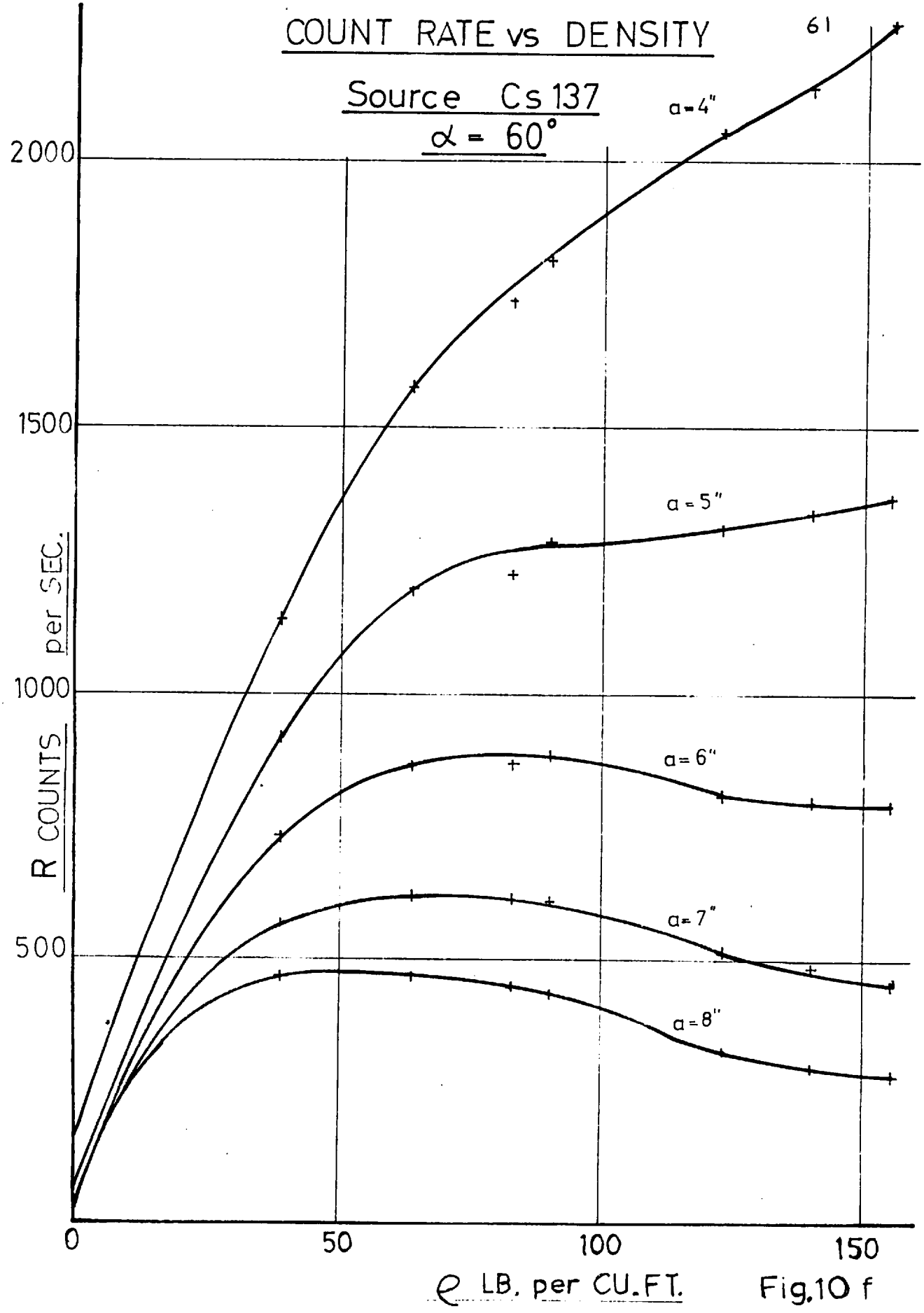


Fig.10 f

COUNT RATE vs DENSITY

Source Co 60

$\alpha = 45°$

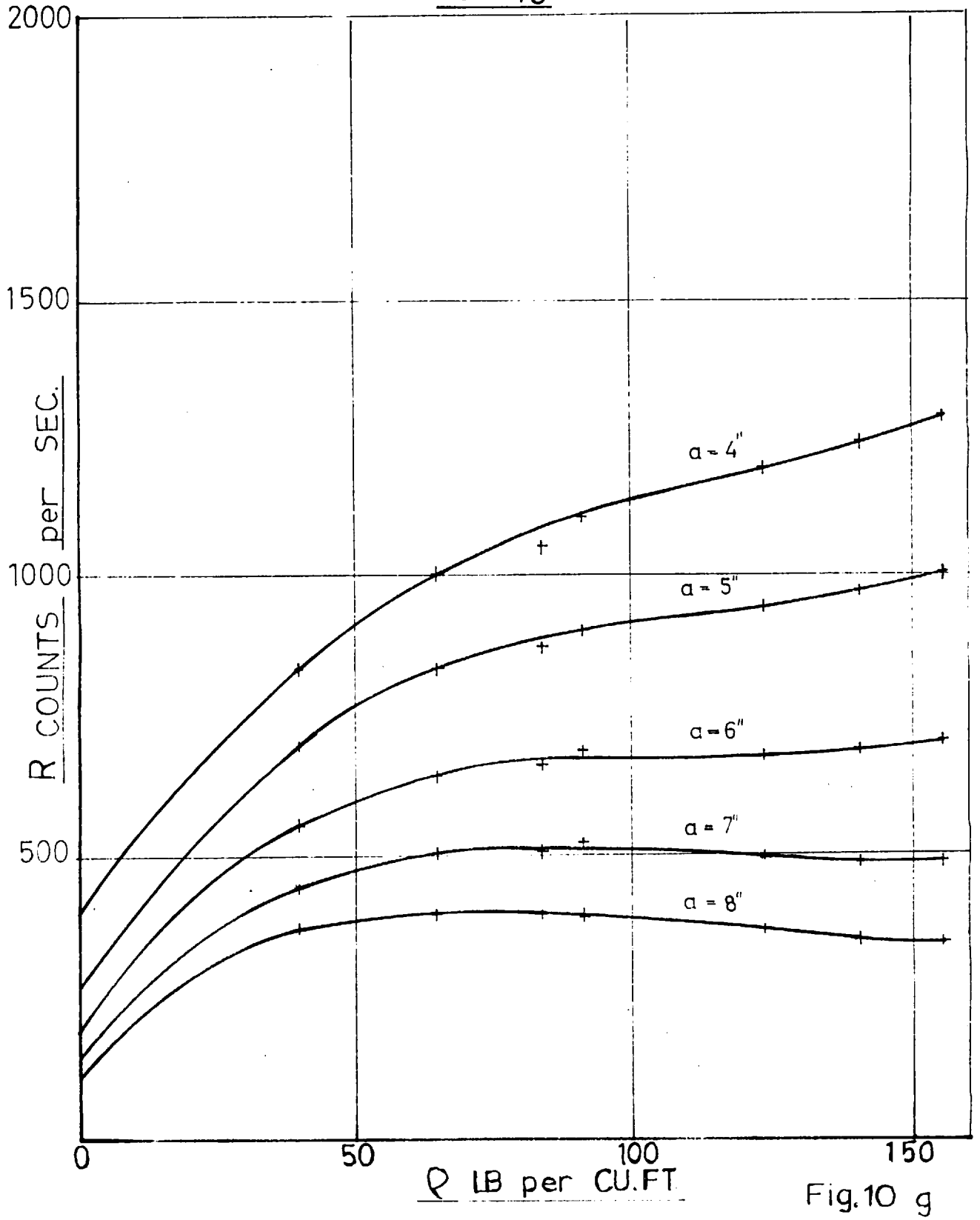


Fig. 10 g

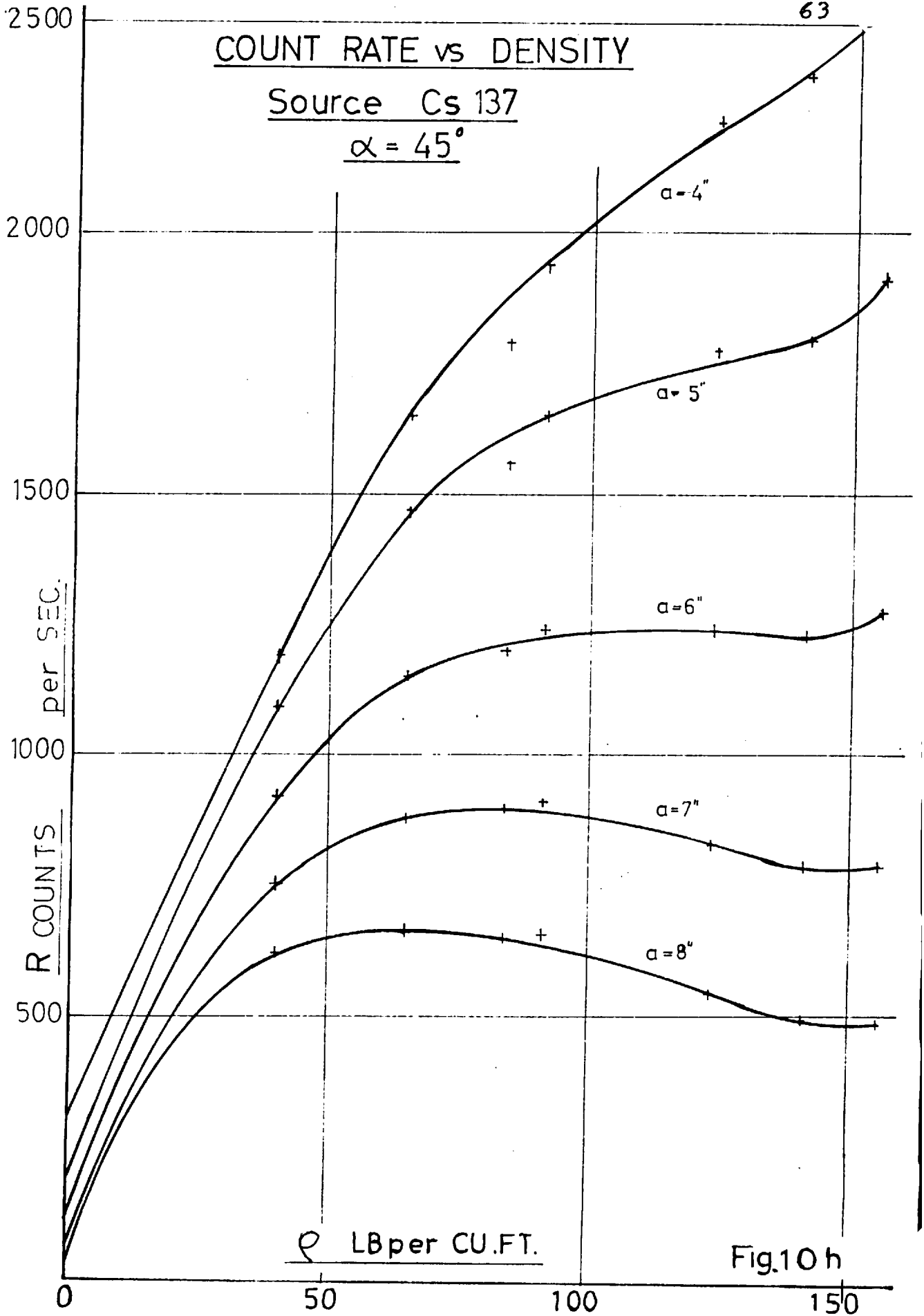

COUNT RATE vs DENSITY
Source Cs 137
α = 45°
a = 4"
a = 5"
a = 6"
a = 7"
a = 8"
R COUNTS per SEC.
ρ LB per CU.FT.
2500
2000
1500
1000
500
0
50
100
150

Fig. 10 h

detector "sees" concrete near the source.

b) The shape of the calibration curve is little affected by source energy.

This may be more clearly understood by considering information obtainable from the detected pulse height spectra.

Figure 11 shows the pulse height spectra observed at a given geometry, $\alpha = 90^{o}$, $a = 5\frac{1}{2}"$ with source Cs 137 on concretes of 156, 64 and 39 lb/cu ft.

The source energy was 0.662 MeV, and the energy after scattering through 120^{o} was calculated from equation 2.2.(3) to be 0.224 MeV. Therefore the highest energy peak was due to the once scattered photons. The peak at about 0.13 MeV was due to twice scattered photons. It has been observed (Hayward and Hubbell 1953 and 1954, Wiechers 1958) that in a system such as this where the photons scatter through a given angle, by one, two or many scatters, the twice scattered photons give a peak in the spectrum. The energy of twice scattered photons has been calculated as a function of scattering angle in Appendix B. There it is shown that for a Cs 137 source and a total angle of scatter of 120^{o}, photons which suffered one large angle scatter had final energy near 0.13 MeV, which gave the peak. Bopp (1937) calculated that peaks should be observed at both high and low energies, but the high energy peak was not observed by Hayward and Hubbell (1953) and (1954) nor

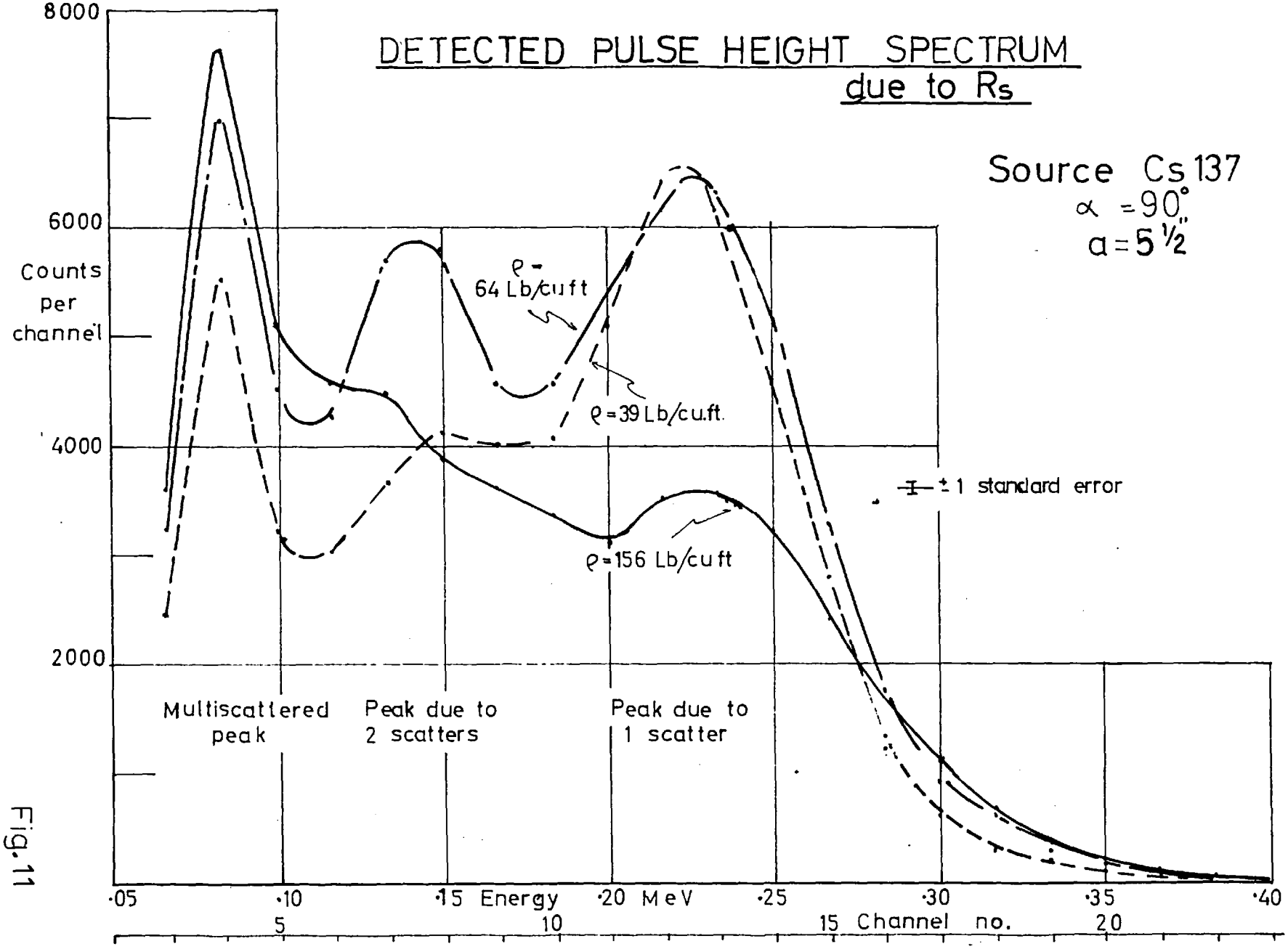

DETECTED PULSE HEIGHT SPECTRUM
due to Rs
Source Cs 137
α = 90°
a = 5 ½"
8000
6000
4000
2000
Counts per channel
ρ = 64 Lb/cu ft
ρ = 39 Lb/cu.ft.
ρ = 156 Lb/cu ft
± 1 standard error
Multiscattered peak
Peak due to 2 scatters
Peak due to 1 scatter
·05
·10
·15 Energy
·20 MeV
·25
·30
·35
·40
5
10
15 Channel no.
20

Fig. 11

Wiechers (1958). The relatively poor collimation of the present apparatus may have obscured this peak, if it occurred. At energies below 0.13 MeV are photons which had scattered many times. If the concrete were a pure Compton scatterer, showing no absorption, the spectrum would reach infinity asymptotically as $E \rightarrow 0$ but because photoelectric absorption eliminated the lowest energy photons a peak was obtained. If the atomic number, Z, of the material were increased, the absorption cross section would be increased and the low energy peak would move to a higher energy.

In Chapter 2.2, it was shown that the absorption cross section depends strongly on the proportions of elements in the concrete, increasing with Z^5/A. Discriminating at an energy of 0.1 MeV would eliminate the low energy peak from the system, so that changes in photoelectric absorption cross section would have no effect on the count rate.

Comparison of the three curves in Figure 11 shows that at a density of 39 lb/cu ft the number of once scattered photons observed was greater than the number of lower energy photons. At 64 lb/cu ft the number of once scattered photons was approximately the same as at 39 lb/cu ft but the relative number of twice and many scattered photons was increased. At 156 lb/cu ft the number of once and twice scattered photons was reduced, and most of the count rate was due to many scattered photons.

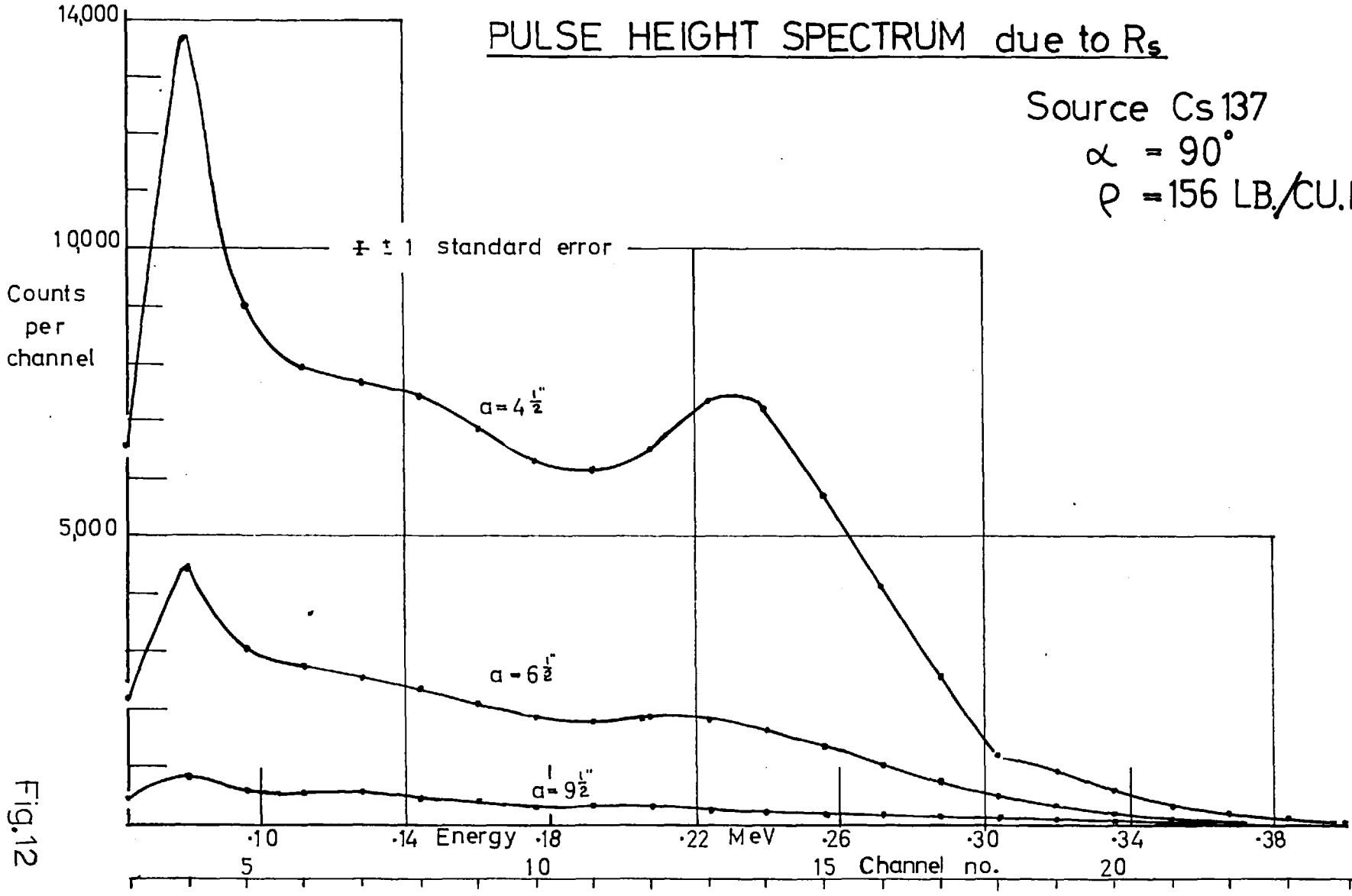

PULSE HEIGHT SPECTRUM due to R_s
Source Cs 137
α = 90°
ρ = 156 LB./CU.FT.
14,000
10,000
5,000
Counts per channel
± 1 standard error
a = 4½"
a = 6½"
a = 9½"
·10
·14
·18
·22
·26
·30
·34
·38
Energy MeV
5
10
15
20
Channel no.

Fig. 12

Figure 12 shows the pulse height spectra at a density of 156 lb/cu ft with a Cs 137 source and $\alpha = 90^{\circ}$, at various source to detector distances. The peaks were due to once, twice and many scattered photons, as in Figure 11. It is seen that as 'a', the distance source to detector was increased, the relative number of once and twice scattered photons decreased. In other words, the count became increasingly due to much scattered, low energy, photons.

Figures 10a to 10h show the curves of count rate vs density for values of $\alpha = 45^{\circ}$, 60°, 75°, 90°, two source energies (Co 60 and Cs 137) and various distances source to detector. These curves are of the general shape described in Chapter 2.4. It was there explained that the rising portion of the curve was due to the enhanced probability of once or twice scattered photons being detected; the falling portion was due to the enhanced probability of multi-scattered photons being detected.

The spectra shown in Figure 11 were observed with the same parameters as the curve marked X on Figure 10b. The spectrum at 39 lb/cu ft is on the rising portion of the curve, the spectrum at 64 lb/cu ft is at the peak, and the spectrum at 156 lb/cu ft is on the falling portion of the curve. Scattering alone may therefore account for the shape of the calibration curve, although in systems where

R_s falls as ρ increases the energy of the detected photons will be low so that the photoelectric absorption process will affect the slope of the calibration curve.

It can be seen by comparing the curves of Figures 10 that the values of R at $\rho = 0$ were far higher for the 1 mC source of Co 60 than for the 5 mC source of Cs 137. It is desirable that R_p be kept low and Cs 137 is therefore a better source than Co 60, for this application.

When photons of energy above about 0.5 MeV scatter in a material, it has been shown that after two or three scatters the energy of the photons is almost independent of the source energy (Hayward and Hubbell 1953 and 1954, Goldstein and Wilkins 1954, Matveev et al 1957, Hyodo 1962). It is therefore to be expected that the shape of the falling portion of the calibration curve, due to multi-scattered photons, be unaffected by source energy. The rising portion of the curve will be influenced, as the collision probability for once and twice scattered photons will depend on the source energy. This probability, however, does not vary very much in the range 0.66 to 1.3 MeV (see Figure 3).

In general, therefore, the value of source energy has little effect on the calibration curve.

Chapter 2.5.5 Discussion of the Effectively Infinite Volume

From Table 5 it is observed that at a density of 140 lb/cu ft the distances b_∞, c_∞, e_∞ and d_∞ hardly varied with distance source to detector or with source energy. As α was decreased, b_∞ decreased while c_∞ increased. For the 30° values, c_∞ was unduly low on account of absorption of scattered radiation by the lead source shield (see Chapter 2.5.6).

In order to be detected, a photon must have had its last collision within the detected beam, and after collision must have been directed towards the detector. The probability that a photon survives from its last collision to the detector is

$$p = e^{-\Sigma_t x} \qquad 2.5.5.(1)$$

where x is the last path distance in the concrete and Σ_t the total cross section. If the effectively infinite volume be defined so as to correspond to a particular value of p, the effectively infinite dimension is seen to depend upon Σ_t.

Now $\Sigma_t = \Sigma_a + \Sigma_s = \rho(\mu_a + \mu_s)$ where μ_s and μ_a each depend upon the elemental constituents of the concrete and the photon energy, so the effectively infinite dimension will depend upon the density and elemental con-

stitution of the concrete and the photon energy spectrum in the detected beam.

The influence of source energy

It has been shown in Chapter 2.5.4 that after a few collisions the energy of a photon was independent of the source energy. The photons reaching the outer regions of the effectively infinite volume were, generally, multi-scattered photons (Hayward and Hubbell 1953 and 1954) and were therefore independent of source energy. The dimension of the effectively infinite volume should therefore have been independent of source energy, if the low energy photons were detected.

The influence of distance source to detector

Whatever the geometrical arrangement of the apparatus, it was the multi-scattered photons which penetrated to the outer regions of the effectively infinite volume, and which therefore determined the extent thereof. After relatively few scatters the multi-scattered photons were at a single energy, which was the low energy peak in Figures 11 and 12, and so Σ_t, which was a function of photon energy, was independent of distance 'a'. The effectively infinite dimension was therefore independent of 'a'. The volume itself did increase as 'a' was increased but the distance beyond the source or detector remained constant.

The influence of angle α

As α was decreased, the detection beam, which was conical, "saw" less concrete beyond the detector, and more beyond the source. b_∞ therefore decreased and c_∞ increased. Knowing an experimental value of d_∞ and the geometry of the detection cone, e_∞, b_∞ and c_∞ were examined to see if they fell within the detection cone. These were plotted in Figure 9 which shows that e_∞ and b_∞ did, while c_∞ fell outside the detection cone. Such behaviour may be expected for the collimated apparatus used.

The probability that a photon penetrates a distance d_∞ through the concrete without collision is calculable from equation 2.5.5.(1) and is tabulated in Table 6 for the experimental densities at two values of photon energy.

TABLE 6

Probability of Last Path Survival

Density lb/cu ft	d inches	$p = e^{-\mu\rho d}$ photon energy 0.05MeV	$p = e^{-\mu\rho d}$ photon energy 0.1MeV
140	4	0.00035	0.021
90	6	0.00046	0.025
39	14	0.00042	0.024

The cross sections μ are for the typical concrete of Grodstein (1957).

The influence of density on effectively infinite depth

Because the effectively infinite depth was determined by photons of a single low energy, Σ_t in equation 2.5.5.(1) was proportional to ρ. For a constant p, therefore, depth d_∞ was inversely proportional to density as is shown in Table 8 of Chapter 2.7.2.

Chapter 2.5.6 The Relation Between Count Rate and Distance Source to Detector

Jacquesson (1954) and (1958), Pocock (1956), Bulatov (1960) and Hyodo (1962) have observed that in a backscattering system the scattered count rate R_s was related to a general distance source to detector x by the relation

$$R_s = Ae^{-Bx} \qquad 2.5.6.(1)$$

where A and B were constants.

Before proceeding further, the effect with this apparatus of absorption by the source shield of photons en route to the detector was examined. The detected beam was a cone and the intersection of the concrete surface and this beam therefore an ellipse. Knowing the geometry of the shields the proportion of the detected beam obscured by the source shield was calculated. All the count rates for $\alpha = 45^\circ$ and the count rate for $\alpha = 60^\circ$, a = 4" were multiplied by the ratio of the total ellipse area to the area "seen" by the detector (see Figure 13a).

This correction was artificial, in the sense that at negative values of x once scattered photons could not have been detected and the spectral composition of the beam would have been different from that which was actually detected.

In equation 2.5.6.(1), ρx seemed to be a more logical variable than x, so curves were drawn of log R_s vs ρx for each density, angle α and source. These are shown in Figures 13a to 13i and appear to be straight lines.

The values of A and B in the equation $R_s = Ae^{-B\rho x}$ were found by least squares fitting. Table 7 shows the sums of squares of residuals obtained, averaged over ρ at each value of α.

TABLE 7

Least Sums of Squares of Weighted Residuals for Fitting $R_s = Ae^{-B\rho x}$, Averaged over 7 Densities

α	Source Co 60	Source Cs 137
90°	17	41
75°	6	14
60°	19	19
45°	144	153

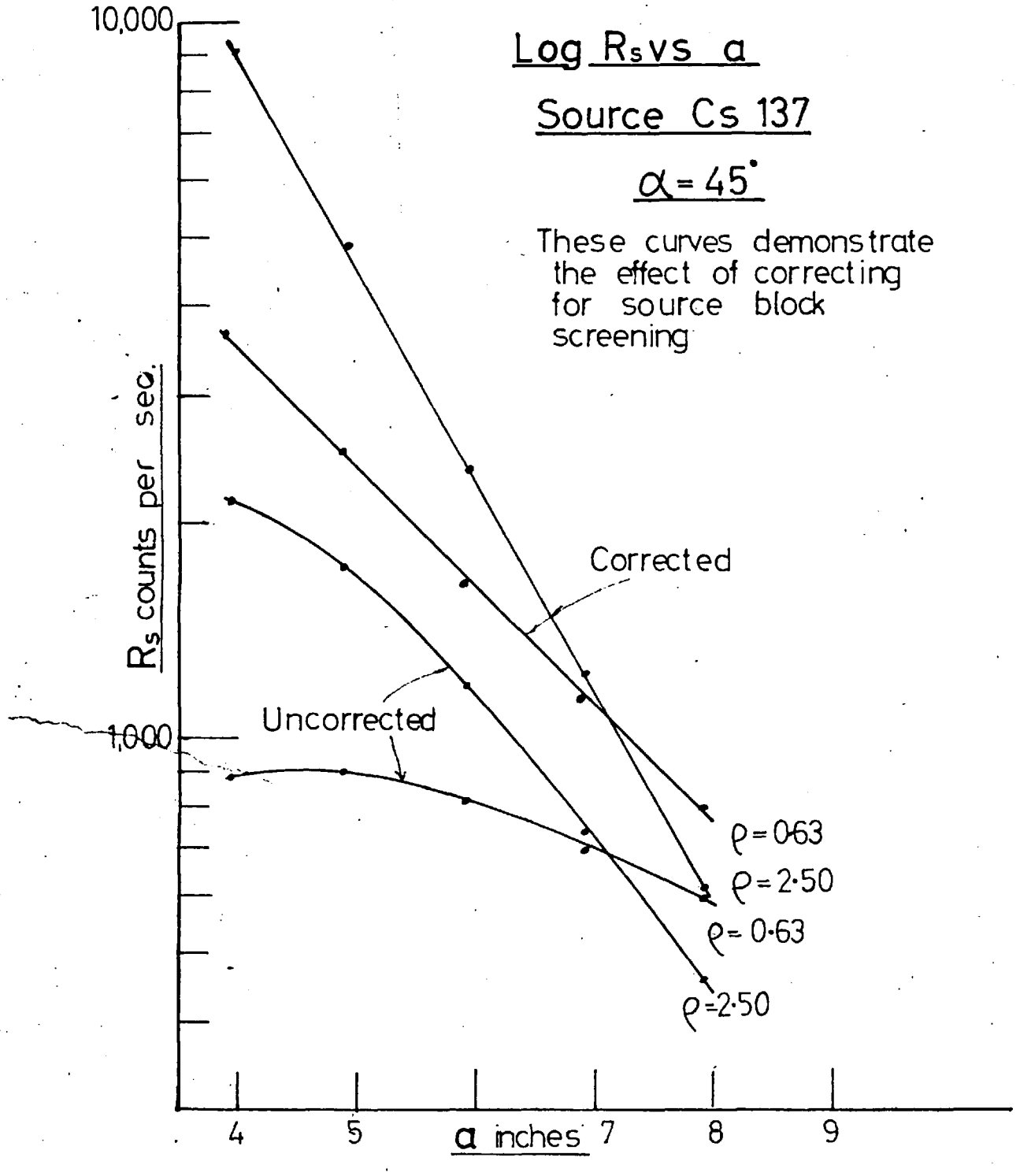

Log Rs vs a
Source Cs 137
α = 45°
These curves demonstrate the effect of correcting for source block screening
10,000
1,000
Rs counts per sec.
Corrected
Uncorrected
ρ = 0·63
ρ = 2·50
ρ = 0·63
ρ = 2·50
4
5
a inches
7
8
9

Fig 13 a

Log R_s vs ρx

Source Co 60

$\alpha = 90°$

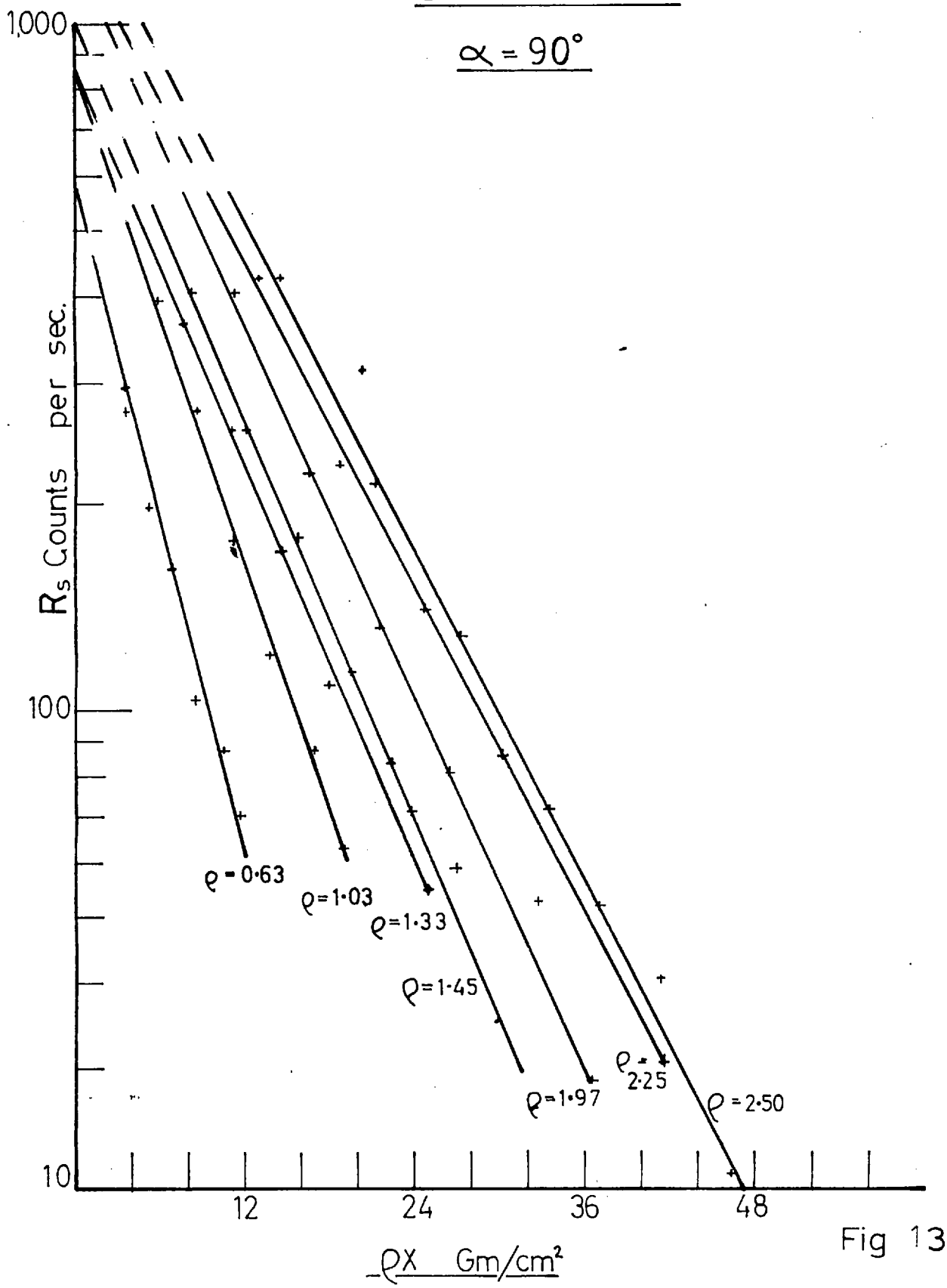


Fig 13 b

Log R_s vs ρx

Source Co 60

$\alpha = 75°$

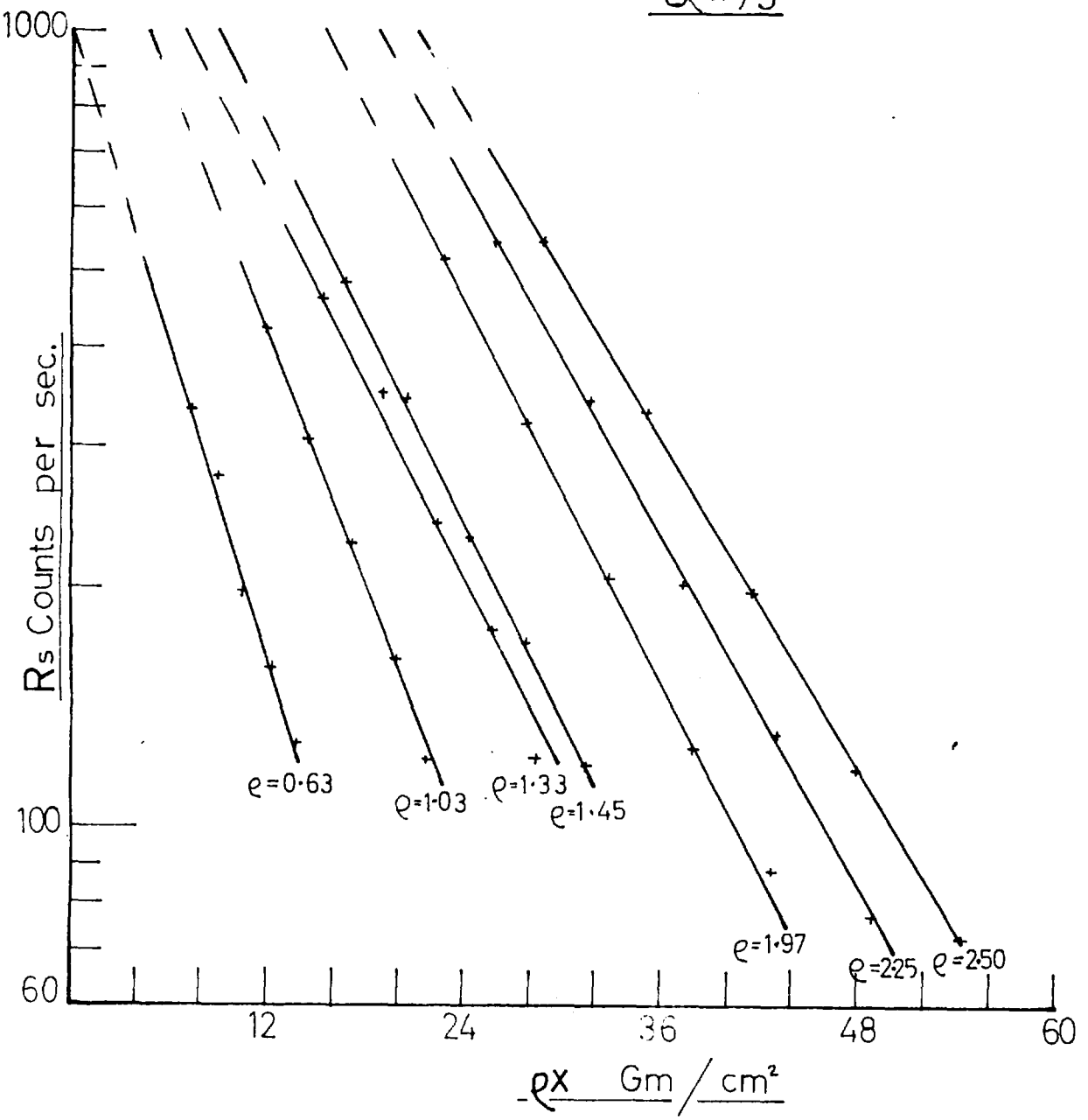


Fig 13 c

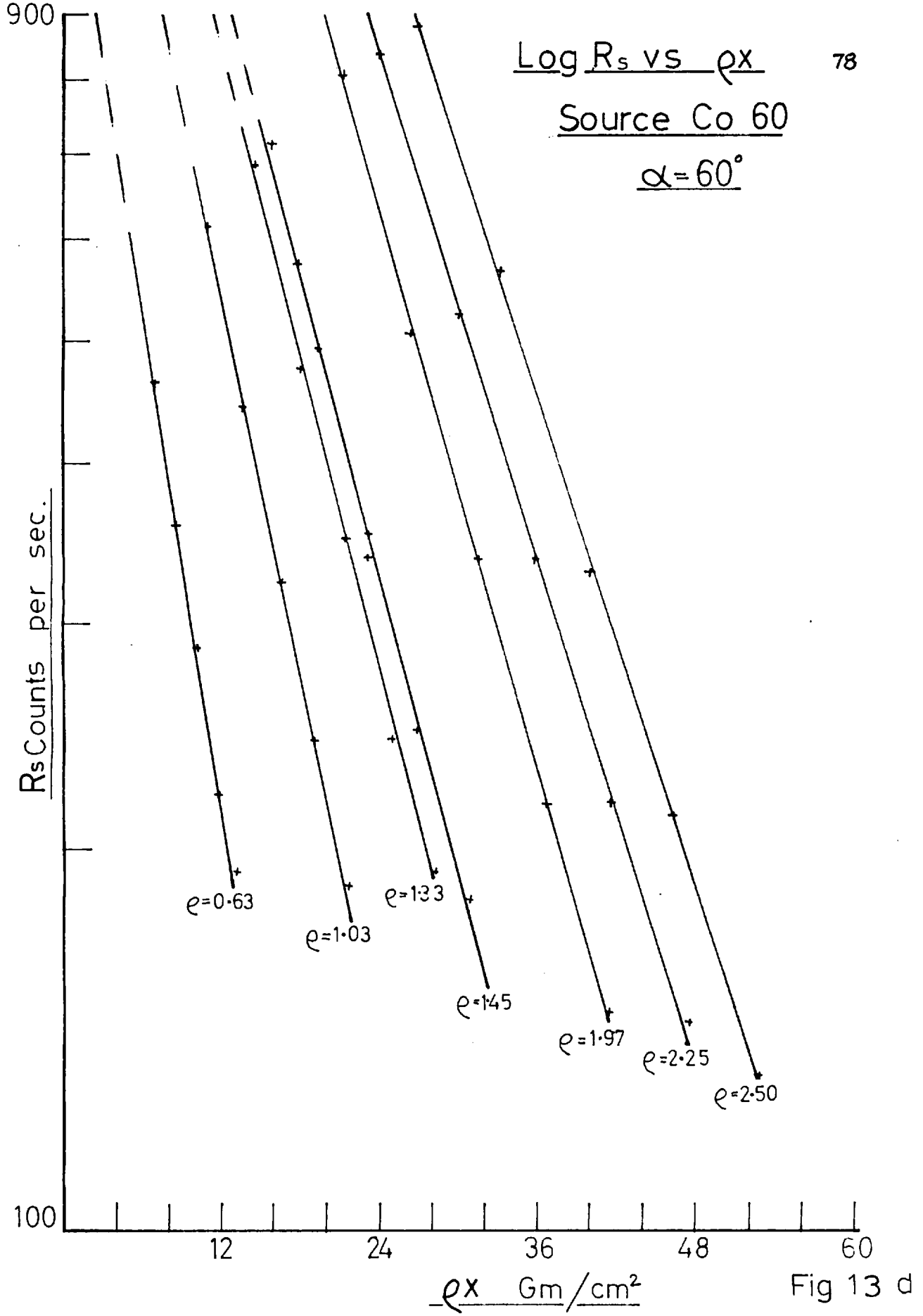

Log Rs vs ρx
Source Co 60
α = 60°
900
100
Rs Counts per sec.
ρ = 0·63
ρ = 1·03
ρ = 1·33
ρ = 1·45
ρ = 1·97
ρ = 2·25
ρ = 2·50
12
24
36
48
60
ρx Gm/cm²

Fig 13 d

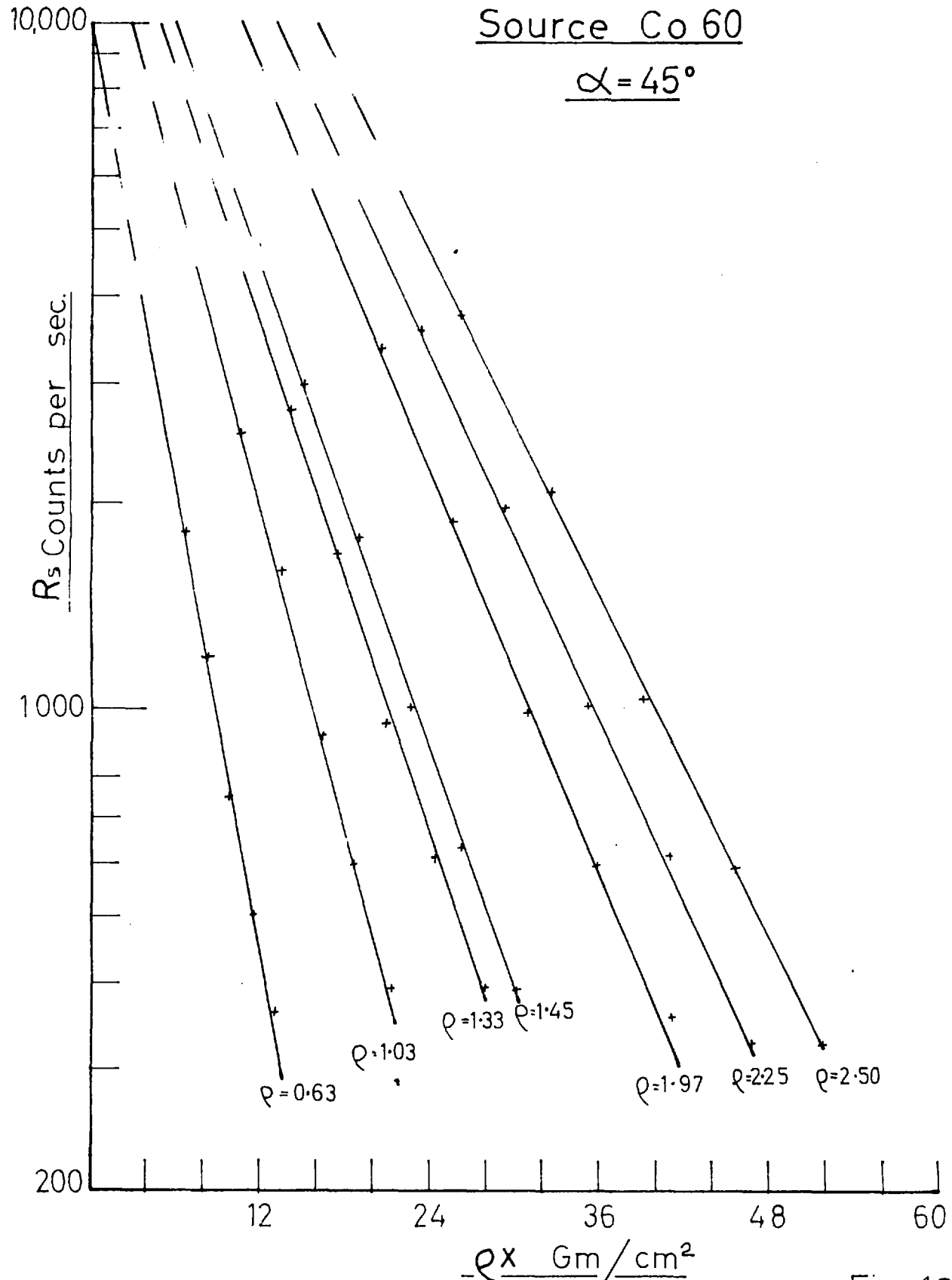

Log Rs vs ρx
Source Co 60
α = 45°
10,000
1000
200
Rs Counts per sec.
ρ = 0·63
ρ = 1·03
ρ = 1·33
ρ = 1·45
ρ = 1·97
ρ = 2·25
ρ = 2·50
12
24
36
48
60
ρx Gm/cm²

Fig 13 e

Log R_s vs ρx

Source Cs 137

$\alpha = 90°$

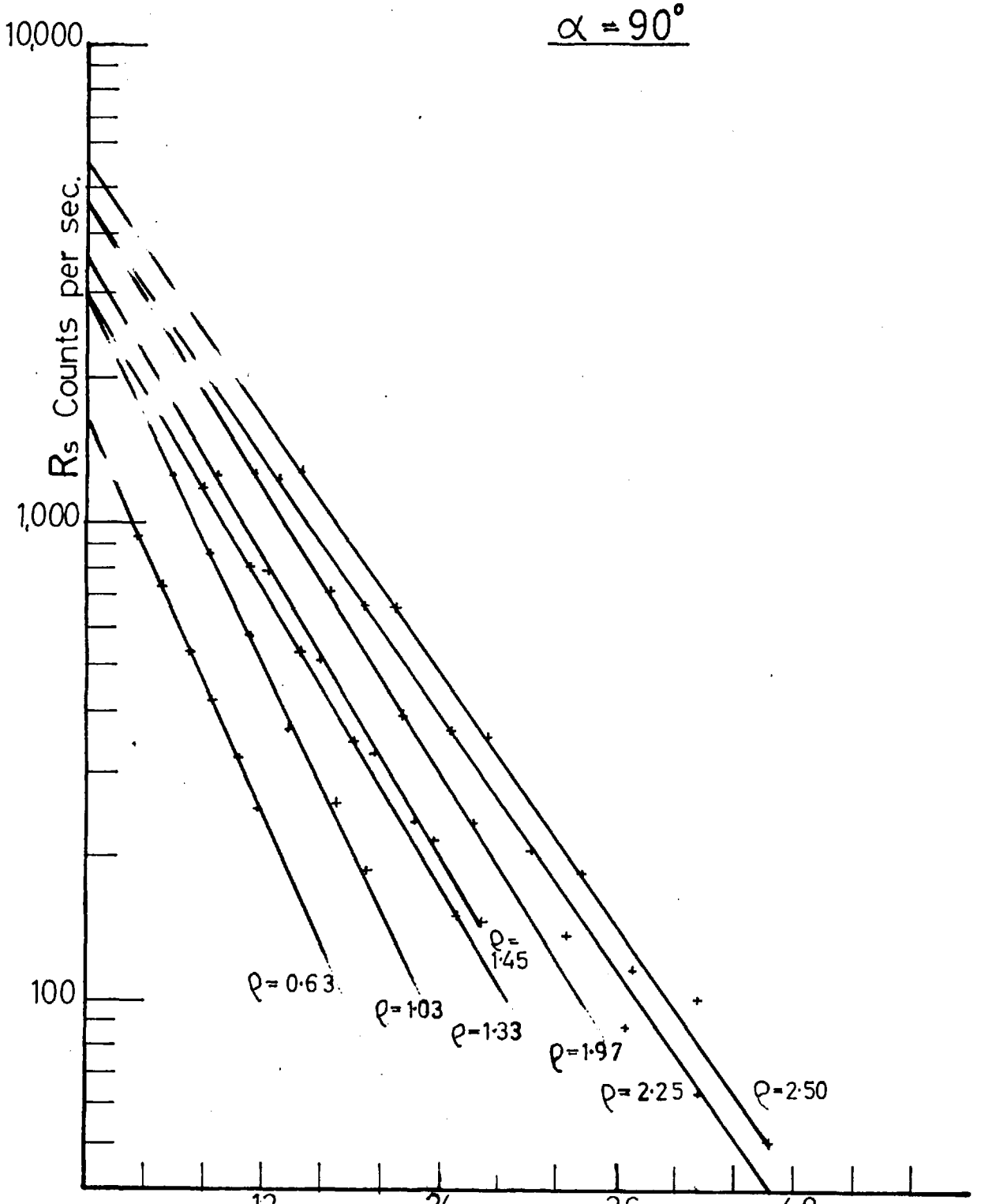


Fig 13 f

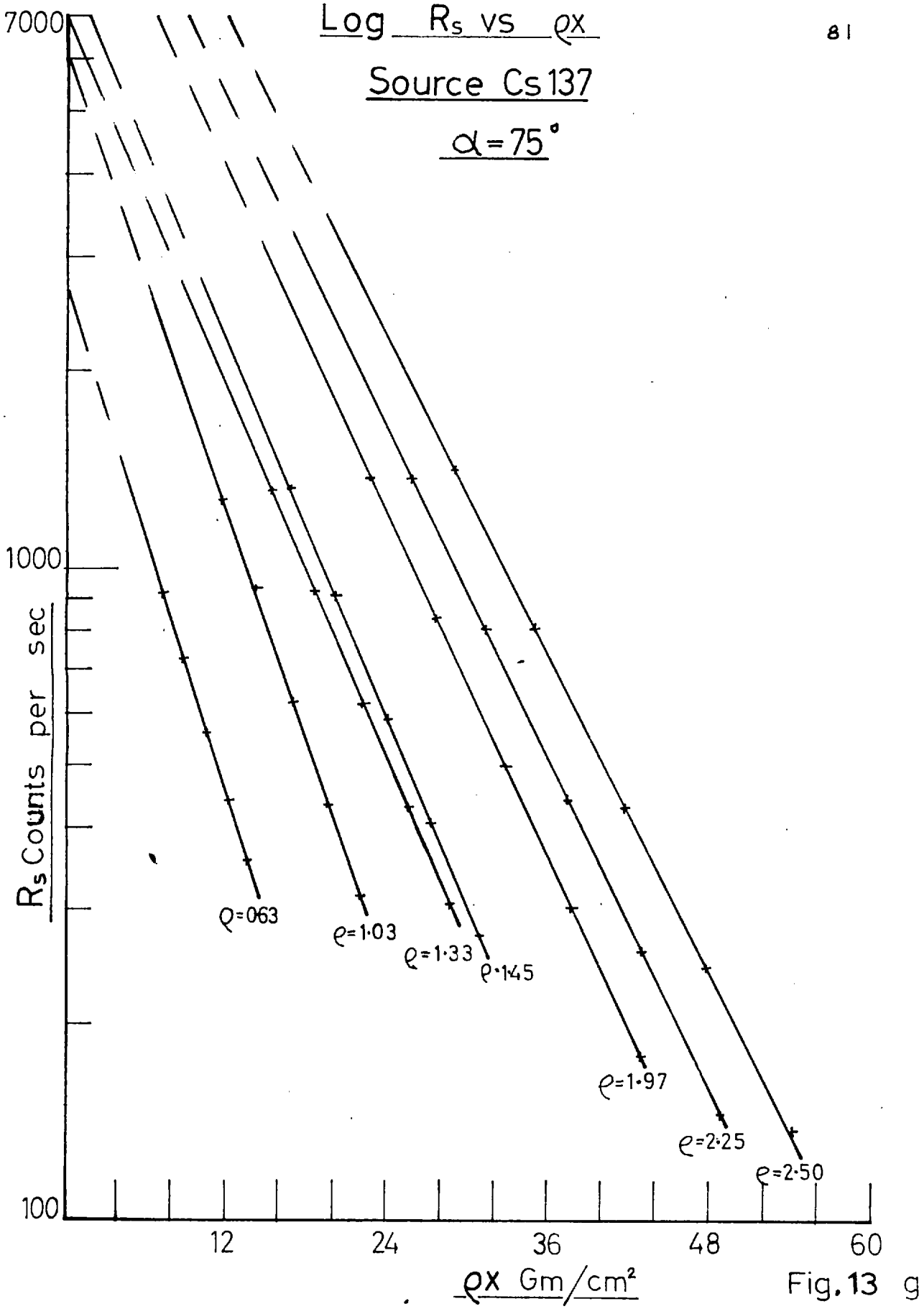

Log Rs vs ρx
Source Cs 137
α = 75°
7000
1000
100
Rs Counts per sec
ρ=063
ρ=1·03
ρ=1·33
ρ·145
ρ=1·97
ρ=2·25
ρ=2·50
12
24
36
48
60
ρx Gm/cm²

Fig. 13 g

Log Rs vs ρx

Source Cs 137

α = 60°

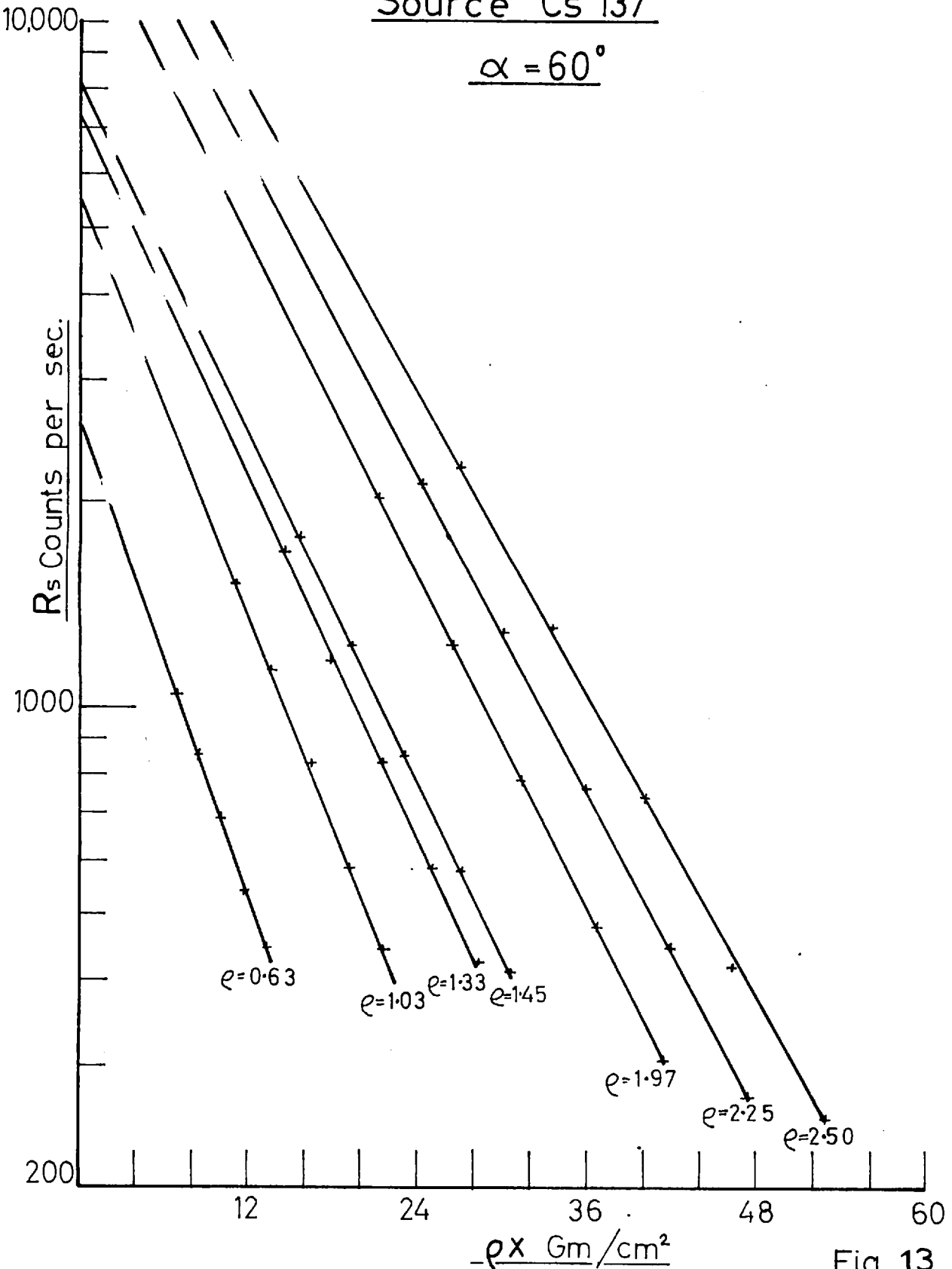


Fig 13 h

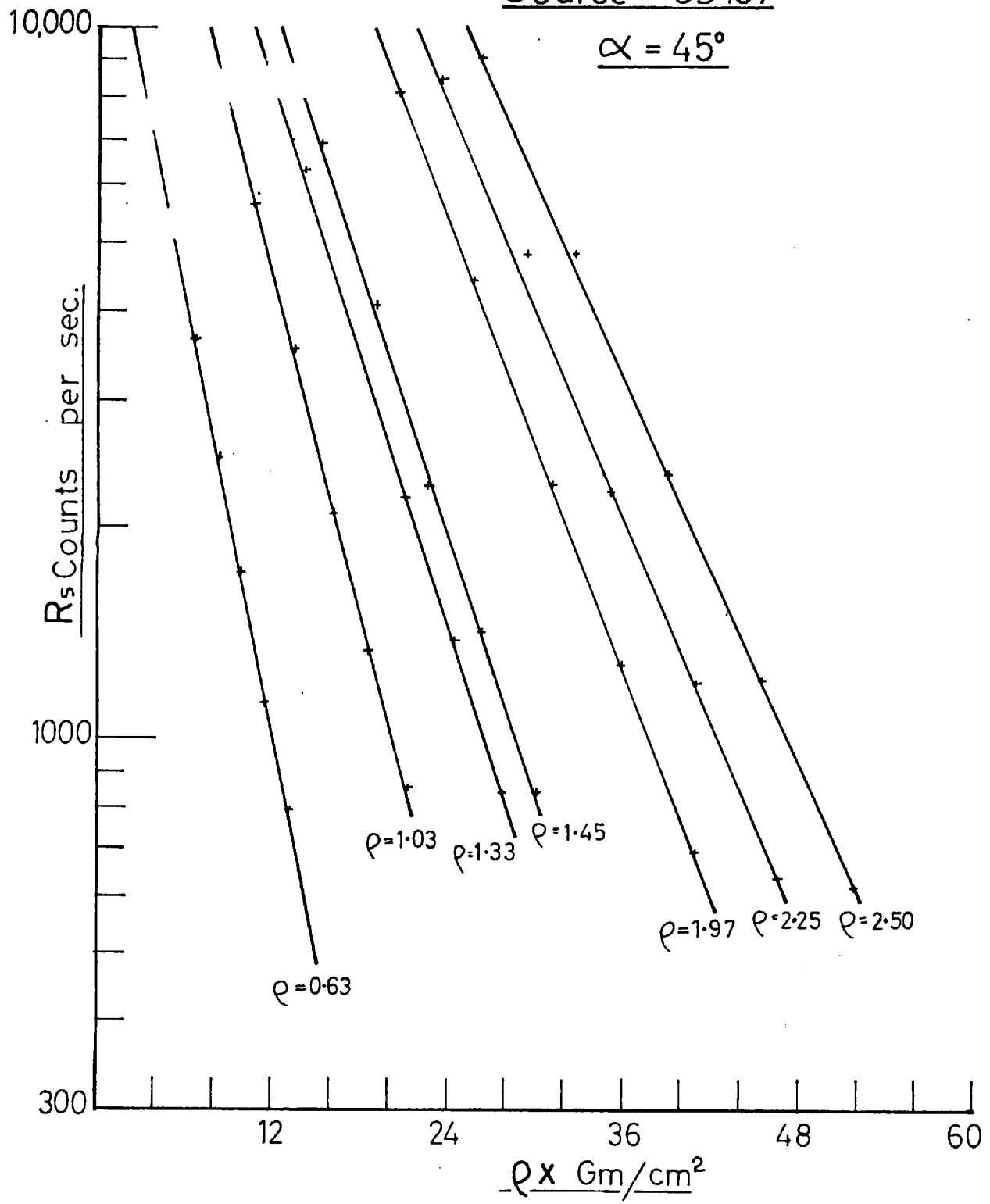

Log Rs vs ρx
Source Cs 137
α = 45°
10,000
1000
300
Rs Counts per sec.
ρ=0·63
ρ=1·03
ρ=1·33
ρ=1·45
ρ=1·97
ρ=2·25
ρ=2·50
12
24
36
48
60
ρx Gm/cm²

Fig. 13 i

For the values with $\theta = 45^{\circ}$, when R_s was adjusted, the residuals were higher than for the unadjusted cases, showing that the adjustment by area proportion did not entirely correct for the count loss.

In calculating A from the curve of R_s vs ρx, the value of A depended upon the datum for x. Distance x was taken from the centre of the detection ellipse to the centre of the source ellipse, which was approximately the horizontal distance at the concrete surface between the centres of source and detected beams, and was not equal to 'a' in Figure 7a.

The sources of error in R_s were:-

a) Nuclear statistical variations.

b) Errors in positioning the shields relative to each other.

c) Non-uniformity of density within each block of concrete.

Weights were assigned to the points (R_s, ρ) assuming that the errors due to b) and c) were negligible.

Chapter 2.5.7 Conclusions

From this series of experiments the following general conclusions were drawn.

a) When the detector "sees" concrete near the source the peak of the calibration curve will be at a density

sufficiently high so that R varies monotonically with ρ over all practical densities.

b) With such a geometry the detected spectrum includes a large proportion of count due to photons of energy greater than 0.1 MeV.

c) Source energy has a very small effect on both the calibration curve and effectively infinite size.

d) The effectively infinite dimensions are little influenced by the distance source to detector.

e) The effectively infinite depth varies inversely as density.

CHAPTER 2.6 DEFINITION OF SENSITIVITY S

As has been shown in Chapter 2.4 the count rate at the detector

$$R_T = R_p + R_s + R_b \qquad 2.6.(1)$$

A further mode of scattering may occur in which photons scatter from the concrete to the lead and then back to the concrete before being detected. Because a photon emitted from Cs 137 will drop to 0.4 MeV with one collision of only 60°, when lead is effectively opaque to gamma energy, any photon which undergoes such scattering can be assumed to be absorbed by the lead.

To determine the density from R_T, R_b must be known. In practice, it should be small. R_p will be a constant

for a given piece of apparatus, detector and source.

Let the expression relating density and count rate at a given source intensity I be $R_s = IF(\rho)$

Now $R_p = K_p I$ K_p a constant.

Therefore $R = IF(\rho) + K_p I$ 2.6.(1)

If the count rate R be derived from N counts in T seconds and if $R_b << R$ the standard deviation of R

$$\sigma_R = \frac{R}{\sqrt{N}}$$

If the second derivative of R with respect to ρ is small, $R(\rho)$ may be assumed to be linear over a small interval and

$$\frac{\sigma_R}{\sigma_\rho} = \frac{dR(\rho)}{d\rho} \equiv R'$$

$$\sigma_\rho = \frac{\sigma_R}{R'} = \frac{R}{R'\sqrt{N}} = \frac{F(\rho) + K_\rho}{F'(\rho)\sqrt{N}} \qquad 2.6.(2)$$

This is an extension of the accuracy defined by Kuranz (1959) and provides a useful basis for the assessment of a particular piece of apparatus.

The factor $\frac{1}{\sqrt{N}}$ depends only upon the number of counts taken.

The lower limit of R/R' is reached as $K_p \longrightarrow 0$, and

is $\frac{F(\rho)}{F'(\rho)}$. For this reason Cs 137 was used. (See Chapter 2.7.1).

The factor R/R' is defined as the sensitivity of the apparatus, designated S. It depends upon the source energy, detector response, and apparatus geometry.

S is a function of ρ. In order to be used as a general measure for gamma backscatter apparatus, the value must be quoted at some standard density. If S is negative at this density, count rate is a falling function of density; if positive it is a rising function. The accuracy obtainable may be completely specified by quoting both S and R at the standard density.

If I_o is the source intensity at the time of calibration of the instrument, and the instrument used at a time t thereafter, then $I_o = Ie^{\lambda t}$ and $e^{\lambda t}$ is a correction factor to apply to R, in order to make the calibration curve valid.

If the ratio of count on specimen to count on standard, r, were used as the ordinate of the calibration curve, then the sensitivity S just defined will be given by

$$S = \frac{r}{r'} \qquad \text{where} \quad r' \equiv \frac{dr}{d\rho}$$

as is shown in the following.

If N_1 counts are taken in T seconds to give a count rate R_1 on a calibration specimen of density ρ_1, and N_2 counts taken in T seconds to give a count rate R_2 on a specimen of unknown density ρ_2 then

$$r = \frac{R_2}{R_1} = \frac{R_\rho + R_{s2}}{R_\rho + R_{s1}} \qquad 2.6.(3)$$

where the suffices have the meanings defined before.

By the law of combination of errors

$$\left(\frac{\sigma_r}{r}\right)^2 = \frac{1}{N_1} + \frac{1}{N_2} \qquad 2.6.(4)$$

From the calibration curve of r against ρ, for small errors

$$\sigma_\rho = \frac{\sigma_r}{r'}$$

$$= \frac{r}{r'}\sqrt{\frac{1}{N_1} + \frac{1}{N_2}} \qquad 2.6.(5)$$

Differentiating 2.6.(3) $r = \frac{R_2'}{R_1}$ because R_1 is a constant, so that $\frac{r}{r'} = \frac{R_2}{R_2'}$ which corresponds to the definition of S given above.

Thus using the ratio gives no change in sensitivity, but the calibration count N_1 must be made several times larger than N_2 to give error comparable with that of the count rate against density curve.

CHAPTER 2.7 DESIGN AND CALIBRATION OF THE BACKSCATTER DENSITY GAUGES

Chapter 2.7.1 Design of the Mark 1 and Mark 2 Gauges.

Using information from Chapter 2.5 a density gauge designated the Mark 1 apparatus was designed.

The shield

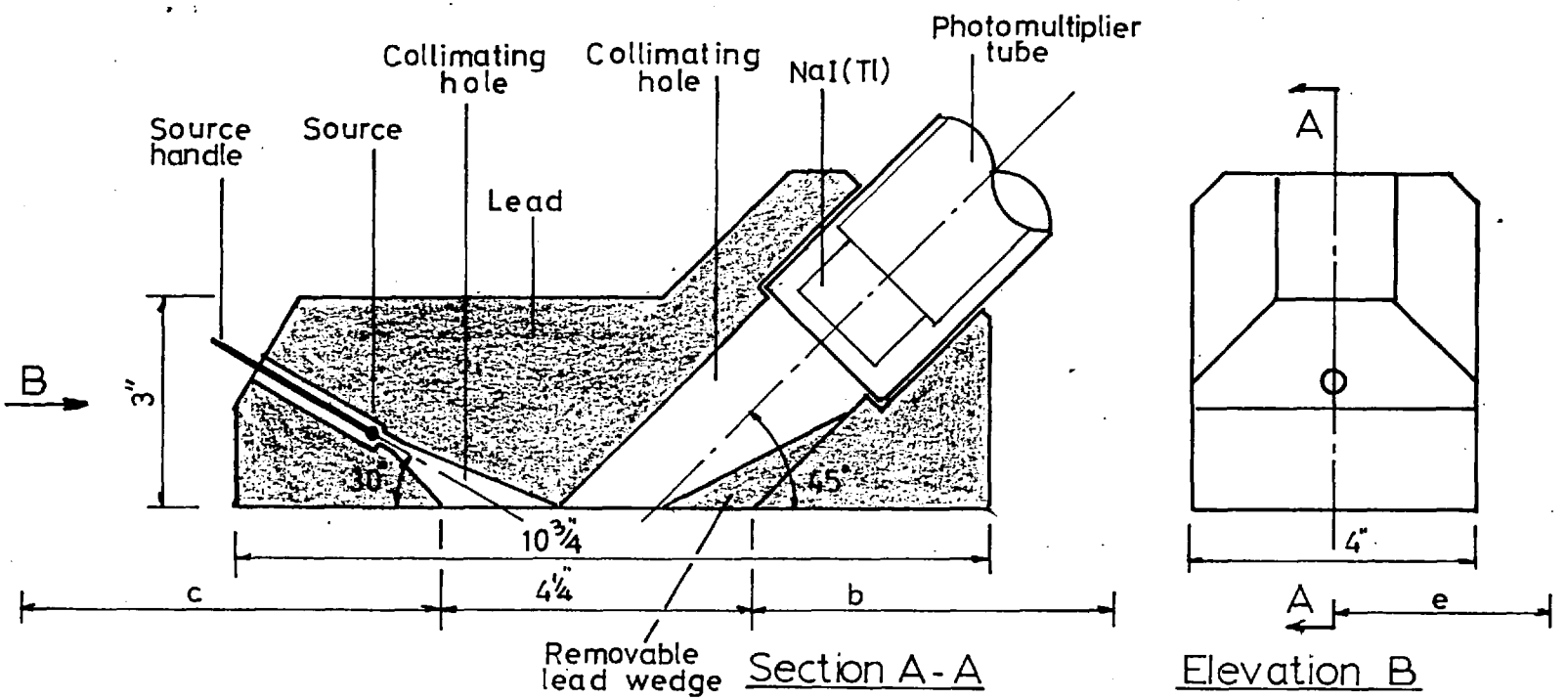
In order that the detected beam should include a high proportion of once and twice scattered photons, so that the calibration curve will be a rising function of density due to photons of energy greater than 0.1 MeV over all practical ranges, the detector must "see" the concrete where the photons enter it. On the other hand, the detector itself must be separated from the source by several inches of lead so as to reduce the component R_p of the count rate due to photons penetrating the lead from source to detector. The geometry of the lead shield, shown in Figure 14, satisfied these requirements.

The source

As has been shown in Chapters 2.5.4 and 2.5.5 the calibration curve and effectively infinite depth are but little affected by the value of source energy. However, because the lower energy photons from Cs 137 are more rapidly absorbed in lead then the higher energy photons from Co 60, R_p is lower if Cs 137 is used. Also, the half life of Cs 137 is longer than that of Co 60. For these reasons, Cs 137 was preferred.

The detector

When establishing the calibration curve, the detector discrimination bias was set at a level corresponding to 0.1 MeV, which as shown in Chapter 2.2. eliminated the



THE MARK 1 SHIELD

NOTES

With the wedge inserted this was the Mark 2 shield.

Dimensions b, c & e, which are the "effectively infinite size" notation, are to the edge of the concrete block.

Scale $\frac{3}{8}$-Fullsize

Fig. 14

effects of photoelectric absorption and therefore minimized the effect of changes in chemical composition of the concrete.

Chapter 2.7.2 Experimental Calibration

The effectively infinite size depended, among other factors, upon the shape of the lead shield. These sizes were determined for this apparatus at various densities by means of the curves of Figures 15a to 15g. The results which are accurate only to within one or two inches are shown in Table 8.

TABLE 8

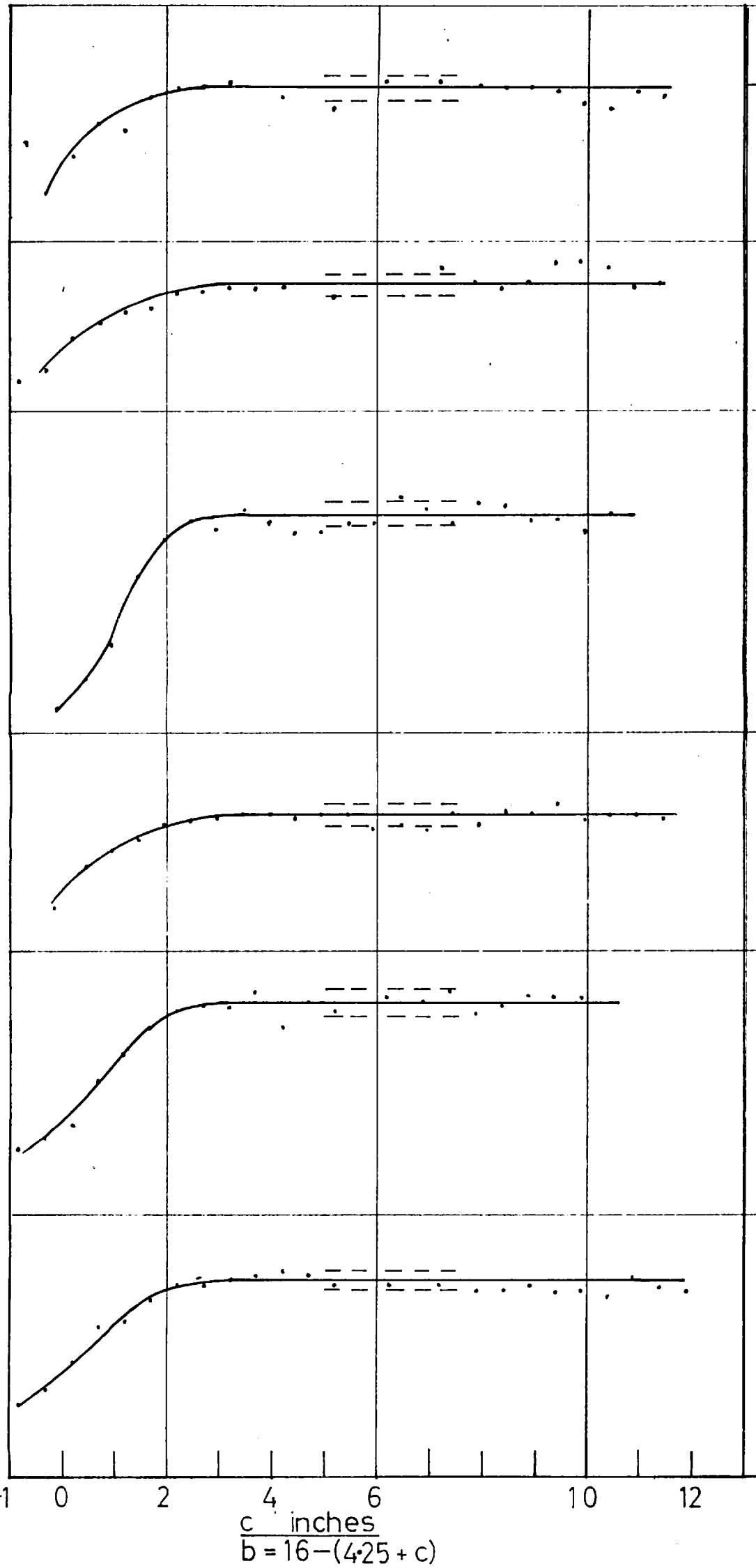
Effectively Infinite Dimensions for the Mark 1 Apparatus

ρ lb/cu ft	Disc. level 0.05 MeV						Disc. level 0.1 MeV					
	c_∞	b_∞	e_∞	d_∞	ρd_∞	$d_{\frac{1}{2}}$	c_∞	b_∞	e_∞	d_∞	ρd_∞	$d_{\frac{1}{2}}$
39	5"	3¾"	7"	12"	470	1.6"	4"	1¾"	7"	16"	620	1.7"
90	5¼"	5¼"	5"	6"	540	1.4"	4½"	4½"	5"	6"	540	1.3"
123	3"	<¼"	2"	-	-	-	3"	<1¾"	2"	-	-	-
140	3"	<¼"	2"	4"	560	0.8"	3"	<1¼"	2"	4"	560	0.8"
156	3"	<¼"	2½"	-	-	-	2½"	< ¼"	1½"	-	-	-

The dimensions b_∞, c_∞, d_∞ and e_∞ are shown in Figure 14. If d_∞ = 14" when ρ = 39 lb/cu ft, then ρd_∞ =546.

DETERMINATION OF c_∞ and b_∞

R vs c

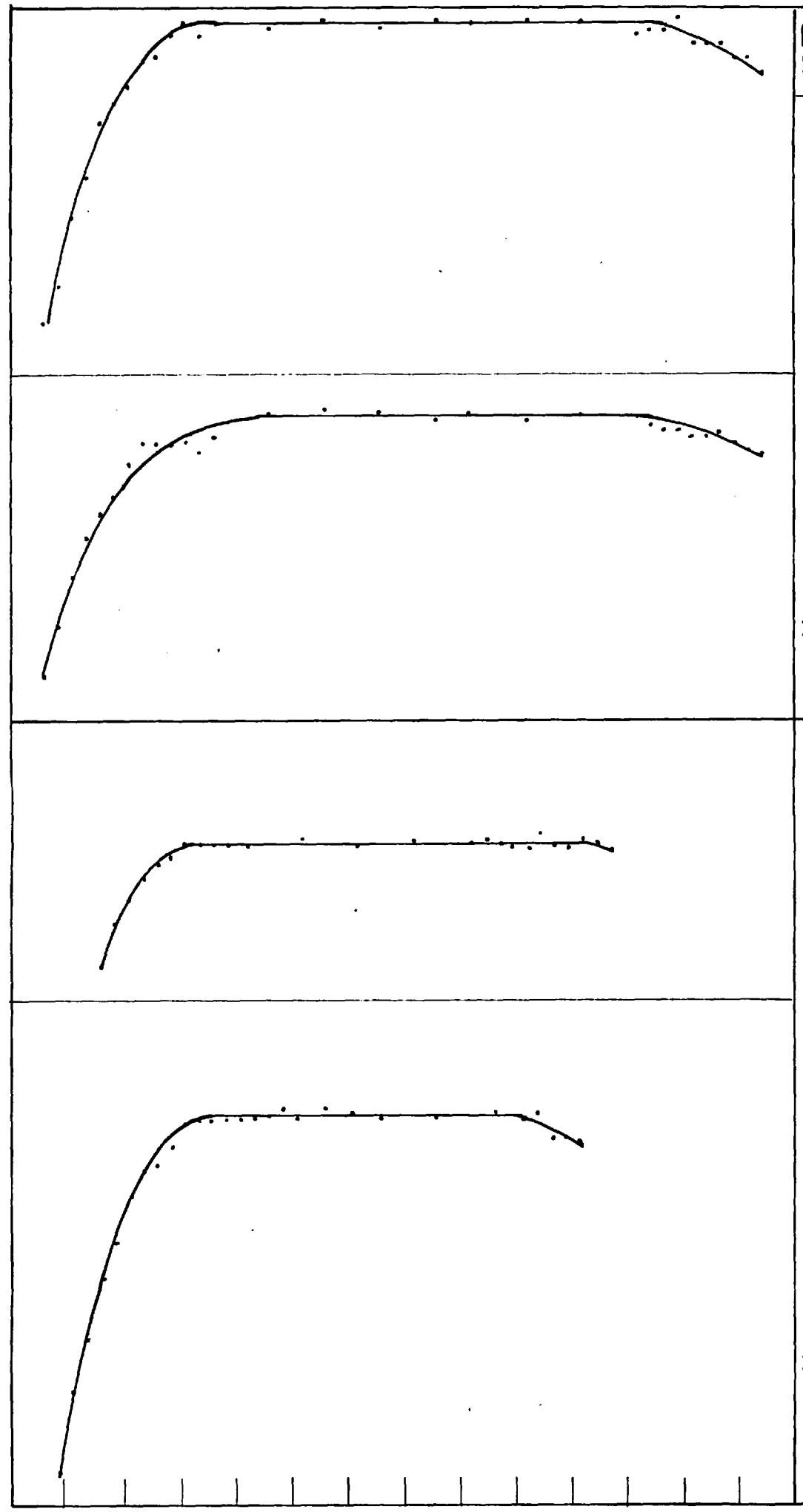


DENSITY Lb/cu. ft.	DISCRIMINATOR LEVEL MeV
156	0·1
156	0·05
140	0·1
140	0·05
123	0·1
123	0·05

Fig. 15 a

DETERMINATION OF c_∞ and b_∞

R vs c

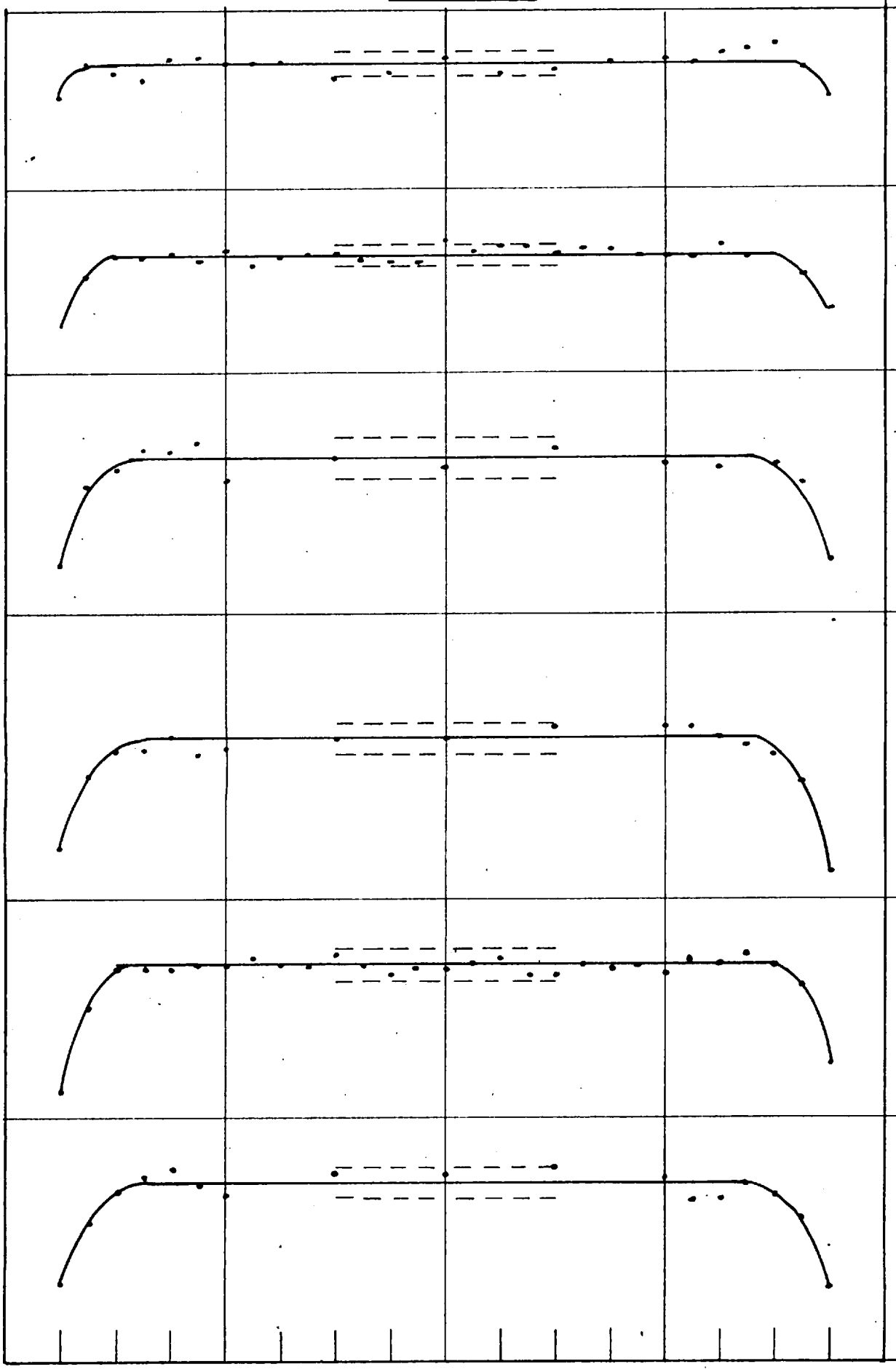


DENSITY Lb./cu.ft.	DISCRIMINATOR LEVEL MeV.
90	0·1
	0·05
b = 30-(4·25+c)	
39	0·1
	0·05
b = 24-(4·25+c)	

Fig. 15 b

DETERMINATION OF e_∞

R vs e



DENSITY LB/CU.FT.	DISCRIMINATOR LEVEL MeV
156	0·1
140	0·1
123	0·1
156	0·05
140	0·05
123	0·05

Fig 15 c

DETERMINATION OF e_∞ at DENSITY 90 LB. per CU.FT.

R vs. e

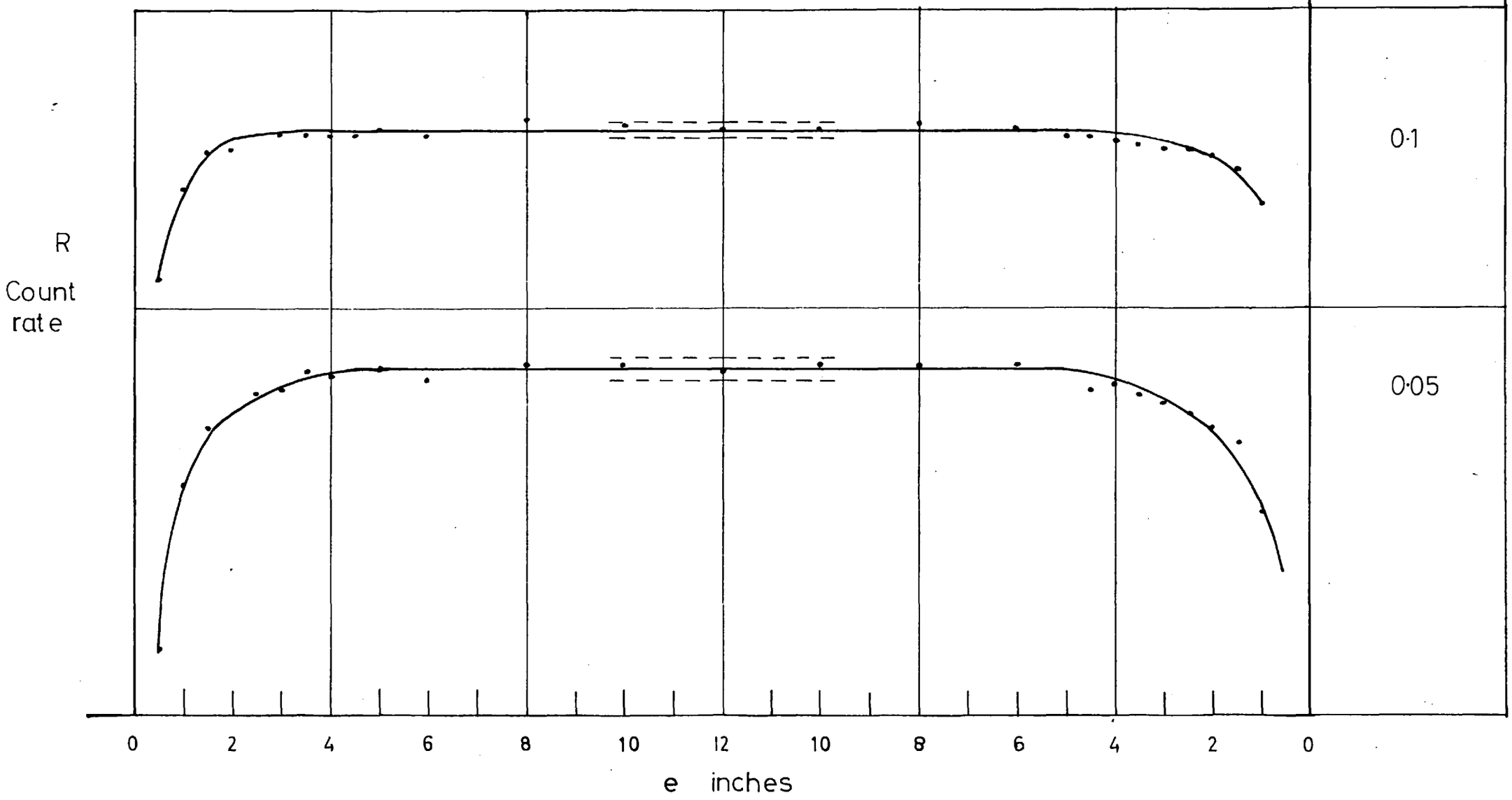


Fig. 15 d

DETERMINATION OF e_{∞} at DENSITY 39 LB. per CU. FT.

R vs e

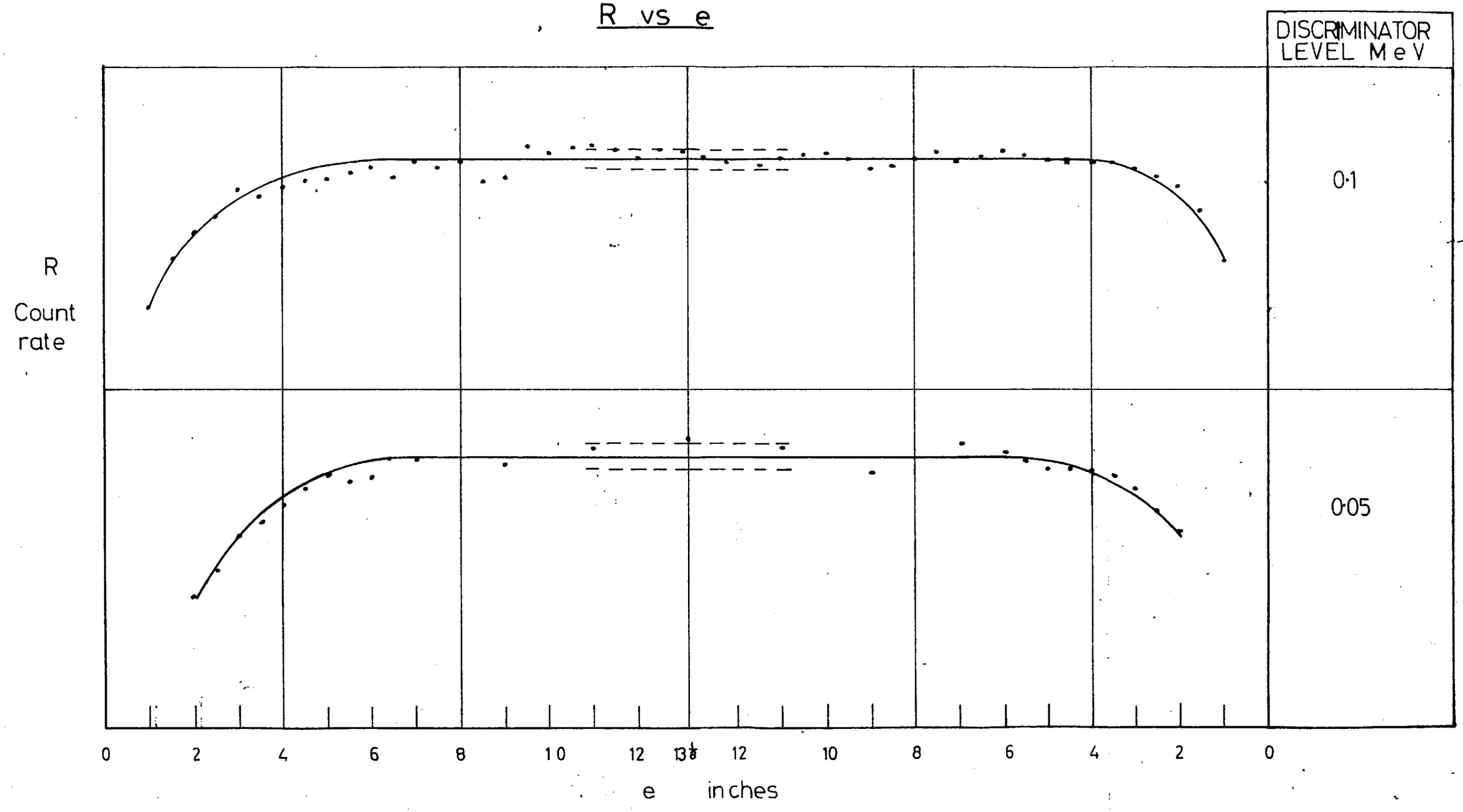


Fig 15 e

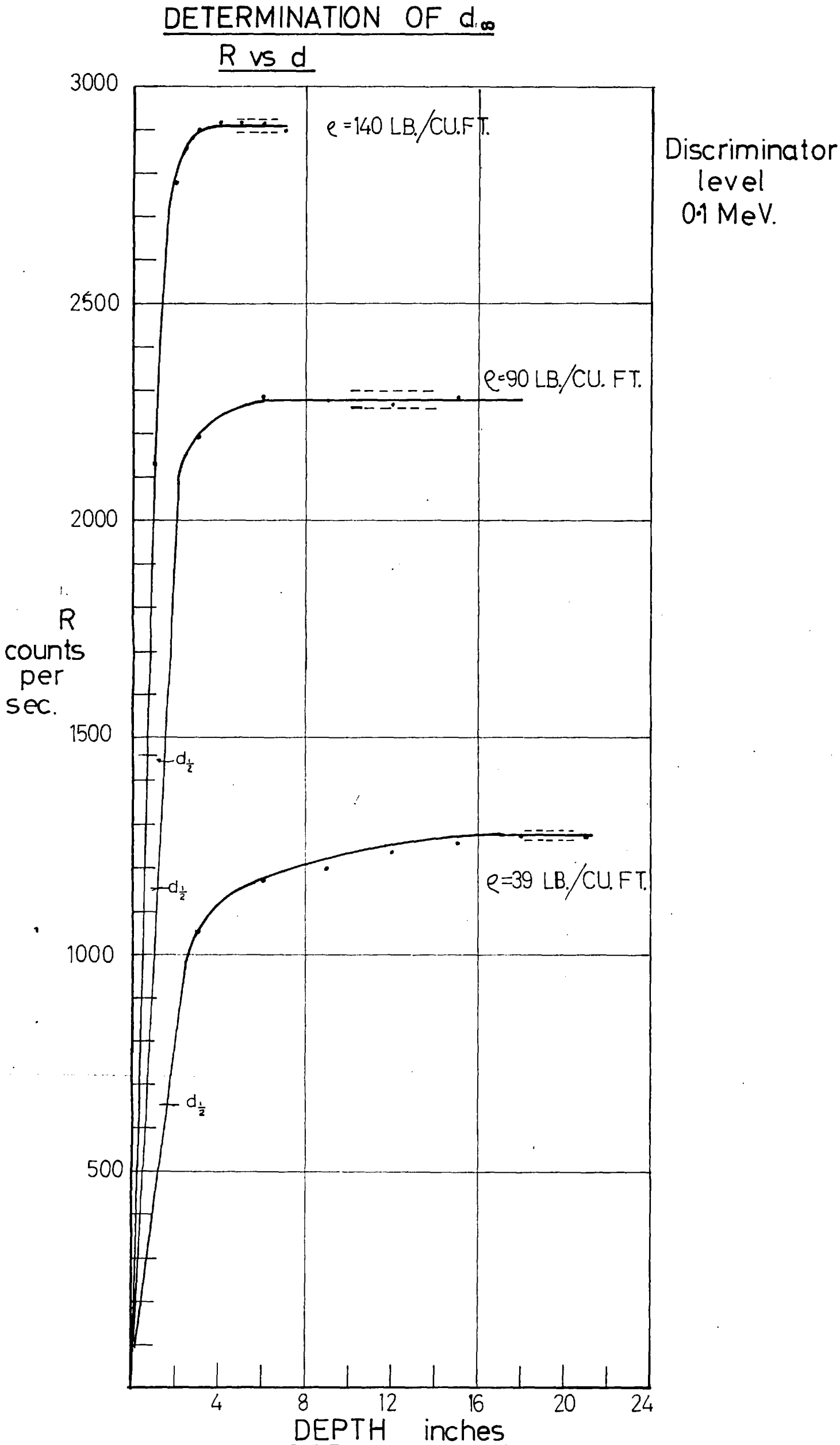

DETERMINATION OF d_∞
R vs d
3000
2500
2000
1500
1000
500
R counts per sec.
ϱ = 140 LB./CU.FT.
ϱ=90 LB./CU. FT.
ϱ=39 LB./CU. FT.
$d_{\frac{1}{2}}$
$d_{\frac{1}{2}}$
$d_{\frac{1}{2}}$
Discriminator level 0·1 MeV.
4
8
12
16
20
24
DEPTH inches

Fig. 15 f

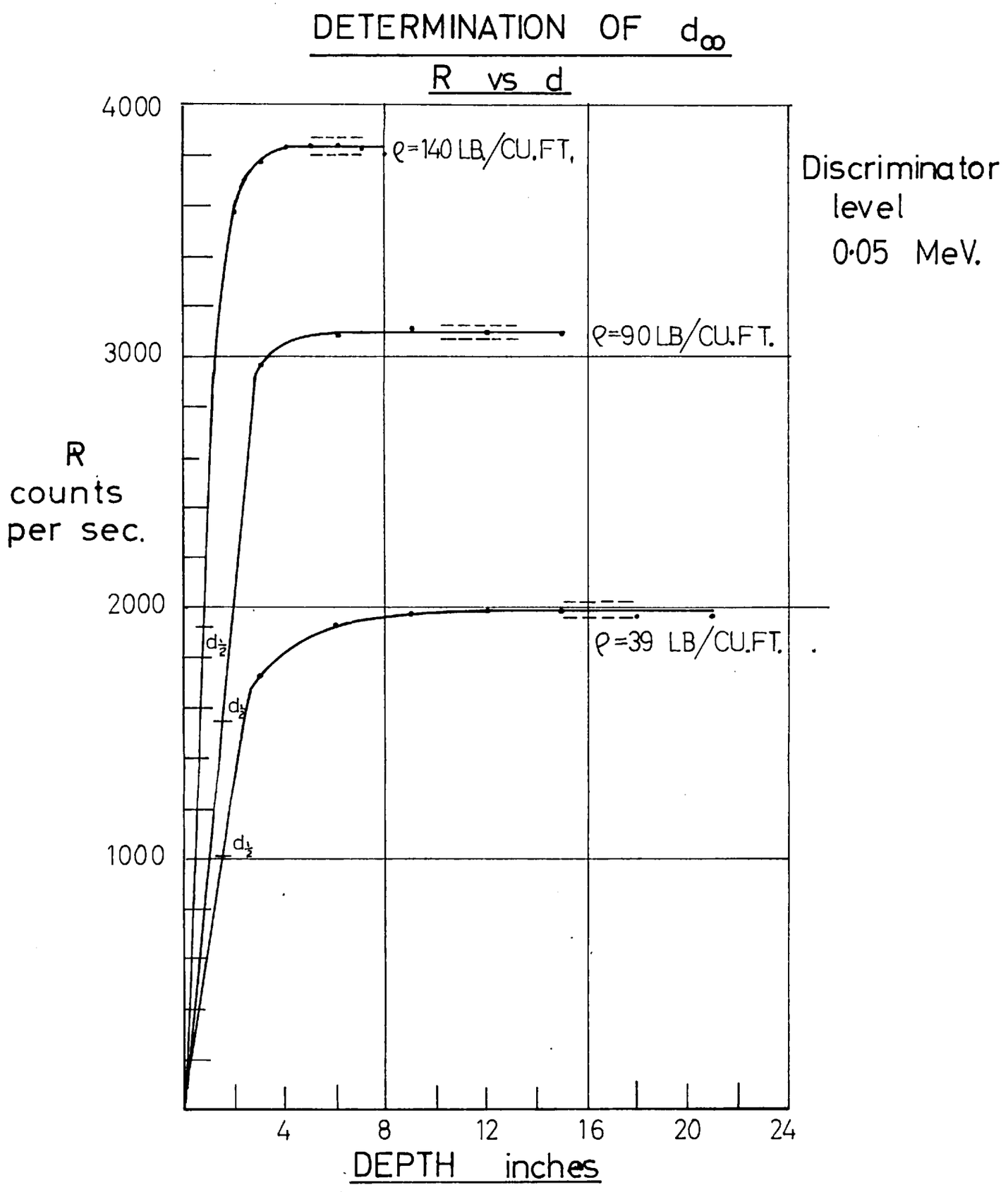

DETERMINATION OF d_∞
R vs d
4000
3000
2000
1000
R
counts
per sec.
ρ=140 LB/CU.FT.
ρ=90 LB/CU.FT.
ρ=39 LB/CU.FT.
Discriminator
level
0·05 MeV.
$d_{\frac{1}{2}}$
$d_{\frac{1}{2}}$
$d_{\frac{1}{2}}$
4
8
12
16
20
24
DEPTH inches

Fig. 15 g

It is observed from this Table that if the mean value d_∞ = 14" is adopted when ρ = 39 lb/cu ft, then $d_\infty \propto 1/\rho$. Figure 16 shows the detected pulse height spectra at various densities.

In order to establish the calibration curve over a practical range of densities, and to show the effects of changes in aggregate and mix proportions, readings were taken on 60 blocks from 30 different concrete mixes.

Five types of aggregate were used and six mixes made with each type. Two blocks from each mix were cast giving a total of sixty specimens. The blocks were each 12" x 10" x 8" which was greater than the effectively infinite size. Table 9 shows the materials and nominal proportions in the mixes. The larger lightweight blocks used in the work described in Chapter 2.5 were also used.

TABLE 9

Details of Concrete Mixes

Types of Coarse Aggregate

A Limestone
B Granite
C River gravel
D "Leca" leightweight
E No coarse aggregate

River sand and ordinary portland cement were used throughout.

The nominal mix porportions.

Code No.	Water	Cement	Sand	Aggregate
1	0.425	1	1.8	2.7
2	0.5	1	1.8	2.7
3	0.5	1	2.4	3.6
4	0.6	1	2.4	3.6
5	0.6	1	3.0	4.5
6	0.675	1	3.0	4.5

PULSE HEIGHT SPECTRUM for MARK 1 APPARATUS

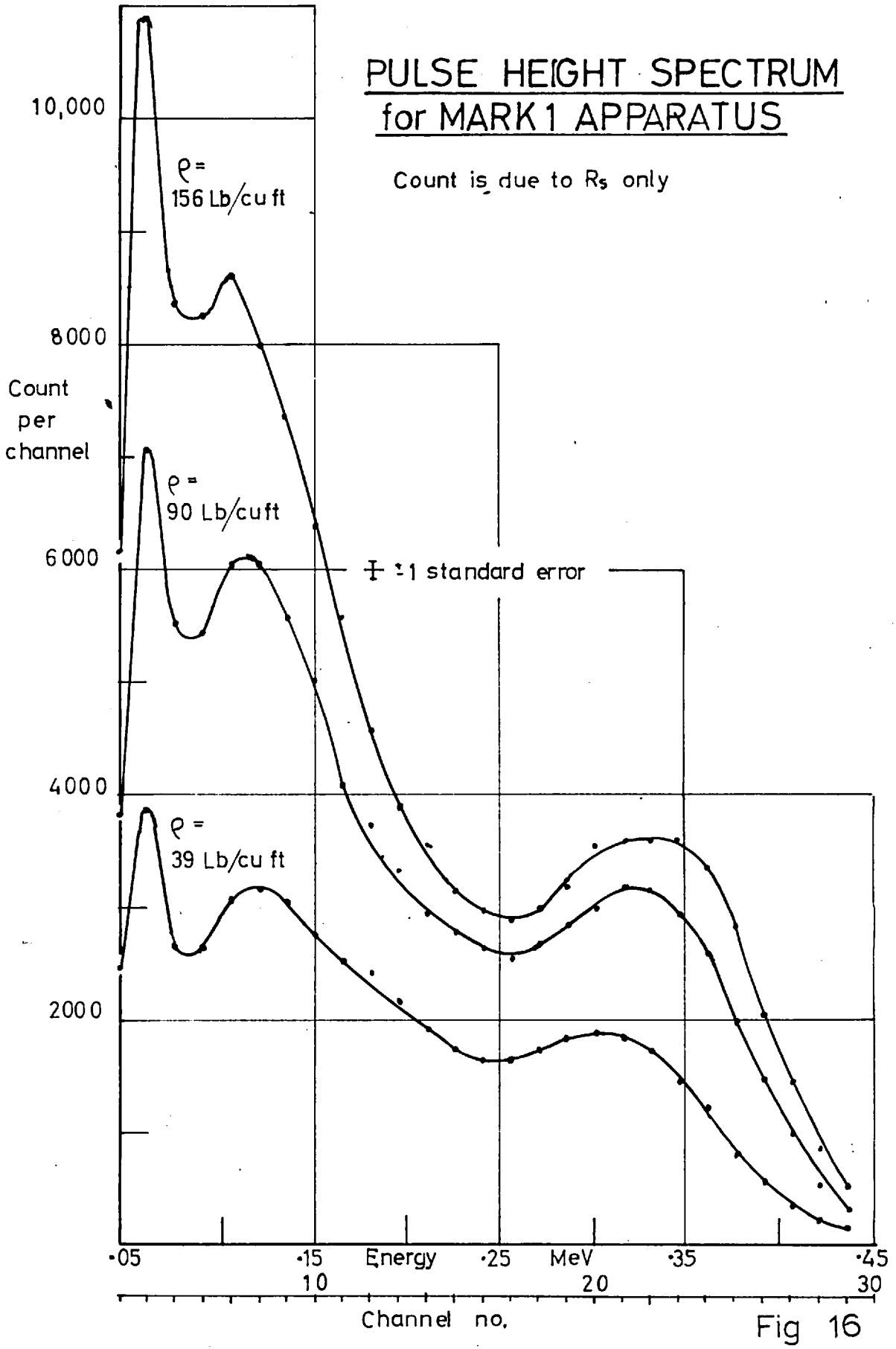


Fig 16

Figure 17 shows a curve or R vs ρ for these concretes. The readings were taken with the apparatus placed centrally on the 12" x 10" face. Each block had two such faces, one of which was roughly finished by hand floating, the other of which was smooth as cast against the mould. The readings on the smooth moulded face are shown and used for the curve. The readings on the rough face, indicated with crosses, are scattered and above the curve. This is because, due to the interface roughness, the centre of the shield, where the beams left and entered the lead, was effectively raised above the concrete surface, so that the photons had a smaller path within the concrete. This is considered further in Chapter 2.8. Figure 18 is a similar curve established some weeks later. The slight differences between this and Figure 17 were due to a changed adjustment of the electronic apparatus, which had meanwhile been used for other work.

Two methods of improving the sensitivity of the calibration curve were tried.

According to the theory of Chapter 2.4, the count rate should be due as much as possible to few times scattered photons. A beam penetrating further into the concrete will have a larger proportion of more scattered photons. A lead wedge which eliminated a portion of the more scattered photons was therefore inserted into the Mark 1 shield. The shield with the wedge was designated the Mark 2 shield.

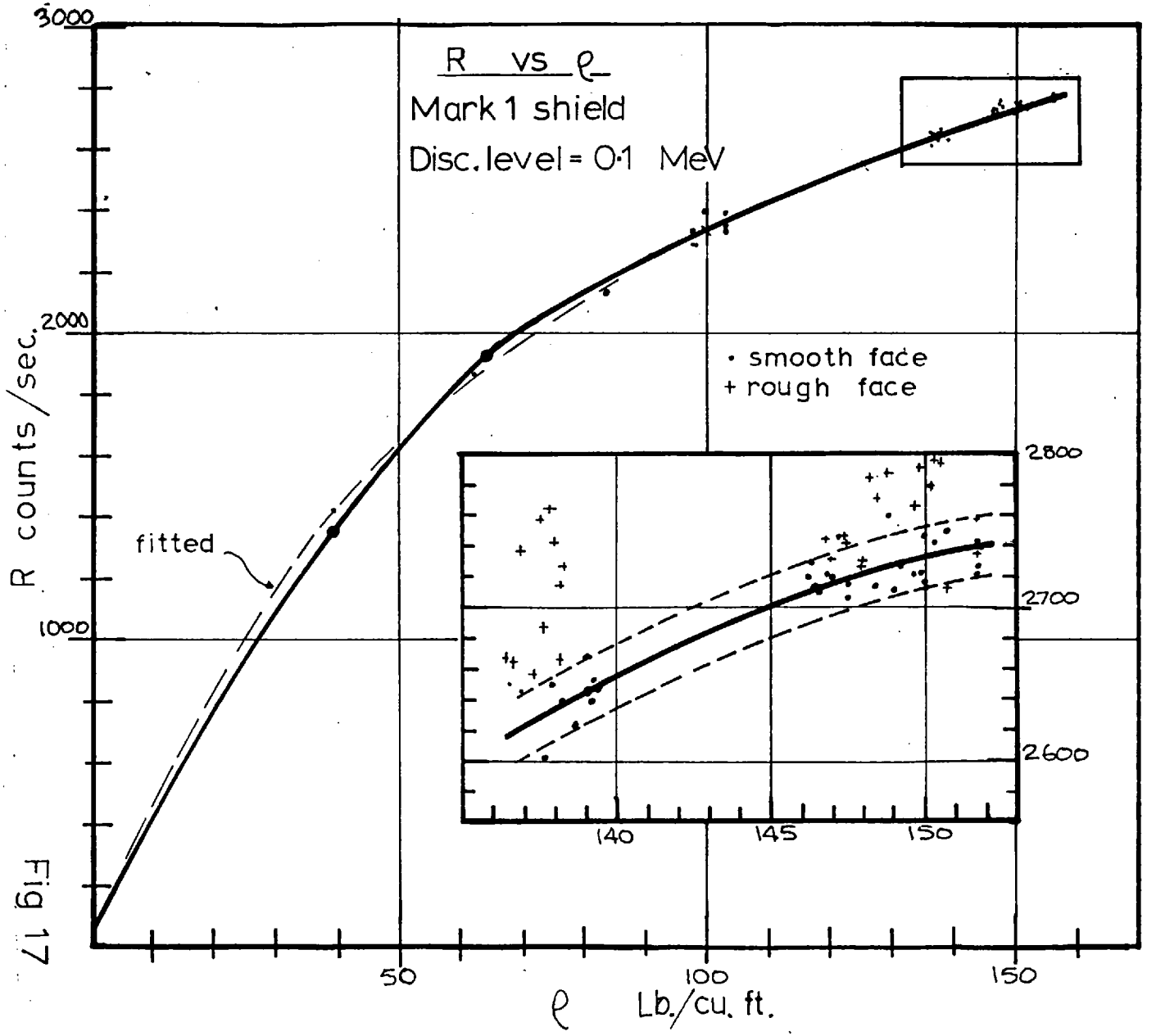

R vs ρ
Mark 1 shield
Disc. level = 0·1 MeV
· smooth face
+ rough face
fitted
R counts/sec.
3000
2000
1000
2800
2700
2600
140
145
150
50
100
150
ρ Lb./cu. ft.

Fig 17

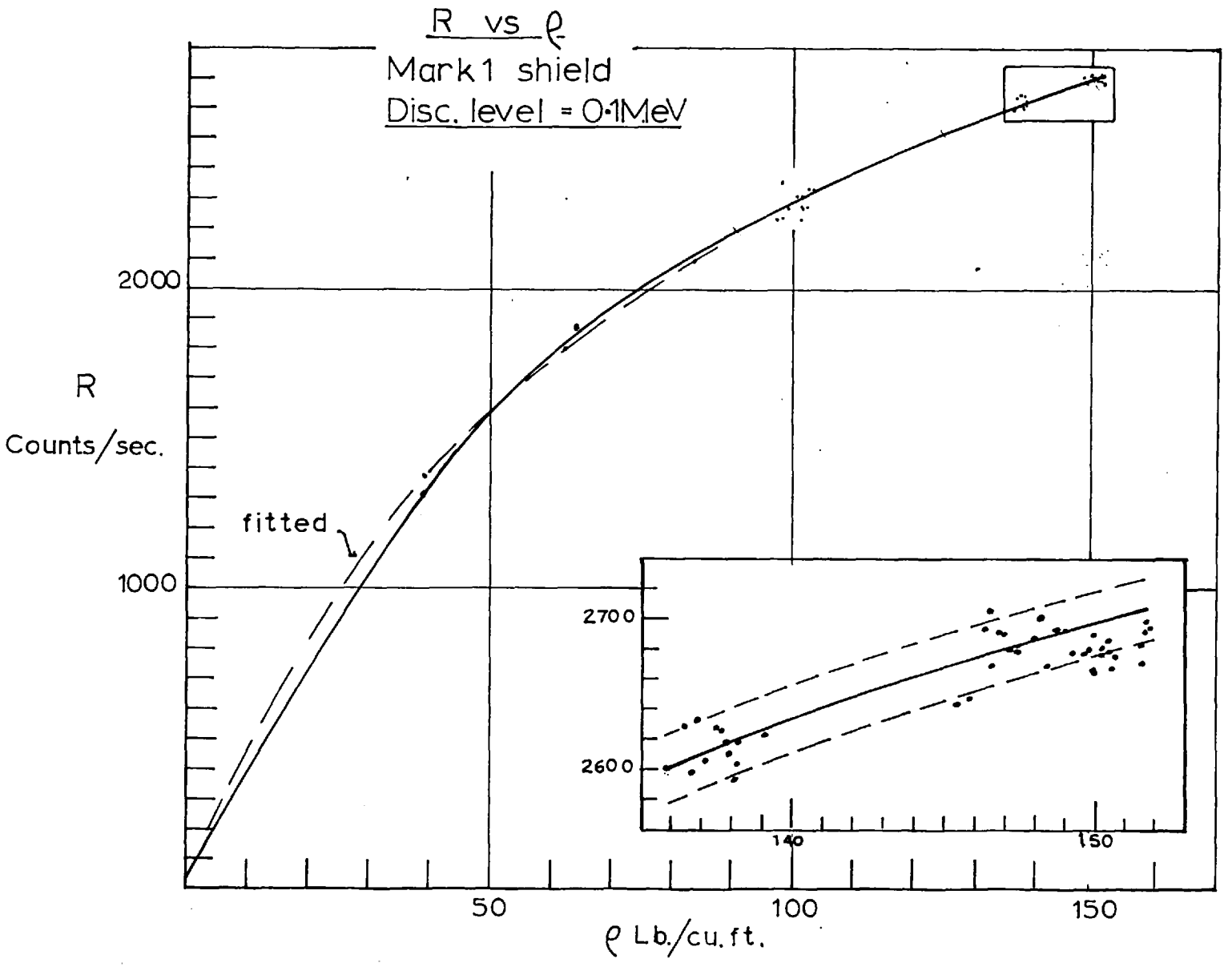

R vs ρ
Mark 1 shield
Disc. level = 0·1MeV
2000
1000
R
Counts/sec.
fitted
2700
2600
140
150
50
100
150
ρ Lb./cu.ft.

Fig. 18

The observed pulse height spectra are shown in Figure 19 and the calibration curve in Figure 20. The sensitivity, shown in Table 11, was improved. The effectively infinite dimensions were determined, showing that they were the same as for the Mark 1 shield.

Examination of Figure 16 showed that the greatest change of count rate with density occurred under the peaks due to twice and much scattered radiation. Accordingly, two further calibration curves were determined; one with the pulse height selector passing only those pulses between 0.05 and 0.1 MeV (the much scattered peak) and one for the channel 0.1 to 0.15 MeV (the twice scattered peak). These curves are shown in Figure 21.

Chapter 2.7.3 The Design and Calibration of the Mark 3 Gauge

The Mark 3 apparatus was designed with following aims:

a) To reduce the weight of lead by having less shielding and by increasing the angle of scatter so that the detector moved nearer to the source.

b) To place the shield on legs in an attempt to reduce the effect of surface roughness.

The shield is shown in Figure 22. The source, detector and concrete calibration blocks were those used with the Mark 1 shield.

PULSE HEIGHT SPECTRUM for MARK 2 APPARATUS

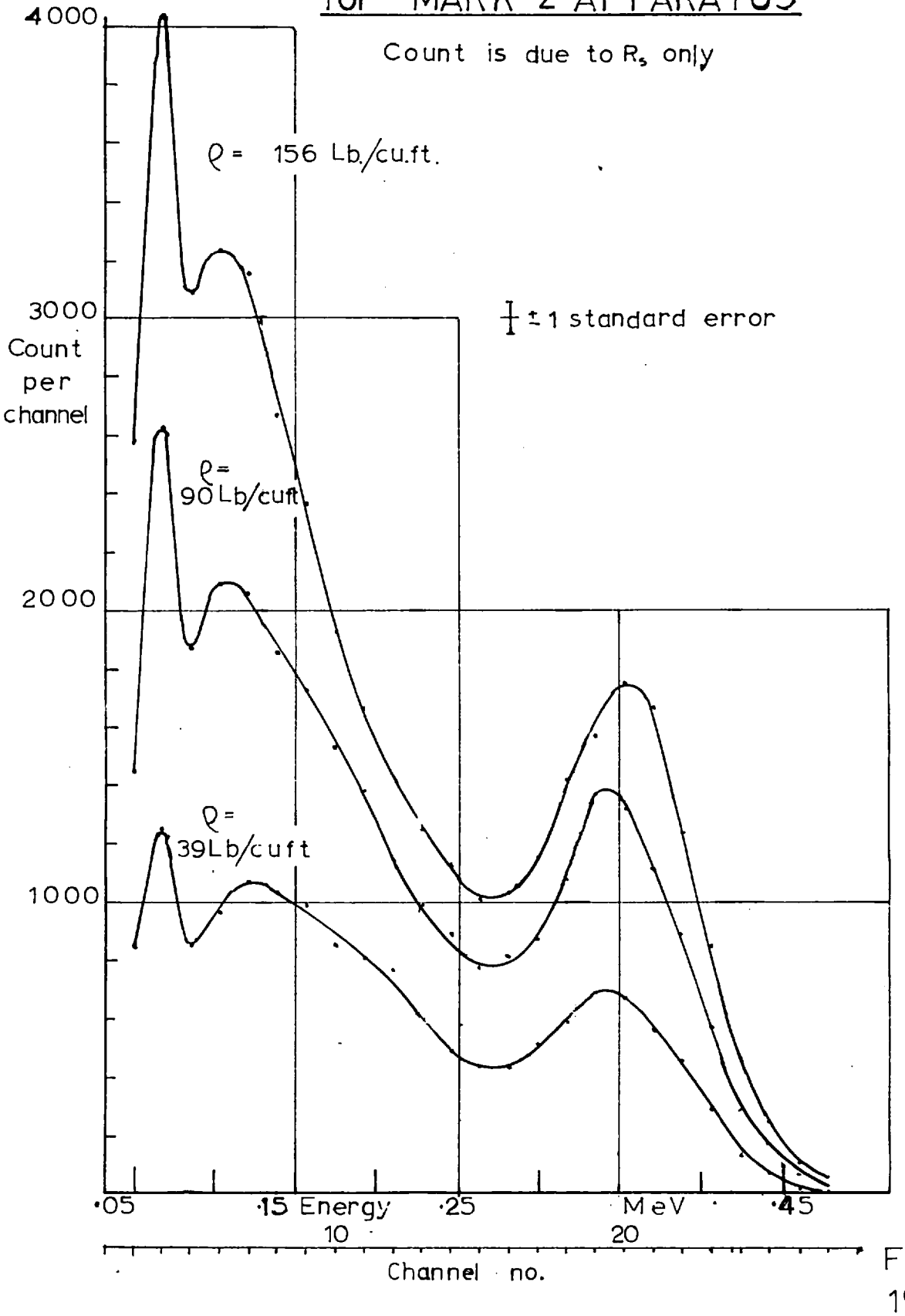


Fig. 19

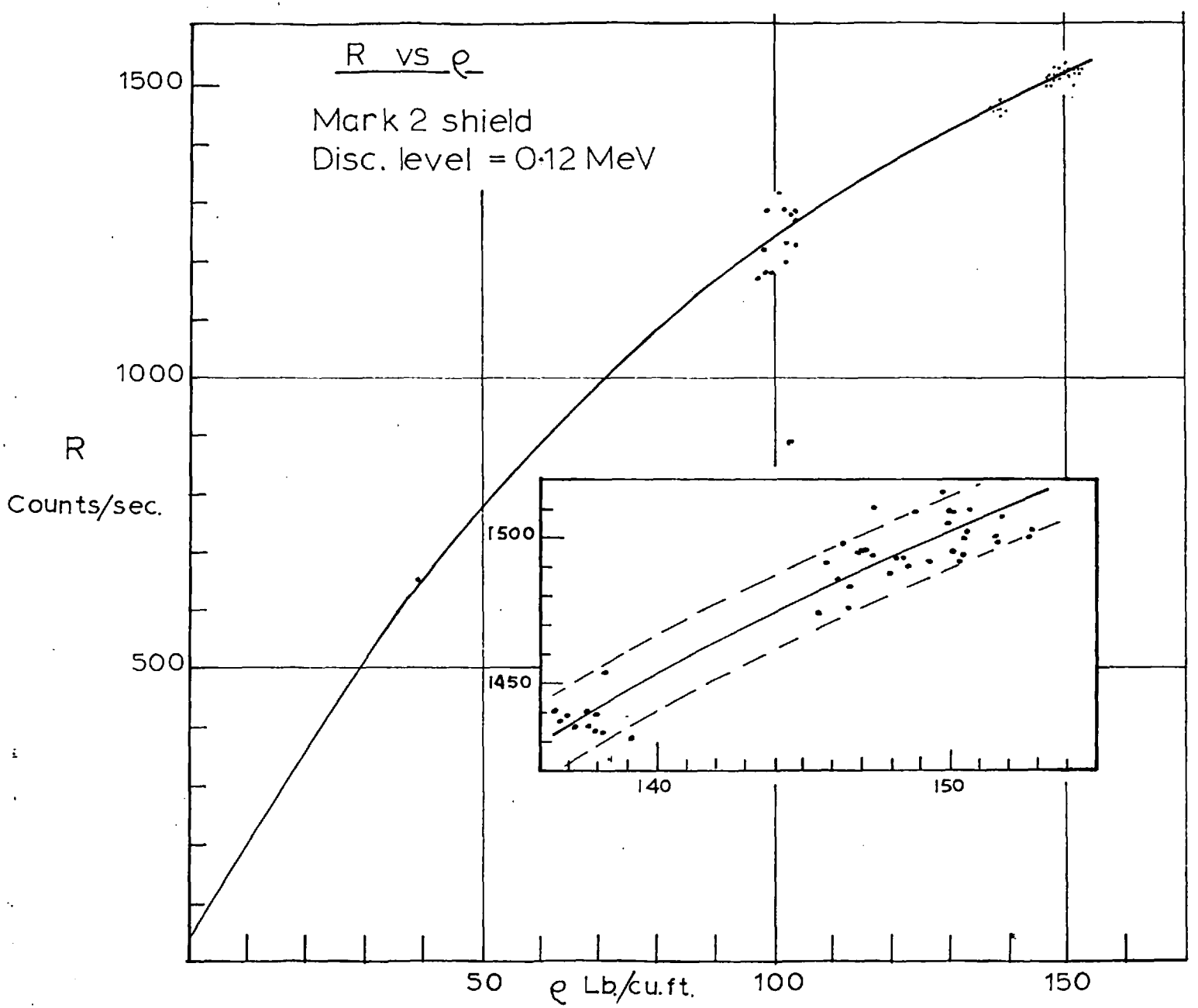

R vs ρ
Mark 2 shield
Disc. level = 0·12 MeV
1500
1000
500
R
Counts/sec.
50
ρ Lb./cu.ft.
100
150
1500
1450
140
150

Fig. 20

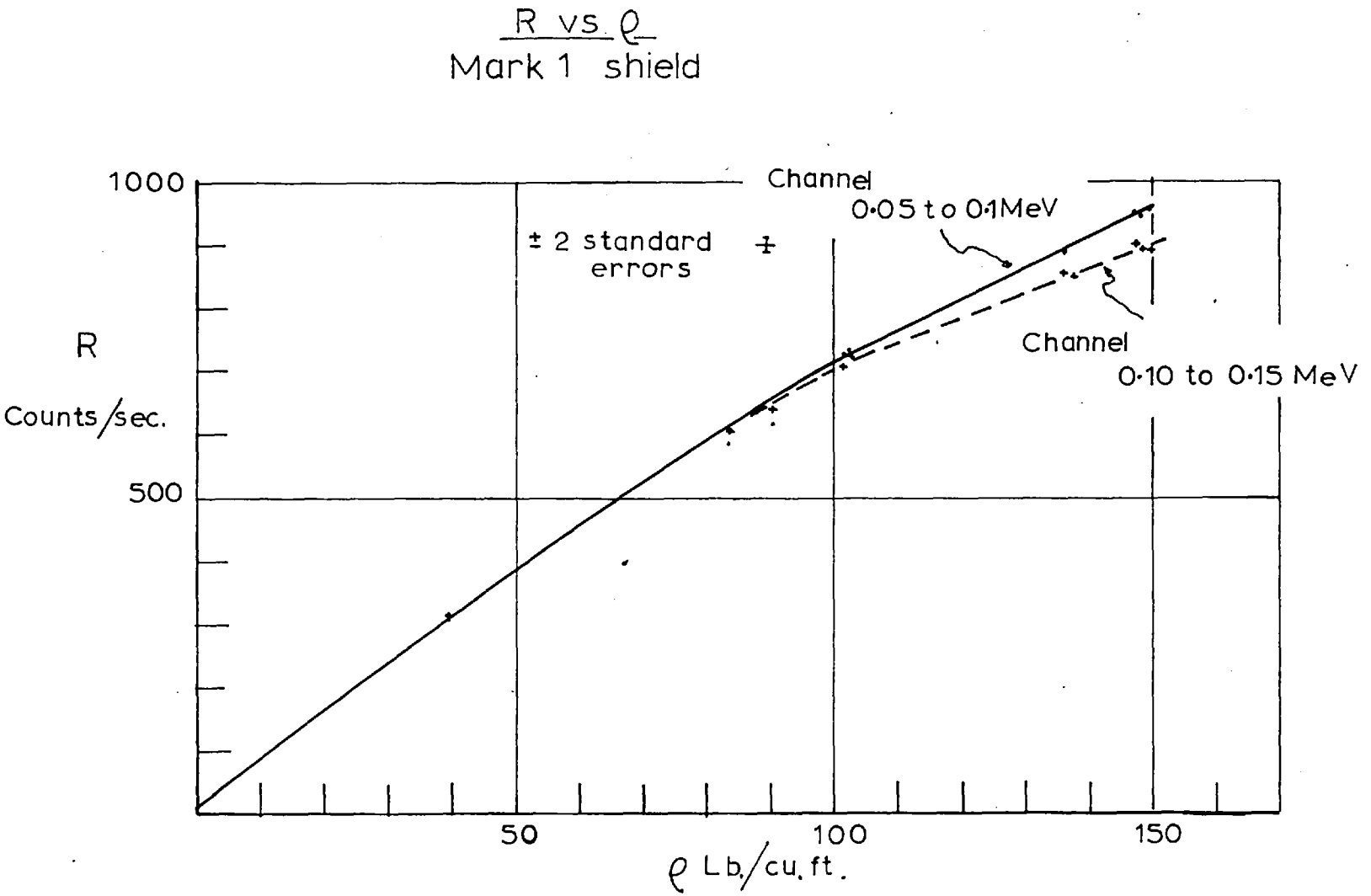
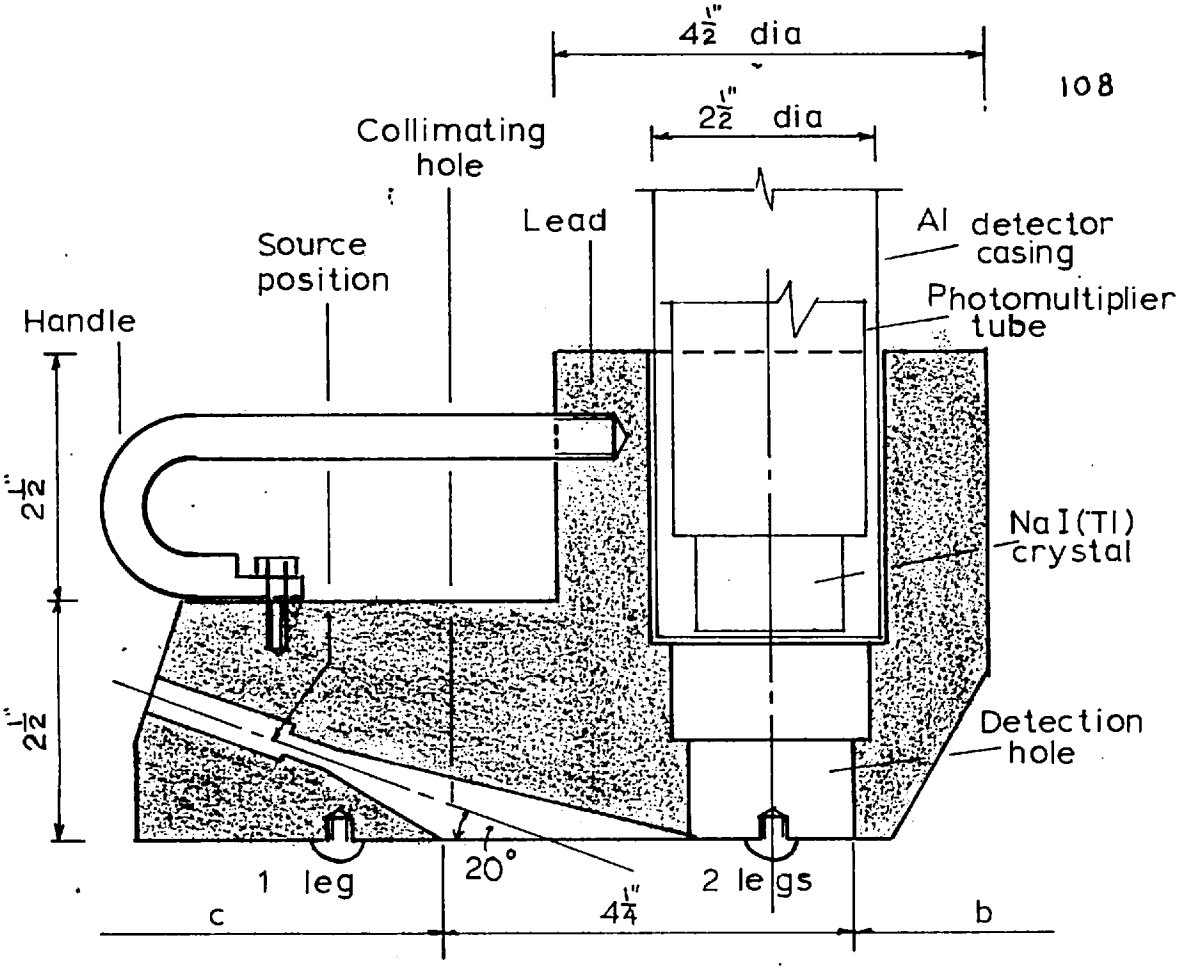
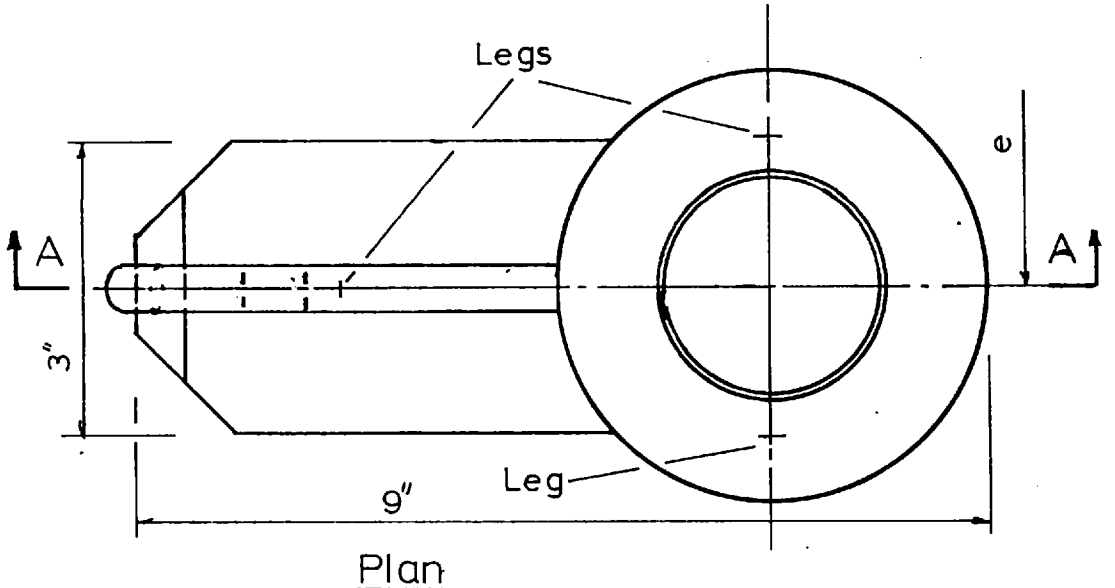

R vs ρ
Mark 1 shield
1000
500
R
Counts/sec.
Channel
0·05 to 0·1MeV
± 2 standard errors
Channel
0·10 to 0·15 MeV
50
100
150
ρ Lb./cu. ft.

Fig. 21



Section A-A



Plan

The Mark 3 Shield Scale ½ fullsize

Dimensions b, c & e defined as for the Mark 1 shield.
Legs are ¼" high.

Fig. 22

The detected pulse height spectra on blocks of various density are shown in Figure 23. The effectively infinite sizes, shown in Table 10, were determined from the curves of Figure 24 in the usual way. The broken lines in Figure 24 and 25 indicate 2 standard errors calculated from nuclear statistics only. The calibration curve is shown in Figure 25.

TABLE 10

The Effectively Infinite Dimensions for the Mark 3 Apparatus

Density lb/cu ft	c_∞	b_∞	e_∞	d_∞	$d_{\frac{1}{2}}$
140	3"	2"	3"	$4\frac{1}{2}$"	$\frac{1}{2}$"
90	3"	$8\frac{1}{2}$"	5"	-	-

By comparing the pulse height spectra with those shown in Figure 16, the peak due to once scattered photons is seen to have moved to a lower energy and that due to twice scattered photons to a higher energy, as expected. When compared with the results for the Mark 1 shield, infinite sizes c_∞, e_∞ and d_∞ are seen to have been little changed but b_∞ was increased because more concrete beyond the detector was "seen". The scatter of the readings

The Mark 3 Shield
Detected Pulse Height Spectra
Due to $R_s + R_p$

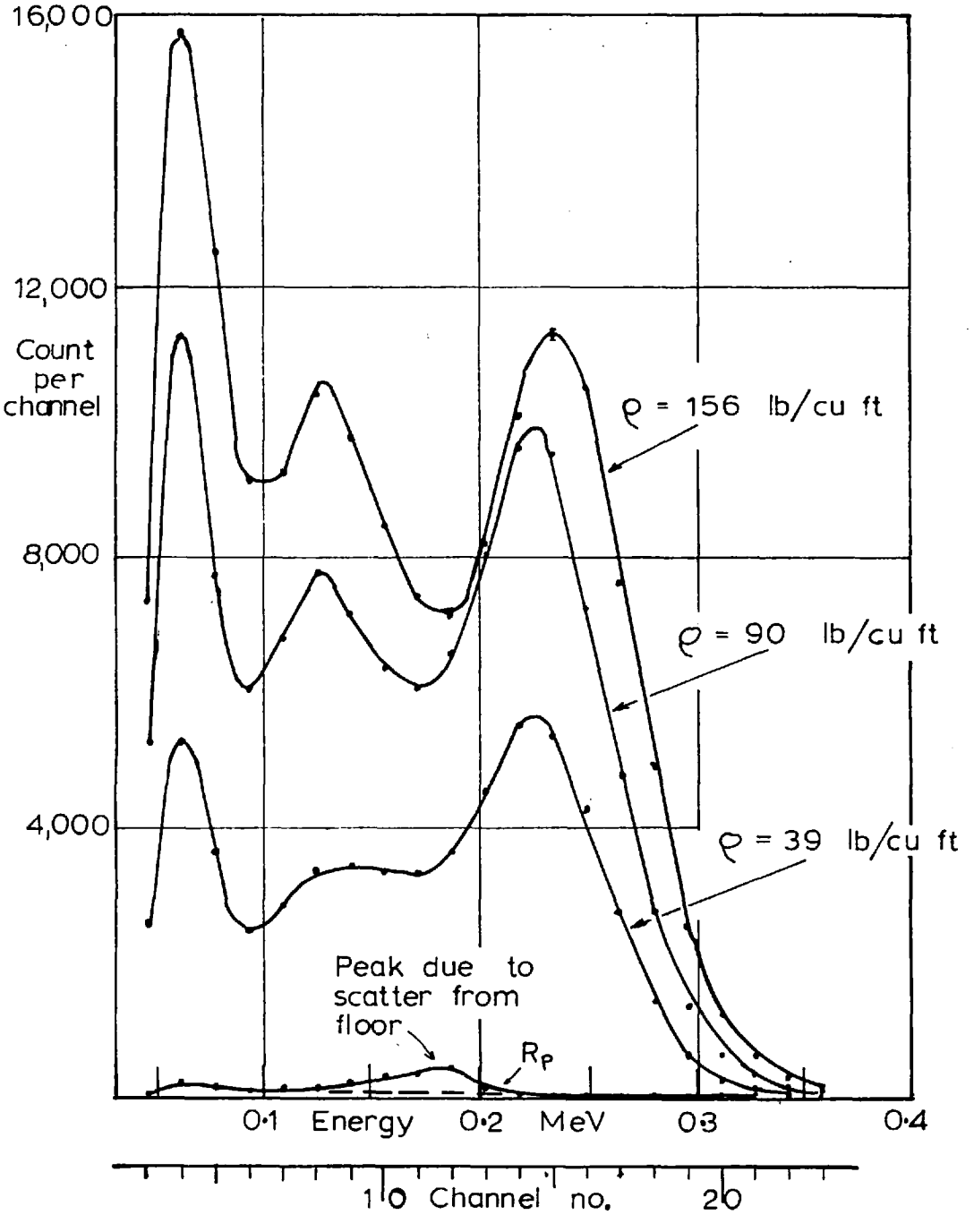


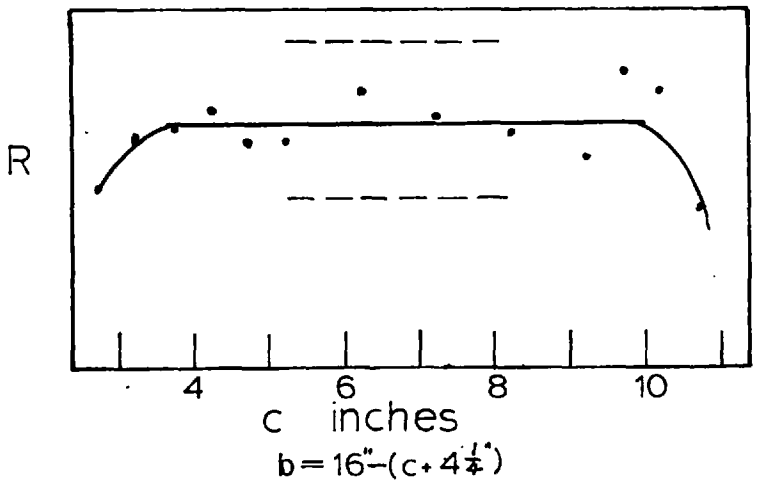
Fig. 23

The Mark 3 Shield

Determination of c_∞ and b_∞

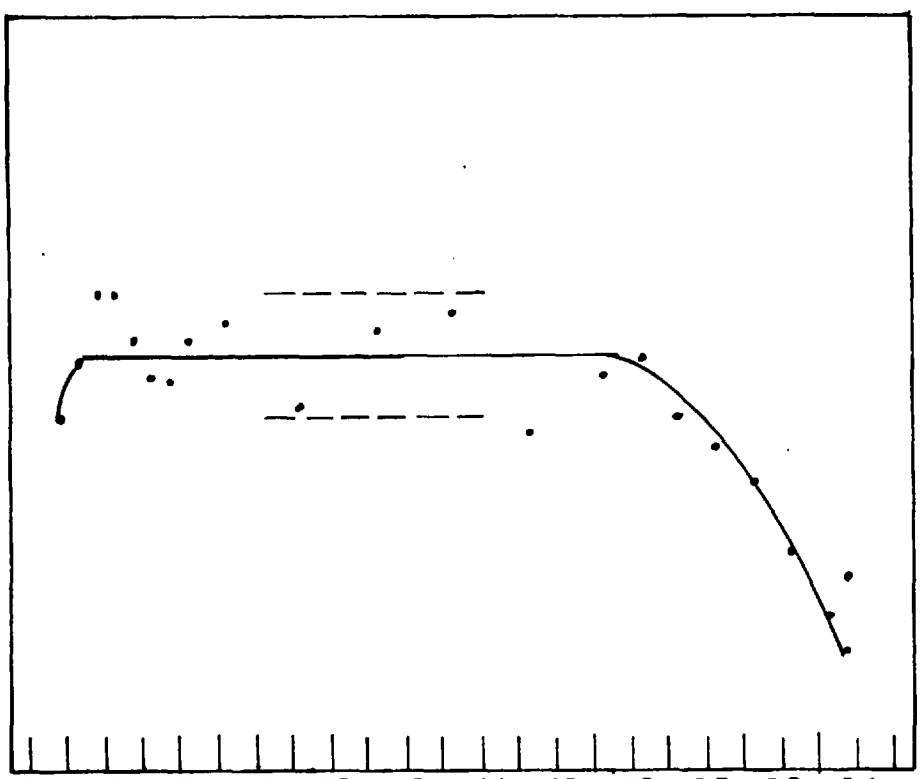
R vs c

Discriminator level = 0·1 MeV



$\rho = 140$ lb/cu ft

$b = 16'' - (c + 4\frac{1}{4}'')$



$\rho = 90$ lb/cu ft

$b = 30'' - (c + 4\frac{1}{4}'')$

Fig. 24a

The Mark 3 Shield
Determination of e_∞ R vs e

Discriminator level = 0·1 MeV

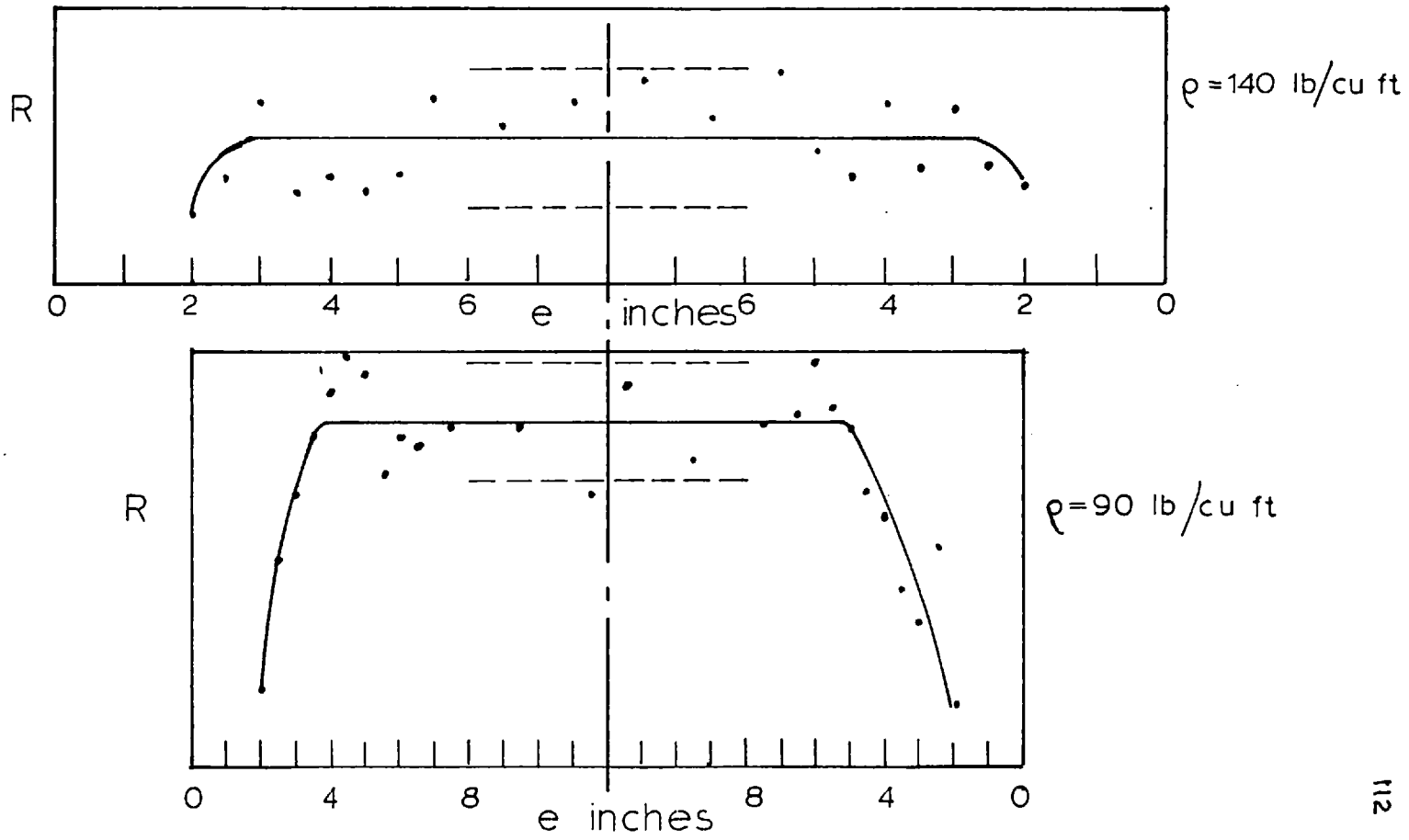


Fig. 24 b

The Mark 3 Shield

R vs d

$\rho = 140$ Lb/cu ft

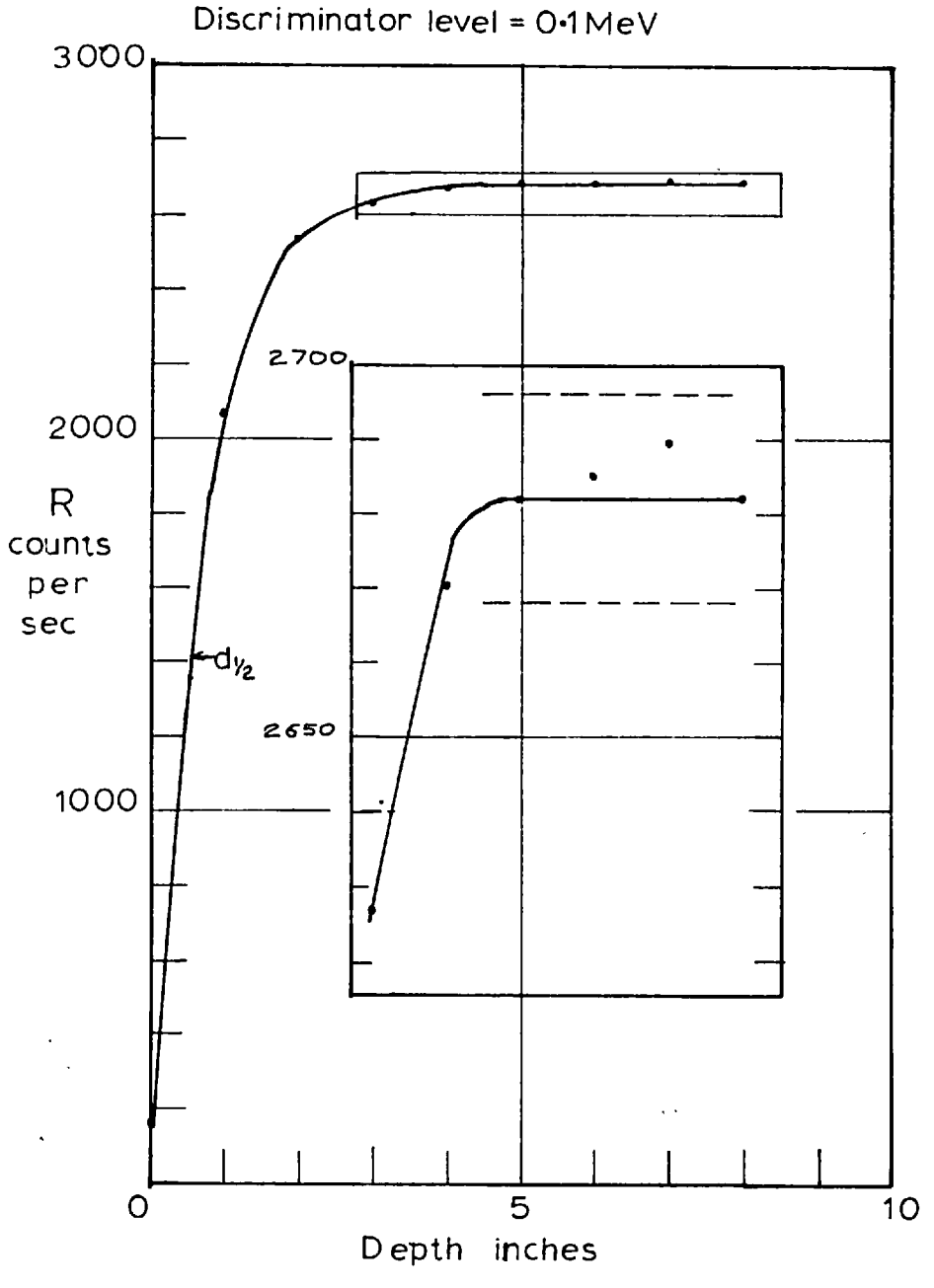


Fig. 24c

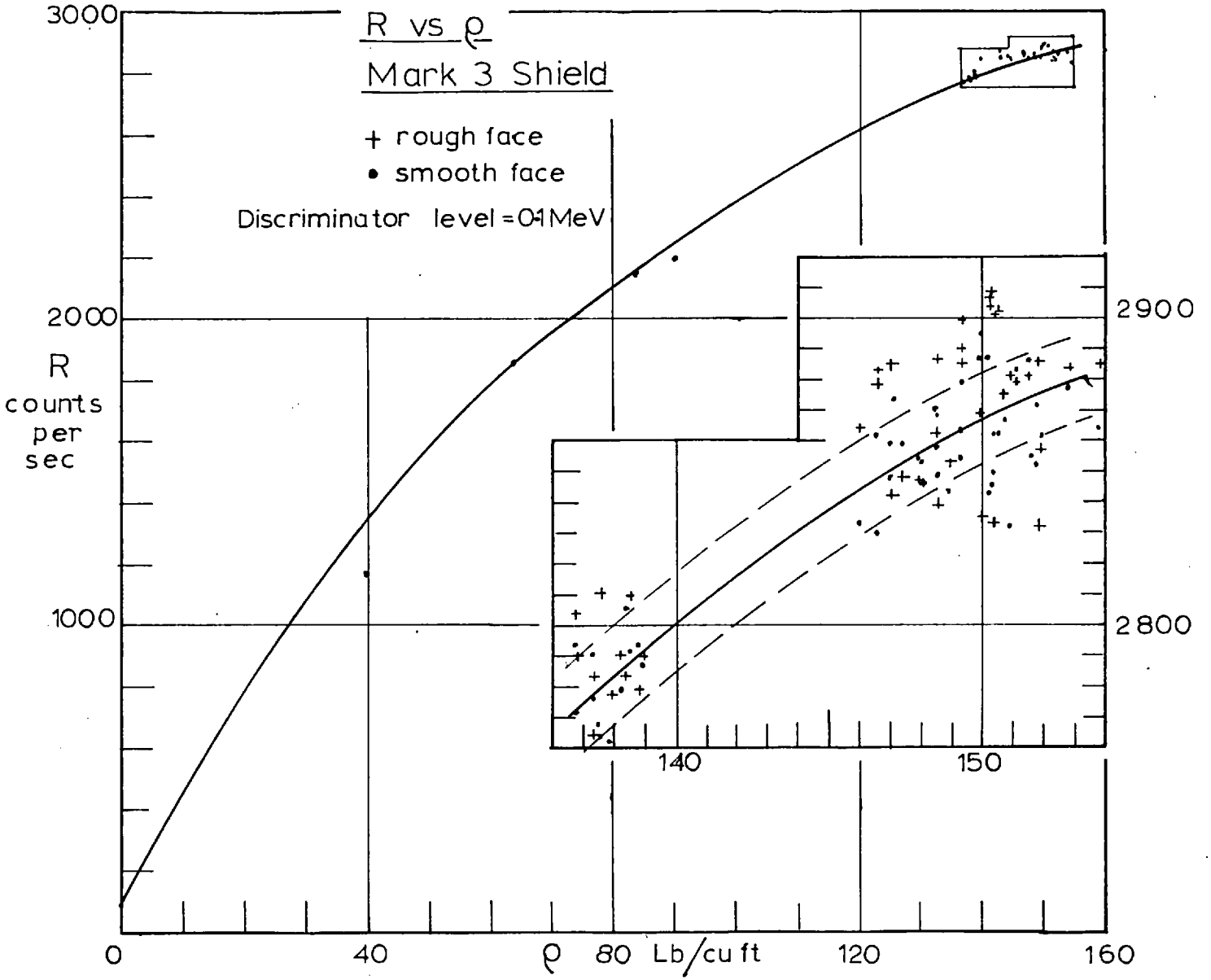

R vs ρ
Mark 3 Shield
+ rough face
• smooth face
Discriminator level = 0·1 MeV
3000
2000
1000
R
counts
per
sec
2900
2800
140
150
0
40
ρ
80
Lb/cu ft
120
160

Fig. 25

on the rough face in Figure 25 is seen to be improved, compared with Figure 17. The scatter of the readings on the smooth face of the mortar specimens at density 138 lb/cu ft in Figures 17, 18, 20 and 25, was less than the scatter of the normal concretes at 150 lb/cu ft. This indicates that the scatter in the calibration curve was due in some part to the heterogeneity of the concrete itself.

The sensitivites, as defined in Chapter 2.6 were calculated for the various calibration curves and are shown in Table 11.

TABLE 11

Sensitivities of Various Calibration Curves at 150 lb/cu ft

Curve	S = R/R' at 150 lb/cu ft	R	N 300 sec.	$\frac{S}{\sqrt{N}}$
Fig.17	535 lb/cu ft	2730 c/s	8.2×10^5	0.59
Fig.18	510	2684	8.05×10^5	0.57
Fig.20	310	1500	4.5×10^5	0.46
Fig.21 Channel 0.05 to 0.10MeV	202	900	2.7×10^5	0.39
Fig.21 Channel 0.10 to 0.15MeV	225	850	2.55×10^5	0.45
Fig.25	375	2866	8.6×10^5	0.41

Chapter 2.7.4 Conclusions

The scatter of points about the calibration curves of Figures 17, 18,20 and 25, where concretes of differing compositions from a wide range of aggregates were used, was not much greater than would be expected on the basis of nuclear statistics only. However, the points on Figure 17, taken on the hand finished faces of the blocks, show a significant scatter. It may therefore be concluded that the Mark 1 apparatus eliminated the effect of chemical composition of the concrete, but the count rate was significantly dependent on the conditions of seating the shield. The readings taken on the rough face with the Mark 3 shield were less scattered than with the Mark 1 shield, but the scatter was still sufficiently great to be a possible practical problem.

Pulse height selection led to an improvement in sensitivity. However, the curve for the 0.05 MeV to 0.10 MeV channel depended on the chemical composition of the concrete as photoelectric absorption was then a significant process. The curve for the channel 0.10 MeV to 0.15 MeV would show no such dependence. Although the sensitivity for this curve was improved, the count rate was lowered, so that there was little reduction in the error for a count of given duration.

The inclusion of the lead wedge in the Mark 2 apparatus

improved the sensitivity, providing some confirmation of the theory of Chapter 2.4.

CHAPTER 2.8 REDUCTION OF THE INFLUENCE OF SURFACE ROUGHNESS ON THE COUNT RATE

The change of count rate with surface roughness may be due to two causes (Lauchaud 1961). If a significant proportion of the count is due to radiation which, after the first scatter, travels parallel to and near the surface of the concrete, then roughness of the surface layer would reduce the effective distance between source and detector so that the count rate would increase. It was considered unlikely that this first mechanism operated here.

Secondly, roughness of a surface may be considered to effectively raise the shield above the "true" surface, reducing the path length between source and detector and therefore increasing the count rate. As the base of the Mark 1 shield was plane, 4" wide by $10\frac{3}{4}$" long, any protuberance over this area would have raised the shield and changed the count rate. Positioning three legs around the source and detector holes in the base is a logical method of reducing this effect (Belcher et al 1952, Carey and Reynolds 1958, Kuhn 1964).

Belcher et al (1952), using the apparatus shown in Figure 1, found that the count rate increased as the apparatus was raised above the surface, but there was very little

difference between the count rates at heights of 7/16" and ½". They concluded that if the legs were ½" long, surface roughness should have little effect. When however using an instrument with ½" legs on site the results were unsatisfactory, and although the cause of error was not found the approach was not pursued. Kuhn (1964) found that the ratio count on legs to count without legs was a function of density independent of the chemical composition of the soils used, and proposed this as a means of eliminating the effect of chemical composition.

By assuming that the detected radiation was all once scattered along a single known path, which was certainly a bad mathematical model of his apparatus, Lauchaud (1961) calculated the theoretical increase of count rate as a function of height above the surface and found fair agreement with experiment. The success of the calculation must however have depended upon the path assumed for the radiation.

The roughness of a surface compared with a plane surface may be defined by that height above the plane which gives the same count rate as the rough surface. Therefore to reduce the effect of roughness the apparatus should be used on legs of height h corresponding to a low value of the slope of the R vs h curve. This curve may easily be established experimentally.

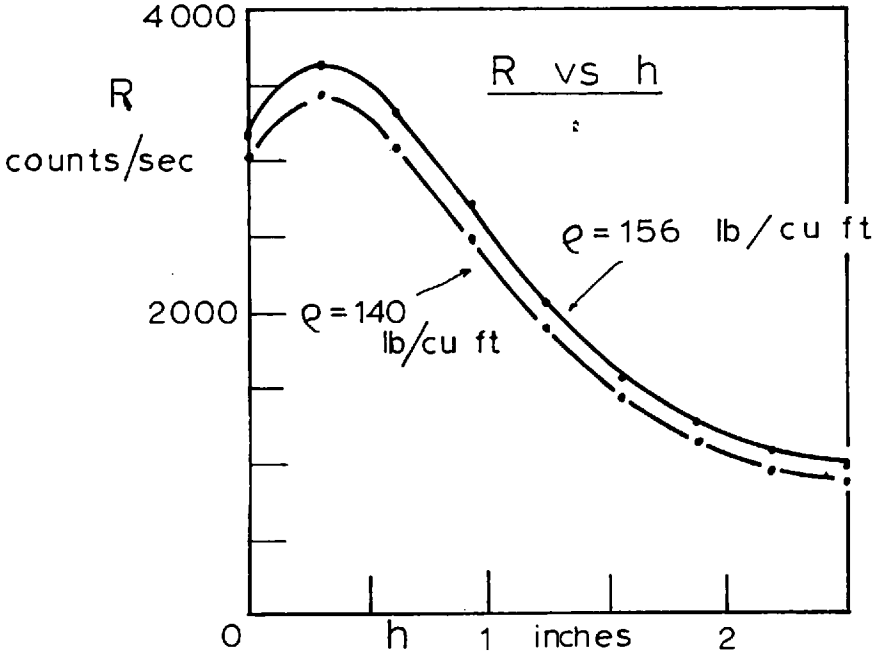
Readings of count rate against height above a plane

surface were taken using the Mark 1 apparatus on two blocks of concrete each 16" x 16" x 8", and of densities 156 lb/ cu ft and 140 lb/cu ft. The curve of count rate against height above the surface is shown in Figure 26.. Sensitivity at 140 lb/ cu ft was calculated assuming a linear calibration curve between 156 lb/cu ft and 140 lb/cu ft; the curve of sensitivity against height is also shown in Figure 26 .

As the shield was raised, less once scattered photons were detected until at h = 2½" the detector and source cones did not intersect in the concrete, so that no once scattered photons were detected. This is demonstrated by the pulse height spectra of Figure 27 in which the different shapes of spectra show that the scattering geometry was changed by raising the shield. These changes account for the shapes of the R vs h and S vs h curves. For elimination of the effect of surface roughness on the reading, the legs should be at a height where the slope of the R vs h curve is a minimum. The peak at h = 0.3" was probably too sharp to entirely eliminate this effect so that a height h = 2½" was the more advisable, for this shield. The statistical accuracy attainable at h = 2½" in a given time was however reduced by changes in both count rate and sensitivity, so that reduction in the influence of surface roughness would have been attained by a sacrifice in time of count or accuracy.

The Mark 1 Shield

Count Rate and Sensitivity vs Height above the Concrete Surface



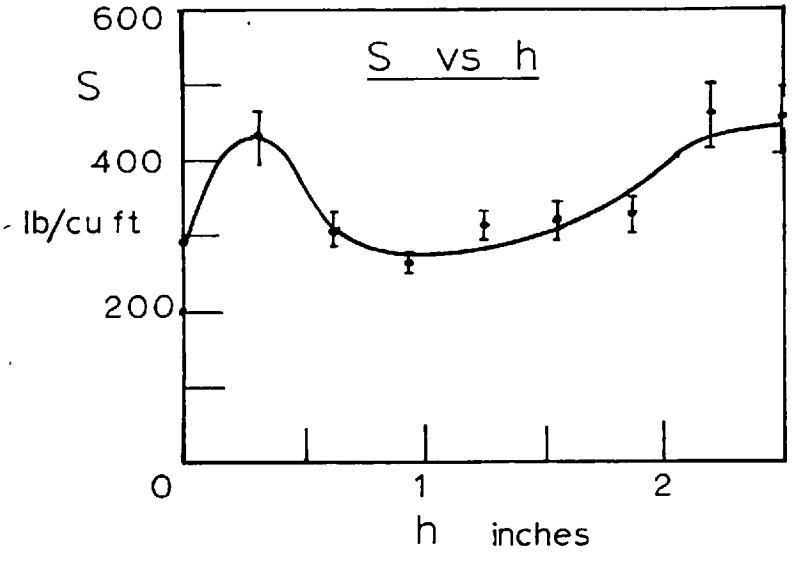


Fig. 26

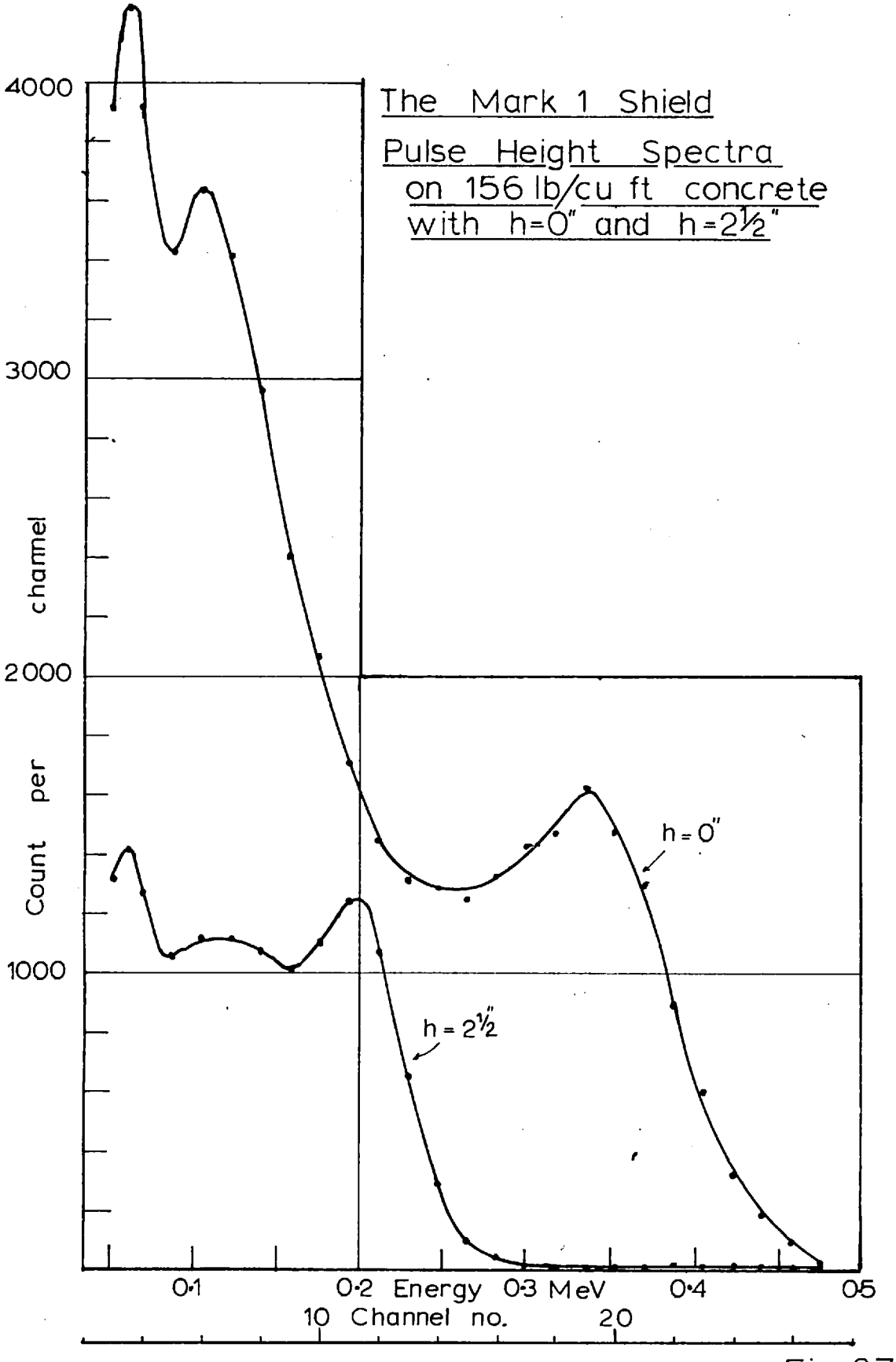

The Mark 1 Shield
Pulse Height Spectra
on 156 lb/cu ft concrete
with h=0" and h=2½"
4000
3000
2000
1000
Count per channel
h = 0"
h = 2½"
0·1
0·2
Energy
0·3 MeV
0·4
0·5
10
Channel no.
20

Fig. 27

The dependence of the reading on surface roughness will depend both upon the design of the apparatus and the condition of the surface and may prove to be the most serious cause of error in practice.

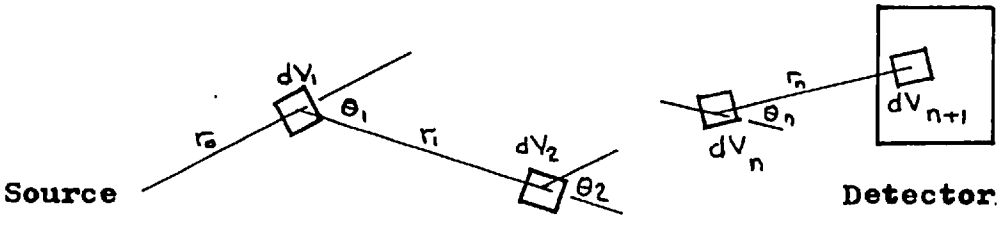
CHAPTER 2.9 THE EQUATION OF THE CALIBRATION CURVE

In an entirely theoretical approach the count rate would have been predicted as a function of source energy, detector characteristics, geometry of the shield and the properties of the tested material. Due to the complexities of this problem such an approach was precluded.

A theoretical investigation was carried out to determine the form of the function expected. Experimental information was then used to determine the constants of this function, which was the equation of the calibration curve.

Chapter 2.9.1 The Theoretical Equation

Consider a source and detector of gamma radiation in a medium which may both scatter and absorb.



Consider a photon travelling distance r_o then colliding within a volume dV_1, travelling distance r_1 to dV_2 and so on until its $(n+1)^{th}$ collision is within the detector.

Let $r_o, r_1 \ldots r_n$ be the path lengths within the medium.

$\theta_1, \theta_2 \ldots \theta_n$ be the angles of scatter

$\Sigma_{so}, \Sigma_{s1} \ldots \Sigma_{sn}$ be the total scattering cross sections along paths 0, 1, ... n.

$\Sigma_{ao}, \Sigma_{al} \ldots \Sigma_{an}$ be the absorption cross sections along paths 0, 1, ... n.

$\Sigma_i = \Sigma_{si} + \Sigma_{ai}$

$\Sigma_{si}(\theta_i)$ be the cross section per unit volume per steradian for scattering through θ_i at point i.

$dA_i = \frac{dV_i}{dr_i}$

$d\Omega_i$ be the solid angle at i subtended by $dA_{i+1} = \frac{dA_{i+1}}{r_i^2}$

$\mu_i = \frac{\Sigma_i}{\rho}$

D_n be the nett current of n times scattered photons into the detector.

η_n be the probability of an n times scattered photon being detected if it enters the detector.

For an isotropic source of 4π photons/sec, the number of photons going in the direction from the source to dV_1 is $\frac{dA_1}{r_o^2}$ photons/sec. The number surviving to dV_1 is $\frac{dA_1}{r_o^2} e^{-\Sigma_o r_o}$ photons/sec, so that the flux at dV_1 is $\frac{e^{-\Sigma_o r_o}}{r_o^2}$ photons/cm^{2}sec. If the photons may be absorbed at this collision, only a fraction $\frac{\Sigma_{so}}{\Sigma_{ao}+\Sigma_{so}}$ will survive. Putting $d\Omega_1 = \frac{dA_2}{r_1^2}$ the number of photons scattering out of dV_1, in the direction of dV_2 is then $\frac{\Sigma_{so}}{\Sigma_o} \frac{e^{-\Sigma_o r_o}}{r_o^2} \Sigma_{s1}(\theta_1)\, dV_1 \frac{dA_2}{r_1^2}$

The differential flux at dV_2 is then

$$\frac{\Sigma_{so}}{\Sigma_o} \frac{e^{-\Sigma_o r_o - \Sigma_1 r_1}}{r_o^2 r_1^2} \Sigma_{s1}(\theta_1)\, dV_1$$

The differential flux at dV_3 is

$$\frac{\Sigma_{so}}{\Sigma_o} \frac{\Sigma_{s1}}{\Sigma_1} \frac{e^{-\Sigma_o r_o - \Sigma_1 r_1 - \Sigma_2 r_2}}{r_o^2 r_1^2 r_2^2} \Sigma_{s1}(\theta_1)\, \Sigma_{s2}(\theta_2)\, dV_1\, dV_2$$

The differential flux at dV_{n+1} is

$$\frac{\Sigma_{so}\Sigma_n}{\Sigma_o \Sigma_{sn}} \frac{e^{-\Sigma_o r_o}}{r_o^2} \prod_1^n \frac{\Sigma_{si}}{\Sigma_i} \frac{e^{-\Sigma_i r_i}}{r_i^2} \Sigma_{si}(\theta_i)\, dV_i \qquad 2.9.1.(1)$$

The flux at the detector due to all the volume is the integral of the above expression over dV_1, dV_2 ... dV_n.

In physical terms, the first integral will give the flux from dV_n at the detector. The second will give the flux at points dV_n from one point dV_{n-1}, the third at points dV_{n-1} from a single point dV_{n-2} and so on.

The above integral may be evaluated numerically for a given physical situation. Such a computation will however require excessive computing time. It is, in fact, the limiting solution of a Monte Carlo calculation, as the number of Monte Carlo processed photons approaches the number of elemental fluxes determined. In applying the equation to the backscatter apparatus some simplifying assumptions were made.

The photons at the detector consisted of once, twice ... m times scattered photons. It was assumed that all once scattered photons travelled in a particular representative path, that all twice scattered photons travelled a representative path, and so on.

As all n times scattered photons travelled the same path, the following quantities were identical for each n times scattered photon.

Angles $\theta_1, \theta_2 \ldots\ldots\theta_n$

Distances $r_o, r_1, \ldots\ldots r_n$

The photon energy along each path, $E_o, E_1 \ldots E_n$

Cross sections $\Sigma_{so}, \Sigma_{s1}, \ldots\ldots \Sigma_{sn}$

$\Sigma_{ao}, \Sigma_{a1}, \ldots\ldots \Sigma_{an}$

The probability of detection η_n, which depended only on the energy E_n and the path within the detector.

Putting $\Sigma = \mu\rho$ in equation 2.9.1.(1)

$$dR_{n+1} = \eta_n dD_n = \eta_n \, e^{-\rho(\mu_o r_o + \mu_1 r_1 + \ldots \mu_n r_n)}$$

$$\times \frac{\mu_{so}\,\mu_n}{\mu_a\,\mu_{sn}\,r_o^2} \prod_1^n \frac{\mu_{si}}{\mu_i} \cdot \frac{\mu_{si}(\theta_i)\,\rho}{r_i^2}\, dV_i \qquad 2.9.1.(2)$$

where $\sum_0^n \mu_i r_i$ and $\prod_1^n \frac{\mu_{si}}{\mu_i} \cdot \frac{\mu_{si}(\theta_i)}{r_i^2} dV_i$ are constant from the above assumptions.

Therefore $R_{n+1} = a_n \rho^n e^{-b_n \rho}$ where a_n and b_n are constants. The total count rate R_s is due to the sum of all 1, 2, ..., m times scattered photons and is therefore

$$R_s = \sum_1^m a_n \, \rho^n \, e^{-b_n \rho} \qquad 2.9.1.(3)$$

Effect of change in Compton scattering factor

A change in Σ_s will change the values of Σ_o, Σ_1, ... Σ_n and $\Sigma_{si}(\theta_i)$. As these cross sections are proportional to X a change from X to X_1, due for instance to a change in water content, should change the value of a_n by $\left(\frac{X_1}{X}\right)^n$.

A change in Compton scattering cross section would also change the values of b_n. In equation 2.9.1(2) μ_o, μ_1, ...μ_n will each change by a factor $\frac{X_1}{X}$ if Σ_a is negligible. If r_o, r_1, ... r_n remain constant,

then equation 2.9.1.(3) may be written

$$R = \sum_{1}^{m} a_n \left(\frac{\rho X_1}{X}\right)^n \exp\left[-b_n \left(\frac{\rho X_1}{X}\right)\right] \qquad 2.9.1.(4)$$

provided Σ_a is negligible, that is, provided photons of energy less than 0.1 MeV are not detected.

The effect of changing X will depend upon the relative values of each a_n and b_n, i.e. upon the apparatus geometry and detector response, but may be evaluated for a particular case.

Determination of the constants

Knowing a number of points on the curve R vs ρ, and deciding on a value of m, one may try to solve for the 2m constants a_n and b_n in equation 2.9.1.(3). This equation is however very badly conditioned, but does become soluble using the experimental information shown in the next section.

Chapter 2.9.2 Consideration of the Curves Log R_s vs ρx.

If $R_s = Ae^{-B\rho x}$ represented the variation of R_s with distance then in equation 2.9.1.(2) all the exponents of e were equal.

i.e. $\rho \sum_{1}^{n} \mu_i r_i = B\rho x$, whatever the value of n.

The exponent of e is the number of mean free paths travelled by the photons, so the conclusion is reached that at a given density and angle α, however many scatters

n a photon underwent before detection it travelled a constant number of mean free paths, and this number varied linearly with the distance source to detector. This conclusion is valid only for this type of apparatus and range of distance and density.

In equation 2.9.1.(2), if all the exponents e were equal for all n, then

$$R_s = \sum_1^m a_n \rho^n e^{-B\rho x} = e^{-B\rho x} \sum_1^m a_n \rho^n$$

Because $R_s = Ae^{-B\rho x}$, $A = \sum_1^m a_n \rho^n$

Log A is plotted against log ρ in Figure 28, and because these curves are straight lines A is given by $A = f\rho^g$ where f and g are constants. Similarly from the curves of log B vs log ρ in Figure 29 $B = h\rho^j$ where h and j are constants.

For a particular shield x is constant and so

$B\rho x = c\rho^{j+1}$, c a constant.

$= c\rho^d$, d a constant.

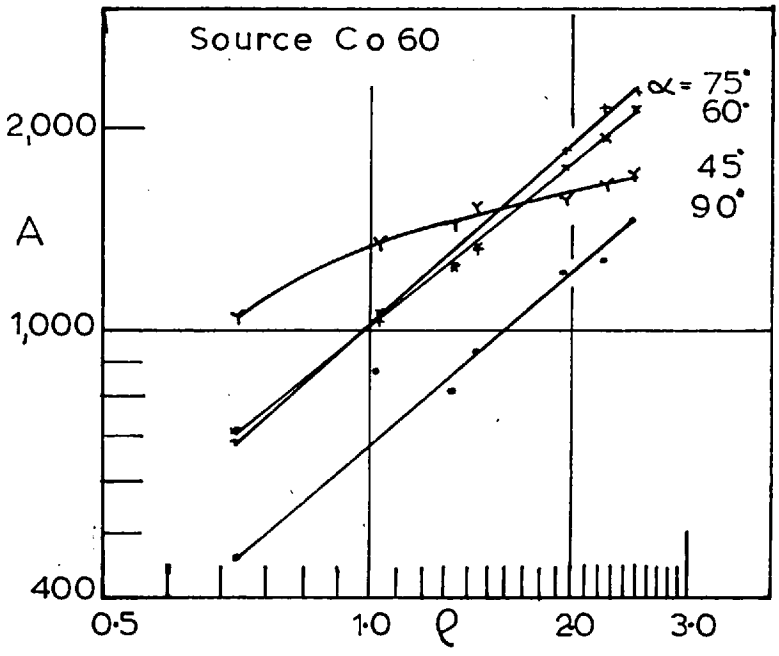
$\sum_1^m a_n \rho^n = A = a\rho^b$, a and b new constants.

Therefore the equation of the backscatter gauge may be written

$$R_s = a\rho^b e^{-c\rho^d} \qquad 2.9.2.(1)$$

If the effect of scattering factor X is included, then by analogy with equation 2.9.1.(4)

Log A vs Log ρ



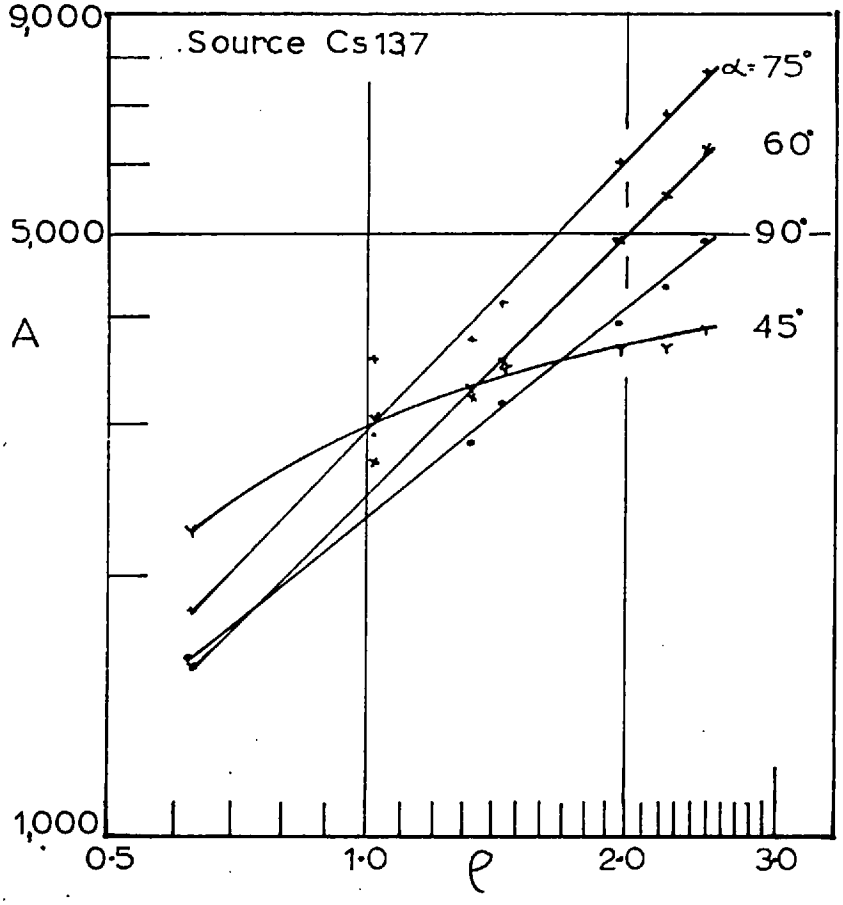


Fig. 28

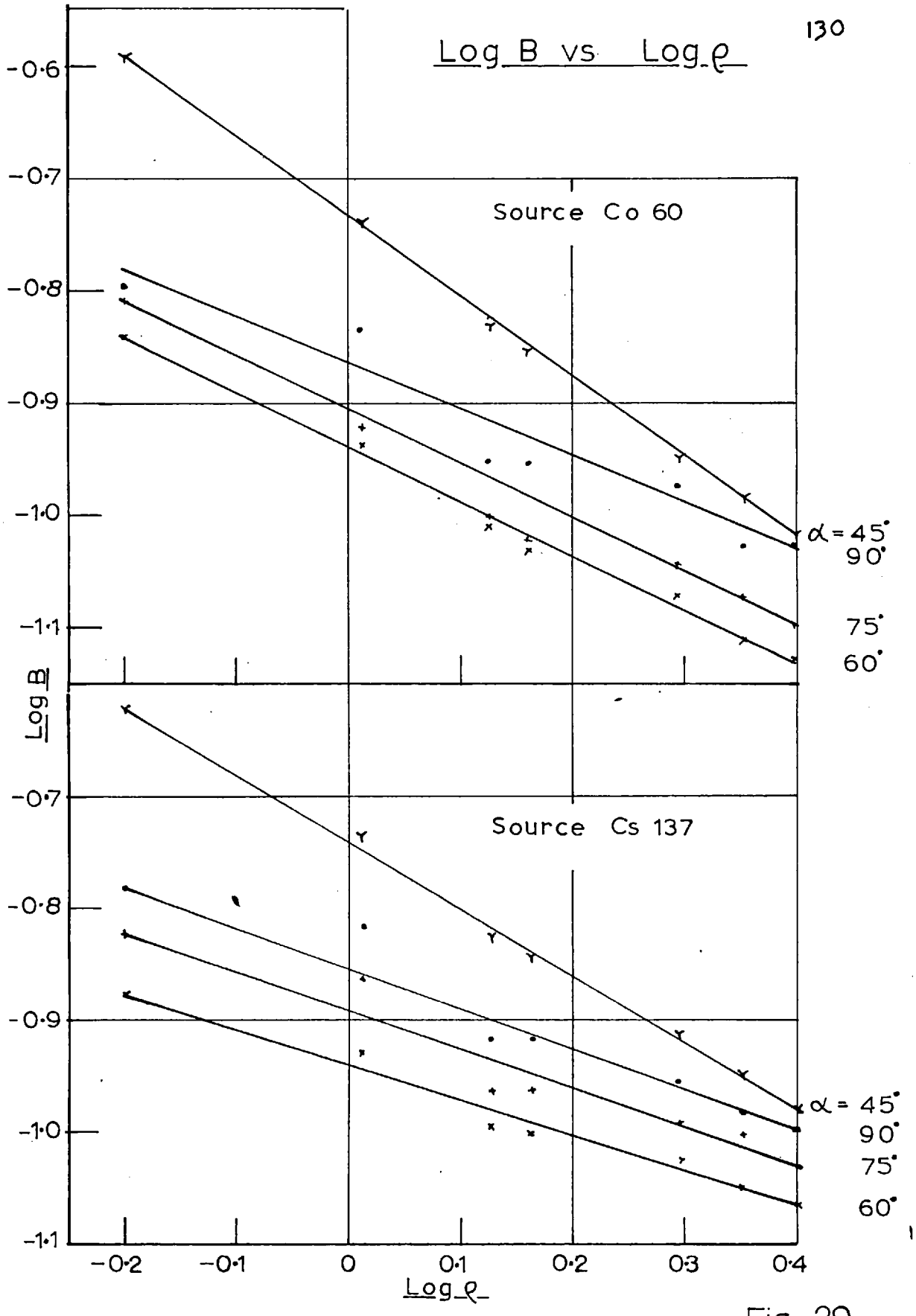

Log B vs Log ρ
Source Co 60
Source Cs 137
Log B
Log ρ
-0·6
-0·7
-0·8
-0·9
-1·0
-1·1
-0·2
-0·1
0
0·1
0·2
0·3
0·4
α = 45°
90°
75°
60°

Fig 29

$$R_s = a\left(\frac{\rho X_1}{X}\right)^b \exp\left[-c\left(\frac{\rho X_1}{X}\right)^d\right] \qquad 2.9.2.(2)$$

Using equation 2.9.2.(2) is equivalent to taking as the independent variable the number of electrons per unit volume of tested material, which is a more rational variable for a gamma backscattering method than the mass per unit volume.

The right-hand sides of equations 2.9.2.(1) and 2.9.2.(2) are ill conditioned. Many different combinations of constants will give a least squares fit. These constants must therefore be determined by experiment.

The values of b and d may be found from the slopes of the curves in Figures 28 and 29, and are given in Table 12. With these known any two points on the curve R vs ρ yielded values of a and c.

TABLE 12

Values Obtained with the Variable Parameter Apparatus for b and d in equation 2.9.2.(1) for R_s in counts/sec and ρ in g/cc

α	Source Co 60		Source Cs 137	
	b	d	b	d
90°	0.84	0.60	0.81	0.65
75°	0.87	0.52	1.05	0.65
60°	0.81	0.53	1.01	0.69
45°	0.27	0.29	0.28	0.41

Chapter 2.9.3 Application of the Equation

Equations 2.9.2.(1) and 2.9.2.(2) were derived using the experimental information of Figures 13, 28 and 29. Further evidence pointing to the validity of these equations was obtained as follows. For each of the blocks used in determining the curves of Figures 17 and 18 the chemical composition and therefore the value X was known. Using values of b and d from Table 12 as initial points, equations 2.9.2.(1) and 2.9.2.(2) were fitted to the curves of Figures 17 and 18 by a minimization routine developed by McConalogue (1962). The constants and standard errors obtained are shown in Table 13 and the fitted curves plotted in Figures 17 and 18. The least squares analysis was carried out using only the observed points above 90 lb/cu ft in order to see how the curve predicted the count rates at lower densities. Agreement is seen to be fairly good.

The error on the fit for equation 2.9.2.(2) was less than for equation 2.9.2.(1), implying that some correction was made for changing X and that equation 2.9.2.(2) represented the physical system. The difference between the constants obtained for the two curves is due probably to the ill-conditioning of the functions.

The change in count rate due to changing X will be small in practice. Should a correction be desired equation 2.9.2.(2) may be used to set up curves of R vs ρ at

different values of X.

TABLE 13

Values Obtained when fitting the Theoretical Functions to the Experimental Calibration Curves.

R in counts/sec and ρ in g/cc.

Curve	Starting Values		Final Values				Error of the Fit	
	b	d	b	d	a	c	Eq.2.9.2. (1)	Eq.2.9.2. (2)
Fig.17	1.05	0.406	1.045	0.4069	5,946	1.198	22.8	22.6
Fig.18	1.05	0.406	1.227	0.2715	21,669	2.497	24.9	24.2

Error of the fit is $\sqrt{\frac{\Sigma vv}{n-4}}$ where v is the residual and n the number of points.

Chapter 2.9.4 Comparison with Other Proposed Equations

Equations proposed for the calibration curve by various authors are shown below.

TABLE 14

Author	Equation	Remarks
Pocock (1956)	$R_s = g(\rho,E_o)\, A^{f_1(\rho,E_o)}\, e^{f_2(\rho,E_o)\chi}$	
Carey and Reynolds (1958)	$R_s = a\, e^{-k\rho}(b\rho + c\rho^2 + d\rho^3)$	a,b,c,d constants
Carey et al (1960)	$R = a_1\, e^{-a_2\rho}$	a,b constants
Lauchaud (1961)	$R_s = B\rho\, e^{-k\rho}$	B,k constants
Huet (1961)	$\rho = -1.7r + 3.04$	

The equations of Carey et al (1960) and Huet (1961) were arbitrarily chosen and fitted to data over a small range of density. Lauchaud (1961) proposed his equation because it gave a curve with zero values at densities of zero and infinity, with a peak between. Carey and Reynolds (1958) considered that the exponential term was due to absorption processes and the polynomial to scattering processes. From equation 2.9.1.(3) it is seen that the equation of Lauchaud corresponded to an assumption that only once scattered photons need be considered, and the equation of Carey and Reynolds corresponded to an assumption that only once, twice and three times scattered photons need be considered, and that the number of mean free paths travelled by each is the same. It is thus seen that these equations are different approximations to the same general equation 2.9.1.(1).

The equation of Pocock (1956) was based upon the experimental fact that the curves of log R_s against x plotted as straight lines.

In his equation $g(\rho, E_o) = 1$

$f_2(\rho, E_o) = -B$ in equation 2.5.6.(1)

$A = R_s + R_p$ at $x = 0$

and $f_1(\rho, E_o) = \frac{\ln R_s}{\ln(R_s+R_p)}$ at $x = 0$

so that his $f_1(\rho, E_o)$ is identical with A as defined in

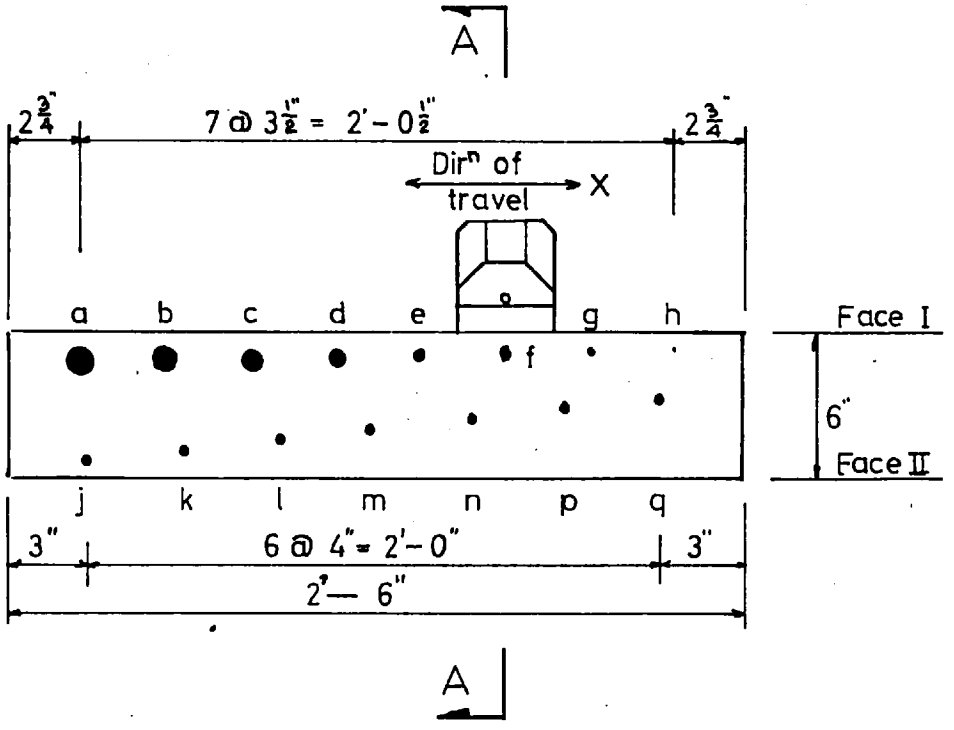
equation 2.5.6.(1). Pocock also found that the curves log $f_1(\rho, E_o)$ and log $f_2(\rho, E_o)$ against log of density ρ plotted as straight lines. His equation is thus identical with equation 2.9.2.(1).

CHAPTER 2.10 USE OF THE APPARATUS TO LOCATE STEEL IN CONCRETE

Steel is denser than concrete. If the apparatus be placed upon concrete near a steel bar, the reading will be greater than that due to plain concrete.

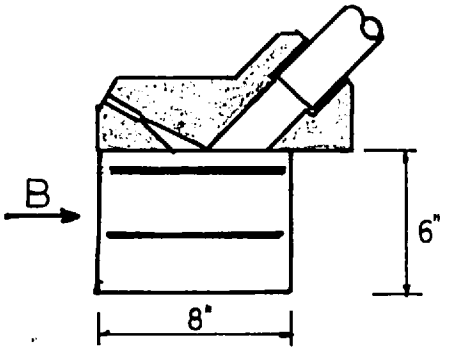
An investigation was carried out to find the effects of cover and bar diameter on the count rate. A beam, section 6" x 8", as shown in Figure 30, was cast. One face of the beam contained bars of different diameter at varying cover. The Mark 1 apparatus, discriminator at 0.1 MeV was placed upon the beam as shown in Figure 30 and a reading taken. It was then moved along the beam, a reading being taken at each position.

Figure 31 shows that the positions of the bars were accurately given by the peaks in the curve. As either the bar diameter decreased or the cover increased count rate fell. In this application the apparatus determined either the cover or the bar diameter, but not both. Further development may produce a method of determining bothvariables.



Elevation B

Fixing bars not shown



Section A-A

Steel bar details

Bar	Dia	Cover
a	1"	
b	⅞"	0·56"
c	¾"	
d	⅝"	
e	½"	
f	⅜"	
g	¼"	
h	3/16"	
j		0·60"
k		1·11"
l	1"/2	1·50"
m		1·92"
n		2·34"
p		2·70"
q		3·00"

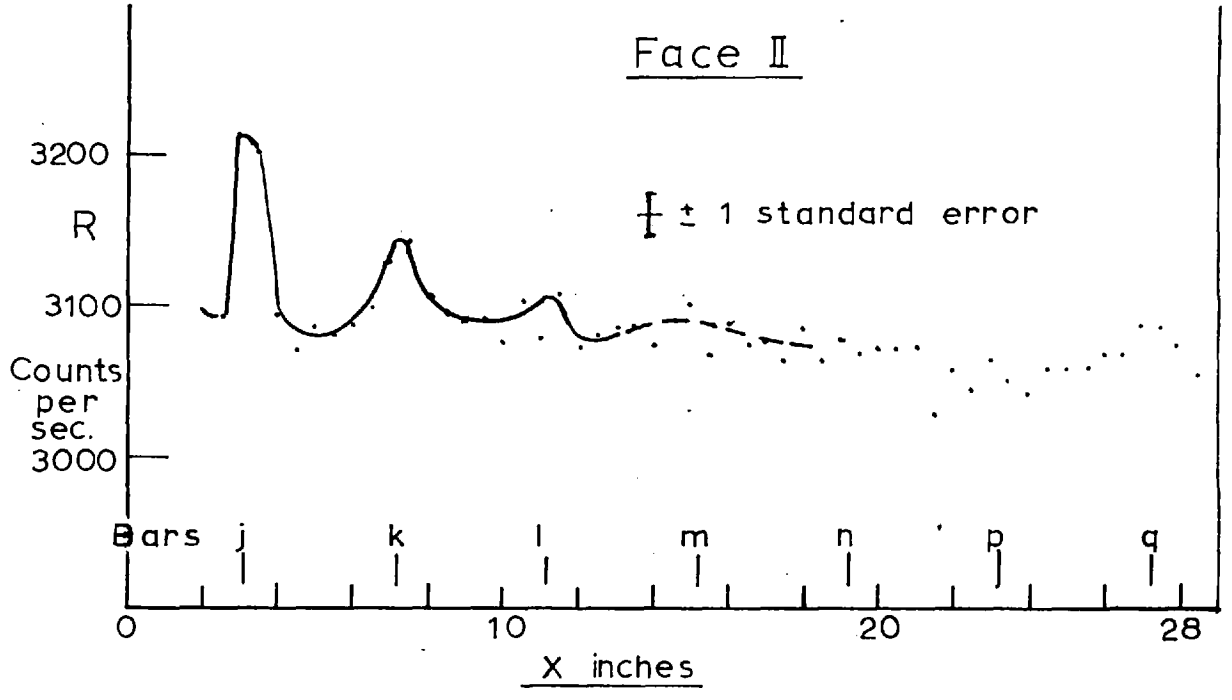
USE OF THE APPARATUS FOR THE DETECTION OF STEEL

1/8 Scale full size

Fig. 30

DETECTION OF STEEL BARS

R vs X (see fig.30)



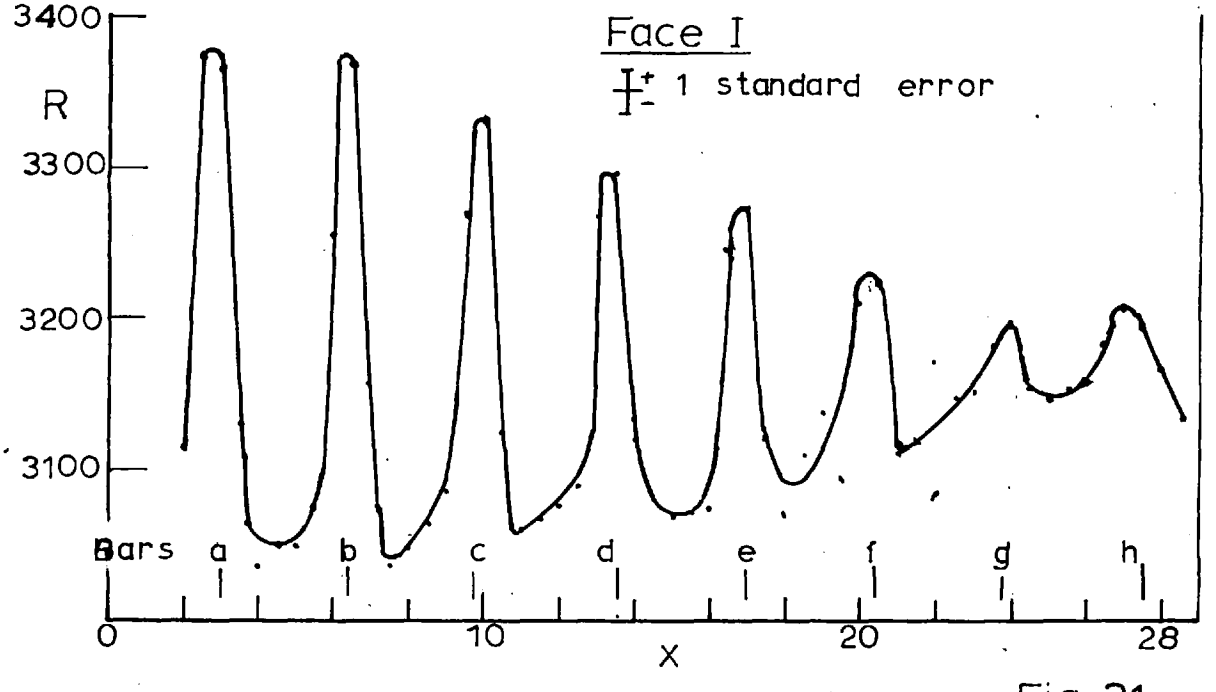


Fig. 31

CHAPTER 2.11 HAZARDS OF GAMMA RAY METHODS

The possible effects of the gamma radiation on both the concrete and the human operator must be considered.

The gamma radiation originating in the Cs 137 will collide with the electrons of the concrete with total energy insufficient to disrupt the chemical and other bonds due to the electrons, and will therefore have negligible effect on the structural stability of the concrete. The energy absorbed by the concrete will eventually appear as heat which will increase the temperature of the concrete.

The energy deposited on the concrete by a 5 millicurie Cs 137 source was calculated. It was assumed that the source was at the centre of a large mass of concrete and that all the source energy appeared as heat within a sphere of radius 5 cm, which is approximately one collision mean free path in concrete of density 2.4 g/cc. These assumptions gave an overestimate of the heating effect.

The heat absorbed by the concrete per second per cc

$$= \frac{\text{Source intensity x energy per emission}}{\text{Volume of sphere}} \text{ MeV/cc sec}$$

$$= 3.8 \times 10^{-8} \text{ watts/cc for a 5 millicurie Cs 137 source in a sphere 5 cm radius.}$$

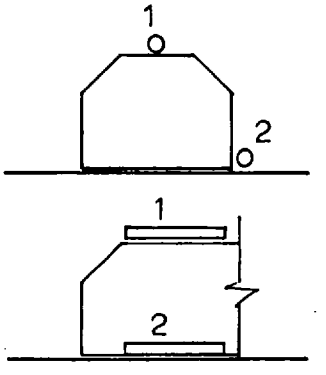
The temperature rise due to this is of the order of 10^{-3} ^{o}C.

Measurements of the dose due to the 5 millicuries Cs 137 source were taken with a quartz fibre pocket dosimeter on the Mark 1 and Mark 3 shields. The former had approximately 2" of shielding about the source and the latter approximately 1½". The measured values of dose are shown in Table 15.

TABLE 15

Doses in millirem per hour Measured on the Mark 1 and Mark 3 Shields

Position	Mark 1	Mark 3
1	2.1	3.1
2	0.8	4.9



Positions 1 and 2 were above and beside the shields respectively, as shown in the accompanying sketch.

The maximum permissible whole body dose (International Atomic Energy Agency, 1958) is 0.1 rem per week, but the extremities of the legs and arms may receive up to 1.5 rem per week. The dose which will be permitted with any apparatus in practice will depend on how it is to be used and who will operate it. The maximum recorded dose rate, 5 millirem per hour, corresponded to 0.2 rem per 40 hour week. As only the hands or feet will experience the dose

at the shield surface, and it is unlikely that they will be thus exposed for as long as 40 hours every week, the 1½" shielding thickness may be reduced.

In practice some interlock system will have to be provided to shield the source hole when the apparatus is not in use.

CHAPTER 2.12 CONCLUSIONS

Gamma backscatter apparatus will give readings of density negligibly dependent on the chemical composition and therefore the types and proportions of constituents of the concrete if Compton scatter is the only operative process. Information useful for the design of apparatus operating on such a principle is given below.

a) The detector must "see" concrete in the region at which radiation enters it, but the detector itself must be shielded from the source.

b) The source energy should be below about 2 MeV.

c) Cs 137 is the best available source, from considerations of shielding, half life and effect on the calibration curve.

d) If a Geiger-Muller tube were used with this apparatus the effect of photoelectric absorption would not be eliminated. Due to the higher proportion of greater energy photons it would however be reduced relative to that shown by other apparatus reported in the literature.

A scintillation counter with discriminator at 0.1 MeV would entirely eliminate the effect of photoelectric absorption.

e) For apparatus designed as above density will be a unique function of count rate.

f) Three peaks will occur in the pulse height spectrum, the highest energy peak being due to once scattered, the intermediate energy peak to twice scattered and the lowest energy peak to multi-scattered radiation.

g) A change in the angle of scatter will change the energy at the peaks due to once and twice scattered radiation, but will not change the energy at the multi-scattered peak.

h) Improved sensitivity may be obtained by using a scintillation counter set to detect only those pulses under the twice scattered peak. This however leads to a reduction in count rate so that there is little gain in accuracy.

i) Change in Compton scattering factor, due to a change in water content, will have only a small effect on the reading. Nevertheless, some correction may be made for this, if very great accuracy is required, by using equation 2.9.2.(2).

j) Roughness of the surface upon which the apparatus is placed will influence the reading. This adverse effect may be reduced by placing the shield on three legs. The height of the legs giving the least surface roughness effect

may be found from the experimental curve of count rate against height, but the statistical error for a given time of count will then be increased.

k) The radiation dose permitted about the apparatus will depend upon how it is used. A shielding thickness of 1½" of lead will give a dose of less than 5 millirem per hour at the surface of the shield.

l) The effectively infinite depth is inversely proportional to density and is little affected by changes in shield geometry.

For satisfactory service the error due to nuclear statistics should be small enough to give useful information about the concrete, and the errors due to all other causes such as surface roughness, chemical composition and electronic drift should be much smaller than that.

Firstly, it has been shown how the error due to chemical composition may be reduced to a negligible magnitude. Secondly, it is important that the electronic system be reliable. Use may be made of a standard specimen with a correcting manual control or of the count on specimen to count on standard ratio, to correct for small amounts of drift. This ratio may also be used to correct for source decay, provided the background count is low. Thirdly, the error due to surface roughness may, in practice, be of magnitude comparable with the error due to

nuclear statistics, even when legs are fixed to the apparatus. The magnitude of this error depends both upon the design of the shield and condition of the surface.

The results of practical experience are needed before any conclusion may be drawn about whether or not the effects of background radiation will be negligible. It may be noted that the higher the count rate, the higher the background rate which may be neglected.

A calibration curve may be established with blocks of any size, but if the blocks are smaller than the effectively infinite volume then the calibration curve will be valid for that size of block only. The effectively infinite depth will be approximately 4" at 140 lb/cu ft, whatever the source, detector or geometry of the shield, and will be inversely proportional to density. The effectively infinite width will be about 4" at 140 lb/cu ft, and will increase as density decreases. The effectively infinite length will depend upon the position and angles of the collimating holes.

The apparatus will measure the density of a weighted volume of concrete, about 50% of the count being due to the uppermost 1" of concrete. This relatively shallow depth may be a disadvantage in some applications.

The count rate will be higher if a steel bar is present in the concrete "seen" by the detector. On the one

hand care must be taken to avoid such bars if the density is being measured; on the other, the apparatus may be used to locate the bars. Further development, in which readings are taken with some parameter of the source, detector or shield varied, may lead to a method of determining both the size and position of a bar.

The calibration curves are in fact curves of local density against overall density of a block. Due to the heterogeneous nature of concrete the density of the surface layer may differ from the overall density of a specimen. When using this apparatus to measure density, the information required and the information actually obtained must be clearly defined.

For all apparatus used in this project the best standard deviation for a five minute count, due to nuclear statistics only, was about 0.5 lb/cu ft, which corresponded to a 95% chance that the reading obtained was within $\pm$1 lb/cu ft of the true value. This error may be reduced by using a more intense source or longer time of count.

PART 3 THE USE OF GAMMA RADIATION TO MEASURE DENSITY BY TRANSMISSION

CHAPTER 3.1 INTRODUCTION

The simple physical law governing the attenuation of radiation, $I = I_0 e^{-\mu\rho x}$, can be applied by placing a source and detector on each side of a known thickness of concrete the density of which is required. This is called the "transmission method".

Sources used by previous workers have usually been Cs 137 or Co 60 with strengths of up to 60 millicuries. Detectors were usually Geiger-Muller tubes although van Bavel (1957) and (1959), Bernhard and Chasek (1955) and (1956) and Zytowitsch and Ferronski (1960) used sodium iodide scintillation counters, and Skopek (1957) used a thimble chamber and electrometer.

Apparatus was made either for use with concrete specimens (Huyghe and Mortier 1955, Brocard 1954 and 1955, Riessauw and Huyghe 1958, Yakhontov 1958, Zhukov et al 1958, Jurenka 1960, Galambos 1960)or for use on soils when the source and detector were inserted in drilled holes between one and seven feet apart (Bernhard and Chasek 1955 and 1956, Vomocil 1954, van Bavel 1957 and 1959, Durante et al 1957, Dobychin 1958, Skopek 1957, Zytowitsch and Ferronski 1960, Stein 1960) or the source was placed in a hole in a concrete road slab with the detector on the

side face (Smith and Whiffin, 1952).

The maximum thickness of concrete which may be tested depends on the type of detector and the maximum strength of source which may be handled. Smith and Whiffin (1952) estimated this thickness to be three feet, but Bernhard and Chasek (1955) used the method on soil of thickness up to seven feet in the laboratory and four feet on site.

The difficulties experienced in making uniform concrete specimens of known density for calibration have been noted by Brocard (1954) and Jurenka (1960) who weighed cubes in air and paraffin and Smith and Whiffin (1952) who measured cores cut from a road slab.

The vertical spatial resolution of this method has been experimentally determined for the two-probe technique in soil, as shown below.

TABLE 16

Author	Effective vertical dimension "seen"	Distance source to detector
Bernhard and Chasek (1955)	$>$18"	$\geqslant$4 ft
Vomocil (1954)	2"	12"
van Bavel (1959)	12 mm	12"
Zytowitsch and Ferronski (1960)	50 cm	40 to 45 cm

A change in count rate due to chemical composition of the material was found experimentally by Lamb (1955), but Bernhard and Chasek (1955) and van Bavel (1959) found no such effect. Smith and Whiffin (1952) and Vomocil (1954) assumed that it did not exist.

In the analysis of Chapter 3.4 it is shown that spatial resolution and occurrence of the chemical composition effect depend on the relative intensities of scattered and unscattered radiation and whether photons of energy less than 0.1 MeV are detected. If no unscattered radiation were detected true narrow beam conditions would hold and the curve of $\ln(R_o/R)$ against the product of density and thickness would be a straight line of slope 0.077 cm^2/g for a Cs 137 source and 0.058 cm^2/g for a Co 60 source (Grodstein 1957). This perfect narrow beam condition cannot be achieved in practice and the graph of $\ln(R_o/R)$ against density times thickness must be expected in general to be curved, with a slope less than that given above.

Most authors (Smith and Whiffin 1952, Brocard 1954 and 1955, Bernhard and Chasek 1955, Durante et al 1957, van Bavel 1959, Jurenka 1960, Galambos 1960) reported that the curve of log count rate against density was linear over the ranges of thickness and density considered. However Vomocil (1954), van Bavel (1957) and Zytowitsch and Ferronski (1960) showed that if a significant amount

of scattered radiation were detected, the magnitude of the slope of this curve decreased with density.

The relative intensity of scattered radiation may be estimated from comparison of the slopes of the lines $\ln(R_o/R)$ against density times thickness, with the narrow beam values given above. van Bavel (1959) using Cs 137, found a value 0.0608 cm^2/g for the slope. Yakhontov (1958) using Co 60 found that the slope was constant at 0.041 cm^2/g for source detector distances in soil exceeding 20 cm, and Dobychin (1958) reported a constant value of 0.042 $\pm$ .001 cm^2/g at distances exceeding 30 cm. Bernhard and Chasek (1955) reported that for distances exceeding 3 ft the collimators used had no effect on the count rate.

Yakhontov (1958), using a Geiger-Muller detector, showed that for Co 60, lead collimators 8.5 cm long of aperture 8 mm gave a slope of 0.0566 cm^2/g, and for Cs 137 a collimator 6.8 cm long of 8 mm aperture gave a slope of 0.0767 cm^2/g. Very little scattered radiation was then detected, but the apparatus was heavy and the count rate low.

The accuracy claimed by various authors is shown below.

TABLE 17

Author	Stated error	Specimen
Smith and Whiffin (1952)	σ = 0.02 g/cc	Concrete road slab
Brocard (1954)	0.5% to 1%	Concrete
Huyghe and Mortier (1955)	1%	8" concrete cubes
Bernhard and Chasek (1955)	3 lb/ cu ft	Soil in laboratory
do.	5 lb/ cu ft	Soil on site
Bernhard et al (1956)	σ = 2.3%	Soil in laboratory
Dobychin (1958)	2%	Soil
Zhukov (1958)	2%	Soil
van Bavel (1959)	σ = 0.03 g/cc	Soil
Jurenka (1960)	1%	Concrete

σ = standard error

In this investigation apparatus was constructed which detected little scattered radiation. The relation between count rate and density was investigated for concretes of thickness 4" and 6" and densities 1.6 to 2.5 g/cc. A simple mathematical relation was found between count rate and the density, thickness and Compton scattering factor of a specimen and showed that neglect of the chemical composition of the concrete, which defined the Compton scatter-

ing factor, could cause errors of up to about 3%. However, using this mathematical relation accurate correction of the count rate for changes in thickness and chemical composition of the concrete, and statistical treatment of the experimental errors, were possible.

The spatial distribution of radiation in the concrete was investigated showing that a narrow conical volume of concrete was "seen" by the apparatus.

The radiographic examination of structures for voids or steel bars may be considered as a case where the pulse detector is replaced by film sensitive to gamma radiation. The detected intensity is measured with far less precision than the present method as only relative intensities are required. Radiography is not discussed in this thesis.

CHAPTER 3.2 DESIGN OF APPARATUS

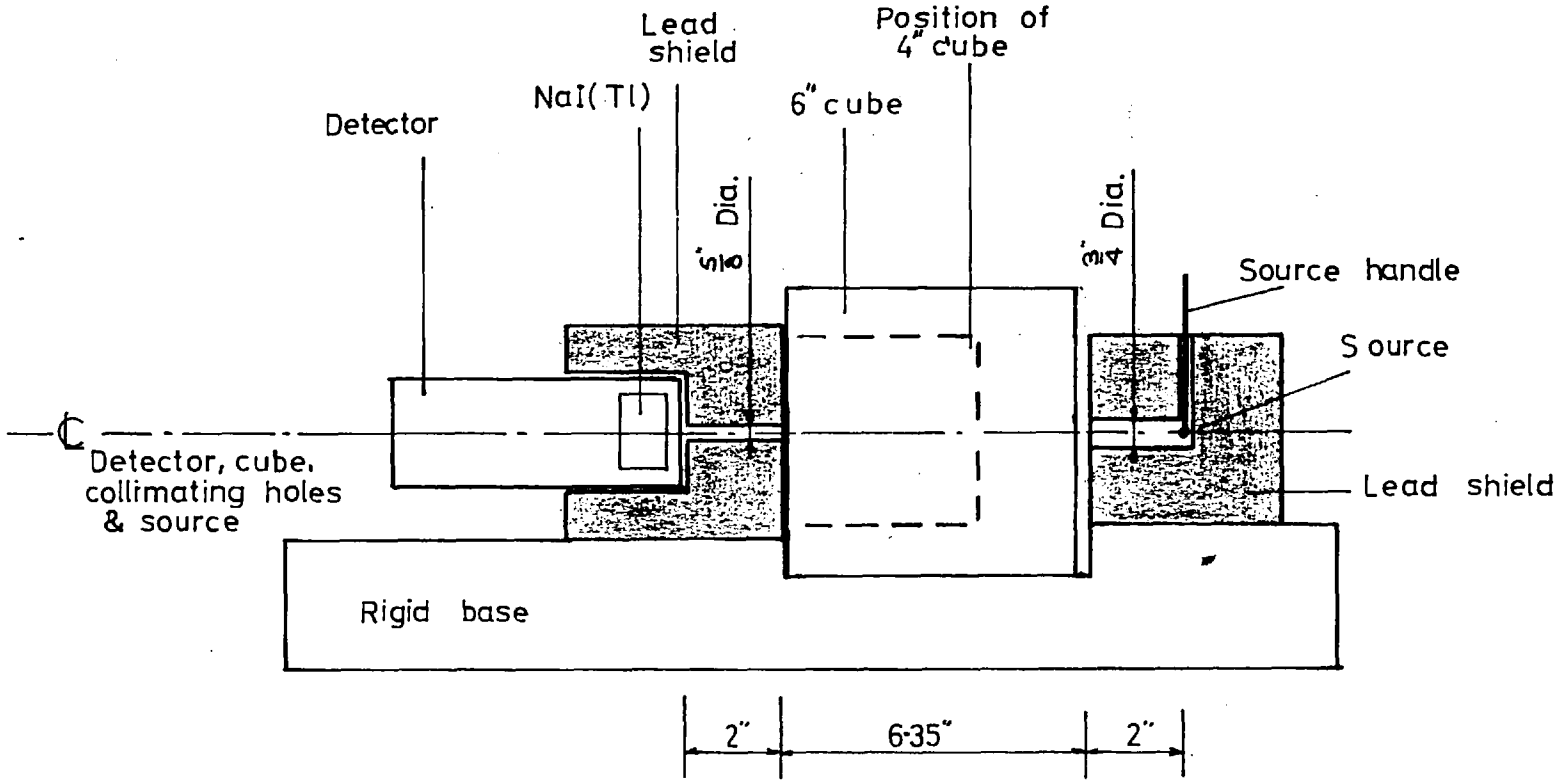
In order for the method to be dependent only on Compton scattering in the concrete, photons below 0.1 MeV had to be eliminated either by using lead collimators or a scintillation counter with appropriate discriminator. Improved collimation led to a lower count rate, so a scinillation counter, which was about 50 times as efficient as a Geiger-Muller tube, was used. With a scintillation counter appropriate selection of a pulse height channel both eliminated low energy photons and gave a

measure of geometrical collimation.

At the source energy of Cs 137, 0.662 MeV, it was shown in Chapter 2.2 that Compton scattering was the only operative process. This relatively low energy is easy to shield and collimate and because the source is mono-energetic may be conveniently used with a pulse height selector covering the source peak, shown in Figure 34. The half life of Cs 137, 33 years, is conveniently long. For all these reasons Cs 137 was chosen, 5 millicuries being used.

Figure 32 shows the arrangement of source, shields and detector used, Figure 33 shows the variation of scattered energy with scattering angle for photons emitted from Cs 137 calculated from equation 2.2.(3), and Figure 34 shows the pulse height spectrum observed on this apparatus with no concrete cube.

The pulse height selector was set to cover the peak due to the 0.662 MeV Cs 137 source photons. In order to minimize the effect of possible drift in the photomultiplier high voltage supply, amplification or discriminator bias, the lower threshold was set at 0.57 MeV, at the valley of the differential bias curve. Figure 33 shows that scattering angle is only weakly dependent on scattered energy for small angles, so that limitation of the angle of scatter by this means would have necessitated setting the lower discriminator at some higher value



THE TRANSMISSION APPARATUS

Scale $\frac{1}{4}$ Fullsize

Fig. 32

SCATTERED ENERGY vs SCATTERING ANGLE

$E_0 = 0.662$ MeV

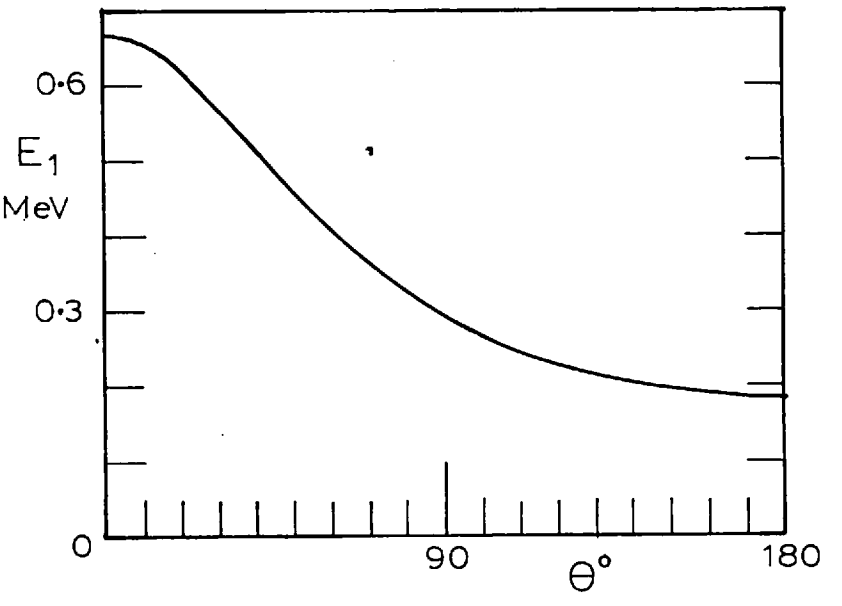


Fig. 33

TYPICAL PULSE HEIGHT SPECTRUM for NaI SCINTILLATION COUNTER

Source Cs137 (·662MeV)

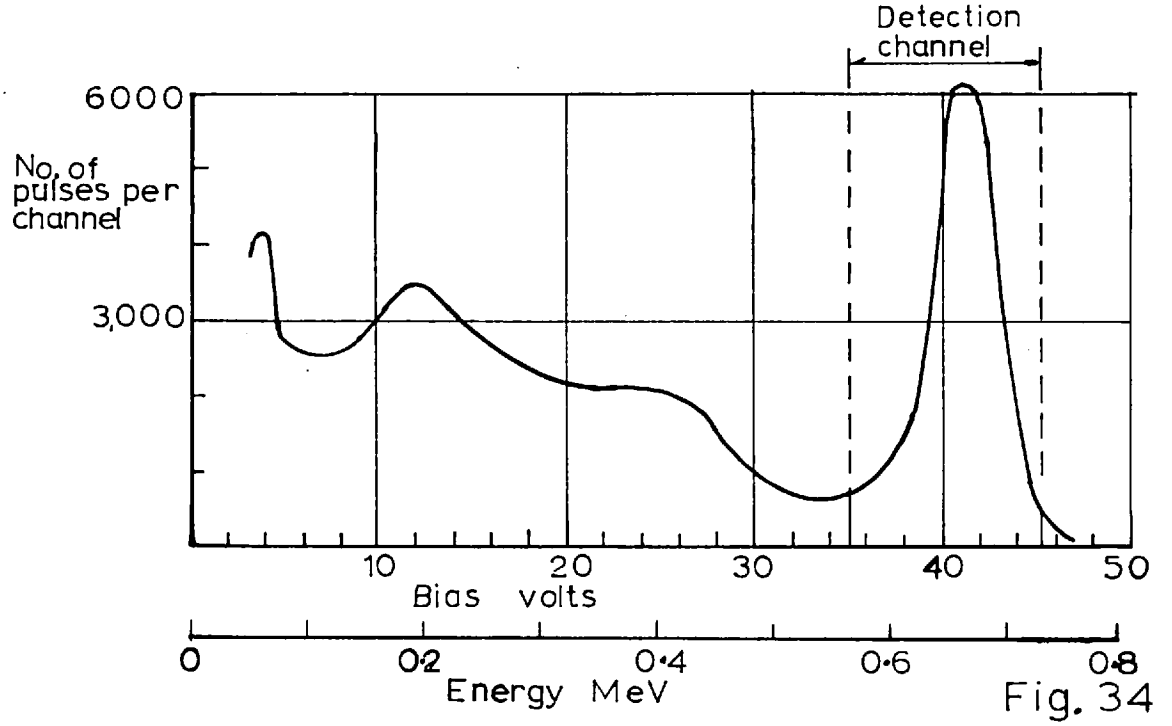


Fig. 34

and the readings would then have been more sensitive to electronic drift. Geometrical collimation was therefore achieved with lead shields, and was designed to give a maximum diameter of 2.2" for the core "seen".

If the detector were capable of detecting low energy scattered photons the effective core "seen" by the apparatus may have extended outside the source and detector beams. However, as used with the pulse height selector, little scattered radiation was detected and the core did not extend beyond the source and detector beams, as was shown experimentally in Chapter 3.3.

The choice of source intensity depended on the resolving time of the detector. For this system 5 millicuries was the upper limit as above this "pile up" of low energy pulses became significant.

CHAPTER 3.3 EXPERIMENTAL CALIBRATION OF THE APPARATUS

Two 4" and two 6" cubes were made from each of the mixes shown in Table 9. From the time of striking the moulds, these were stored under water.

Each cube was placed in the apparatus and the count rate determined in two mutually perpendicular directions, with the hand floated face uppermost, giving four values for each size cube, for each mix. The dimensions of each cube in each direction were measured with a micrometer, and each cube was weighed in air and water to determine

the density. The Compton scattering factor, defined in Chapter 2.2, was calculated for each cube from knowledge of the chemical compositions and proportions of the components.

A count was taken with no concrete in the apparatus. All counts were corrected for pulse resolving time losses and background count.

This information could have been used simply to draw curves of count rate against density for a given thickness, but in order to gain a better understanding of the method the procedure outlined in the next chapters was followed.

The diameter of the core "seen" by the apparatus was determined by moving a 4" mortar cube past the apparatus in steps of 0.1", taking a count at each step. The result is shown in Figure 35 where the broken lines indicate ± 2 standard errors calculated from nuclear statistics only.

The pulse height spectra obtained with 4" and 6" cubes of low and high density in the apparatus, plotted in Figure 36, show differences between the peaks for cubes of different densities which are significant compared with the statistical errors in the counts. This figure shows that with the denser cubes the mean energy of detected photons was lower than with the lighter cubes, on account of the increased proportion of scattered photons detected. The differences between the spectra were, however, small.

THE TRANSMISSION APPARATUS

Determination of the maximum diameter of concrete "seen." by the apparatus.

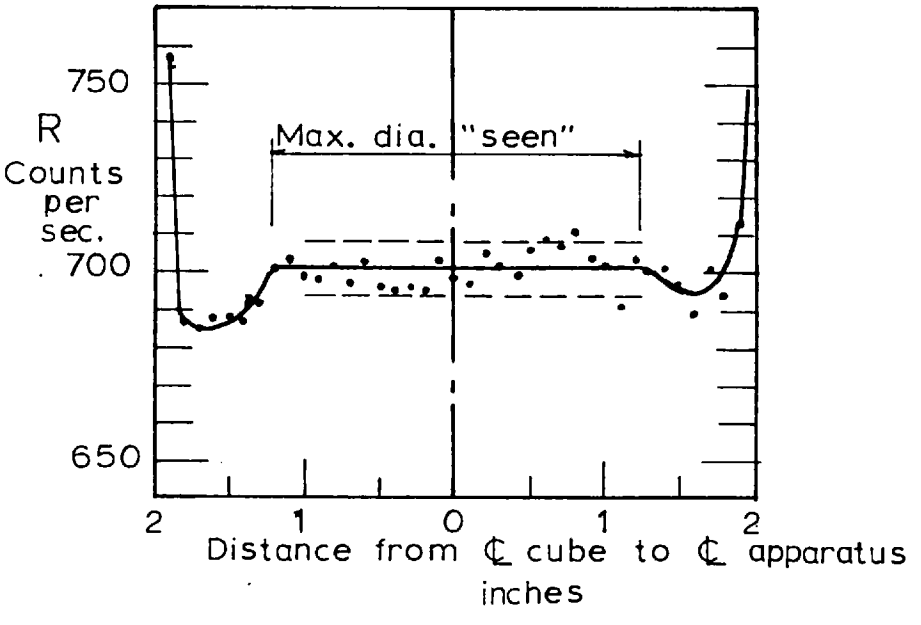


Fig. 35

Pulse Height Spectra Detected with 4" and 6" Cubes of Low and High Densities

Area under peak of low density cube normalized to that of the high density cube in each case.

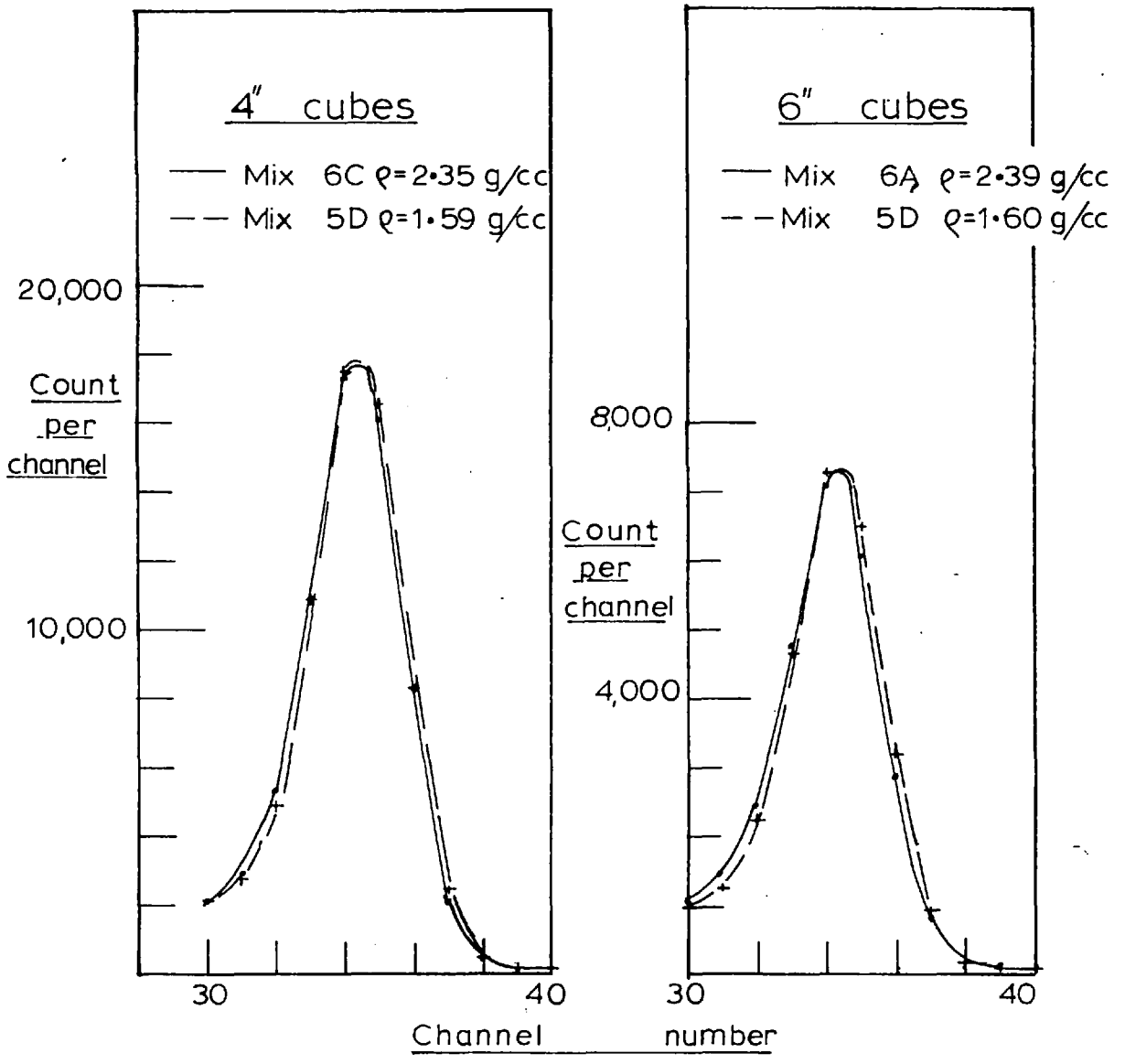


Fig. 36

CHAPTER 3.4 ANALYSIS OF THE APPARATUS

Chapter 3.4.1 The Curve $\ln(R_o/R)$ vs ρ

The total detected intensity comprised both unscattered and scattered radiation

$$I = I_u + I_s \qquad 3.4.1.(1)$$

Assuming that the detector efficiency remained constant over the detection channel.

$$R = \eta I = \eta(I_u + I_s) = R_u + R_s \qquad 3.4.1.(2)$$

The unscattered count rate was then given by

$$R_u = R_o e^{-\Sigma x} = R_o e^{-N_A \rho X \xi x} \qquad 3.4.1.(3)$$

ξ, the Compton cross section for a 0.662 MeV photon is 0.256 barns/electron. Density ρ, Compton scattering factor X and thickness x were determined separately for each cube and R_o was the count rate with no concrete in the apparatus.

A quantity β, the apparent cross section per electron was defined such that

$$R = R_o e^{-N_A \rho X \beta x}$$

$$\text{i.e. } \beta = \frac{\ln(R_o/R)}{N_A \rho X x} \qquad 3.4.1.(4)$$

As R_s was, in general, a function of the density and the thickness of a specimen, β may have been expected to be

dependent on these parameters. Table 18 shows the values of β. These are the averages of the four values obtained for each mix and size of cube.

TABLE 18

Values of the Apparent Cross Section per Electron β

Mix	X	6" Cubes				4" Cubes			
		ρ	R_s/R_u	$\bar{\beta}$	$\bar{\bar{\beta}}$	ρ	R_s/R_u	$\bar{\beta}$	$\bar{\bar{\beta}}$
1A	.5035	2.410	.33	.2307		2.406	.19	.2323	
2A	.5044	2.379	.33	.2305		2.380	.21	.2304	
3A	.5032	2.406	.34	.2300	.2297	2.405	.19	.2322	.2319
5A	.5033	2.376	.32	.2307		2.369	.19	.2320	
6A	.5038	2.379	.40	.2268		2.374	.19	.2325	
1B	.5025	2.440	.36	.2289		2.445	.20	.2323	
2B	.5029	2.404	.33	.2303		2.412	.20	.2311	
3B	.5021	2.420	.33	.2306	.2301	2.432	.22	.2300	.2309
4B	.5024	2.384	.31	.2315		2.396	.19	.2319	
5B	.5020	2.406	.34	.2300		2.415	.21	.2308	
6B	.5027	2.394	.35	.2291		2.414	.22	.2291	
1C	.5035	2.391	.38	.2274		2.351	.20	.2308	
2C	.5041	2.345	.31	.2313		2.349	.20	.2311	
3C	.5033	2.355	.31	.2311	.2297	2.367	.22	.2292	.2307
4C	.5040	2.340	.28	.2331		2.351	.21	.2299	
5C	.5032	2.343	.40	.2252		2.353	.19	.2317	
6C	.5036	2.339	.32	.2303		2.361	.19	.2316	
1D	.5080	1.658	.24	.2288		1.640	.17	.2257	
2D	.5082	1.666	.23	.2302		1.671	.16	.2281	
3D	.5071	1.683	.21	.2316	.2323	1.721	.17	.2266	.2282
4D	.5078	1.663	.22	.2310		1.659	.19	.2226	
5D	.5080	1.600	.18	.2339		1.587	.15	.2286	
6D	.5079	1.586	.14	.2384		1.602	.08	.2413	
1E	.5065	2.209	.26	.2334		2.211	.19	.2307	
2E	.5076	2.208	.26	.2333		2.211	.19	.2311	
3E	.5073	2.192	.27	.2323	.2324	2.192	.17	.2327	.2314
4E	.5075	2.202	.28	.2317		2.203	.19	.2312	
5E	.5064	2.172	.28	.2320		2.180	.18	.2314	
6E	.5072	2.175	.28	.2315		2.174	.18	.2314	

Mean for all 6" cubes = 0.2308
Mean for all 4" cubes = 0.2307
Grand mean = $\bar{\bar{\beta}}$ = 0.2308
Tabulated ρ is the mean of 2 values for each mix.
Values were used separately in the calculations.
$\bar{\beta}$ is the mean of 4 values obtained for each mix.
$\bar{\bar{\beta}}$ is the mean for each type of cube.

The values of $\bar{\beta}$ were divided into ten groups, each group comprising the values from one type of concrete and one size of cube. An analysis of variance, shown in Table 19a, was done to see whether the between-type or between-size variance was significantly greater than the within-group variance. The low values of F found may have been due to the questionable assumption of homogeneity of group variances, but this would not have upset the conclusion that $\bar{\beta}$ was constant. As a further check the differences between the group means and the grand mean were then investigated as shown in Table 19b, where the error of the difference was found assuming that the grand mean $\equiv{\bar{\beta}}$ was known with zero error, thus overestimating the value of t. Nevertheless, only one possibly significant difference was found between the grand mean and the group mean, for the 6" cubes E, but as the density of these cubes lies between those of groups A to C and group D it is reasonable to assume that this was due to chance and that β was constant over the ranges of density, thickness and chemical composition of concrete tested.

STATISTICAL TESTS ON VALUES OF β

TABLE 19a

ANALYSIS OF VARIANCE

Two classes are assumed, being the 5 types A to E and the two sizes of cubes.

	Mean sums of squared errors	Degrees of freedom	Ratio F	5% Level of F
Within groups	6.9×10^{-6}	50	-	
Between types	5.1×10^{-6}	4	0.73	2.56
Between sizes	1.6×10^{-7}	1	0.02	4.03

TABLE 19b

t TEST FOR SIGNIFICANCE OF GROUP MEANS

Group	$\bar{\bar{\beta}} - \bar{\bar{\beta}}$	s	t	p
6" A	.00106	.00168	1.42	.23
6" B	.00072	.00096	1.85	.14
6" C	.00106	.00288	0.90	.40
6" D	-.00153	.00342	1.10	.33
6" E	-.00158	.00081	4.78	<.01
4" A	-.00109	.00084	3.20	.02
4" B	-.00008	.00120	0.16	.87
4" C	.00007	.00100	0.17	.82
4" D	.00197	.00650	0.74	.48
4" E	-.00063	.00068	2.27	.07

$$s^2 = \frac{\sum_n (\bar{\bar{\beta}} - \bar{\beta})^2}{n-1} \qquad t = \frac{(\bar{\bar{\beta}} - \bar{\bar{\beta}})\sqrt{n}}{s}$$

p = the probability of that value of t being exceeded by chance.

Following from this result, if the densities of specimens of various thicknesses and chemical compositions are required a simple correction using equation 3.4.1.(4) is possible and statistical treatment of the errors which assumes a constant value of β in that equation valid.

The concrete specimens used to obtain these values of β covered the range of densities from 1.6 to 2.5 g/cc and the entire practical range of chemical compositions, but thicknesses of only 4" to 6".

Table 4 in Chapter 2.2 showed that the Compton scattering factor, which defines the chemical composition of the concrete, may vary by up to 3%. Neglect of this factor would cause an error of that magnitude in the density.

Rewriting equation 3.4.1.(4), the density is given by

$$\rho = \frac{\ln(R_o/R)}{N_A \beta x X} \qquad 3.4.1.(5)$$

Chapter 3.4.2 Determination of the Relative Intensity of Scattered Radiation

The count rate due to unscattered radiation was calculated from equation 3.4.1.(3) and then the ratio of scattered to unscattered count calculated from equation 3.4.2.(1)

$$\frac{R_s}{R_u} = \frac{R}{R_u} - 1 \qquad 3.4.2.(1)$$

The results are shown in Table 18 where it may be observed that the relative intensity was greater for greater thickness or density of specimen, agreeing with the observations of the pulse height spectra in Figure 36.

The intensity of once scattered radiation was calculated theoretically as follows.

For an isotropic source of 4π photons/sec, the count rate due to uncollided photons

$$R_u = \eta \frac{\pi g^2}{a^2} e^{-\Sigma_o c} \qquad 3.4.2.(2)$$

where g, a and c are shown in Figure 37 and Σ_o is the total collision cross section for source photons in the concrete.

Adopting an approach similar to that of Chapter 2.9.1 an equation for the count rate due to once scattered photons was derived (see Appendix C)

$$R = 2\pi\eta \int_{0}^{\alpha_o \text{ max.}} \int_{r_o \text{ min.}}^{r_o \text{ max.}} \zeta(\theta)\Omega N_A \rho X \sin\alpha_o \, e^{-N_A \rho X(\xi_o r_o + \xi_1 r_1)} dr_o d\alpha_o \qquad 3.4.2.(3)$$

where $\zeta(\theta)\Omega$ is the cross section per electron for scattering through angle θ into solid angle Ω, and ξ_o and ξ_1 are the total Compton cross sections per electron before and after collision. The limits of α_o and r_o were determined by the size of the specimen tested and the holes in the source and detector shields.

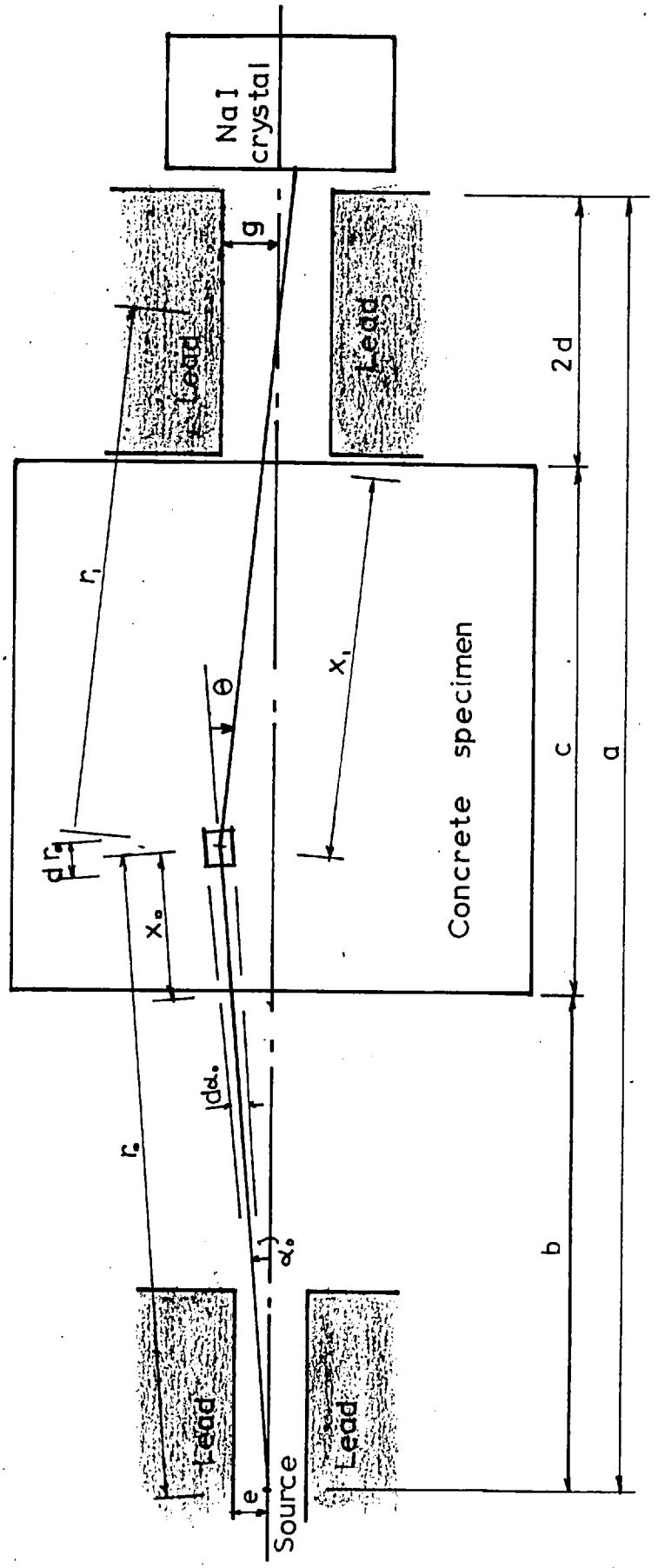

NaI crystal
Lead
Lead
Lead
Lead
Source
Concrete specimen
g
2d
c
a
b
e
θ
r_1
x_1
x_0
dr_0
r_0
dx_0
r
α_0

Fig.37

Similar equations may have been written for twice and more scattered photons but the solution required extensive computation.

Equation 3.4.2.(3) in differential form, gave the count due to photons scattering within a differential volume at (α_o, r_o). This was integrated for various densities and sizes of cube. The apparent cross section β and the ratio R_s/R_u were calculated and are shown in Table 20.

TABLE 20

Values of β and R_s/R_u obtained by considering only once scattered photons

Density ρ	Scattering factor X	Concrete thickness	β Theoretical	R_s/R_u Theoretical	R_s/R_u From expt.	Difference in R_s/R_u due to multiple scattering
2.4	0.5	4"	0.2353	0.108	0.20	0.09
2.2	0.5	4"	0.2352	0.099	0.18	0.08
1.6	0.5	4"	0.2349	0.073	0.16	0.09
2.4	0.5	6"	0.2358	0.160	0.34	0.18
2.2	0.5	6"	0.2357	0.147	0.27	0.12
1.6	0.5	6"	0.2353	0.108	0.20	0.09

These results show that about 10% of the count was due to once scattered photons, so about 10% must have been due to twice and many scattered photons.

Chapter 3.4.3 Determination of the Spatial Distribution of Radiation within the Specimen

It can be shown from the ratios R_s/R_u in Table 18 that between 75% and 90% of the detected beam was unscattered and therefore passed only through the cone defined by the holes in the source and detector shields. About half the scattered radiation was once scattered. By considering the cube divided into a three dimensional mesh the count rate due to the once scattered photons scattering within each small volume was calculated, giving some idea of the distribution of radiation in the cube. These values, shown in Table 21, are the number of photons scattering per second from a ring 1.016 cm square in section at the position shown, into the detector, for a source of $10^6/\eta$ photons/steradian second.

TABLE 21

Theoretical Spatial Distribution of Once Scattered Photons in Typical Concrete Cubes for a Source of $10^6/\eta$ Photons/ster sec.

10 x 1.016 cm = 4"

5 x 1.016cm = 2"										
	0	0	0	0	0	0	0	0	0	0
	0	0	0	0	0	0	0	0	0	0
	0	0	1.2	0.6	0	0	0	0	0	0
	3.7	3.5	3.4	3.3	3.1	2.8	2.2	0.4	0	0
	1.9	1.9	1.9	1.9	2.0	2.2	2.4	2.7	3.2	4.0

℄

Source end — cube and apparatus

Parameters ρ = 2.4 g/cc, X = 0.5, c = 4"

10 x 1.016 cm = 4"

5 x1.016cm = 2"										
	0	0	0	0	0	0	0	0	0	0
	0	0	0	0	0	0	0	0	0	0
	0	0	1.5	0.7	0	0	0	0	0	0
	4.7	4.5	4.3	4.1	3.9	3.6	2.8	0.5	0	0
	2.4	2.3	2.3	2.4	2.5	2.7	3.0	3.4	4.0	5.0

℄

Source end — cube and apparatus

Parameters ρ = 1.6 g/cc, X = 0.5, c = 4"

TABLE 21 (Cont.)

Theoretical Spatial Distribution of Once Scattered Photons in Typical Concrete Cubes for Source of $10^6/\eta$ Photons/ster sec.

15 x 1.016 cm = 6"

7 x 1.016cm=2.8"

0	0	0	0	0	0	0	0	0	0	0	0	0	0	0
0	0	0	0	0	0	0	0	0	0	0	0	0	0	0
0	0	0	0	0	0	0	0	0	0	0	0	0	0	0
0	0	0	0	0	0	0	0	0	0	0	0	0	0	0
0	0	0	0	0	0	0	0.5	0.2	0	0	0	0	0	0
0	0	1.8	1.7	1.5	1.4	1.4	1.3	1.3	1.2	1.1	0.9	0.2	0	0
1.3	1.1	0.9	0.9	0.8	0.8	0.7	0.7	0.7	0.7	0.8	0.9	1.1	1.3	1.6

℄ Cube and apparatus

Source end

Parameters = 2.4 g/cc, X = 0.5, c = 6"

15 x 1.016 cm = 6"

7x1.016cm=2.8"

0	0	0	0	0	0	0	0	0	0	0	0	0	0	0
0	0	0	0	0	0	0	0	0	0	0	0	0	0	0
0	0	0	0	0	0	0	0	0	0	0	0	0	0	0
0	0	0	0	0	0	0	0	0	0	0	0	0	0	0
0	0	0	0	0	0	0	0.8	0.4	0	0	0	0	0	0
0	0	3.2	2.9	2.7	2.5	2.4	2.3	2.2	2.1	1.9	1.5	0.3	0	0
2.2	1.9	1.6	1.5	1.4	1.3	1.3	1.3	1.3	1.3	1.4	1.6	1.8	2.2	2.7

℄ Cube and apparatus

Source end

Parameters = 1.6 c/cc, X = 0.5, c = 6"

The spatial distribution of the twice scattered photons was considered. Every photon made its first scatter within the cone defined by the source shield. If it was twice scattered and then detected, the second scatter must have been within the detection cone. If, after the first collision the photon scattered back so as to leave the volume defined by the source cone, its energy after the second scatter would have dropped to below the discriminator threshold. A twice scattered detected photon must therefore have remained within the source and detected cones. Similar reasoning showed that the probability that a three or more times scattered photon left the cones and then re-entered and was detected, was small.

The radius of circle of intersection of the cones was 1.1". The radius of the core of concrete "seen" by the apparatus was found from the curve of Figure 35 to be between 1.1" and 1.25", confirming the above discussion.

Chapter 3.4.4 Analysis of Errors

Equation 3.4.1.(5) gave the relation between count rate, density and the other variables. From this the relation between the errors in the variables was obtained by the laws of combination of errors

$$\left(\frac{\sigma_\rho}{\rho}\right)^2 = \left(\frac{\sigma_x}{x}\right)^2 + \left(\frac{\sigma_X}{X}\right)^2 + \left(\frac{\sigma_\beta}{\beta}\right)^2 + \frac{1}{(N_A \rho X x \beta)^2}\left[\left(\frac{\sigma_R}{R}\right)^2 + \left(\frac{\sigma_{R_o}}{R_o}\right)^2\right] \qquad 3.4.4.(1)$$

β and R_o are determined for apparatus at the time of calibration, x is determined by measuring a specimen and X calculated from knowledge of the chemical composition of the concrete.

If the apparatus is very accurately calibrated

$$\frac{\sigma_\beta}{\beta} \doteq 0 \quad \text{and} \quad \frac{\sigma_{R_o}}{R_o} \doteq 0$$

Because X depends primarily upon the hydrogen, and therefore water content, of a concrete, normal chemical analyses of cements or aggregate which may have a closure error of 2% are sufficiently accurate for calculating this factor. With conventional engineering equipment, such as a micrometer, it is possible to measure x to 0.1% for a well made specimen. A micrometer may be permanently incorporated in apparatus for this purpose.

If a scaler-timer is used to determine count rate, $\frac{\sigma_R}{R} = \frac{1}{\sqrt{N}}$.

The apparatus measured the density of a well defined core of concrete, as shown in Chapter 3.4.3, but was calibrated against overall density of a cube. A difference between the local and overall densities appeared as error in the calibrated value of β. This led to a method of measuring uniformity of concrete described in the next chapter.

CHAPTER 3.5 USE OF THE METHOD

Chapter 3.5.1 To Measure Uniformity of a Concrete Specimen

Because the aggregate and mortar will be evenly distributed throughout a perfectly uniform concrete specimen, the uniformity of one or more specimens may be defined thus:-

If cores are cut from one or more specimens, each core being reasonably long compared with the maximum size of aggregate, the concrete is perfectly uniform if the overall densities of the cores are equal.

For each mix and type of cube four values of β were determined from equation 3.4.1.(4). If the concrete were perfectly uniform the standard error of β would have been given by

$$\left(\frac{\sigma_\beta}{\beta}\right)^2 = \left(\frac{\sigma_w}{w}\right)^2 + \left(\frac{\sigma_x}{X}\right)^2 + \left(\frac{\sigma_\rho}{\rho}\right)^2 + \frac{1}{(N_A \rho X \times \beta)^2}\left[\left(\frac{\sigma_R}{R}\right)^2 + \left(\frac{\sigma_{R_0}}{R_0}\right)^2\right] \qquad 3.5.1.(1)$$

Assuming β to be a normal variate, the ratio $\frac{\sum_n(\bar{\beta}-\beta_i)^2}{\sigma_\beta^2}$ would be distributed as a χ^2 with n-1 degrees of freedom, where σ_β^2 is calculated from 3.5.1.(1) and $\bar{\beta}$ is the mean of the n determinations of β_i.

In this work n = 4 and the following values were used:

$$\sigma_x = 0.002"$$

$$\frac{\sigma_\rho}{\rho} = 0.15\% \text{ for } 6" \text{ cubes}$$

$$= 0.30\% \text{ for } 4" \text{ cubes}$$

$$\sigma_x = 0$$

$$\frac{\sigma_R}{R} = 0.5\% \text{ because } N = 4 \times 10^4 \text{ count}$$

The estimates of errors σ_x and σ_ρ were based on experience in measuring the thickness and density of cubes in these experiments.

For each mix and size of cube the ratio was calculated and from χ^2 tables the probability derived that the four readings were obtained from a perfectly uniform mix. This is shown in Table 22.

TABLE 22

MEASUREMENT OF UNIFORMITY

Mix	6" Cubes			4" Cubes		
	σ_β	χ^2	p	σ_β	χ^2	p
1A	.0006	1.17	.77	.0042	0.64	.88
2A	.0018	10.80	.01	.0001	0.05	>.99
3A	.0009	2.88	.42	.0011	4.20	.25
5A	.0012	5.16	.13	.0016	9.41	.03
6A	.0039	53.3	<.01	.0017	10.50	.02
1B	.0009	2.76	.44	.0007	1.72	.64
2B	.0014	7.06	.07	.0013	6.65	.08
3B	.0007	1.60	.67	.0004	0.61	.89
4B	.0011	4.24	.24	.0008	2.64	.50
5B	.0013	5.56	.13	.0005	1.00	.81
6B	.0005	0.93	.82	.0012	5.45	.14
1C	.0023	17.60	<.01	.0013	6.36	.09
2C	.0017	9.85	.02	.0019	13.44	<.01
3C	.0008	2.32	.52	.0006	1.30	.74
4C	.0014	7.00	.07	.0009	3.01	.30
5C	.0026	22.60	<.01	.0010	3.24	.36
6C	.0019	12.20	<.01	.0006	1.20	.77
1D	.0044	36.4	<.01	.0032	26.8	<.01
2D	.0063	73.3	<.01	.0016	6.38	.09
3D	.0051	47.0	<.01	.0042	45.0	<.01
4D	.0027	13.8	<.01	.0065	107.8	<.01
5D	.0048	41.5	<.01	.0018	8.50	.04
6D	.0028	14.0	<.01	.0043	48.2	<.01
1E	.0018	10.00	.02	.0005	0.86	.84
2E	.0007	1.42	.70	.0003	0.40	.93
3E	.0005	0.80	.85	.0004	0.52	.90
4E	.0002	0.17	.97	.0006	1.21	.76
5E	.0007	1.57	.58	.0002	0.20	.97
6E	.0011	3.80	.28	.0006	1.34	.73

$$\sigma_\beta^2 = \frac{\sum_1^4 (\bar{\beta} - \beta_i)^2}{3}$$

$$\chi^2 = \frac{\sigma^2}{\sigma^2_{\text{expected}}}$$

p = probability that the readings were obtained from perfectly uniform specimens.

This was not an absolute measure of that probability because few values of β were used and because it depended upon the values of errors used in the right hand side of equation 3.5.1.(1), but future experience in developing the method should show the range of errors acceptable.

The method may be generalized as follows. If it is desired to measure the uniformity of one specimen the density is measured by conventional means and n readings of count rate R and thickness x taken. The n values of β are calculated using equation 3.4.1.(4) and from these $\bar{\beta}$ and the χ^2 ratio obtained, giving a value of probability from χ^2 tables. As the Compton scattering factor X will not vary from one reading to another a nominal value may be assumed. This will produce an error in the value of $\bar{\beta}$ but will not change the sum of squares in the numerator of the ratio. In calculating the expected error from equation 3.5.1.(1) it may be assumed that there is no error in ρ, X or R.

When comparing the uniformities of batches comprising many specimens, X and ρ must be determined for each specimen and values of the errors in determining x, X, ρ and R must be considered when calculating the expected error, in order that the values of χ^2 found will be due only to non-uniformity of the density distribution in the concrete.

To facilitate calculation of the Compton scattering factor X for concretes, this factor is listed in Table 23

for various aggregates, cement and water. The value of X for a concrete will be given by

$$X = \frac{\sum_n G_i X_i}{\sum_n G_i} \qquad 3.5.1.(2)$$

where G_i and X_i are the mass fraction and Compton scattering factor for the n components of the concrete, which will be water, cement and one or more aggregates.

TABLE 23

The Compton Scattering Factor X for Typical Aggregates, Cement and Water

Item	X	Reference for Chemical Analysis
Granite	0.4949	(a) of Table 1
Granite	0.4957	(c) of Table 1
Basalt	0.4989	(b) of Table 1
Limestone	0.4995	(d) of Table 1
Hornsfels	0.4944	(e) of Table 1
Thames River Sand	0.4989	Special Analysis
Ordinary Portland Cement	0.4992	As Table 1
Water	0.5551	

Chapter 3.5.2 To Measure Density of Concrete

Apparatus suitable for measuring the density of hardened laboratory specimens or fresh concrete in laboratory moulds was made. Experience in setting up this apparatus showed

that although good quality laboratory equipment was used drift of the electronic system was significant, and that scatter of readings due to non-uniformity of the concrete specimens affected significantly the accuracy of the calibration.

Dealing with the latter point first, it is recommended that in calibrating the apparatus concrete containing coarse aggregate should not be used. Suitable materials would be aluminium, glass, perspex, carefully made specimens of mortar concrete, or similar materials. The calibration may then be done taking long counts and with sufficient care that $\frac{\sigma_\rho}{\rho}$ and $\frac{\sigma_{R_o}}{R_o}$ in equation 3.4.4.(1) may be neglected.

When determining the density of an unknown specimen the accuracies attainable in x and X are $\frac{\sigma_x}{x} = 0.001$ by using a conventional engineering micrometer and $\frac{\sigma_x}{X} = 0.002$ by calculating from ordinary chemical analysis of the constituents as used for Table 23. If the count rate is determined from a scaler-timer, then with $N = 4 \times 10^4$ counts, which here took $\frac{1}{2}$ minute on 4" cubes and 1 minute on 6" cubes, the error in density from equation 3.4.4.(1) is

$\frac{\sigma_\rho}{\rho} = 0.004$ for 4" cubes of density 2.4 g/cc

$= 0.003$ for 6" cubes of density 2.4 g/cc

Improvements in this would be possible by taking a longer count and by improving the accuracy of the determination of x and X but would probably not be realistic

as the error due to non-uniformity of a specimen would give errors of this order. A better procedure would be to take a number of readings of density at various points, and use the mean of these.

The drift of the apparatus may be checked using the value of R_o with no concrete in the apparatus. The value of R_o at any time after calibration should be $R_o = R_{oc}e^{-\lambda t}$ . . . where R_{oc} is the value of R_o at the time of calibration. When the apparatus has warmed up R_o can be brought to this value by adjustment of the pulse height selector.

The effect of source decay must be allowed for either by applying a correction $e^{\lambda t}$ to the count rate or by using different calibration curves as time proceeds.

If a ratemeter is used instead of a scaler-timer, both drift and source decay may be allowed for as follows. The reading of R_o at the time of calibration is balanced against a stable potential obtained, for instance, from a standard cell. In subsequent use, when the apparatus has warmed up, the value of R_o is balanced against the calibrated potential by means of a variable resistor in the ratemeter circuit. This applies a scale factor to the count rate R so that the ratemeter will read in units as calibrated. The scale factor will alter the error due to nuclear statistics, but as the half life of Cs 137

is 33 years, and because drift should cause only a small change in count rate, the change in error should, in practice, be very small.

CHAPTER 3.6 CONCLUSIONS

Apparatus for measuring density by the transmission method can, with the use of a scintillation counting system, a Cs 137 source and lead collimators, be made to give good spatial resolution and accuracy adequate for the needs of concrete technology.

Statistical tests showed that the apparent cross section per electron, β, was constant over the range of concrete specimens tested, making possible accurate correction to the count rate for the effects of thickness and chemical composition and validating statistical tests for the uniformity of concrete. The value of $\bar{\beta}$, 0.2308 barns/electron, corresponded to a value of 0.0695 cm^2/g for the slope of the curve $\ln(R_o/R)$ against the product of density and thickness. This may be compared with the values obtained by other authors and reported in Chapter 3.1. The range over which β was found to be constant included all practical chemical compositions, densities from 1.6 to 2.5 g/cc and thickness of 4" to 6".

The accuracy required in determining the thickness and Compton scattering factor may be achieved by simple

techniques and using these values an accuracy in the density measurement of 0.5%, which is two standard errors, is easily achievable. At this order of accuracy, however, the heterogeneity of the concrete itself becomes significant, so more accurate density determinations may be meaningless unless correctly interpreted.

The source and detector must be accurately held in the same position relative to each other. This may be achieved by attaching both to a U frame which may be placed around a member to be tested. In practice this would mean that only laboratory specimens, beams, columns and other members small enough to fit within the U frame may be tested.

The effect of the position of the concrete in the apparatus, defined by dimension 'b' of Figure 37, would be small on account of the small proportion of scattered radiation detected. There is however no reason why the specimens tested should not be placed in a standard position in the apparatus, and this should be done in practice.

In general, the background count rate must be allowed for, but if the scintillation counter is used over the Cs 137 peak and the detector shielded, as in this investigation, that count will be small and may well be negligible in practice.

With an adequately shielded source the only hazard to health would be in the region directly in front of the source shield. With correct procedure it is never necessary

for the hands to be in this region, but a mechanism whereby a specimen is placed on a movable platform away from the source and then moved into position, is advisable. The dose scattered from a 6" concrete cube in the apparatus described here was measured and found to be less than 2.5 millirad per hour and was therefore tolerable.

This method may be used both on hardened specimens and fresh concrete in the forms. In the latter case calibration would have to be done with the forms in the apparatus. If no scattered radiation were detected the effect of formwork would be uniquely defined by the product of the total thickness, the Compton scattering factor and the density of the formwork "seen" by the apparatus. In that case R_o, but not β, would be affected by the presence of forms. As apparatus is in fact designed to detect little scattered radiation and because the forms are thin relative to the concrete that product will probably be the only parameter required to define the effect of formwork on the count rate. If that is so, R_o and β, which define the calibration curve, need be found experimentally only as a function of that parameter of the formwork. Timber formwork containing fresh concrete may absorb moisture and change its density, thus upsetting the calibration for timber moulds.

Neither the effect offorms nor the effect of concrete of thickness greater than 6" on the apparent cross section

per electron, β , has been investigated. This deserves further study.

If the apparatus "sees" a steel bar the count rate would decrease because steel is denser than concrete. This may be used to locate steel bars by moving the apparatus across a member and observing the count rate, and should give accurate results because of the good spatial resolution of the apparatus.

The specimens used for calibration must themselves be uniform and of accurately known density. When using the apparatus subsequently, care must be taken to correct the count rate for electronic drift and source decay. Accurate calibration is possible whatever the dependence of the apparent cross section per electron β on density and specimen size but in the range where β may be taken as constant, log of count rate varies linearly with density, thickness or Compton scattering factor so that fewer specimens are needed to establish the curve.

If a relation can be found between the uniformity of specimens as found with this method and the scatter in other properties of concrete, then this method will provide a measure of the error in those experimentally determined properties, due to the heterogeneous nature of the concrete.

PART 4 THE USE OF NEUTRON RADIATION TO MEASURE THE WATER CONTENT OF CONCRETE

CHAPTER 4.1 INTRODUCTION

Neutron radiation methods, which determine the total mass of water per unit volume of a material, have been more extensively used on soils than on concretes. As will be shown in Chapter 4.2 the chemical structure of the concrete must be expected to influence the reading with a particular piece of apparatus, so that results obtained on soils may not be entirely valid on concrete. However, some useful information about the method may be obtained from reports dealing with soils so these are first discussed, then their application on concrete described. This review deals mainly with surface instruments but the results obtained on probes are quoted where useful.

Use of soils

Sources used have been radium-beryllium, polonium-beryllium, radium D-beryllium and americium-beryllium. Detectors used included foils with Geiger-Muller tubes, boron lined counters, zinc sulphide and boron scintillators, lithium iodide scintillators and in most more recent work boron trifluoride tubes. The response of the detector to gamma radiation was a problem with some detectors (Roy and Winterkorn 1957).

There has been no systematic analysis, for surface

instruments, of the optimum distance from source to detector. The source was usually placed as near as possible to the detector, taking into account the need for lead shielding with gamma sensitive detectors.

The calibration curve of count rate against density of water in mass per unit volume, d', was usually a straight line, or very close to straight (Kuranz 1959, Neville and van Zelst 1960, Carlton 1960, Gnaedinger 1960, Carey et al 1960, Huet 1961 and 1962).

Holmes (1956), neglecting all elements other than hydrogen, applied the Fermi age equation for plane geometry to a probe with a boron trifluoride detector and found good agreement with experiment. This equation was applied by Huet (1962) to both probes and surface instruments, and by Dobychin (1958) to an unspecified instrument which was apparently a probe.

The chemical composition of the soil may have affected the count rate either by change of scattering cross section due to chemical or crystalline bonding or by a change in absorption cross section due to boron, lithium, chlorine or other strong neutron absorbers. Burn (1963) using a probe with an actinium-beryllium source and lithium iodide scintillator observed discrepancies of 11% between the calibrated count and the count observed on a site clay. After investigation this was attributed to 7% iron in the clay. Dobychin (1958) using a silver foil detector found

that both the mineralogical composition of the soil and the presence of absorbers affected the count rate. Gnaedinger (1960) and Mintzer (1960) also found an effect of the type of soil but van Bavel et al (1956), Carey et al (1960) and Huet (1961 and 1962) found no such effect for the soils used. In general it must be assumed that the chemistry of the soil may affect the results and it will be shown in Chapter 4.3 how this may occur.

The effective depth of penetration of a surface gauge was found by various authors as shown below.

TABLE 24

Author	Depth
Belcher et al (1952)	$\not>$ 6"
van Bavel et al (1956)	$6(d')^{-\frac{1}{3}}$ inches (see below)
Kuranz (1959)	5" to 16"
Neville and van Zelst (1960)	6"
Huet (1962)	$4.5(d')^{-\frac{1}{3}}$ inches (see below)

van Bavel et al (1956) neglecting all elements except hydrogen and assuming spherical symmetry proposed the cubic function shown above. The relation between depth and water density is discussed in Chapter 4.5.3. The horizontal area required depended upon the geometry and charact-

eristics of each instrument and the water content of the material. van Bavel et al (1956), using radium-beryllium and a boron lined counter 12" long by 1½" dia. separated by distances up to 10 cm, found that on a "dry" soil a plan area of 1500 cm^2 (approximately 15" square) was sufficient.

The accuracies reported by various authors are shown below.

TABLE 25

Author	Stated Accuracy
Belcher et al (1952)	1 lb/cu ft
van Bavel et al (1956)	σ = 1%
Kuranz (1959)	0.5 lb/cu ft
Carlton (1960)	σ = 0.9 lb/cu ft
Gnaedinger (1960)	2%

Whether on site or in the laboratory, the instrument readings were calibrated against water density found by drying and by conventional replacement or volumeter methods. Kuhn (1960) after statistical analysis of the instrument readings compared with sand replacement and oven drying tests, concluded that the nuclear method was at least as accurate as the conventional method.

When calibrating an instrument, a number of uniform specimens of soil of known water content were required. In sands at low water contents, water concentrated in local pockets and at high water contents drained under gravity. Burn (1960 and 1963) conducted a thorough investigation into the use of substitute hydrogeneous materials and inorganic materials other than sand. He used calgon water solutions for high water contents, bentonite, sand and water mixtures for medium water contents and dextrose, sand and water mixtures for low water contents, but difficulty was experienced in placing the last uniformly. Huet (1962) used mixtures of ammonium aluminium sulphate and sand.

Instruments were usually checked by taking a count on a standard specimen which was most often paraffin wax. In order to overcome the effects of electronic drift or source decay Kuranz (1959), Neville and van Zelst (1960) and Huet (1961 and 1963) used the ratio of count on specimen to count on standard instead of count rate.

Lauchaud (1962) tried a transmission method for determining the water content of soil specimens 20 mm thick. From the thermal source, which was radium-beryllium in wax, the neutrons passed through the specimen and into a boron trifluoride counter. The count rate thus detected was a function both of overall density and water density, so

calibration against dry specimens was first necessary, and the difference in count between wet and dry specimens used. The method gave large errors.

Use on concrete

Brocard (1954) constructed a cylindrical cadmium-indium-cadmium sandwich 28 cm long by 2.8 cm diameter. The cylinder with a radium-beryllium source within was placed in a hole in the concrete. He established a calibration curve on alum powder mixtures. As the process of moving the indium to a Geiger-Muller counter was tedious, he replaced the foil by a boron trifluoride counter (Brocard 1955).

Huyghe and Mortier (1955), Mortier and Huyghe (1955) and Riessauw and Huyghe (1958) used a radium-beryllium source with indium or silver foils and with a boron trifluoride counter on the surface of various concretes. Initial investigations showed the half life of indium to be too long, and because the half life of the silver β activity was 2.44 minutes they attempted to measure the saturation activity with a Geiger-Muller detector, with the source, 25 millicuries radium-beryllium, 12.5 cm from the detector. The β activity was masked by the intense radium activity detected. They then used a boron trifluoride detector. The calibration curve was a straight line.

Yaltakaya and Senturk (1962) used the neutron water content method as an indirect method for determining the cement content of concrete by assuming that the bound water content was proportional to the cement content. They constructed a steel container 216 mm high by 143 mm diameter and in a central tube 27 mm diameter placed a 1 curie polonium-beryllium source and a boron trifluoride counter. Concrete was dried, powdered and placed in the cylinder so that the count rate gave a measure of cement content. The accuracy of the apparatus was fairly good.

Pawliw and Spinks (1957) used 50 millicuries of radium-beryllium and a boron trifluoride counter 0.75" diameter by 4" effective length on concrete. The source was next to the detector and both were covered with a 1" steel reflector which increased the count rate by a factor of 2.35. The effectively infinite depth, determined with mixtures of sugar and sand, varied from 4" for water to 8" for an equivalent water density of 0.135 g/cc. When the source was on the centre line of a cylindrical container the minimum radius required varied from 4" for water to 10" at an equivalent water density of 0.135 g/cc.

They established a calibration curve on a concrete cylinder 8.75" high by 18" diameter. Readings on water and on concrete were taken, the concrete weighed and dried at 130°F, another pair of readings taken, and so on until

all the evaporable water was removed, when it was heated to 1000°C to determine the total water content. The curve of the ratio count on concrete to count on water against water density in g/cc was found to be a straight line, to which was fitted the equation of Holmes (1956). This was

$$r = d'F \qquad 4.1.(1)$$

where r is the ratio count on concrete to count on water, d' is the density of water in g/cc of concrete and

$$F = \frac{e^{-(\bar{r}/L)d'}\left[1-\operatorname{erf}\left(\frac{L_s}{L}-\frac{\bar{r}\,d'}{2L_s}\right)\right]+e^{(\bar{r}/L)d'}\left[1-\operatorname{erf}\left(\frac{L_s}{L}+\frac{\bar{r}\,d'}{2L_s}\right)\right]}{e^{-(\bar{r}/L)}\left[1-\operatorname{erf}\left(\frac{L_s}{L}-\frac{\bar{r}}{2L_s}\right)\right]+e^{(\bar{r}/L)}\left[1-\operatorname{erf}\left(\frac{L_s}{L}+\frac{\bar{r}}{2L_s}\right)\right]} \qquad 4.1.(2)$$

When L_s, the slowing down length in water was 6.80 cm and L, the diffusion length 2.88 cm $\bar{r}$, the effective distance source to detector, was found by fitting the function to the experimental line to be 3 cm.

Comparatively little work has been done with the neutron scattering method on concretes. No investigation has been reported of how nuclear processes other than scattering by hydrogen may affect the apparatus reading although experience on soils showed that the presence of an absorber such as iron or chlorine could upset the reading.

In the chapters following the various processes which may have an effect on the count rate are discussed. It is

shown how the effect of absorbers or chemical bonding of the hydrogen may be eliminated by using a cadmium covered detector and various experimental assemblies employing this principle were tested. For a system where source and detector are on one face of a specimen the source, detector and geometry giving a count rate least dependent on perturbing processes and giving the most accurate reading of water content in a given time, was determined.

CHAPTER 4.2 DESCRIPTION OF THE RELEVANT NUCLEAR PROCESSES

a) Elastic scattering

When a neutron collides with an atomic nucleus by elastic scatter, kinetic energy and momentum are conserved. In collisions between light or medium atomic weight materials and neutrons of energy up to approximately 10 $A^{-\frac{2}{3}}$ MeV (Price et al, 1957), the angular momentum of the incident neutron may be neglected so the scattering will be isotropic in the centre of mass system.

From conservation of kinetic energy and momentum the ratio of the energy after collision E_1 to the energy before collision E_o is given by

$$\frac{E_1}{E_o} = \frac{A^2 + 2A\cos\varphi + 1}{(A+1)^2} \qquad 4.2.(1)$$

where A is the atomic number and φ the angle of scatter in the centre of mass system. The scattering angle

in the laboratory system, θ , is related to φ by

$$\cos\theta = \frac{A\cos\varphi + 1}{(A^2 + 2A\cos\varphi + 1)^{1/2}} \qquad 4.2.(2)$$

For hydrogen the maximum value of θ is 90°, and E_1 may range from E_o to zero, when the neutron reaches thermal equilibrium with the scatterer. In a purely scattering medium at $21^{\circ}C$ the energy corresponding to the maximum thermal flux per unit energy is 0.0253 eV.

In an approximate sense neutron energies are described as "thermal" for energies up to about 0.2 eV, "slow" up to about 10 eV, "intermediate" up to about 0.5 MeV and "fast" up to about 20 MeV.

As a consequence of the isotropy of the scattering it can be shown that the average logarithmic energy decrement per collision, $\varsigma = \overline{\ln(E_1/E_o)}$ is dependent only on the atomic weight of the scatterer. The quantity ς may be used to calculate the average number of collisions required for a neutron of initial energy E_1 to be scattered to a final energy E

$$n = \frac{\ln (E_1/E)}{\varsigma} \qquad 4.2.(3)$$

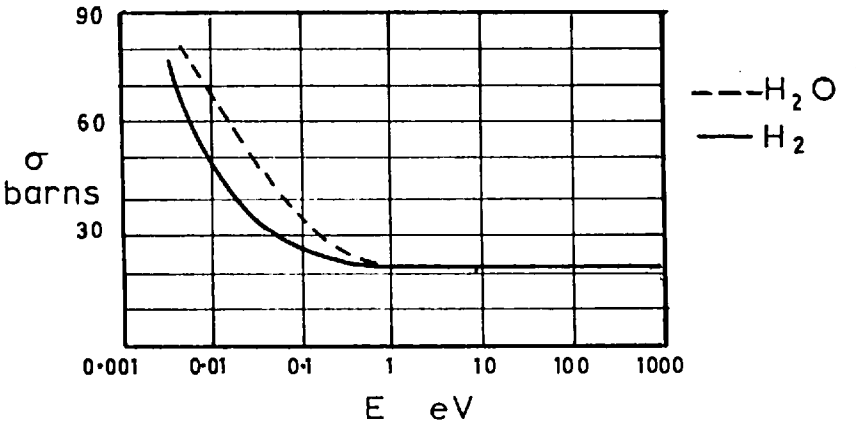
Table 26 shows the average number of scatters required off various elements in concrete for a 3 MeV neutron to reach 0.0253 eV and 0.4 eV respectively.

TABLE 26

Element	ς	n for 0.4 eV	n for 0.0253 eV
H	1	15.8	18.6
C	0.1589	100	117
O	0.1209	131	154
Al	0.0730	217	255
Si	0.0702	226	265
Ca	0.0495	320	376
Fe	0.0357	443	521

The values of ς are from Etherington (1958).

The elastic scattering cross section will be constant for an unbound nucleus at low neutron energies, but for a lightnucleus,if the binding energy is not negligible compared with the neutron energy, the scattering cross section will be increased. For collisions with bound hydrogen the nuclei may be regarded as free if the incident energy is greater than 0.8 eV (Evans 1955). Figure 38, from Weinberg and Wigner (1958), shows the total cross section of hydrogen both free and bound in water.



The scattering cross section of H

Fig. 38

When the wavelength of a neutron is of the order of magnitude of the interatomic dimensions, crystal diffraction scattering will occur. This process will occur at energies below approximately I eV, when the wave length is 0.29Å.

b) Resonance reactions

If a nucleus absorbs a neutron with energy such that the compound nucleus has energy equal to an excited level of that nucleus, a resonance peak in the cross section is observed. The energy spacing of the peaks depends upon the atomic weight of the nucleus. The lowest resonance energy falls as atomic weight increases but for the light and medium weight elements in concrete the resonances will usually occur above thermal energies.

The decay of an excited nucleus may, in general, be by the emission of any particle or energy. In nuclei up to atomic weight of about 60 re-emission of the incident particle, that is scattering, is more likely than absorption but for heavier nuclei and energies up to about I keV absorption is more probable.

c) Thermal absorption

If the neutron energy is well away from a resonance, the absorption cross section will vary with $E^{-\frac{1}{2}}$. This may be a significant process at thermal energies.

CHAPTER 4.3 THE INFLUENCE OF THE NUCLEAR PROCESSES ON THE APPARATUS

When a fast neutron source and slow neutron detector are placed in a fixed geometry near concrete, the count rate at the detector will be influenced by

a) elastic scattering off the hydrogen nuclei in the concrete, which is the primary process

b) changes in the scattering cross section due to changes in the chemical bond on the hydrogen

c) scattering by elements other than hydrogen

d) absorption of neutrons by even small quantities of absorber.

e) gamma radiation, if the detector is sensitive to that.

Because neutrons are slowed in fewer collisions by hydrogen than by other elements and because the scattering cross section is greater for hydrogen than other elements the slowing down length of fast neutrons in concrete is almost entirely due to the hydrogen content. For source neutrons at 2 MeV the slowing down length to 0.025 eV is 5.6 cm in water but is 19 cm in graphite of density 1.6 g/cc (Price at al,1957) and will be greater in heavier elements. If therefore the source and detector are not more than about 15 cm apart moderation by elements other than hydrogen should be negligible.

The bonding forces on the hydrogen in a hydrated concrete will, in general, be different from one concrete to another or, for one mix, from one age to another. In order that the calibration curve established for a water content gauge be universally applicable to concretes the effects of differing hydrogen bonding forces, which change the scattering cross section, should be eliminated. It was shown in Chapter 4.2 that hydrogen bonding effects and diffraction scattering may be neglected for neutrons of energy above 0.8 eV so neutrons below 0.8 eV should not be detected.

If the concrete being tested contains even a small quantity of absorber more than in the material used for calibrating the instrument the count rate will be depressed

and a wrong value of water content obtained. Typical absorbers which may occur in aggregates are boron, lithium, iron, phosphorus and the halogens. Because the thermal absorption cross section decreases as energy increases the effects of absorption may be eliminated by not detecting low energy neutrons.

If the detector is capable of detecting fast neutrons then neutrons scattered off elements other than hydrogen will give an unwanted component of count rate dependent on the bulk density of the concrete. Similarly, if the detector is sensitive to gamma radiation then the count rate due to photons emitted from the source and scattered from the concrete will depend upon the bulk density.

It is not possible in practice to shield the detector from all the source neutrons emitted directly towards it. This count, designated R_p as in Chapter 2.4, must be kept as low as possible.

An ideal detector for this purpose may be specified as follows:

a) It must not detect neutrons below 0.8 eV.

b) It must not detect fast neutrons which may be direct from the source or scattered off elements other than hydrogen.

c) It must not detect gamma radiation.

d) It must have a high detection probability for neutrons which are slow but above 0.8 eV.

It is not possible, with conventional neutron detectors, to discriminate at a neutron energy of 0.8 eV. However, a cadmium cover placed over the detector would absorb neutrons below about 0.4 eV, as shown by the cross section in Figure 39a. In the work reported here cadmium covers 0.015" thick were used. These had a penetration probability of 8.6×10^{-6} at 0.2 eV, 0.17 at 0.3 eV and 0.58 at 0.4 eV.

At 0.4 eV the change of hydrogen cross section due to bonding is shown by Figure 38 to be small; the neutron wavelength is 0.5 Å so that the effect of diffraction scattering will be negligible; and the absorption cross section will be $\frac{1}{4}$ that at 0.025 eV.

The influence of resonance reactions was not eliminated by the use of a cadmium cover. This effect was however expected to be small because the total width of resonances is small compared with the range of energies of the scattered neutrons.

If the effects of absorption and changes in chemical bond are eliminated and if fast scattered neutrons and gamma radiation are not detected then the count rate will depend only on the number of hydrogen atoms per unit volume. As concretes will contain at most a negligible amount of organic material the hydrogen may be considered to be due only to the water. The count rate will be a measure of the mass of water per unit volume d', and not

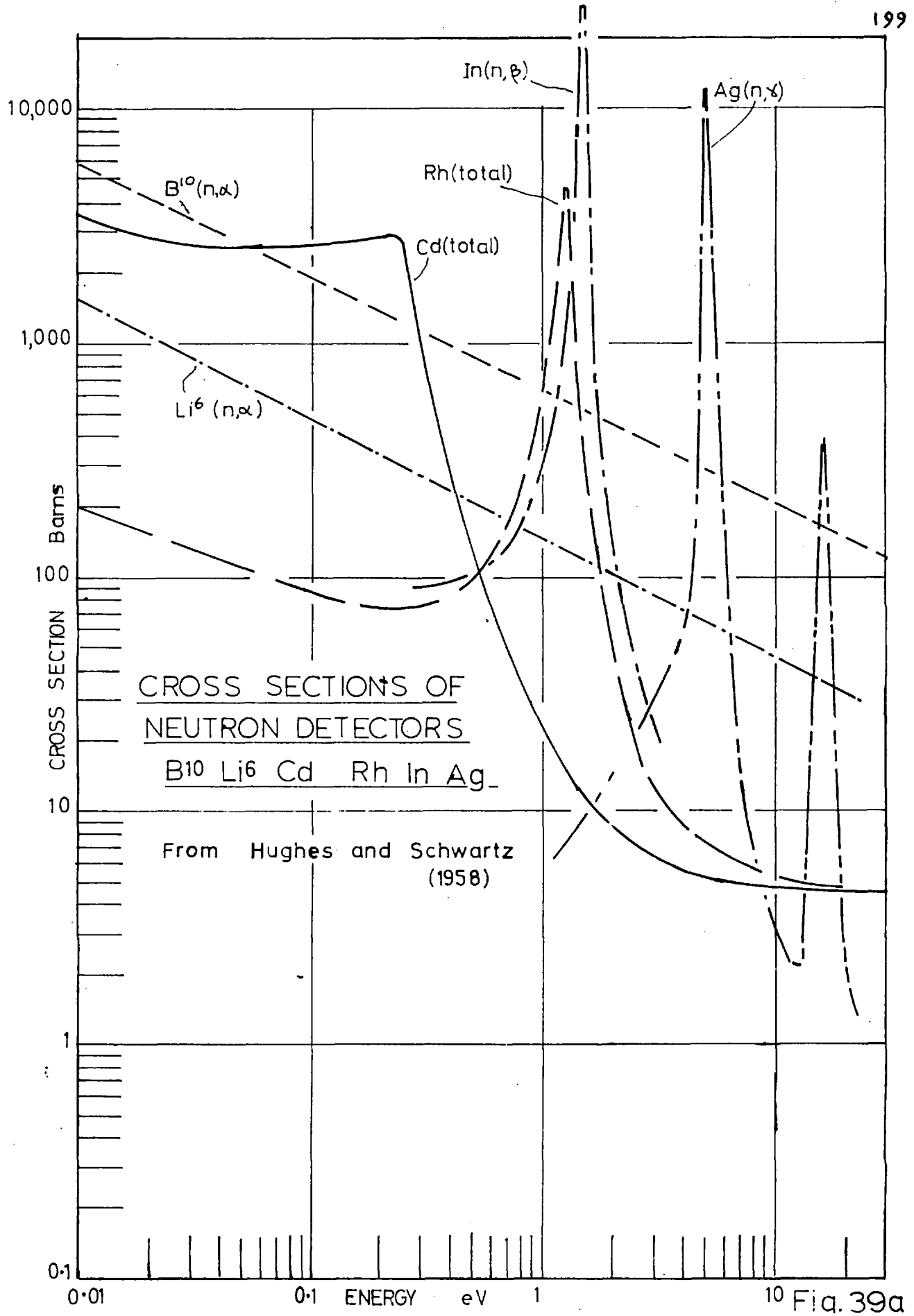

In(n,β)
Ag(n,γ)
Rh(total)
B10(n,α)
Cd(total)
Li6 (n,α)
10,000
1,000
100
10
1
0·1
CROSS SECTION Barns
CROSS SECTIONS OF
NEUTRON DETECTORS
B10 Li6 Cd Rh In Ag
From Hughes and Schwartz
(1958)
0·01
0·1
ENERGY eV
1
10

Fig. 39a

DETECTION (n,α) CROSS SECTIONS FOR B^{10} and Li^6

From Hughes and Schwartz (1958)

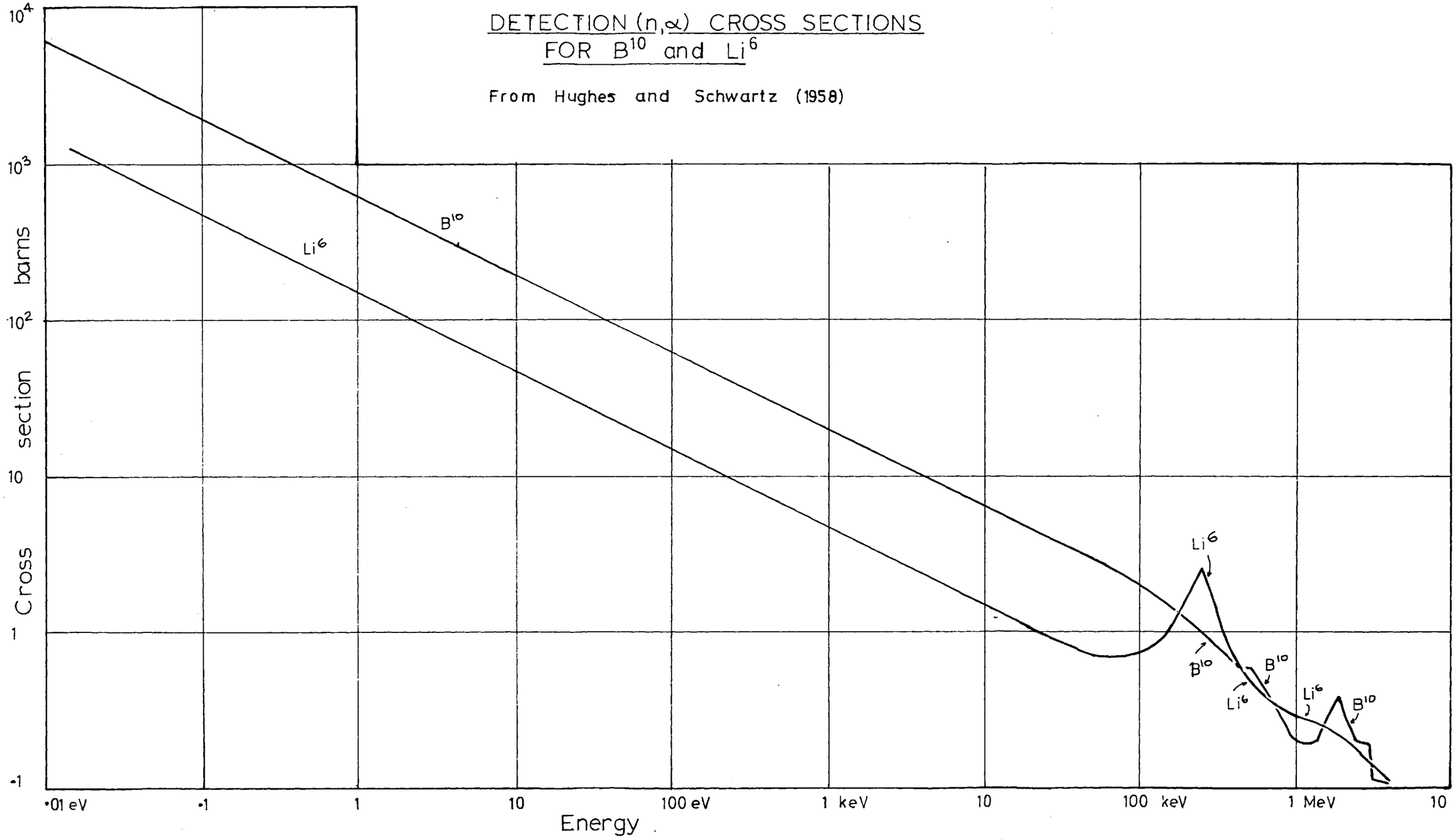


Fig. 39 b

the water content which is the mass of water per unit mass of concrete.

CHAPTER 4.4. THE SERIES I EXPERIMENTS

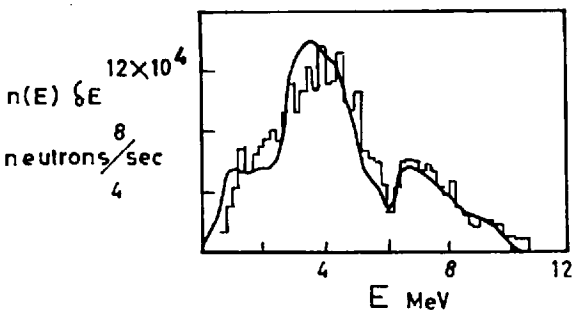
Chapter 4.4.1 The Source

A source with low gamma activity was desirable both to reduce the count rate due to gamma radiation and to reduce the health hazard and weight of shield with a site instrument. Four sources of polonium-beryllium, with a half life of 138.4 days, were used during the course of the work. Each had a nominal initial activity of one curie which gave emission of 2.5×10^6 neutrons per second. The neutron energy spectrum, as measured by Notarrigo et al (1962) for a similar source, is shown in Figure 40.

The dose from a 1 curie polonium-beryllium source is 2.5 millirem per hour at 105 cm, due to fast neutrons. The source had therefore to be handled at a distance, although short carefully controlled periods of work were permitted at lesser distances.

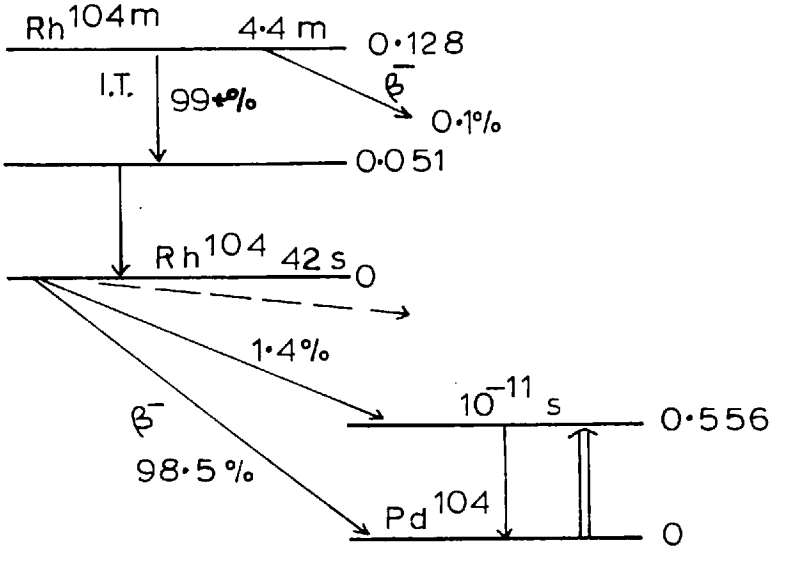
Chapter 4.4.2 The Detectors

Because neutrons are not charged particles they cannot themselves give rise to ionisation and electric charge in a detector. The most common method of detection is to let



Po-Be source energy spectrum
theoretical and experimental

Fig. 40



The decay scheme for Rh^{104}

Fig. 41

the neutrons collide with a target, making it radioactive, and then to detect the decay of the activated target. The target may be a foil, the decay of which is detected by a Geiger-Muller tube or scintillation counter, or it may be included in the detector itself as was the case for the lithium glass scintillator and boron trifluoride tube which were used in this project. The activation cross sections for the detectors used were shown in Figures 39a and 39b.

As epi-cadmium neutrons were to be detected, the possibility of using foils showing suitable resonance activation reactions was examined. Such a foil was required to have a resonance above the cadmium cut-off, yield decay products which were detectable and separable from background activity, and to have a reasonably short half life.

Indium, silver and rhodium foils, the cross sections of which were shown in Figure 39a, were tried. Indium had an inconveniently long half life of 54 minutes, and silver yielded a gamma activity difficult to distinguish from background. Rhodium, with a half life of 42 seconds, was used.

Natural rhodium is 100% Rh 103. The thermal activation cross sections are 12 barns for the formation of the 4.4 minute and 140 barns for the 42 second half life activities. (Hughes and Schwartz 1958). The decay of Rh 104 is shown in Figure 41 (Strominger et al 1958).

Calculation using this data in Appendix D showed that the activity due to the 4.4 minute state was small for activation up to three minutes. This was verified experimentally for activation by both thermal and epi-cadmium neutrons.

The foil used, 0.010" thick and $1\frac{1}{2}$" diameter, was placed against a 1 cm thick by $1\frac{3}{4}$" diameter plastic scintillator. This was used with a conventional arrangement of photomultiplier, cathode follower, amplifier, discriminator, scaler and timer as shown in Figure 4. The differential bias curve for the system is shown in Figure 42. The discriminator setting chosen for neutron detection was 7 volts.

Two neutron sensitive scintillators were also used. The first was a cerous glass scintillator, 2 mm thick by $1\frac{3}{4}$" diameter, containing 7% Li 6. (NE 905, Nuclear Enterprises (G.B.) Ltd.). The pulse height spectra due to neutrons and gamma radiation in the geometry used in Chapter 4.5 are shown in Figure 43. The discriminator was set a channel 32. The second was a boron-zinc sulphide scintillator 1" diameter (NE 401, Nuclear Enterprises (G.B.) Ltd.).

Chapter 4.4.3 The Apparatus

The apparatus, designed for use with a 6" cube of

PULSE HEIGHT DISTRIBUTION
due to decay of a rhodium foil 0·010" thick on a 1cm thick plastic scintillator

Counting interval = 3 min.

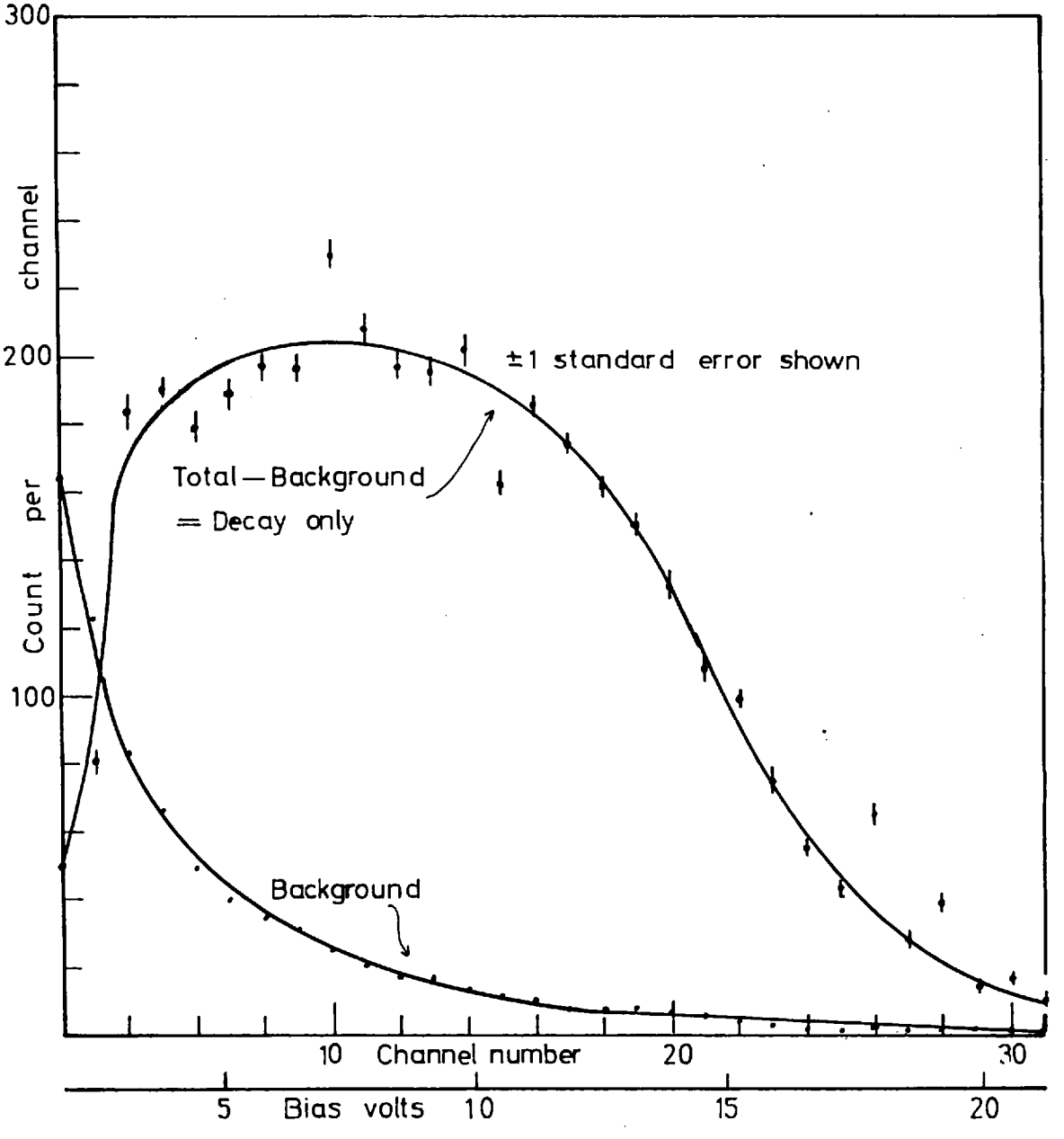


Fig.42

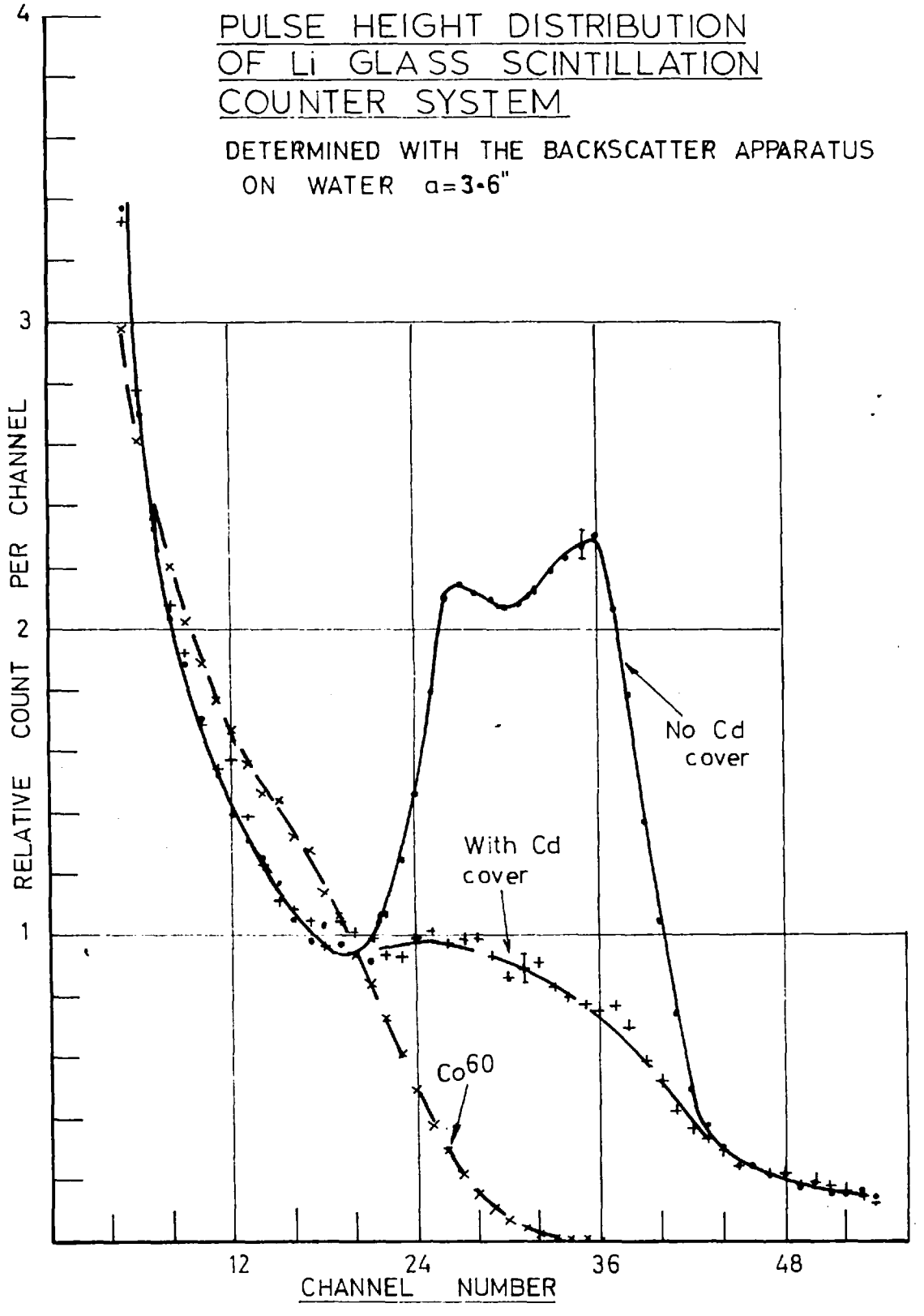

PULSE HEIGHT DISTRIBUTION
OF Li GLASS SCINTILLATION
COUNTER SYSTEM
DETERMINED WITH THE BACKSCATTER APPARATUS
ON WATER a=3·6"
RELATIVE COUNT PER CHANNEL
4
3
2
1
No Cd
cover
With Cd
cover
Co60
12
24
36
48
CHANNEL NUMBER

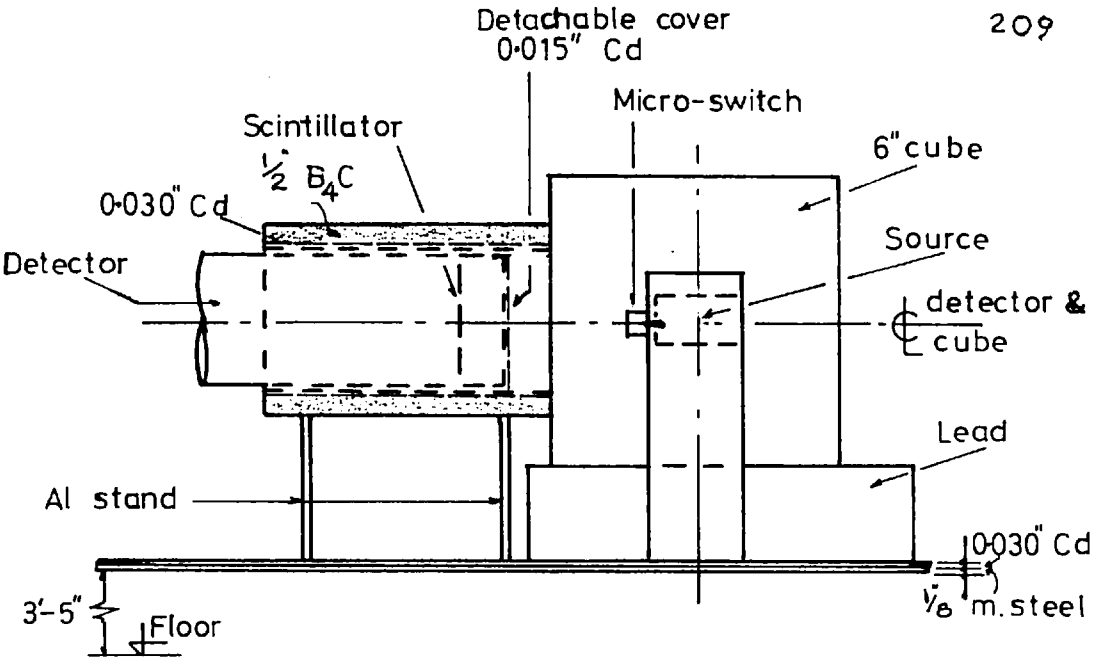
Fig. 43

concrete, is shown in Figure 44. The source, enclosed in a stainless steel capsule at the end of a handling rod, was held in position by a mild steel stand which served also as a reflector to increase the intensity of fast neutrons entering the cube. The detector was placed on the centre line of a face perpendicular to the source face. When the neutron scintillators were used the detector was held in a cylindrical shield which included 0.030" cadmium and ½" of boron carbide powder, but when the rhodium foil and plastic scintillator were used it was held in a lead cube of 4½" side.

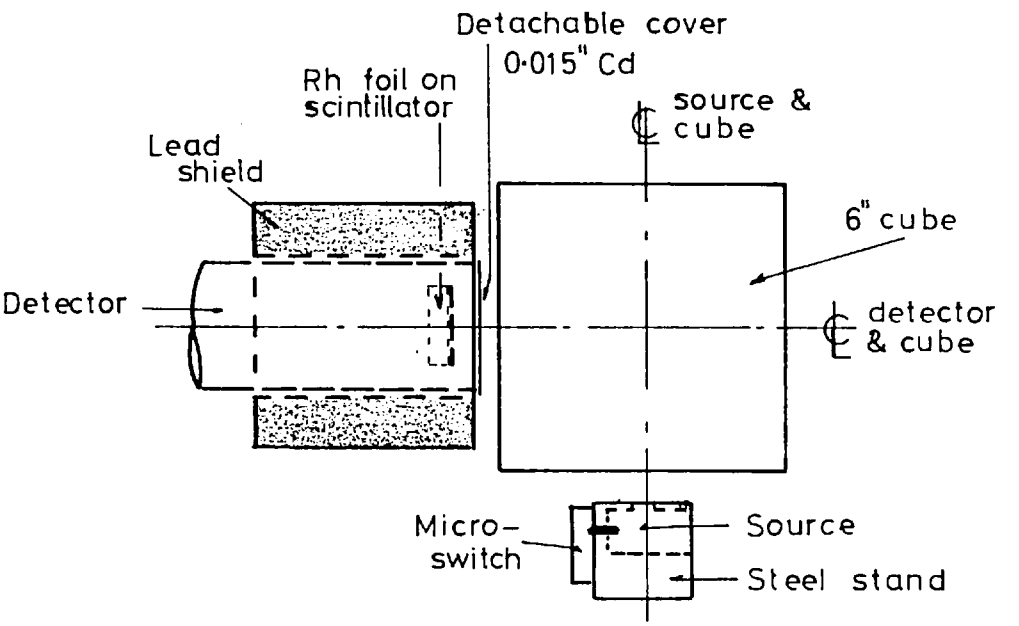
The use of the micro-switch is explained in the next chapter.

Chapter 4.4.4 Establishment of the Calibration Curve

Because the count rate at the detector was a function of the total water per unit volume there was no need to make concrete cubes to establish the calibration curves. Instead, mixtures of other materials and water in a 6" cubic aluminium tank were used. Brocard (1954), Pawliw and Spinks (1957), Burn (1960) and (1963) and Huet (1962) used various materials as discussed in Chapter 4.1. In this work organic hydrogeneous materials were avoided because it was felt that high concentrations of carbon may have had some moderating effect. Mixtures of silica



ELEVATION SHOWING LITHIUM GLASS SCINTILLATION COUNTER IN CADMIUM/BORON SHIELD



PLAN SHOWING RHODIUM FOIL SCINTILLATION COUNTER IN LEAD SHIELD

THE SERIES I WATER CONTENT APPARATUS

Scale $\frac{1}{4}$ fullsize

Fig. 44

gel, water and Thames river sand were used. A calibration specimen was required to have water uniformly distributed in the solid material, and the material uniformly placed in the tank. The silica gel saturated at a water content of about 30%, and the sand at about 1%. Saturated silica gel and sand were prepared and mixed in different proportions, giving a range of specimens of water content from 1% to 30%.

With each detector the calibration curves were established as follows. The 6" cubic container was filled with dry sand and four counts taken. It was then filled in turn with dry silica gel, wet sand, wet sand-gel mixtures, wet silica gel and water, and counts taken. The container of known volume was weighed with each material and samples of the material weighed, dried at 300°C for about twelve hours and weighed again, thus determining the water density. Previous experience had shown that there was no loss of weight of solid matter caused by drying at 300°C.

With the lithium glass and boron zinc sulphide scintillators counts were taken with the source in position, but when the rhodium foil was used the gamma activity from the source obscured the decay of the foil. For that reason the following cycle of events was used.

TABLE 27

Time	Event
0 min 0 sec	Start irradiation
3 0	Move source to coffin
3 5	Start scintillation counter
5 35	Stop scintillation counter
6 0	Repeat cycle

Four such cycles were repeated with each specimen, and an interval of six minutes left between specimens. The residual activity due to the 4.4 minute and 42 second states, when used as above, has been calculated in Appendix D.

The five second period from source removal to start of counting was measured by an electro-mechanical timer. This was started by the micro-switch which closed when the source was removed and after five seconds passed a pulse which closed a relay to start the scintillation counter.

When a foil decays in a constant background there is an optimum time of count to give the least coefficient of variation of the count due to the foil. This was calculated in Appendix D for various ratios of foil to background activity and for the ratios observed the counting time of 2.5 mean lives was close to the optimum.

THE SERIES I APPARATUS
COUNT RATE vs WATER DENSITY
DETECTOR - B(Zn S) SCINTILLATOR

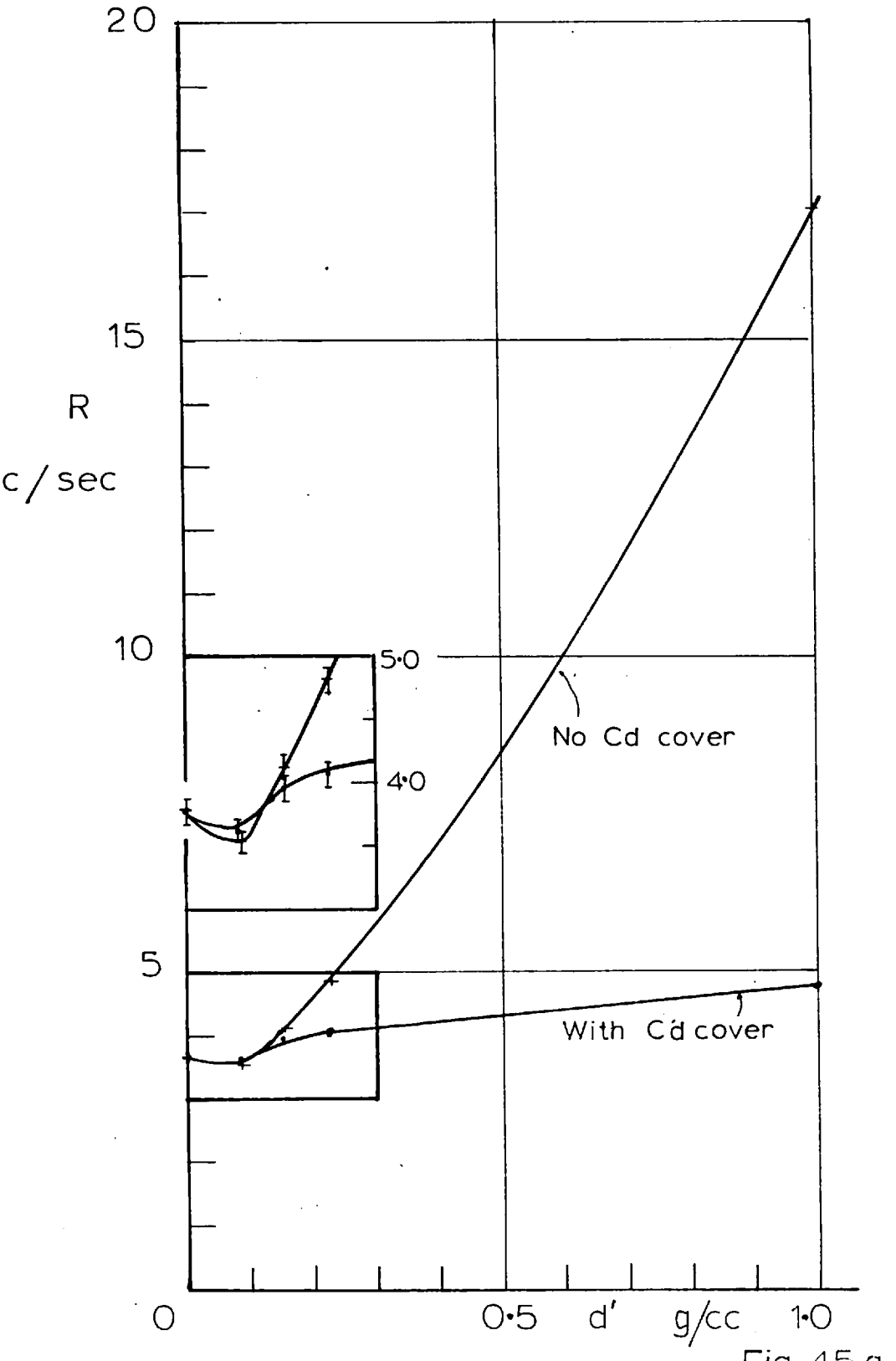


Fig 45 a

THE SERIES I APPARATUS
COUNT RATE vs WATER DENSITY

DETECTOR – Li GLASS SCINTILLATOR

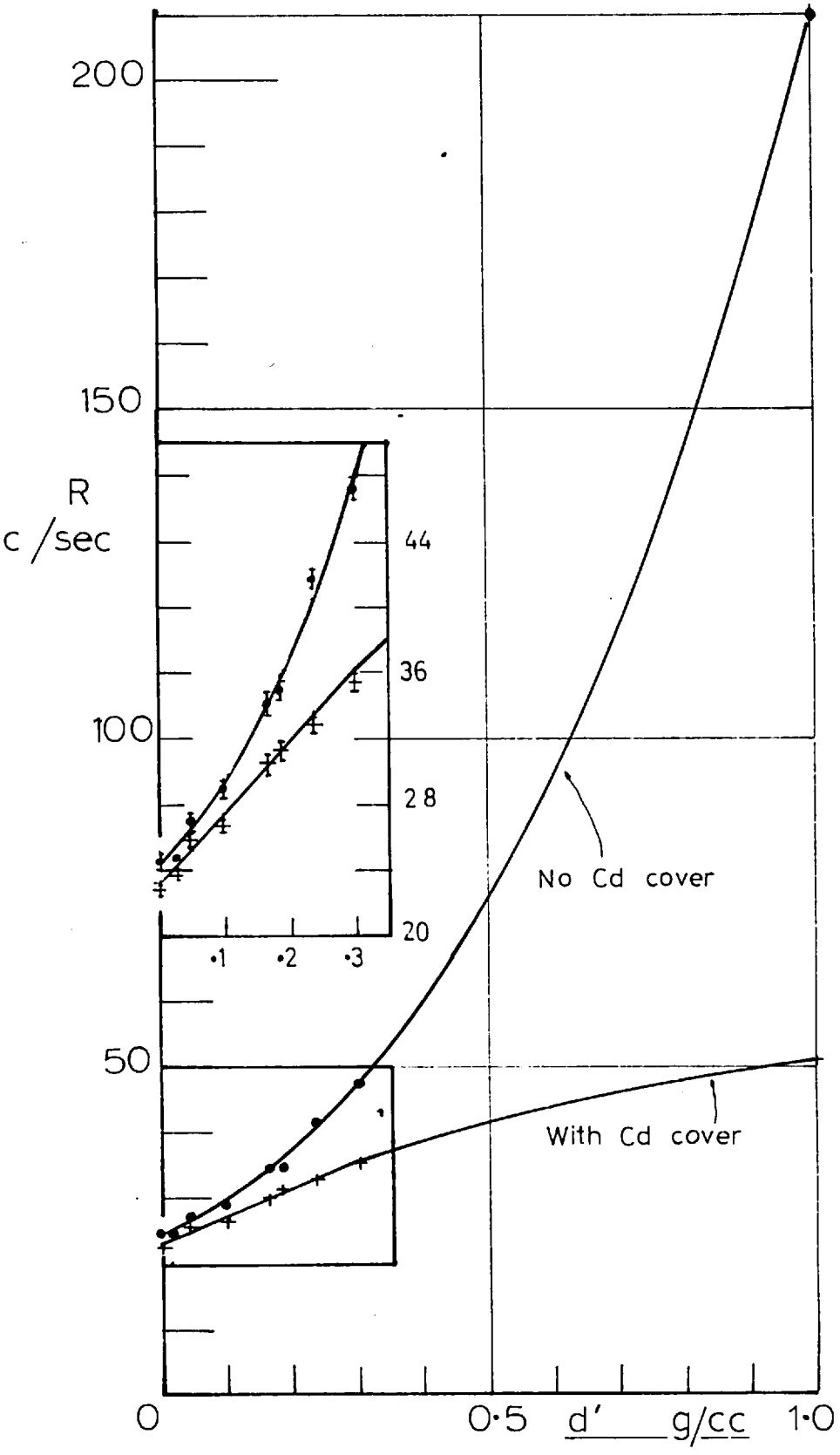


Fig. 45 b

THE SERIES I APPARATUS
TOTAL COUNT vs WATER DENSITY

DETECTOR— Rh FOIL

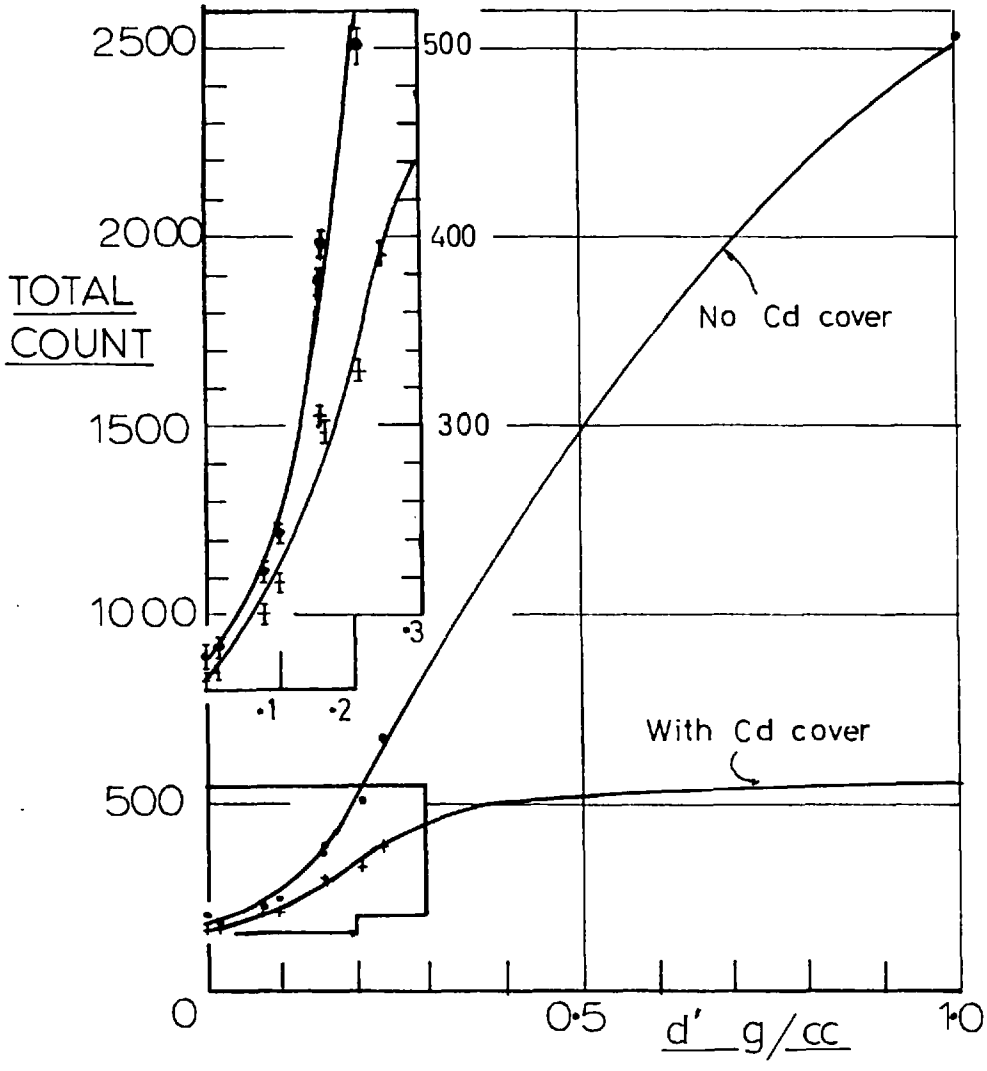


Fig 45c

The calibration curves are shown in Figures 45a to c. The curves for the boron-zinc sulphide scintillator were not as good a measure of water density as those obtained with the other two detectors.

At low water densities the counts both with and without cadmium covers were equal but as water density was increased the count with cadmium cover became progressively less than the count rate without because the detected neutron energy spectrum became "softer" and more neutrons were absorbed in the cadmium.

Applying the definition of sensitivity derived in Chapter 2.6, the following values of standard error attainable in five minutes with the lithium glass scintillator were calculated.

TABLE 28

Curve	S g/cc at d' = 0.3 g/cc	R c/sec	N for T = 300	$\sigma_{d'} = \frac{S}{\sqrt{N}}$
With Cd cover	0.94	35.5	10,650	0.0091 g/cc
No Cd cover	0.40	47.3	16,190	0.0031 g/cc

The standard errors in the last column, which would represent between one and three percent of the water density of concretes, could have been improved by taking more counts.

The definition of sensitivity used above was not appli-

cable to the rhodium foil detector because the counting interval was long compared with the half life of rhodium. If the total count consisted of N_d due to the foil and N_b due to background, then

$$\frac{\sigma_{N_d}}{N_d} = \frac{N' \sigma_{d'}}{N_d} \qquad 4.4.4.(1)$$

The slopes of the calibration curves and the coefficients of variation to give a standard error of 0.005 g/cc in the water density at d' = 0.3 g/cc are shown below.

TABLE 29

Curve	N' counts per g/cc	N_d	R_o c/sec	$\frac{\sigma_{N_d}}{N_d}$ for $\sigma_{d'}$=0.005 g/cc
With Cd cover	1410	440	8.0	0.016
No Cd cover	2400	840	15.3	0.014

The best available coefficient of variation is shown as a function of R_o and R_b in Figure 62 of Appendix D from which it is seen that the least attainable coefficient of variation is best reduced by reducing the background count, which was difficult. The accuracy attainable with the foil detector was thus limited.

Chapter 4.4.5 Determination of the Effectively Infinite Volume

The volume of the 6" cube which influenced the count

was determined for water, using the cadmium covered lithium glass detector. To find the effectively infinite depth the tank was filled in ½" intervals, a reading being taken at each step. To find the effectively infinite dimensions in the horizontal directions the tank was filled with plates of duralumin, which was effectively vacuum to the fast neutrons. The plates were removed in order, each replaced by an equal volume of water and a count taken.

The curves of nett count rate against water thickness are shown in Figure 46 and show that a volume 5" from the source by 2½" from the detector by 6" high contributed to the count. As the curve of count against depth had not reached a maximum at the full depth of 6", the calibration curves were dependent on the geometry of the apparatus. The effectively infinite sizes were presumably greater in lower water density media, but this was not investigated.

Chapter 4.4.6 The Effect of Neutron Absorbers

Experiments were performed to find to what extent the cadmium cover reduced the effects of thermal neutron absorbers in the concrete. Sodium chloride was chosen as an experimental absorber because chlorine has a high thermal absorption cross section, exceeded in the light and medium atomic weight elements only by lithium, boron, technetium, rhodium, cadmium and indium, and sodium has a large resonance of 350

SERIES I WATER CONTENT APPARATUS

DETERMINATION OF EFFECTIVELY INFINITE DIMENSIONS

MATERIAL – WATER

DETECTOR – Li GLASS SCINTILLATOR

LIMITS ± 2 STANDARD ERRORS ARE SHOWN

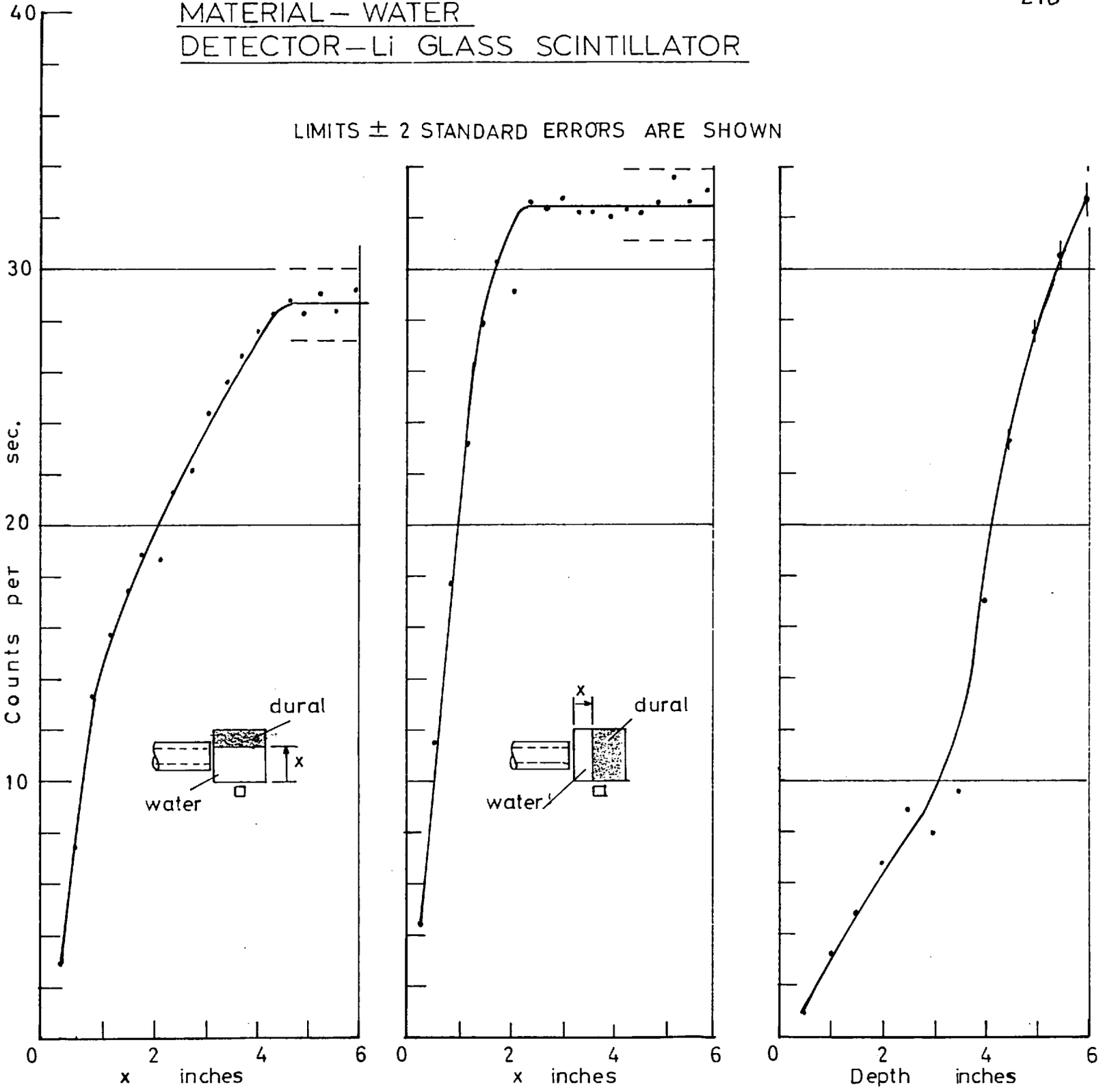


Fig. 46

barns peak at 2.85 keV. The sodium chloride was used in water rather than in material of lower water density. As the neutron energy spectrum was "softer" in water, this increased the effect of the absorber.

The tank was filled with water and readings taken both with and without a 0.015" cadmium cover. Five percent by weight of salt was added and readings again taken. The results are shown below.

TABLE 30

Salt content	0.05 gram salt/gram water
Density of solution	1.03 g/cc
Water density of solution	0.98 g/cc

Detector		Water		Solution	
		Reading	σ	Reading	σ
Rhodium foil	.015" Cd cover	483 counts	6	474 counts	3
	No Cd cover	2152	8	1721	5
Lithium glass	.015" Cd cover	49.7 c/s	0.5	50.4 c/s	0.5
	No Cd cover	200.8	1.0	171.9	1.0

Standard errors quoted were calculated on the basis of nuclear statistics only.

The results showed that the high concentration of absorber used had no significant effect on the count rate.

Chapter 4.4.7 Conclusions

The use of a fast neutron source and cadmium covered detector in this geometry was found to give a reasonably accurate measure of water density independent of the presence of absorbers and presumably independent of bonding forces on the hydrogen, but the calibration curve was valid only for the size of cube and geometry used.

Although the curve established with a cadmium cover was less accurate a measure of water density than the curve without a cover, the use of the cadmium cover made the readings negligibly dependent upon the effects of neutron absorption and chemical bonding on the hydrogen, and were therefore negligibly dependent on the chemical composition of the concrete.

Improvements in accuracy were attainable with a continuously counting detector by simply taking a larger count but the accuracy attainable with the rhodium foil detector was limited by the background activity. For this reason and because the procedure of source removal and insertion was considered impractical for site use, the rhodium foil detector was not further investigated.

CHAPTER 4.5 THE BACKSCATTER METHOD WITH A LITHIUM GLASS SCINTILLATOR

The work described in Chapter 4.4 showed that the lithium glass scintillator was the best of the detectors used. The aim of the work in this chapter was to use that

detector in apparatus which required access to only one face of a specimen.

The calibration curves, effects of absorbers and effects of gamma radiation and scattered fast neutrons were observed at various distances source to detector.

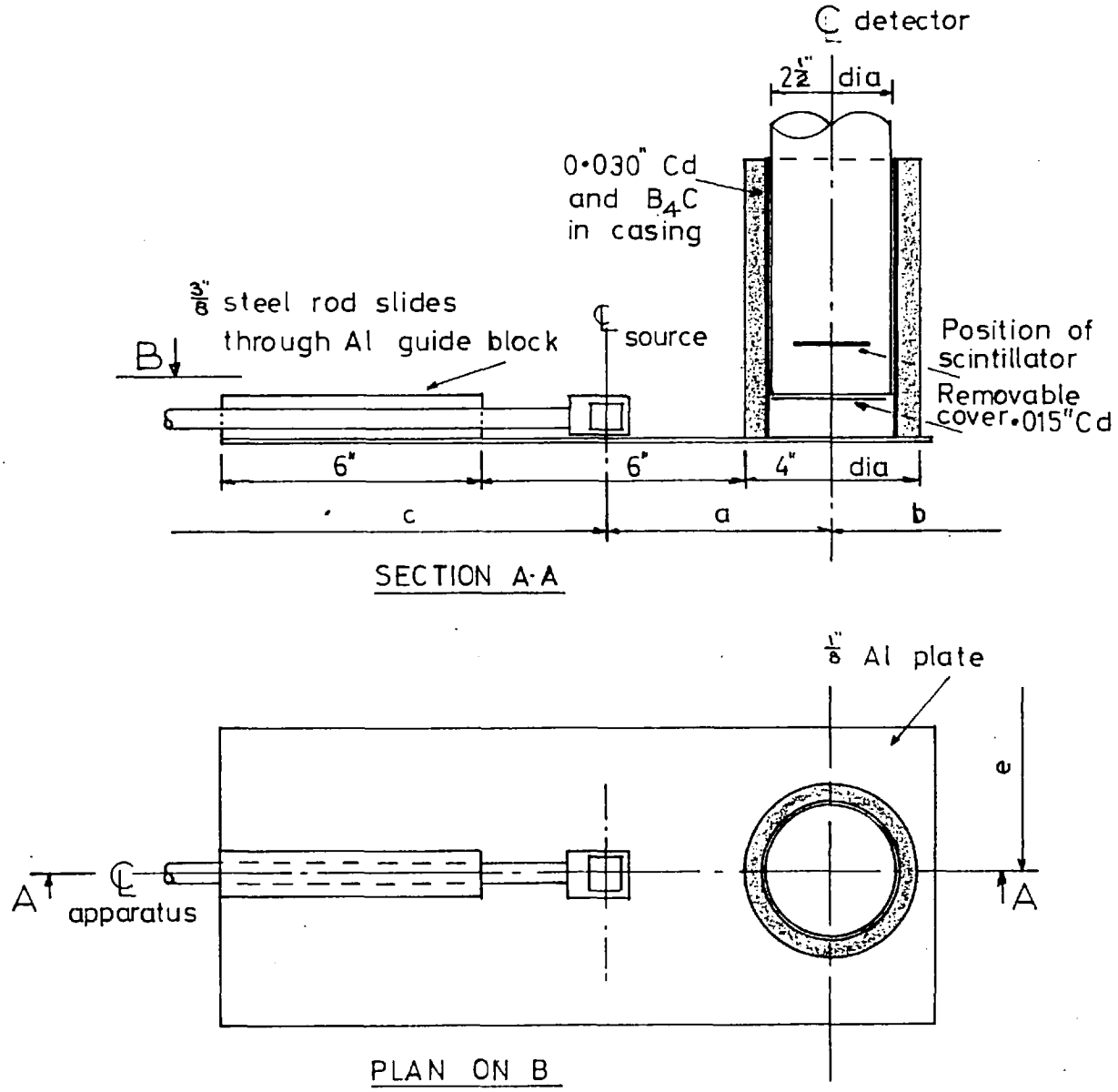
Chapter 4.5.1 The Apparatus

The sources, each originally one curie of polonium-beryllium, and the detector, in a cadmium-boron shield, were mounted on a $\frac{1}{8}$" aluminium plate as shown in Figure 47. The distance between source and detector could be varied by sliding the handling rod in a guide.

The detected pulse height spectrum for the apparatus on water with the source adjacent to the shield was shown in Figure 43. The peak obtained was broader than for a symmetrical neutron flux and was apparently due to the variation of flux over the diameter of the detector. Only the pulses in the ten channels 32 to 41 were passed by the pulse height selector.

Chapter 4.5.2 Establishment of the Calibration Curves

The materials used for establishing the calibration curves are listed below.



NOTE

Dimensions b,c & e which are the effectively infinite size notation are to the edge of the block of material.

BACKSCATTER METHOD WITH SCINTILLATION COUNTER APPARATUS DETAILS

Scale ¼ fullsize

Fig 47

TABLE 31

d' g/cc	Description
0	A frame table covered with 0.030" cadmium, 3'6" above the floor.
0.06 approx.	Damp sand in a tank 20" x 20" x 15".
0.076 and 0.089	Aerated concrete slabs forming a block 30" x 24" x 18".
0.248	Mortar concrete, nominally 1 : 2 with water-cement ratio 0.45. One block 16" x 16" x 8" plus eight slabs 16" x 16" x 1".
0.75	Solution of calgon in water, in a tank 1'10" diameter by 1'3" deep.
1	Water in a tank 1'10" diameter by 1'3" deep.

The count was considered to consist of components R_b, R_p and R_s as defined in Chapter 2.6 for density methods.

R_b was measured by taking a count with source removed and R_p was determined by taking a reading on the cadmium covered frame. Readings previously taken at various heights above a tank of water had established that at

heights exceeding 2'0" no epi-cadmium neutrons were scattered back to the detector and above 2'6" no scattered neutrons at all were detected, so the reading taken on the frame was indeed R_p.

The sand was carefully placed in the tank, uniformity in density being achieved by placing weighed quantities in 1" layers. Samples from each layer and from several positions on the surface were weighed and oven dried at 300°C to determine the water content.

The densities of the concretes were determined by measuring and weighing the blocks and the total water content determined from chemical analysis carried out by the Associated Portland Cement Manufacturers Research Laboratory.

Calgon dissolved in water up to concentrations of approximately 0.5 grams per gram of solution, which corresponded to about 0.75 grams of water per cubic centimetre of solution. A curve of density of calgon solution against water density had been set up and using this the water density could be derived from the overall density which was measured with a specific gravity bottle.

Counts were taken on the materials with various values of distance source to detector, with and without a 0.015" thick cadmium cover and the curves thus obtained are shown in Figures 48a and b.

As the distance source to detector 'a' or the water

THE BACKSCATTER METHOD WITH SCINTILLATION COUNTER

R vs d'

With Cd cover

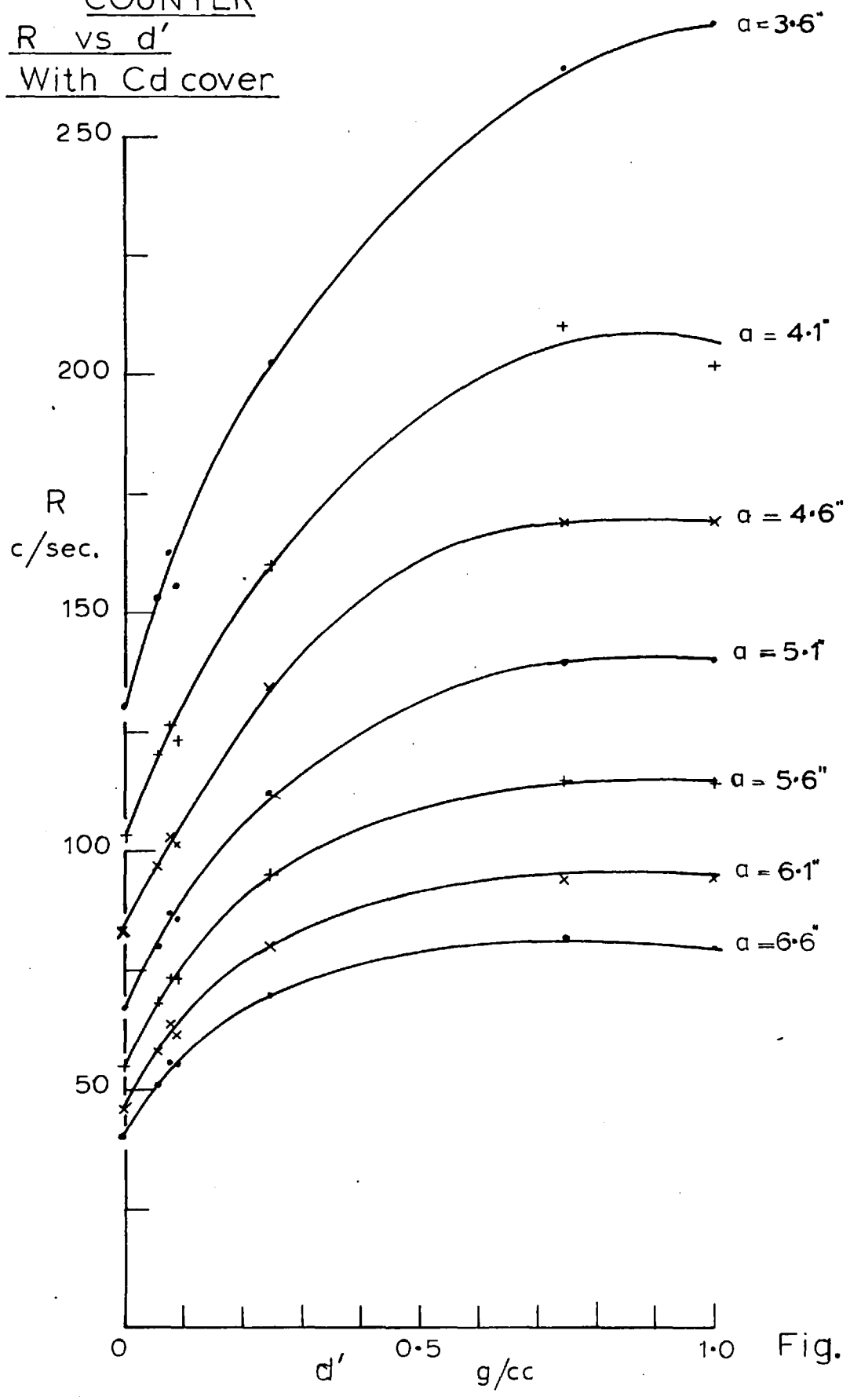


Fig. 48a

THE BACKSCATTER METHOD WITH SCINTILLATION COUNTER

R vs d'

No Cd cover

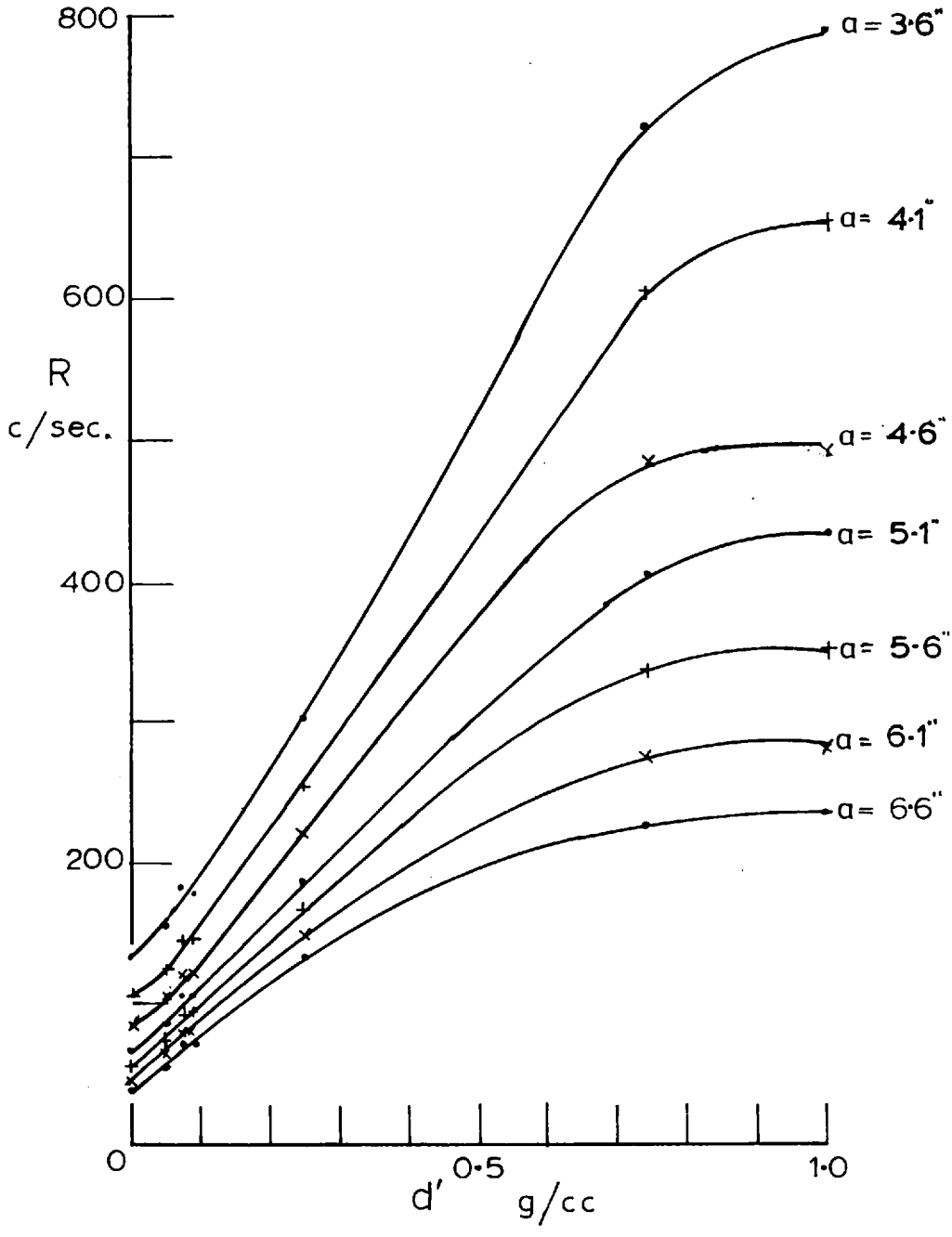


Fig. 48 b

density were increased, the slopes of the calibration curves decreased. The mechanism here appears similar to that described in Chapter 2.4 for gamma radiation density back-scatter apparatus where it was shown that as the radiation was more scattered, due to increasing source-detector distance or density, the slope of the curve decreased. As water density was increased the curves established with the cadmium covered detector dropped more and more below the curves for the bare detector, due to the "softening" of the detected neutron energy spectrum.

The accuracy of the calibration curves is discussed in Chapter 4.6.5.

Chapter 4.5.3 Determination of the Effectively Infinite Dimensions

The effectively infinite depth d_∞ on a material was determined by taking readings with the apparatus on various thicknesses of that material. The thickness at which the count rate reached a steady value was the effectively infinite depth.

The effectively infinite dimensions b_∞, c_∞ and e_∞, shown in Figure 47, were determined by moving the apparatus across the surface of a material, taking a reading at each point. The distance from the edge of the material to the position at which the count rate became constant

was the effectively infinite dimension. When one effectively infinite dimension was being determined, care was taken that the other dimensions were themselves greater than effectively infinite.

For these experiments the water, calgon solution and sand were placed in a tank 20" x 20" x 15" deep, made of 1/16" mild steel, standing on the cadmium covered frame.

The curves obtained are shown in Figures 49, where the broken lines represent ± 2 standard errors calculated from nuclear statistics only, and the resulting dimensions in Table 32.

TABLE 32

The Effectively Infinite Dimensions for the Backscatter Apparatus with Lithium Glass Scintillator

d' g/cc	a	With Cd Cover				No Cd Cover			
		b_∞	c_∞	e_∞	d_∞	b_∞	c_∞	e_∞	d_∞
1	3.6"	3"	1"	4"	4"	3"	1"	4"	4"
	6.6"	2"	0"	4"	3"	3"	-½"	4½"	4½"
0.74	3.6"	3"	2½"	5"	4½"	3"	3"	5"	5"
	6.6"	3"	2½"	5"	3½"	4"	1"	5"	5"
0.248	3.6"	3½"	2½"	4"	6"	4"	3½"	4"	8½"
	6.6"	3½"	2"	4"	5"	4"	1"	5"	8½"
0.053	3.6	3½"	4"	-	-	4"	3½"	-	-
	6.6"	3½"	5"	-	-	3"	2"	-	-
0.058	3.6"	-	-	5"	12"	-	-	5"	10"
	6.6"	-	-	6"	10"	-	-	5"	11"

The values of e_∞ and b_∞ were plotted against d_∞, where d_∞ was assumed to be the last path length in the material, in Figure 50, which shows that b_∞ and c_∞ for

DETERMINATION OF b_∞ and c_∞ FOR THE APPARATUS SHOWN IN FIG. 47

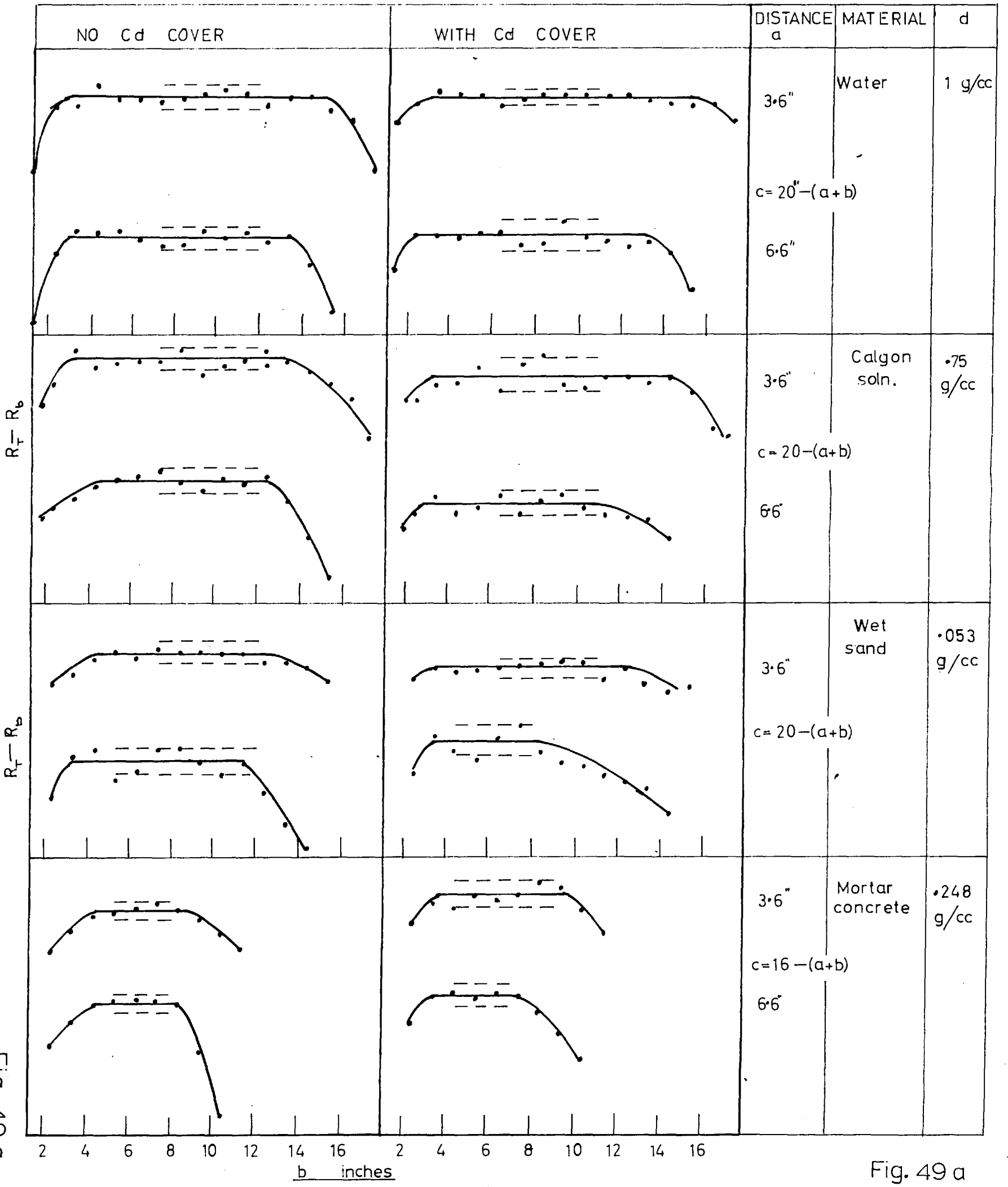


Fig 49 a

Fig. 49 a

DETERMINATION OF e_∞ FOR THE APPARATUS SHOWN IN FIG. 47

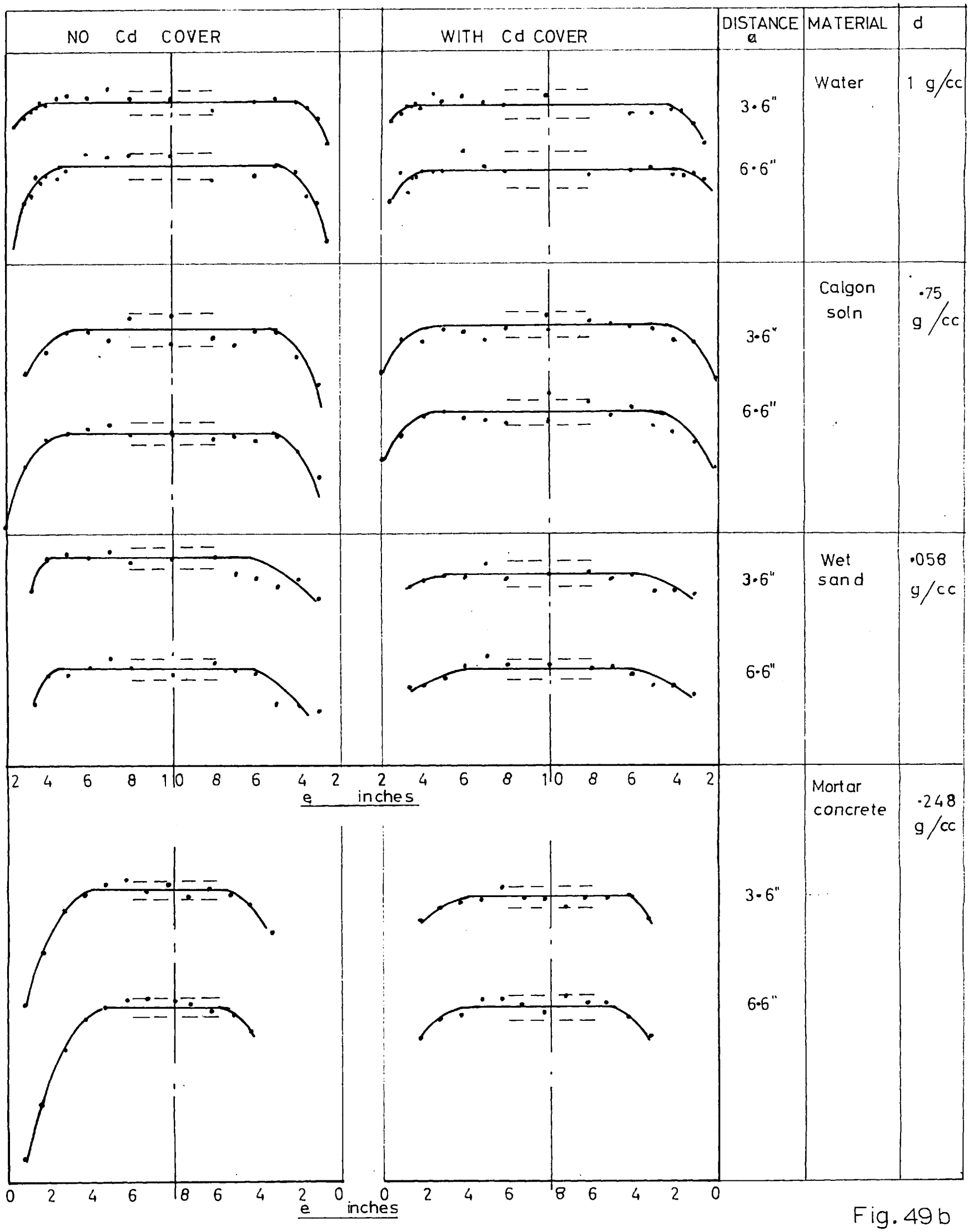
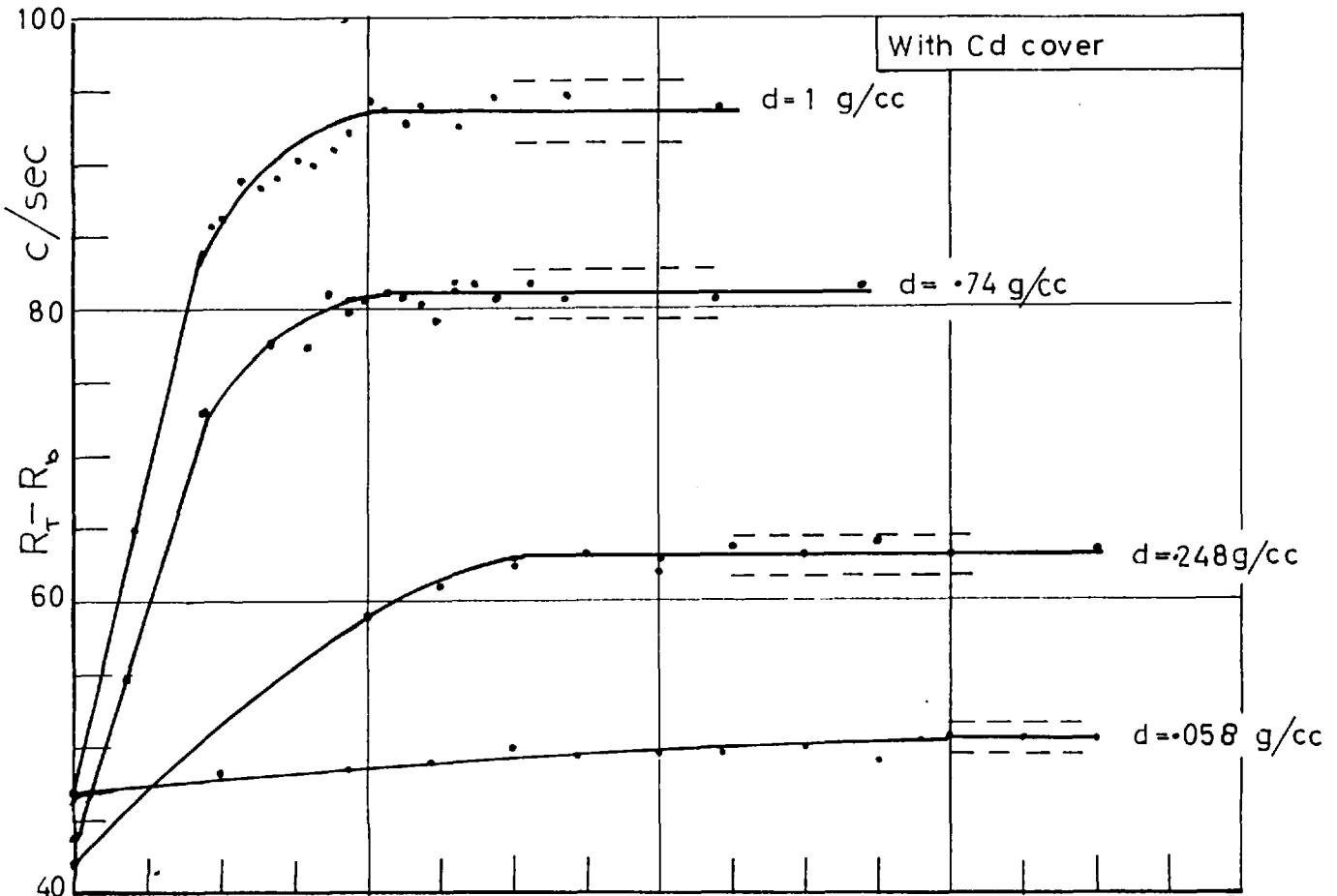


Fig. 49b

DETERMINATION OF d_∞ FOR THE APPARATUS SHOWN IN FIG. 47

DISTANCE a = 3·6"



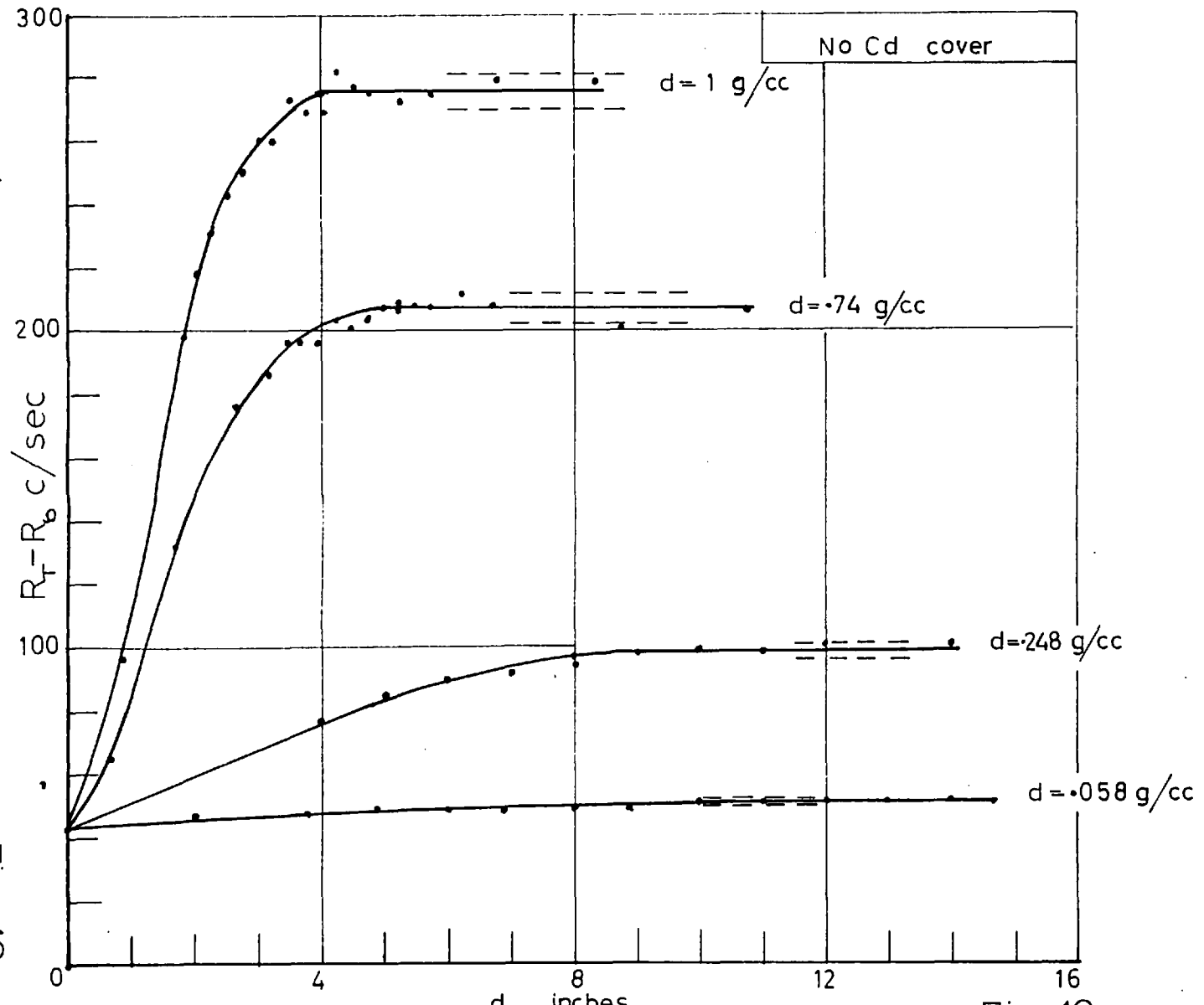


Fig 49c

Fig. 49c

DETERMINATION OF d_∞ FOR THE APPARATUS SHOWN IN FIG. 47

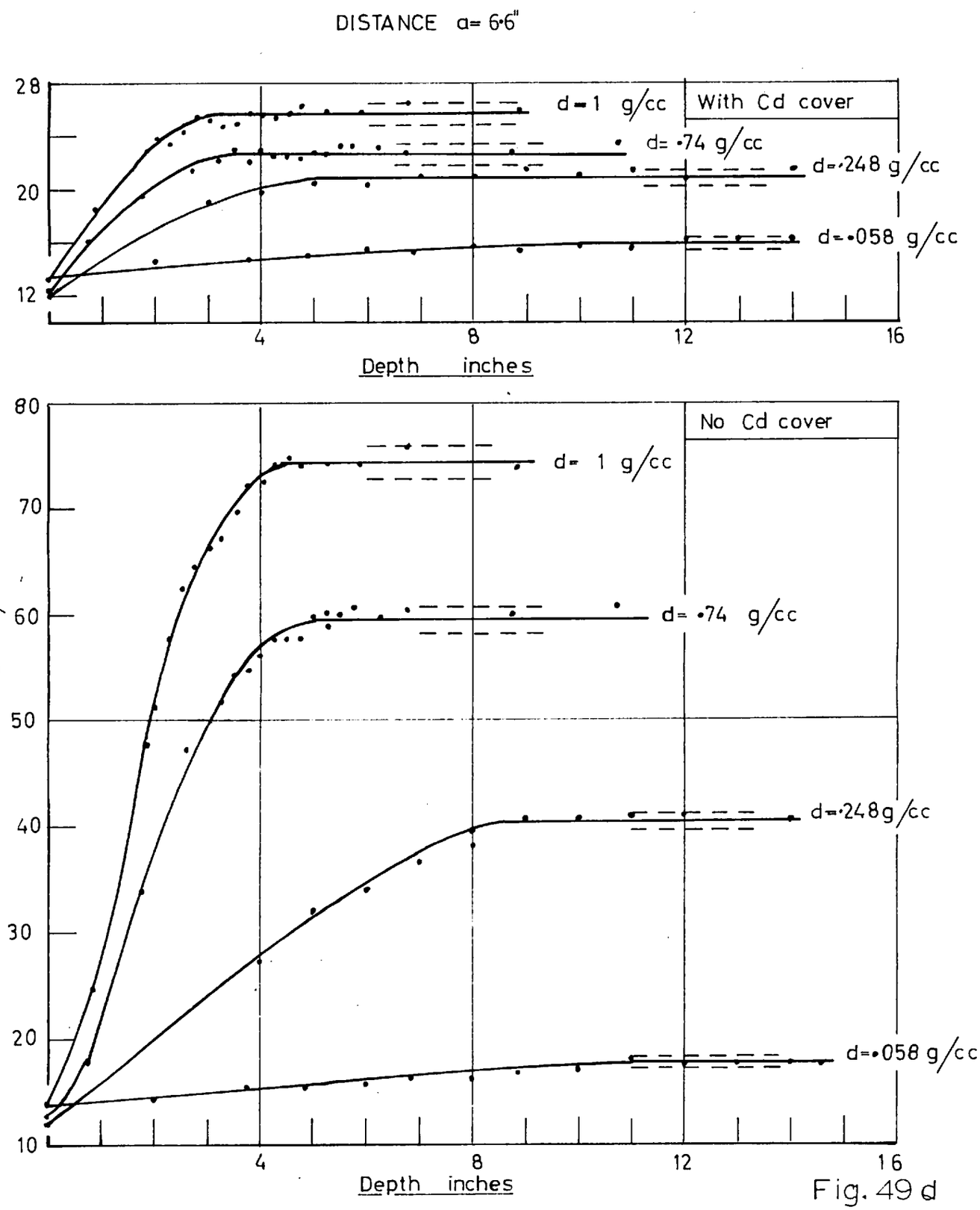


Fig. 49 d

Fig 49d

THE BACKSCATTER METHOD WITH SCINTILLATION COUNTER

PLOT OF THE EXTREME POINTS OF THE EFFECTIVELY INFINITE VOLUME

CODE

Prefix	d g/cc	Suffix	a	Cd cover
A	1	1	3·6"	No
B	·75	2	6·6"	Yes
C	·248	3	36"	No
D	·058	4	6·6"	Yes

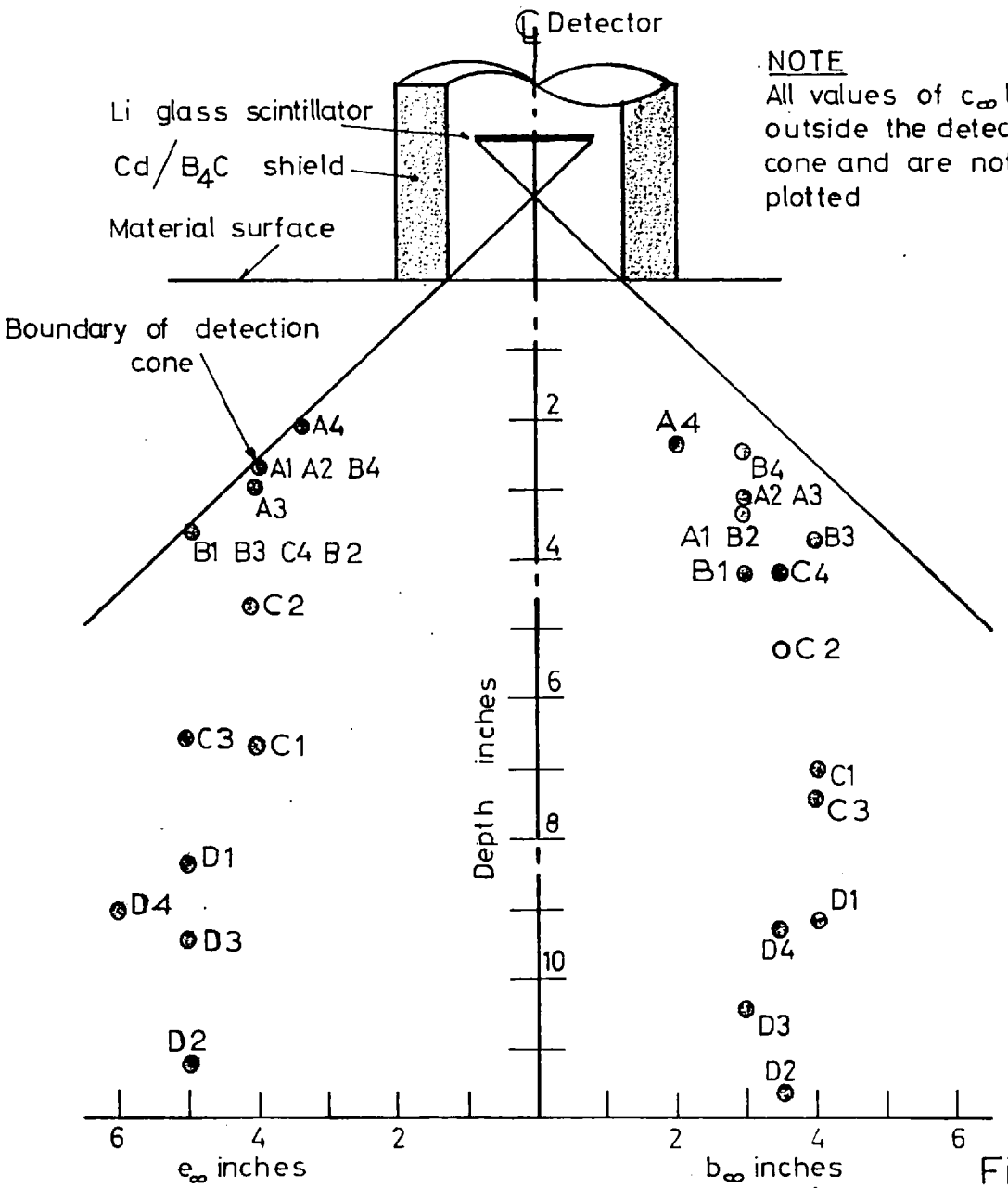


Fig. 50

water densities 0.248 g/cc and 0.058 g/cc were not determined by the collimation of the detector but by the neutron distribution in the material.

The slowing down length for fast neutrons in a hydrogeneous moderator is greater than the diffusion length. Provided the source and detector are not far apart the effectively infinite depth will be determined by the probability that the neutrons penetrate from the edge of the effectively infinite volume to the detector.

This probability for a diffusing medium in plane geometry is given by

$$p = e^{-d\omega/L}$$

where L is the diffusion length.

From Table 33, which shows the calculated thermal transport cross sections for a number of materials, it is seen that the cross sections of materials other than water are small but not negligible. However, neglecting the cross sections of components other than water, for constant weak absorption in the medium

$$L \propto (\Sigma_{tr})^{-\frac{1}{2}}$$

$$\propto (d')^{-\frac{1}{2}}$$

TABLE 33

Material		Calculated Σ_{tr} at 0.025 eV cm^{-1}
Water		3.08
Granite	(a)	0.13
Basalt	(b)	0.12
Granite	(c)	0.20
Limestone	(d)	0.12
Hornfels	(e)	0.16
Portland Cement	(f)	0.14
Thames River Sand	(g)	0.09
Calgon	(h)	0.12

Analyses:- (a) to (f) as Table 4

(g) special analysis

(h) manufacturer.

Cross sections are from Hughes and Schwartz (1958) except for a proton in water which was 44 barns/atom (Soodak 1962).

If the effectively infinite depth corresponded to a particular value of p above, then

$$d_\infty \propto (d')^{-\frac{1}{2}}$$

THE BACKSCATTER METHOD WITH SCINTILLATION COUNTER

d_∞ vs $(d')^{-1/2}$

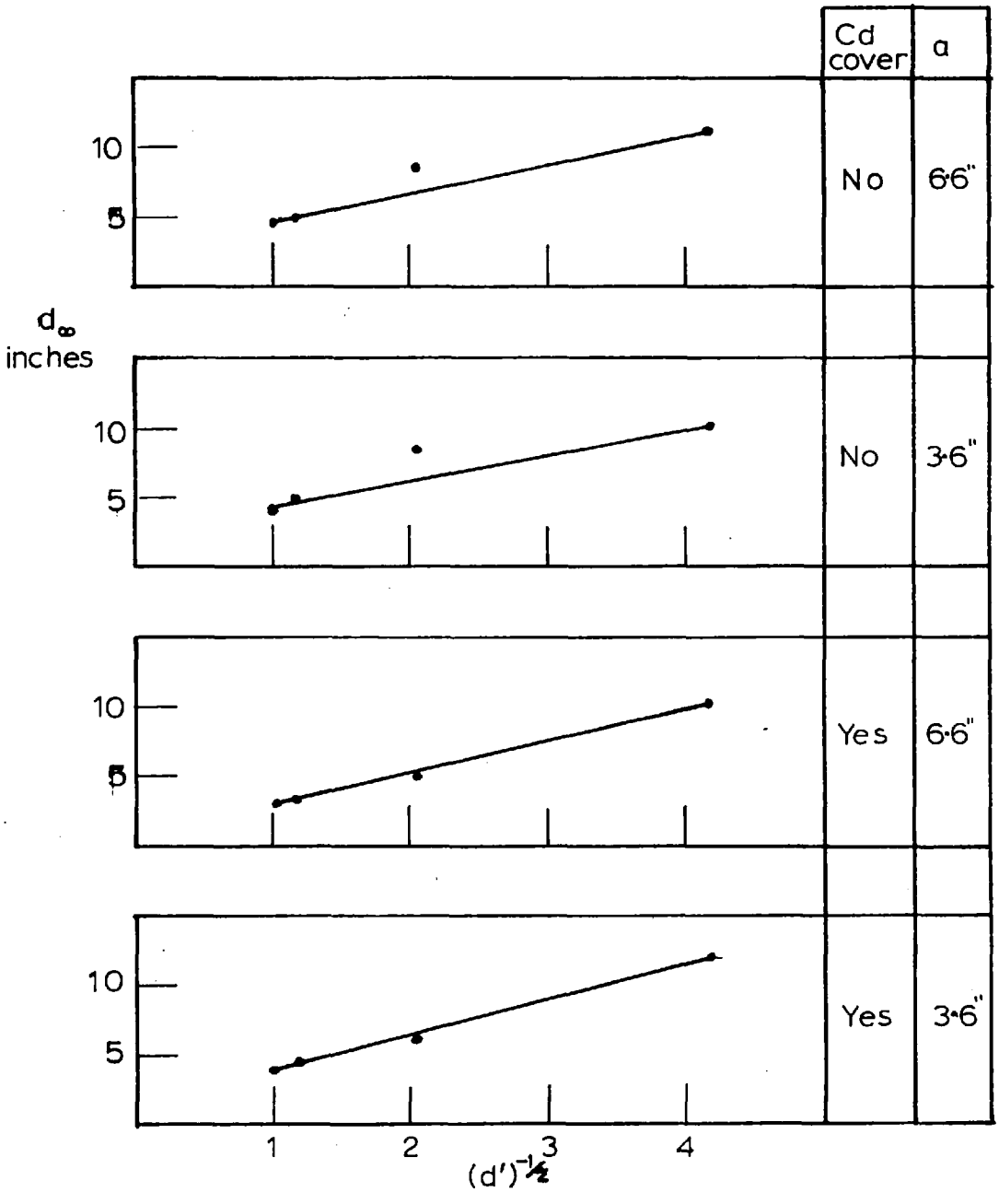


Fig. 51

Figure 51 shows the curves of d_∞ against $(d')^{-\frac{1}{2}}$. For the cadmium covered detector they plot as straight lines but for the bare detector the depth for mortar concrete at $(d')^{-\frac{1}{2}} = 2.02$ was anomalously great. Paterson et al (1963) showed that the thermal transport cross section per proton in concrete decreased as the bound water content rose, and for the largest bound water content they considered, 4.6% by weight, was $\frac{3}{4}$ the cross section of a proton in water, If the cross section for the concrete used here, which contained 8% bound water and 3% evaporable water, were about half that of a proton in water, this would explain the anomalously large values of d_∞.

Chapter 4.5.4 The Effect of Neutron Absorbers

Sodium chloride was used as absorber, 5% by weight being added to water. Readings with and without cadmium covers were taken as before, and the results are shown in Table 34.

TABLE 34

Distance 'a'	Bare Counter				.015" Cd Cover				.030" Cd Cover			
	On Water		On Salt Solution		On Water		On Salt Solution		On Water		On Salt Solution	
	R	σ	R	σ	R	σ	R	σ	R	σ	R	σ
3.6"	241	2.4	212	2.1	82.9	0.8	83.4	0.8	80.5	0.8	79.5	0.8
4.1"	198	2.0	174	1.7	66.0	0.7	69.3	0.7	64.1	0.6	64.3	0.6
4.6"	161	1.6	137	1.4	53.0	0.5	54.2	0.5	51.3	0.5	51.4	0.5
5.1"	128	1.3	110	1.1	43.5	0.4	43.8	0.4	42.4	0.4	41.4	0.4
5.6"	106	1.1	88	0.9	35.0	0.4	36.1	0.4	34.3	0.3	33.7	0.3
6.1"	85	0.9	73	0.7	28.9	0.3	29.5	0.3	28.2	0.3	28.3	0.3
6.6"	70	0.7	59	0.6	24.4	0.2	24.8	0.2	23.7	0.2	24.1	0.2

R is in counts per second, $\bar{\sigma}$ is the standard error in counts per second estimated on the basis of nuclear statistics only.

It is seen that with a cadmium cover 0.015" thick the effect of absorption by the high concentration of sodium chloride was not significant.

Chapter 4.5.5 Investigation of the Count due to Gamma Radiation and Fast Scattered Neutrons

If the detector were sensitive to gamma radiation or fast scattered neutrons the reading would have depended on the bulk density of the material as well as moisture den-

sity and this was clearly undesirable.

A Co 60 source was obtained with a gamma intensity equal to that of a Po-Be source. The count rates R_p due to the Po-Be and due to the Co 60 were determined, as was the count rate $R_p + R_s$ due only to the Co 60, on concrete of density 140 lb/cu ft. The count rates obtained are shown in Table 35.

TABLE 35

Source	a = 3.6"		a = 6.6"		Material
	R	σ	R	σ	
Po-Be	39.45	0.42	10.71	0.13	Cd frame
Co 60	0.30	0.07	0.23	0.07	Cd frame
Co 60	0.41	0.07	0.20	0.06	Concrete

Values in counts per second.

The count due to gamma radiation was between 1% and 2% of R_p, with no apparent increase due to scattering from the concrete.

The count due to fast scattered neutrons was measured by placing the apparatus on a container 1'9" high by 1'4" diameter, filled with $\frac{3}{4}$" Thames river gravel previously dried at 300°C until no loss of weight occurred. Readings were taken on the cadmium covered frame and on the dry gravel and are shown in Table 36. The gravel had a bulk density of 1.409 g/cc and after the experiment a check of

the water content showed it to be 0.003 g/g, which gave rise to an error of less than 1½% in R_{fast}.

TABLE 36

a	d' = 0		d' = 0.248 g/cc	
	$\frac{R_{fast}}{R}$	σ	$\frac{R_{fast}}{R}$	σ
3.6"	0.10	0.02	0.06	0.01
4.1"	0.09	0.02	0.06	0.01
4.6"	0.07	0.02	0.05	0.01
5.1"	0.11	0.02	0.06	0.01
5.6"	0.10	0.02	0.06	0.01
6.1"	0.11	0.02	0.06	0.01
6.6"	0.08	0.02	0.05	0.01

The contribution of fast scattered neutrons was between 10% and 5% of the count for water density up to d' = 0.25 g/cc.

Chapter 4.5.6 Conclusions

When a cadmium cover was used the apparatus gave a reading independent of the presence of absorbers normally found in concrete. Fast scattered neutrons contributed between 5% and 10% of the count in a manner which depended

upon the bulk density of the concrete. The contribution of gamma radiation was negligible.

The effectively infinite depth varied inversely as the square root of water density for the cadmium covered detector but for the bare detector the depth was greater in the concrete than in the materials containing uncombined water on account of the change in hydrogen transport cross section with bound water content.

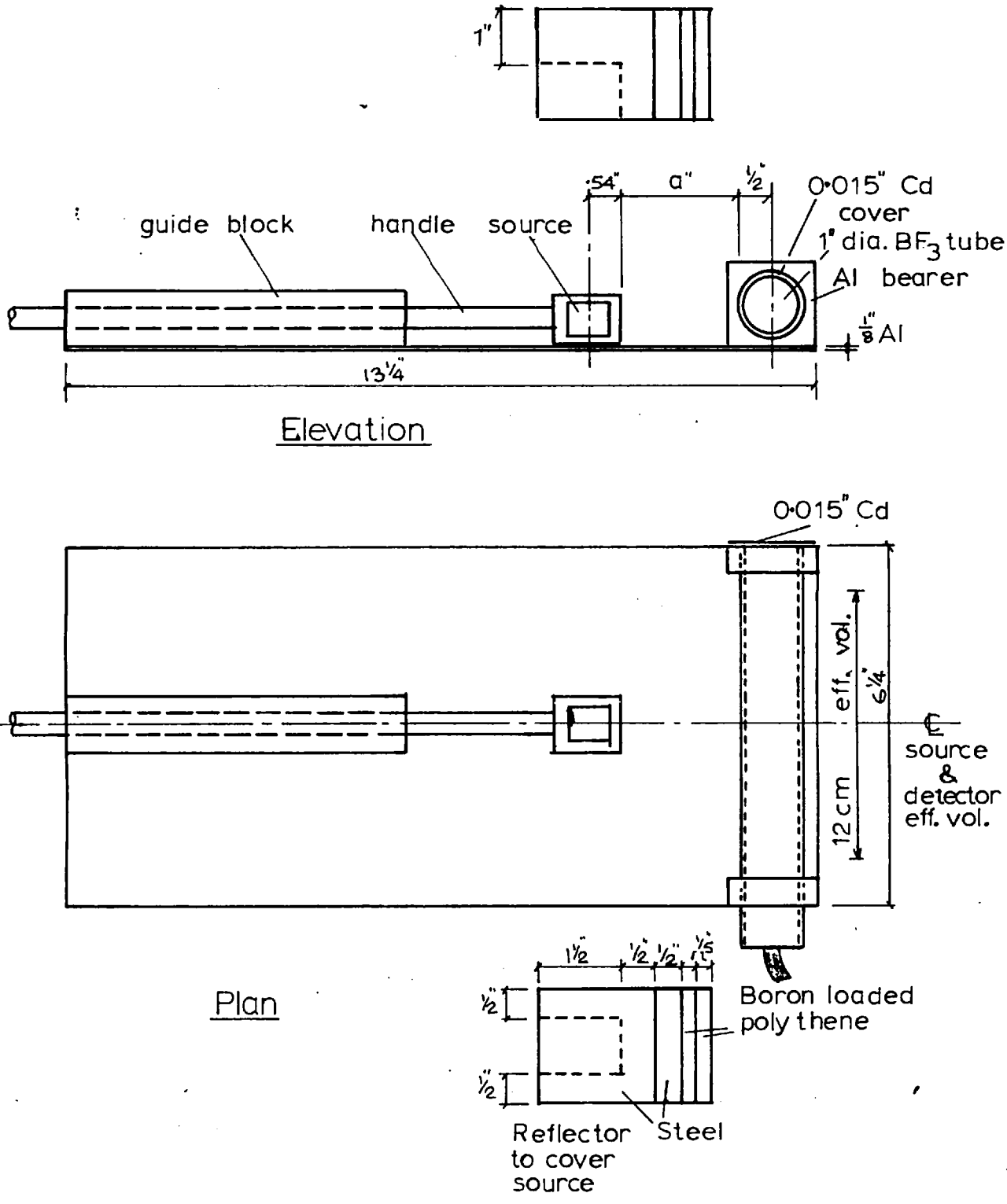
The performance of this apparatus was satisfactory but further tests, reported in Chapter 4.6, were carried out using a boron trifluoride counter. Although the count rate with a BF_3 counter is less than that with a lithium glass scintillator, the electronic stability demanded by a BF_3 tube is lower and therefore more suitable for both civil engineering site and research work.

The detection cross section for boron 10 was shown in Figure 39b.

CHAPTER 4.6 THE BACKSCATTER METHOD USING A BORON TRIFLUORIDE COUNTER

Chapter 4.6.1 The Source, Detector and Apparatus

Figure 52 shows the detector, a 12EB40 of 20th Century Electronics Ltd., effective volume 12 cm by 2.54 cm diameter, and the source, originally 1 curie of polonium-beryllium, on a $\frac{1}{8}$" aluminium plate. The detector was held



THE BACKSCATTER APPARATUS WITH BF_3 COUNTER

Scale $\frac{3}{8}$ fullsize

Fig. 52

in position by two aluminium bearing pieces and the source, in a stainless steel capsule, could be moved by sliding the handling rod in the guide block.

The use of the source reflector is described in Chapter 4.6.6.

Chapter 4.6.2 Determination of the Effect of Neutron Absorbers

To find the effect of absorbers on the count rate, readings were taken, with and without a cadmium cover, on water and on a 5% sodium chloride solution, and are shown in Table 37 from which it is seen that when a cadmium cover 0.015" thick was used there was no significant depression of the count rate due to the salt. It is not however reasonable to expect the cadmium cover to entirely eliminate the effect of neutron absorption because some $E^{-\frac{1}{2}}$ and resonance absorption will occur above the cadmium cut-off. In order to find a relation between count rate and concentration of absorber counts were taken, with the cadmium cover on the counter and distance a = 1", on water to which sodium chloride was progressively added. The result is shown in Figure 53. The slope of the straight regression line showed that the fractional change of count rate was 0.12 $\pm$ 0.04 per g/cc of NaCl.

TABLE 37

a	Bare Counter				0.015" Cd Cover			
	On Water		On Salt Solution		On Water		On Salt Solution	
	R	σ	R	σ	R	σ	R	σ
0"	596.3	6.0	507.0	5.1	69.6	0.7	69.0	0.7
½"	547.4	5.5	465.0	4.7	52.0	0.5	51.8	0.5
1"	484.5	4.8	413.9	4.1	41.0	0.4	41.3	0.4
1½"	414.4	4.1	368.1	3.7	33.5	0.3	33.8	0.3
2"	362.0	3.6	309.4	3.1	26.9	0.3	27.9	0.3
2½"	308.6	3.1	267.3	2.7	22.1	0.2	22.1	0.2
3"	258.2	2.6	223.2	2.2	17.9	0.2	18.3	0.2

R is in counts per second

σ is the standard error calculated from nuclear statistics.

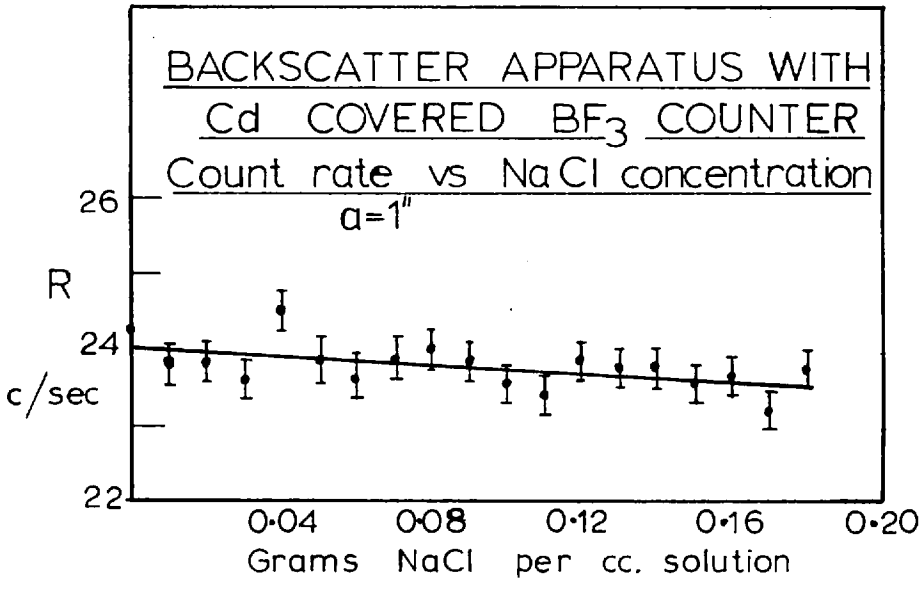


Fig. 53

Concentrations of other absorbers having the same thermal absorption cross section are shown in Table 38, compiled from Hughes and Schwartz (1958).

TABLE 38

Element	$\mu_a cm^2/g$	Concentration in g/cc equivalent to 1 g/cc NaCl
Li	6.09	0.054
B	41.87	0.0079
Cl	0.53	0.62
Sc	0.32	1.03
Co	0.38	0.87
Tc	0.61	0.54
Rh	0.87	0.38
Cd	13.66	0.024
In	0.99	0.33

The relation between error in water density and absorber concentration is derived in Chapter 4.6.5.

Chapter 4.6.3 Determination of the Effect of Gamma Radiation and Fast Scattered Neutrons

No counts due to gamma radiation were observed.

The count rate due to fast scattered neutrons was determined by taking readings on dry ¾" Thames river gravel and on the cadmium covered frame as in Chapter 4.5.5. The results are shown in Table 39.

TABLE 39

a inches	d' = 0		d' = 0.248 g/cc	
	$\frac{R_{fast}}{R}$	σ	$\frac{R_{fast}}{R}$	σ
0"	0.09	0.03	0.06	0.02
1"	0.07	0.03	0.04	0.02
2"	0.10	0.03	0.04	0.01
3"	0.18	0.04	0.06	0.01

It is shown later that the optimum distance 'a' was about 2", and at that distance the ratio of scattered to total count varied between 4% and 10% depending upon the water density.

The scattering mean free path due to all the elements in concrete other than hydrogen is approximately equal to that of 0.662 MeV gamma quanta. The dependence of the fast neutron scattered count on bulk density at a given

distance 'a' and density ρ may be expected to be similar to the dependence of scattered gamma radiation on density.

Figures 10a to 10h showed that in the range of densities from 1.4 to 2.4 g/cc (87 to 150 lb/cu ft), at a = 4" or 5" and α = 90° or 75°, which corresponded closest to the geometry of the neutron apparatus, scattered count rate showed very little change with density.

An upper limit for the expected effect of scattered fast radiation may be calculated by assuming a linear relation between scattered count and bulk density. In that case, at density 2.4 g/cc the ratio $\frac{R_{fast}}{R} = \frac{2.4}{1.4} \times 4 =$ 7%, at d' = 0.248 g/cc. A change of bulk density of as much as 10% would therefore change the count rate by 0.7%. Although the assumption of a linear relation was very pessimistic the change in count rate due to a change in concrete density was small, so that in practice it should be negligible. Dependence of the reading on bulk density has not been reported in the previous work reviewed in Chapter 4.1.

Chapter 4.6.4 Establishment of the Calibration Curves

The specimens used to establish the calibration curves were similar to those described in Chapter 4.5.2. The apparatus was placed on each specimen in turn, readings being taken at various source to detector distances, with

and without a 0.015" thick cadmium cover. The curves, shown in Figures 54, are of the same general shape found with the lithium glass scintillator.

Chapter 4.6.5 Assessment of the Results and Comparison with the Lithium Glass Scintillator

The curves of R_s/R at d' = 0.248 g/cc against 'a' in Figure 55 show that this ratio was higher for the BF_3 than the lithium glass scintillator, and that it increased as the source was moved farther from the detector. The sensitivity of the apparatus with the BF_3 counter was better than with the lithium glass scintillator but because the detection efficiency of the BF_3 counter was lower the time to reach a given standard error, shown in Figure 56, was less for the lithium glass scintillator.

The time required for a given standard error was a function of sensitivity S and count rate R, and therefore depended on the relative magnitudes of $R = R_s + R_p$ and R_S. When the source was near the detector R_p was high and as it was moved from the detector both R_p and R_s decreased. The initial reduction in R_p gave an improvement in S and a lower time for a given accuracy, but at greater distances the increase in sensitivity was insufficient to counteract the reduction in count rate with the result that at a particular optimum distance the time to achieve a given

THE BACKSCATTER APPARATUS WITH Cd COVERED BF_3 COUNTER

R vs d'

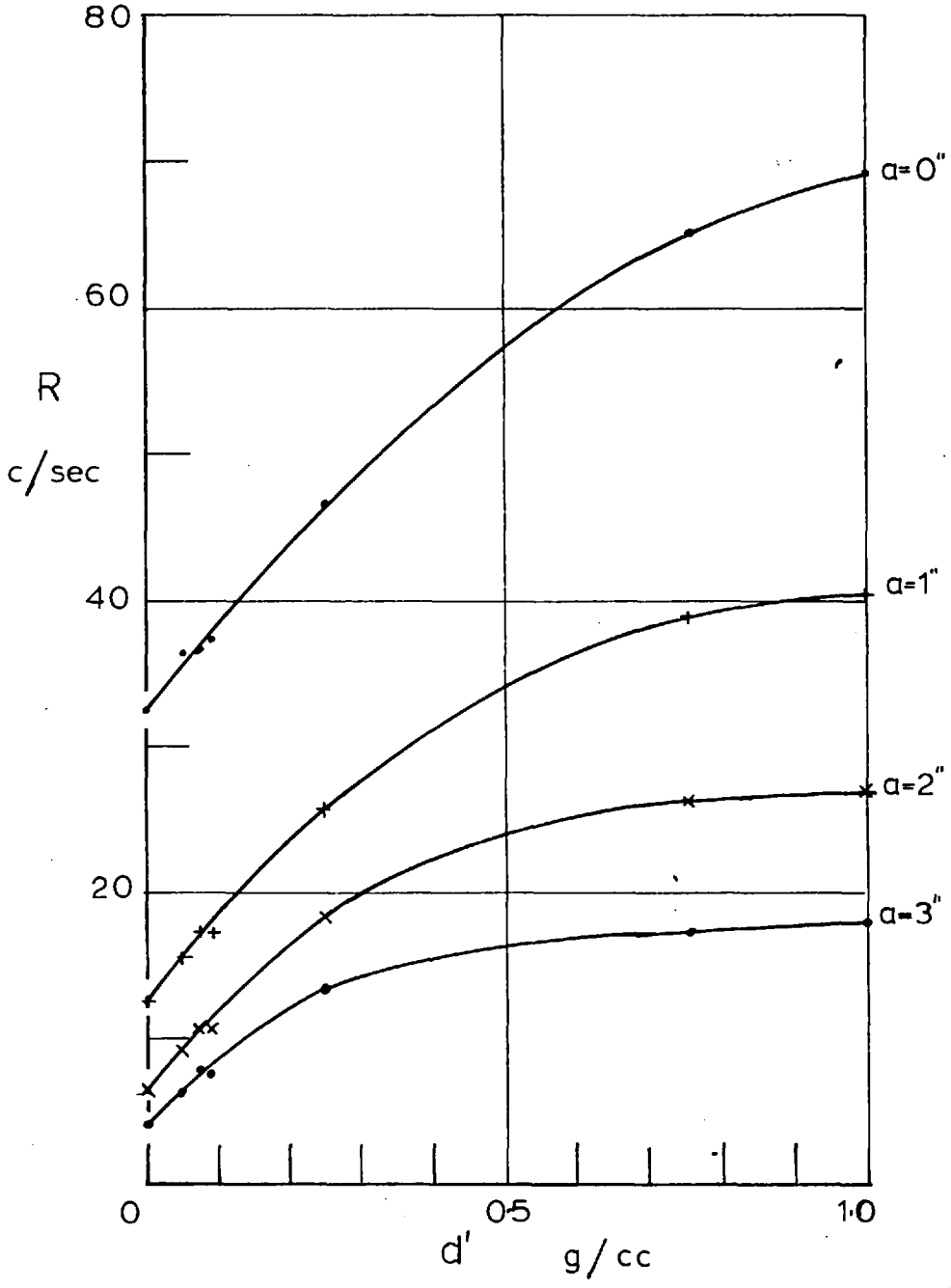


Fig.54 a

THE BACKSCATTER APPARATUS WITH BARE BF_3 COUNTER
R vs d'

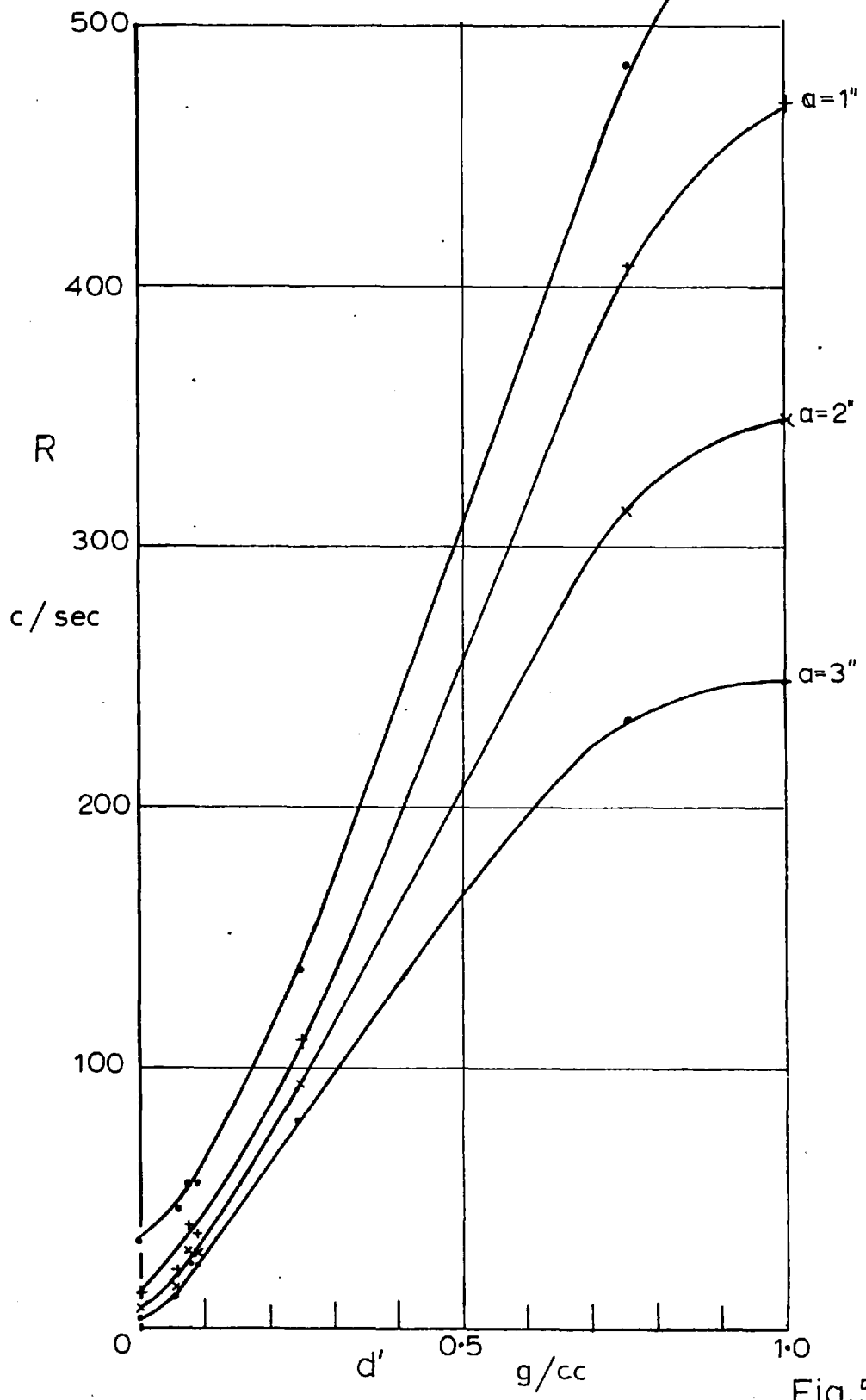
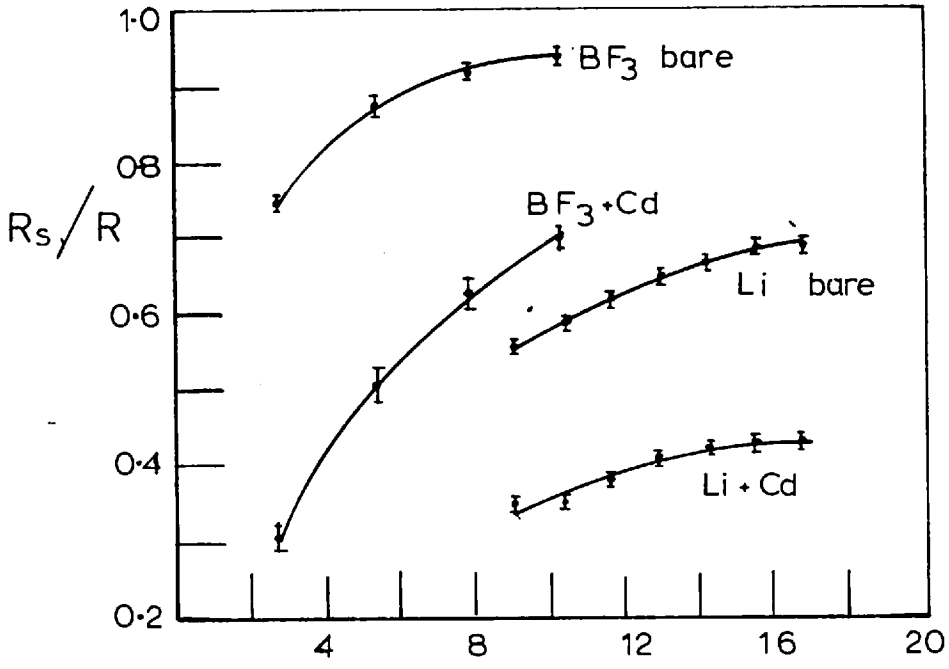


Fig. 54 b

R_s/R & S vs Distance from centre of source to centre of detector

$d' = 0.248$ g/cc



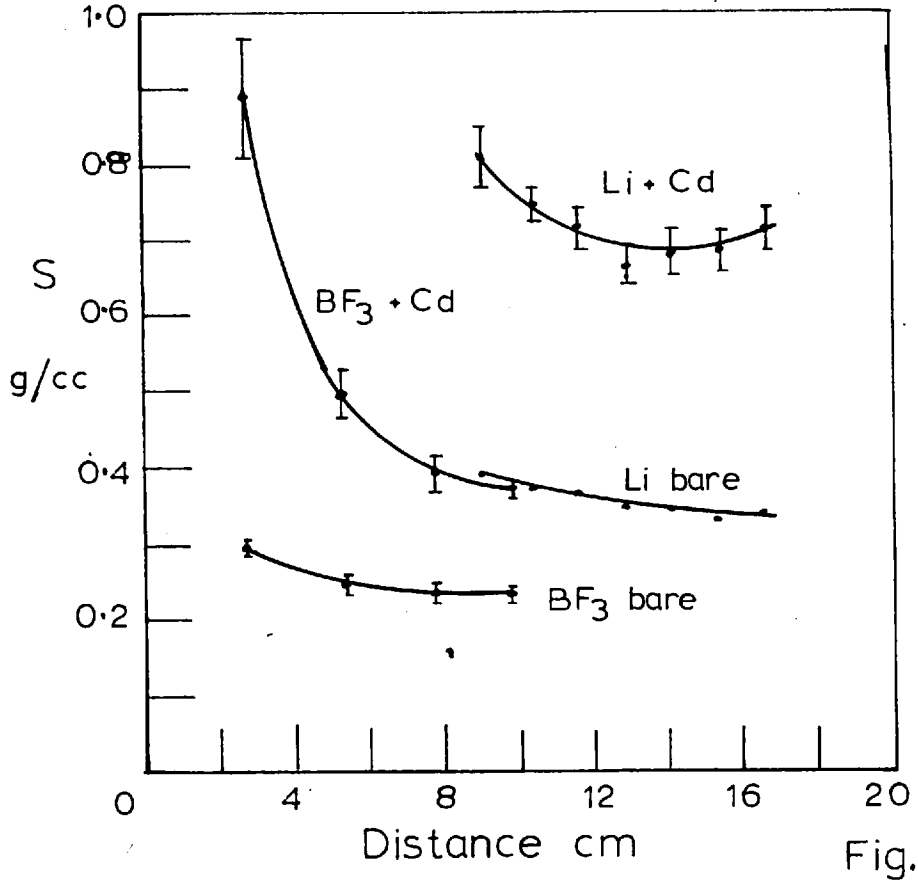


Fig.55

TIME FOR $\sigma_{d'}$ 0·01 g/cc vs DISTANCE FROM CENTRE OF SOURCE TO CENTRE OF DETECTOR

$d' = 0{\cdot}248$ g/cc

Source intensity $= 2{\cdot}4 \times 10^6$ n/sec

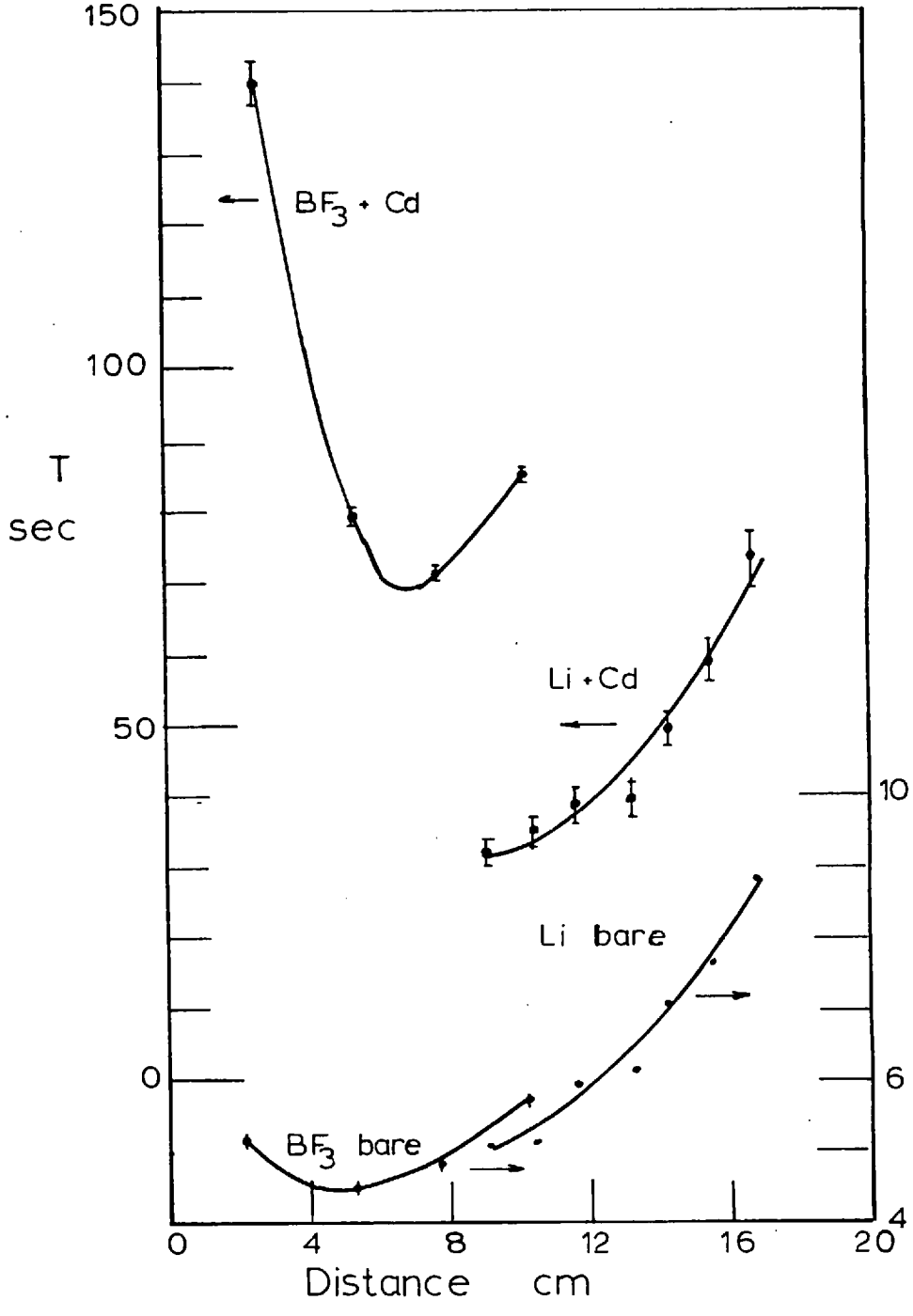


Fig. 56

accuracy passed through a minimum.

The relation between concentration of absorber and water density was found knowing a value of sensitivity.

$$\frac{\sigma_R}{R} = \frac{\sigma_{d'}}{S} \qquad 4.6.5.(1)$$

At the optimum, for the cadmium covered BF_3 counter, S = 0.4 g/cc. The relative change of count rate corresponding to $\sigma_{d'}$ = 0.005 g/cc was found from equation 4.6.5.(1) to be 0.0125. This change would be produced by a sodium chloride concentration of $\frac{0.0125}{0.12}$ = 0.1 g/cc, or an equivalent of any other absorber, listed in Table 38. The concentrations required to produce a change of 0.005 g/cc in the assumed water density are greater than would be found in structural concretes.

Comparing the results for the BF_3 counter and lithium glass scintillator:

a) The BF_3 counter gave a greater sensitivity than the lithium glass scintillator.

b) The time to achieve a given accuracy with a cadmium covered BF_3 counter was about twice that for a lithium glass scintillator.

c) The lithium glass scintillator did detect a small count due to gamma radiation but the BF_3 counter did not.

d) The scattered fast neutron count was of the same order of magnitude for each and would be expected to give a negligible change in count rate with bulk density over

the range of normal concretes.

e) Instrumentation for a portable BF_3 counter would be cheaper and more reliable than for a scintillation counter.

Considering all the points of comparison, the BF_3 counter was considered the better detector for this application.

Chapter 4.6.6 Some Considerations in the Design of a Practical Instrument

An instrument requiring access to only one face of a specimen was considered to be the most useful, and is discussed here.

The BF_3 counter was found to be the most satisfactory detector. Although it is not necessary, with this detector, to use a source with low gamma intensity, the use of such a source rather than radium-beryllium is worthwhile in order to reduce the cost and weight of shielding required.

Assuming that a low gamma activity source is used, the shield design will be determined by the allowed fast neutron dose. The shield must be arranged so as to scatter a minimum of neutrons into the detector because these would increase the count rate R_p and reduce the sensitivity of the instrument.

The choice of source strength is a compromise between

the accuracy required in a given time and the shielding requirement. The relation between time of count and accuracy was obtained from the derivation of sensitivity S.

$$\sigma_{d'} = \frac{R}{R'\sqrt{N}} \qquad \text{from 2.6.(2)}$$

$$T = \frac{N}{R}$$

$$= \frac{S}{R' \sigma_{d'}^2} \qquad 4.6.6.(1)$$

R' will be proportional to source intensity I_o, so

$$T \propto \frac{S}{R' I_o \sigma_{d'}^2} \qquad 4.6.6.(2)$$

Figure 56 shows that at the optimum source detector distance a standard error of 0.01 g/cc was attained after 70 seconds with a source of 2.4×10^6 neutrons per second. Using this information in equation 4.6.6.(2) it was calculated that a source of 10^7 neutrons per second would give a standard error of 0.0025 g/cc in 250 seconds.

A steel reflector placed around the source would increase R_s and decrease R_p. Experiments were carried out with such a reflector, shown in Figure 52. Distance 'a' was set at 1" and readings taken with the BF_3 counter both bare and cadmium covered, on concrete of water density 0.248 g/cc and on the cadmium covered frame. The results are shown in Table 40.

TABLE 40

Arrangement	Ratio of $S_{reflected}$ to S_{bare}		Ratio of $Time_{reflected}$ to $Time_{bare}$	
	With Cd Cover	No Cd Cover	With Cd Cover	No Cd Cover
Reflector	1.32	1.05	0.45	0.63
Reflector + ½" steel plate	1.37	1.05	0.43	0.64
Reflector + ½" steel plate + 200 mg B in 0.2" polythene	1.25	1.03	0.53	0.71
Reflector + ½" steel plate + 400 mg B in 0.4" polythene	1.27	1.03	0.48	0.73

The boron loaded polythene was not helpful because the moderating effect of the polythene was greater than absorption by the boron. A 1" thickness of steel between source and detector increased the sensitivity, and halved the time required for a given accuracy.

For an instrument comprising a source of 10^7 neutrons per second, a 1" steel reflector and a BF_3 counter effectively 12 cm by 2.54 cm diameter, the time required to reach a standard error of 0.0025 g/cc at d' = 0.25 g/cc should be about two minutes.

The recommended permissible dose on the hands, forearms, legs, feet and ankles is 1.5 rems per week (I.A.E.A.

1958). Making the safe assumption that this dose will be tolerated for 40 hours per week, a dose of 37.5 millirem per hour would be permitted. The flux of neutrons between 1 and 5 MeV corresponding to this dose is 270 neutrons/ cm^2 sec. (Imperial College 1962) and the distance in air from a source of 10^7 neutrons/sec giving this flux is 54 cm.

If a wax shield 3" thick were placed 12" from the source, then assuming a slowing down length in wax of 7 cm, the fast flux at the wax surface would be approximately 185 neutrons/cm^2 sec.

Some mechanism would be required to shield the source from below when not in use.

The neutron radiation may affect the concrete either by activating nuclei constituting it, by disruption of chemical bonds or by heating the concrete. The activation and disruption due to a source of 10^7 neutrons per second for the time that apparatus may be on concrete would be negligible (Price et al 1957).

The heating effect was calculated assuming that the average energy per neutron is 3 MeV, and that all the energy is lost by proton collisions within one slowing down length. The slowing down length L_s in concrete of water density 0.25 g/cc would be four times that of water, which is given by Price et al (1957) to be 5.6 cm. The energy deposited per cubic centimetre for a source of 10^7 neutrons per second is given by

$$\text{Energy/cc} = \frac{\text{Energy per neutron x source intensity}}{\text{Volume of concrete}}$$

$= 1.2 \times 10^{-10}$ watts per cc for the values above. The temperature rise will therefore be negligible.

Chapter 4.6.7 Conclusions

Neutron backscatter apparatus using a BF_3 counter covered with 0.015" cadmium will give readings of water content negligibly dependent upon the presence of neutron absorbers, hydrogen bonding, or the bulk density of the concrete.

There exists an optimum source detector distance, found to be 7 cm between centre lines of source and detector. For a 12EB40 (20th Century Electronics Ltd.) detector and a source of 10^7 neutrons per second in a 1" steel reflector placed 7 cm apart, the time required to reach a standard error of 0.0025 g/cc at d' = 0.25 g/cc should be about 2 minutes. Greater accuracy could be achieved by taking a longer count, using a more intense source, or by using several shunt connected detectors which may be on one or both sides of the source depending upon the extent of the volume of concrete over which the reading is required to be averaged.

CHAPTER 4.7 THE EQUATION OF THE GAUGE

Logarithm of the scattered count rate R_s was plotted against the horizontal distance between centre lines of source and detector, x, in Figures 57a to d for both lithium glass and BF_3 detectors, for the various materials used. These were straight lines to which were fitted the equation

$$R_s = Ae^{-Bx} \qquad 4.7.(1)$$

A and B were found by least squares fitting and the logarithms of these values were plotted against logarithm of d' in Figures 58 and 59. These are seen to be straight lines up to about d' = 0.8 g/cc giving the empirical equations

$$A = jd'^{k} \qquad 4.7.(2)$$

$$B = md'^{n} \qquad 4.7.(3)$$

where j, k, m and n are constants for a given source and detector arrangement.

Substituting in 4.7.(1)

$$R_s = jd'^{k}\exp(-md'^{n}) \qquad 4.7.(4)$$

where m is now equal to mx before.

The values of the slopes of the straight portions of the curves are shown in Table 41.

LOG R_s vs DISTANCE FROM CENTRE OF SOURCE TO CENTRE OF DETECTOR

Cd covered Li glass scintillator

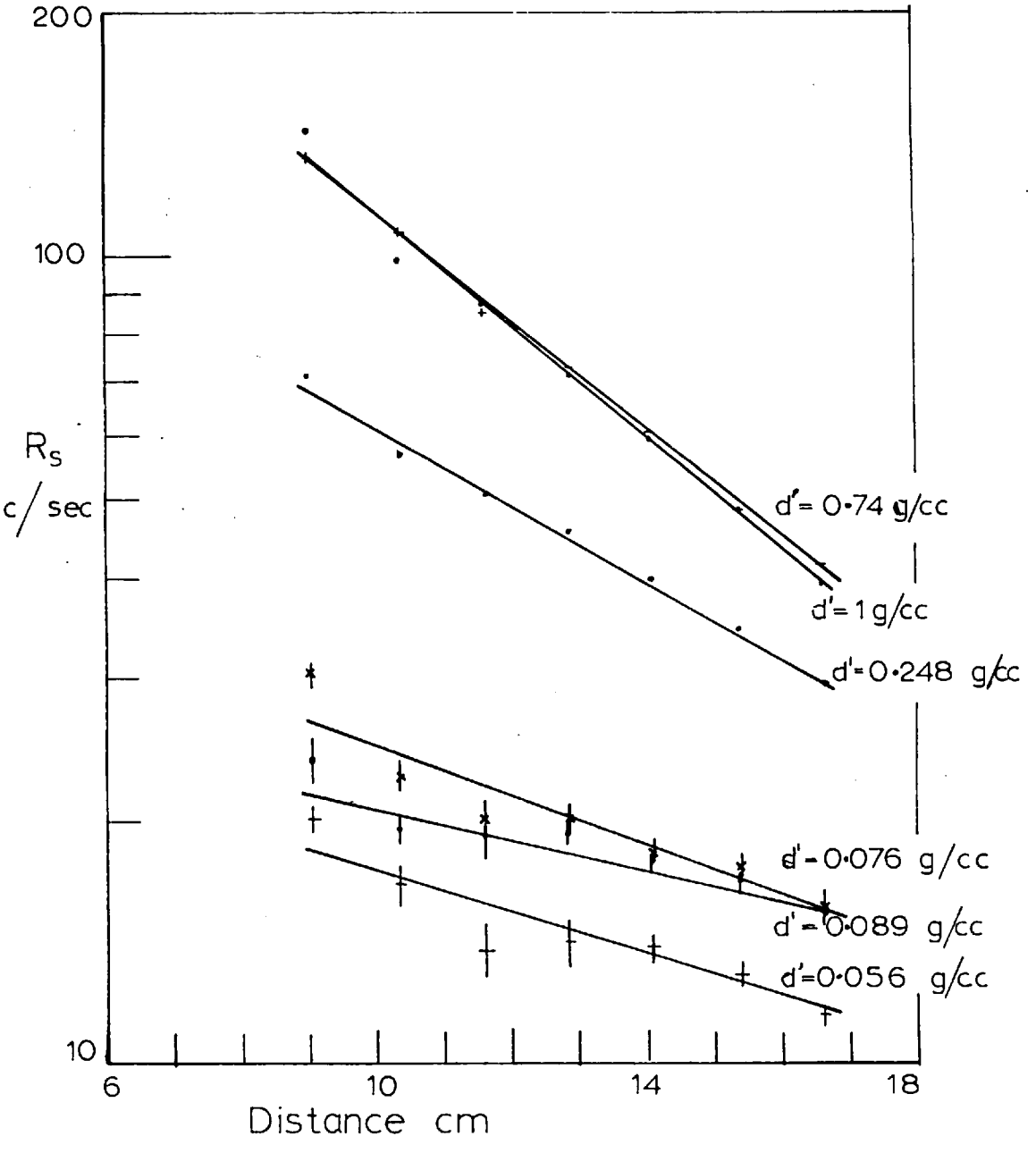


Fig.57a

LOG R_s vs DISTANCE FROM CENTRE OF SOURCE TO CENTRE OF DETECTOR

Li glass scintillator without Cd cover

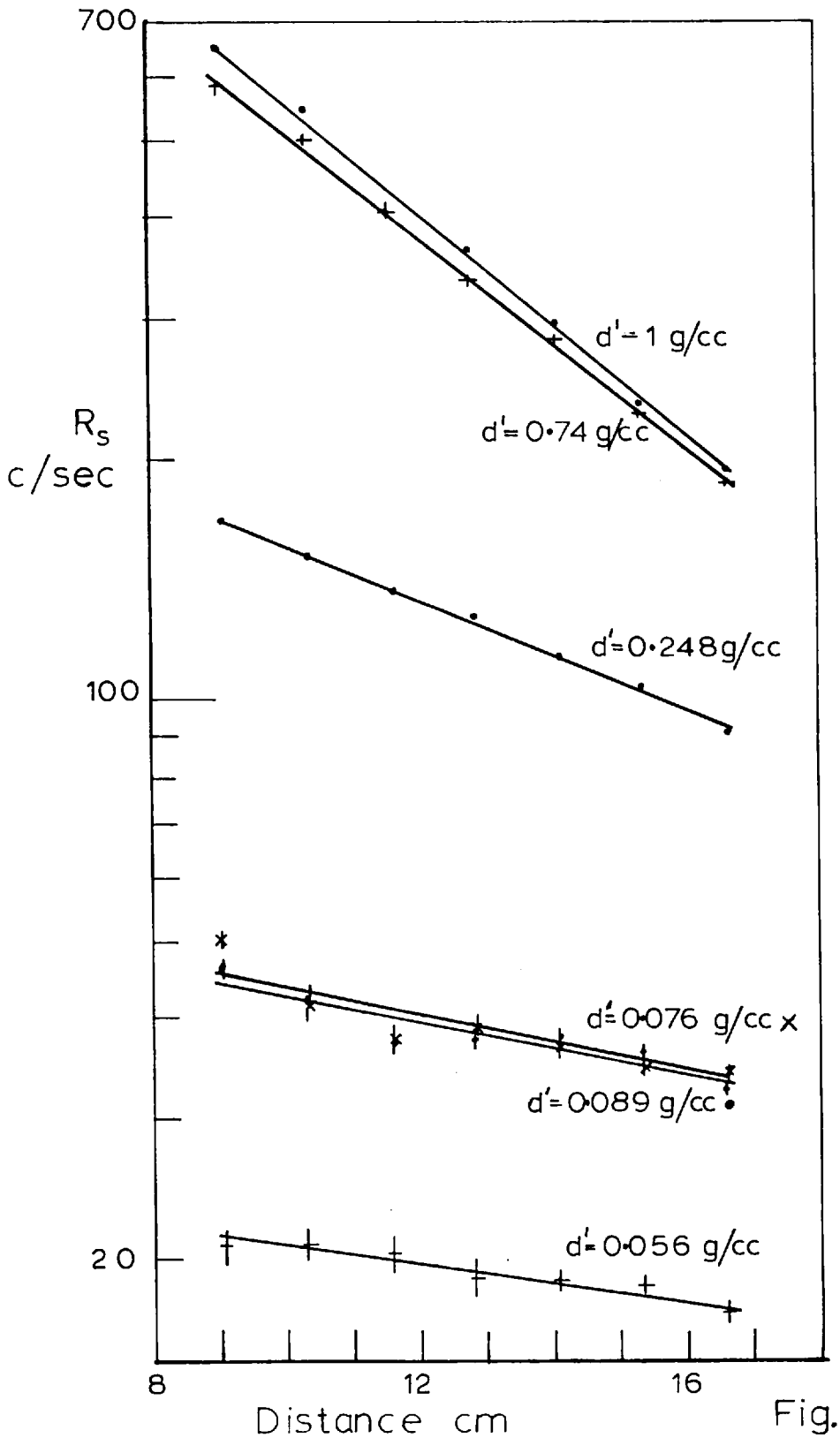


Fig.57b

LOG R_s vs DISTANCE FROM CENTRE OF SOURCE TO CENTRE OF DETECTOR

Cd covered BF_3 counter

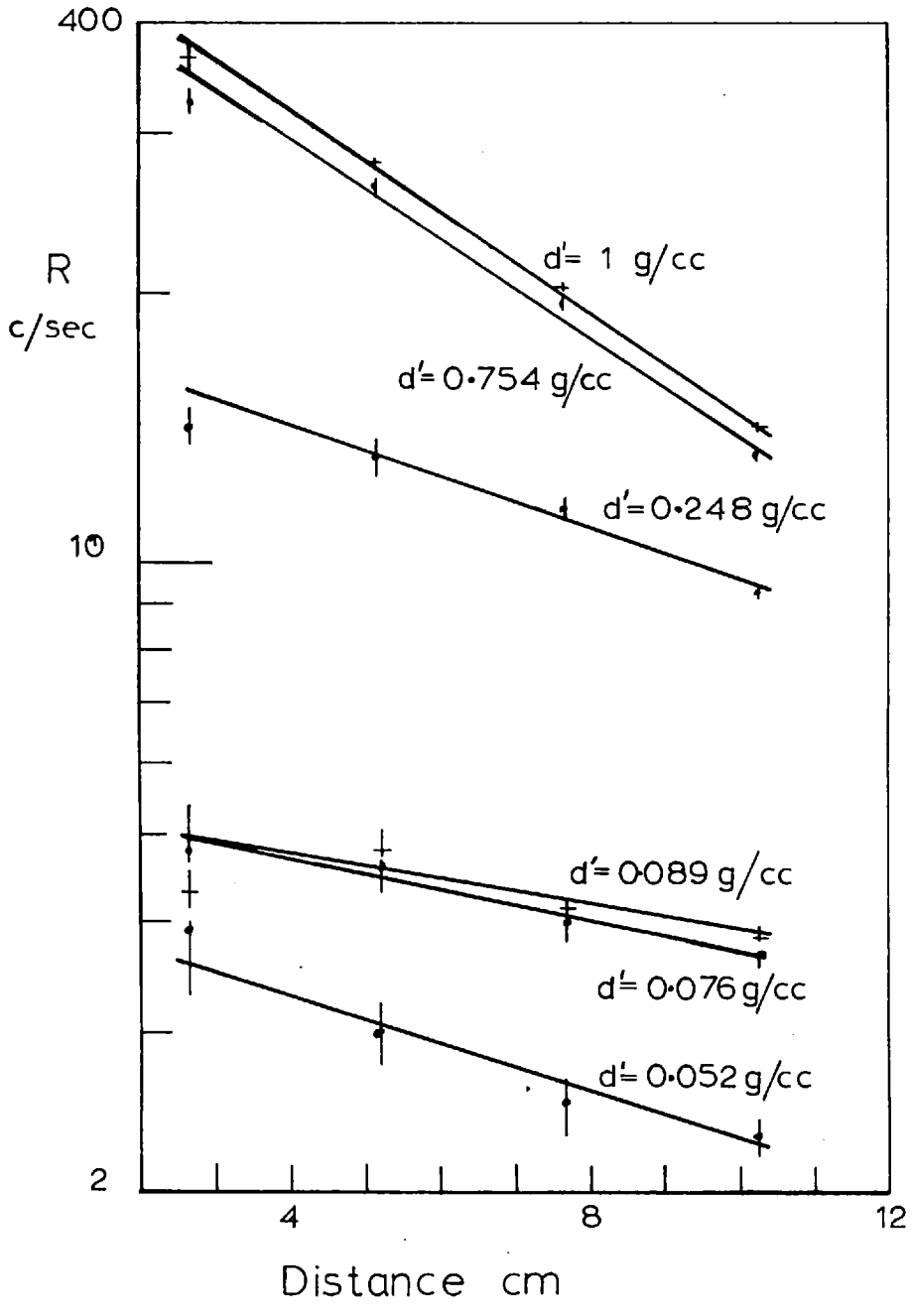


Fig. 57c

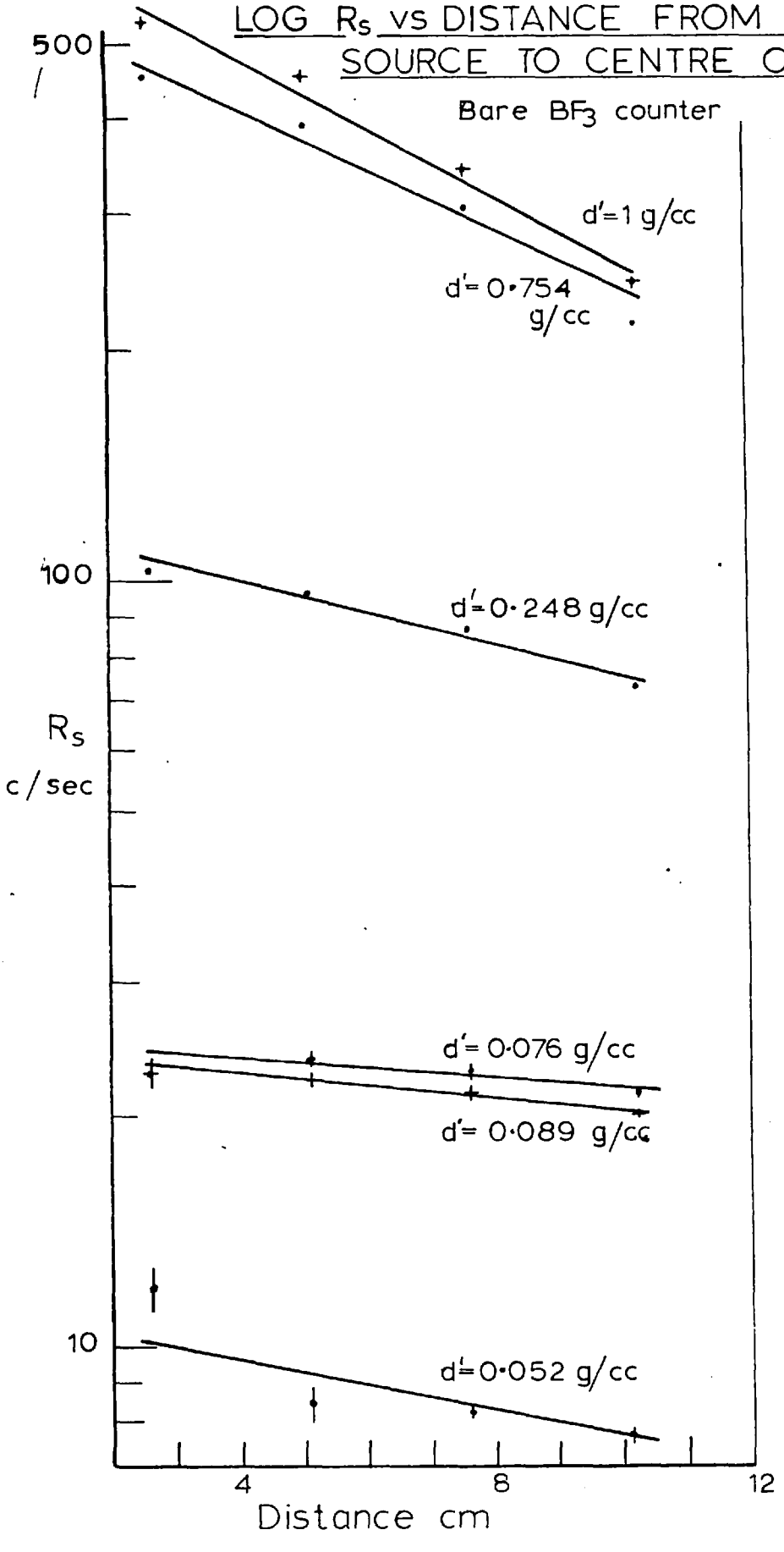

LOG R_s vs DISTANCE FROM CENTRE OF SOURCE TO CENTRE OF DETECTOR
Bare BF_3 counter
d'=1 g/cc
d'= 0·754 g/cc
d'= 0·248 g/cc
d'= 0·076 g/cc
d'= 0·089 g/cc
d'= 0·052 g/cc
500
100
10
R_s
c/sec
4
8
12
Distance cm

Fig. 57d

LOG A vs LOG d'

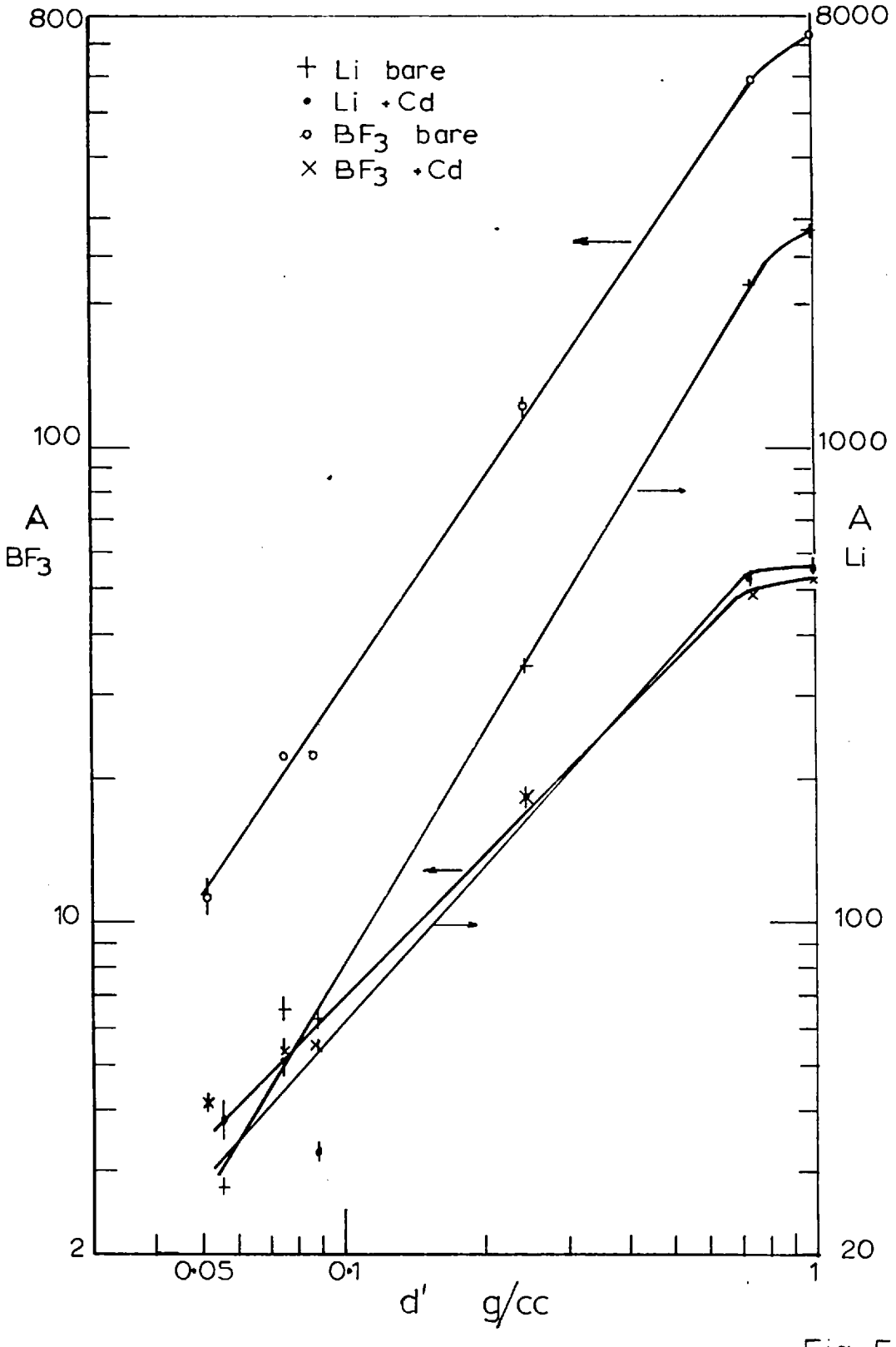


Fig. 58

LOG B vs LOG d'

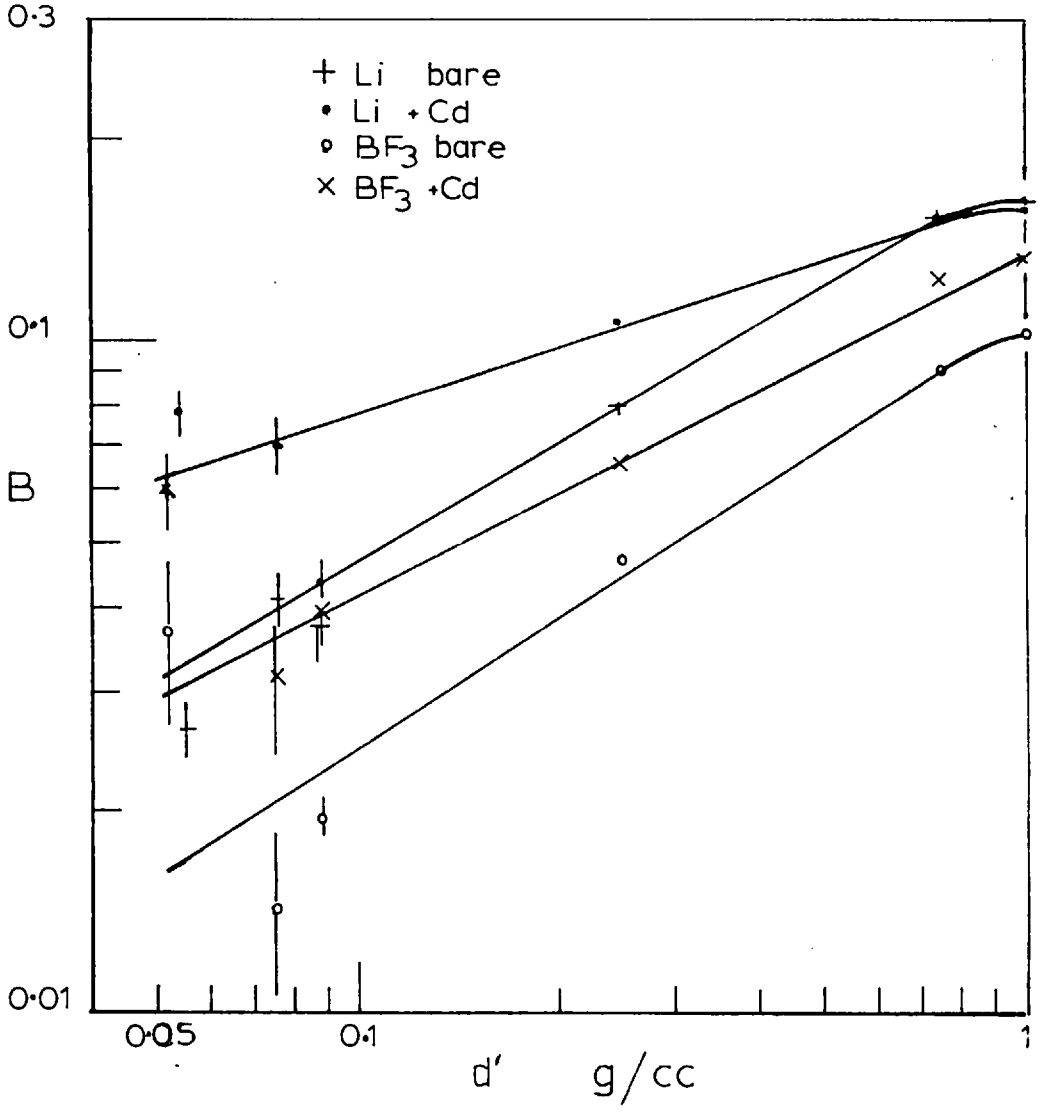


Fig. 59

TABLE 41

Detector	K	σ_K	n	σ_n
Li, Cd cover	1.13	0.12	0.35	0.06
Li, bare	1.72	0.04	0.61	0.02
BF_3, Cd cover	1.00	0.07	0.45	0.10
BF_3, bare	1.48	0.07	0.66	0.11

Although the experimental evidence is rather slender it is interesting to note that this result is similar to that for the gamma backscatter density gauge, discussed in Chapter 2.9.

CHAPTER 4.8 CONCLUSIONS

A neutron scattering water content gauge should give a reading of water density independent of fast scattered neutrons, gamma radiation, presence of neutron absorbers, or of bonding on the hydrogen atoms. The instrumentation should also be as simple and reliable as possible. With a boron trifluoride counter covered with 0.015" cadmium, the changes in count rate due to changes in fast scattered neutron flux with bulk density, due to the presence of any absorbers which may reasonably be found in concrete and due to hydrogen binding force were negligible. The portable instrumentation required for a BF_3 counter is

easily acquired and usually more reliable than that for a scintillation counter so that detector was considered the most satisfactory for a water content gauge.

Elimination of the effects of chemical composition, achieved by using a cadmium cover, was gained at the expense of the time required to reach a given standard error. Even with the cover, however, the time required to reach a standard error of 0.0025 g/cc was only about 2 minutes.

The use of foil detectors was limited either by the long half life of a foil or by the limitation in statistical accuracy due to the presence of background radiation.

A long half life low gamma intensity neutron source should be used in order to avoid the weight of gamma ray shielding. Plutonium-beryllium and americium-beryllium are such sources. The source spectrum of plutonium-beryllium is similar to that of polonium-beryllium (Notarrigo et al 1962) and that of americium-beryllium, although not yet experimentally determined, should also be similar, so that the results quoted for a polonium-beryllium source should be applicable to these sources.

If polonium-beryllium is used the correction to the count rate due to the decay of the source is about $\frac{1}{2}\%$ per day, which is considerable, and frequent replacement of the source would be expensive. The correction for americium-beryllium is 0.15% per year and for plutonium-beryllium is 0.285% per century, which is negligible.

Both these sources would outlive an instrument and could be used again.

The source and detector may be placed in any geometrical relation such as that discussed in Chapter 4.4 for 6" cubes, but then the calibration curve would depend upon the size of specimen used.

For backscatter apparatus requiring access to only one face of a specimen the optimum distance between centres of source and detector is 7 cm. A coefficient of variation of 1% due to nuclear statistics should be attainable in a reasonable time with a source of 10^7 neutrons per second inside a 1" steel reflector.

The effectively infinite depth d_∞ varies from about 4" in water to 12" in damp sand ($d' = 0.06$ g/cc) and appears to vary inversely as $(d')^{\frac{1}{2}}$. The effectively infinite surface dimensions will depend upon the detailed geometry of an instrument, but the distance from the detector to the edge of the volume should not exceed d_∞.

The possible causes of errors may be classed as:

a) electronic instability

b) nuclear statistics

c) geometrical errors, which include such items as surface roughness and the change of position of the source or detector due to bad instrument design.

The presence of steel bars and the non-uniformity of moisture distribution in concrete are not classed as errors,

because if these occur the apparatus will nevertheless measure the moisture content of the effectively infinite volume, giving a weighted average over this volume. This is discussed later.

In apparatus of the geometry described in Chapter 4.4, geometrical errors may arise due to inaccuracy in positioning the specimen, which may be a standard cube or a container holding fresh or hardened concrete. The specimen must be placed in an accurately reproducible position, and if a container of fresh concrete is used it must be carefully levelled off. Whether or not these elementary precautions will reduce the geometrical errors to insignificance must be determined by future experience.

If backscatter apparatus is correctly designed and manufactured then neither source nor detector will move and geometrical errors will be due to roughness of the surface of the concrete. Workers who have used both gamma ray and neutron backscatter apparatus in the same location and who have observed an effect of surface roughness with density apparatus have not reported any such effect for neutron apparatus (Belcher et al 1952, Carlton 1960).

As the surface roughness affects the count rate by changing the effective path of radiation in the concrete, the magnitude of the effect will increase with water density. Neutron backscatter apparatus may for this purpose be con-

sidered as analogous to gamma ray backscatter apparatus where the water densities found in concretes correspond to low densities and so the effect of surface roughness is expected to be less than with density apparatus. The use of three legs on gamma ray backscatter apparatus was seen to reduce this effect, so although the error due to surface roughness is expected to be small with neutron back-scatter apparatus the use of legs may be beneficial. As the neutron apparatus is uncollimated the change of sensitivity, count rate and optimum distance, due to short legs, should be small but would require investigation.

Neutron water density apparatus measures the total water content weighted over an effectively infinite volume which in concretes will extend from 5" to 10" from the detector, depending upon the water density. When calibrating an instrument the count rate is plotted against water density derived from weighing and drying samples of concrete. In order to determine the total water content the samples have to be heated at an elevated temperature and the evaporated water analysed for carbon dioxide. The accuracy of the calibration will depend upon whether the samples are representative of the effectively infinite volume and whether the analysis of the samples is accurate. Accurate calibration by this procedure is possible but requires that the concrete specimens be carefully made and cured and that a considerable number of samples be taken

from each in order to establish the uniformity of moisture distribution in the specimen and to reduce the errors in analysing the samples.

In order to test experimentally the effect of surface roughness and to test the reliability of a particular instrument, the procedure described above should be followed. As this investigation has shown that the neutron backscatter method is capable of fairly good accuracy, further development which included such a procedure would be worthwhile.

The presence of steel bars in the effectively infinite volume would affect the count rate and should therefore be avoided. This was not investigated.

The background count due to cosmic neutron radiation would be negligible.

A portable instrument for determining the water density may be used for quality control on either fresh or set concrete or may be used to determine the water content of an existing structure or specimen, which would be useful in research and routine testing of concrete. In order to find the water content from water density the density of the concrete must be known. This may be found using the gamma radiation techniques described in Parts 2 and 3.

PART 5 GENERAL CONCLUSIONS

It has been shown in this thesis that in the determination of both density and water density of concrete by the use of radioactive isotopes, the effect of the chemical composition of the concrete, which may be a significant cause of error, can be made negligible by the correct design and use of apparatus. The apparatus need then only be calibrated once and this curve, when corrected for source decay and possible electronic instability, will be valid on all concretes.

The method of determining density by gamma ray backscatter has the advantage that only one surface of a member need be accessible in order to take a reading. The depth of concrete "seen" is about 4" with about half the count due to radiation which does not penetrate beyond the first inch. There is therefore no way of directly calibrating the apparatus, as the usual method of determining the density is to weigh and measure a block overall. The most significant possible cause of error, apart from electronic instability in badly designed apparatus, will be roughness of the concrete surface. Provided the surface is reasonably smooth three legs in the base of the instrument should reduce this effect, but in some cases grinding of the concrete may be necessary. The accuracy attained by such an instrument should be about 1 lb/cu ft, which is

two standard errors.

The transmission method, although requiring access to opposite faces of a member, is capable of greater accuracy than the backscatter method. This is achieved by using the simple relation governing count rate, density and other variables, to make accurate allowances for the effect of chemical composition, shown in the Compton scattering factor, and surface condition, defined by the thickness of a specimen. This apparatus "sees" a narrow pencil of concrete and determines the density of that small volume which will usually be different from the overall density of a specimen, so that accurate direct calibration is not possible. The accuracy of the density as determined by the transmission method is limited by non-uniformity of the concrete itself, so this apparatus is as accurate as may be required for concrete testing.

Both the above methods may be used for locating steel bars in concrete.

The neutron water density method determines the total water density of concrete which must be divided by the overall density to give the total water content. It is fortunate that the most practical neutron detector, the boron trifluoride tube, is suitable from other points of view. When covered with 0.015" cadmium and used in apparatus requiring access to only one face of a specimen, with a

reflected source the optimum distance away, the accuracy attainable should be 1%, which is two standard errors. The apparatus "sees" a depth of approximately 8" in concrete, so accurate direct calibration with conventional techniques is difficult.

The accuracy of radioisotope methods is limited by the statistics of nuclear counting and by geometrical factors as defined in Chapter 4.8. As was shown in Part 2, the accuracy to be expected from backscatter density apparatus is about 1%, provided the concrete surface is smooth. Transmission density apparatus can determine the density to an accuracy of $\frac{1}{2}$%, as discussed in Part 3, and water density apparatus should give an accuracy of 1%, as shown in Part 4.

The magnitude of the accuracy which would be sufficient depends on the property being investigated, the effects of density and water density on it and the precision required in evaluating that property. For example, the relation between density, water content and cube crushing strength has been experimentally determined and it is known that a 5% decrease in cement/water ratio (Fulton 1957) or a 1% decrease in density (Jones 1962) would cause a 5% decrease in cube crushing strength. In order therefore to determine the cube crushing strength to an accuracy of 5%, an accuracy of 5% would be sufficient for the water density

and 1% for the density determination. If used for this purpose the density backscatter apparatus may be insufficiently accurate on a rough surface but the density transmission apparatus and the water density apparatus would be accurate enough.

The use of these methods makes available an entirely new approach to the control of concrete quality because the water content and density of a concrete can be determined immediately after placing and unsatisfactory concrete removed before setting.

The development of radioisotope methods as standard tests for concrete will depend whether they give useful information sufficiently accurately and whether or not this information is made available by other methods.

The density and moisture content of a concrete made from given materials are basic to the properties of that concrete. Most properties of concrete are found experimentally in terms of the aggregate/cement and water/cement ratios and for a given air voids ratio these quantities determine both the density and the water density. As density and water density may be determined by non-destructive tests, this knowledge, if sufficiently accurate, could be used to determine other useful properties of concrete.

Ever since the classical work of Abrams earlier this century it has been realised that the water content is an

important variable in concrete, and water content is usually carefully controlled at the mixing point but is not measured on the finished structure. Although correctly placed concrete has a uniform density which can be specified for given concrete components, density is not measured on a structure because, until the advent of radioisotope techniques, this has not been possible. Even the usual laboratory technique of weighing in air and water is applicable only to saturated specimens.

If quantitative relations were established between density, water density and fundamental properties of interest in concrete, these properties could be determined on a structure using the methods described in this thesis.

All the results obtained are applicable to soils, making it possible to eliminate the "soil type effect" observed with previous instruments.

LIST OF REFERENCES

Belcher D.J., Cuykendall T.R. and Sack H.S. 1952
U.S. Civil Aero. Admin., Tech. Dev. Report No.161.

Bernhard R.K. and Chasek M. 1955
A.S.T.M., Proc. Vol. 55, p.1198

- and Griggs P. 1956
A.S.T.M., Proc. Vol. 56, p 1288.

Bopp F. 1937 Annalen der Physik Vol. 30.

Brocard J. 1954 RILEM Bulletin No.20 (old series), Dec.

- 1955 Revue des Materiaux de Construction et de Travaux Publics, No.482-483, p 142, Nov./Dec.

Bulatov B.P. 1960 Kernenergie p 494

Burn K.N. 1960 A.S.T.M., Spec.Tech.Publ. 293

- 1963 Inter.Symp. Humidity and Moisture, Washington.

Carey W.N. and Reynolds J.F. 1958. U.S. Highway Research Board Special Report 38.

Carey W.N., Shook J.F. and Reynolds J.F. 1960
A.S.T.M. Spec. Tech.Publ. 293

Carlton P.F. 1960 A.S.T.M. Spec. Tech. Publ. 293

Dobychin V.P. 1958 D.S.I.R., N.L.L. Boston Spa, Translation RTS 2165

Durante V.A., Kogan J.L., Ferronsky V.I. and Nösal S.I. 1957 Proc. 4th Inter. Conf. on Soil Mechanics and Foundation Engineering Vol.1 p 216

Etherington H. 1958 "Nuclear Engineering Handbook", McGraw Hill.

Evans R.D. 1955 "The Atomic Nucleus", McGraw Hill.

Forrester J.A. 1960 Hochschule fur Bauwesen, Leipzig, Symposium. See U.S.A.E.C. Translation tr - 5632.

Fulton F.S. 1957 "Concrete Technology", The Concrete Association, South Africa.

Galambos S. 1960 Hochschule fur Bauwesen, Leipzig, Symposium. See U.S.A.E.C. Translation tr - 5632.

Goldstein H. and Wilkins J.E. 1954 U.S.A.E.C., N.Y.O. Report 3075.

Gnaedinger J.P. 1960 A.S.T.M. Spec. Tech. Publ. 293.

Grodstein G.W. 1957 U.S. Nat. Bur. Stds. Circular 583.

Hayward E. and Hubbell J. 1953 U.S. Nat.Bur. Stds. Report 2264.

- 1954 J.Appl.Phys. Vol.25, No.4, p 506.

Her Majesty's Stationery Office, D.S.I.R. 1931 "Chemical Analyses of Igneous Rocks, Metamorphic Rocks and Minerals".

- 1956a "Chemical Analyses of Igneous Rocks, Metamorphic Rocks and Minerals 1931 - 1954".

- 1956b "The Limestones of Scotland, Chemical Analyses and Petrography".

- 1960 "Sources of Road Aggregate in Great Britain".

Holmes J.W. 1956 Aust.J.Appl.Sci., Vol. 7, No.1.

Huet J. 1961 Centre de Recherche Routieres, Brussels, Report 75/JH/1961.

- 1962 RILEM Bulletin 15, June.

Hughes D.J. and Schwartz R.B. 1958 U.S.A.E.C., B.N.L. Report 325.

Huyghe G. and Mortier P. 1955 Institut Interuniversitaire des Sciences Nuclaires, Brussels, Symposium.

Hyodo T. 1962 Nucl.Sci. and Engng., Vol.12, No.2, p 178.

Imperial College, London, 1962, "Code of Practice against Radiation Hazards".

International Atomic Energy Agency, Vienna, 1958 "Safe Handling of Radioisotopes".

Jones R. 1962 "Non-Destructive Testing of Concrete" Cambridge University Press.

Jurenka J. 1960 Hochschule fur Bauwesen, Leipzig, Symposium. See U.S.A.E.C. Tranlsation tr - 5632.

Jacquesson J. 1954 RILEM Bulletin 20 (Old series).

- 1958 J. Phys. Radium, Vol.17, No.11, p 176A.

Kuhn S.H. 1960 Civ. Engr. in South Africa, Vol.2, No.5, May.

- 1964 Highway Research Board, Washington, 43rd Annual Meeting.

Kuranz J.L. 1959 A.S.T.M., Spec. Tech. Publ. 268.

Lamb D.R. 1955 A.S.T.M. Proc. 55, p 1217.

Lauchaud R. 1961 RILEM Bulletin 13, Dec.

- 1962 RELEM Bulletin 15, June.

Matveev V.V., Sokolow A.D. and Shlypnikov R.S. 1957 J. Nucl. Energy, Vol. 4, p 415.

McConologue D.J. and Strickland R.E. 1962 Instn. Mech. Engrs. London, Symposium.

Mintzer S. 1960 A.S.T.M., Spec. Tech. Publ. 293.

Mortier P. and Huyghe G. 1955 Institut Interuniversitaire des Sciences Nuclaires, Brussels, Symposium.

Neville O.K. and van Zelst T.W. 1960 A.S.T.M., Spec. Tech. Publ. 293.

Notarrigo S., Parisi R., Riccamo R. and Rubbino A. 1962 Nucl. Phys., Vol. 29, No.3, p 507.

Paterson W.J., Etherington B.W. and Berenbaum R. 1963 Brit.J. App.Phys. Vol.14, No.12, Dec.

Pawliw J. and Spinks J.W.T. 1957 Con. J. Technology, Vol. 34, No.8, March.

Pocock B.W. 1956 Michigan State Highway Dept., Res. Lab. Report No.261.

Price B.T., Horton C.C. and Spinney K.T. 1957 "Radiation Shielding", Pergamon Press.

Riessauw F.G. and Huyghe G. 1958 Rijksuniversiteit, Ghent, Belgium, Revue C Tijdschrift I, No.5.

Roy E.R. and Winterkorn H.F. 1957 U.S. Highway Research Board Bulletin 159.

Skopek J. 1957 Proc. 4th Inter. Conf. on Soil Mechanics and Foundation Engineering Vol.1, p 107.

Smith E.E. and Whiffin A.C. 1952 The Engineer, 29th Aug.

Soodak H. 1962 "Reactor Handbook", Interscience.

Stein G. 1960 Hochschule fur Bauwesen, Leipzig, Symposium. See U.S.A.E.C. Translation tr - 5632.

Strominger D., Hollander J.M. and Seaborg G.T. 1958 Rev. Mod. Phys. Vol. 30, No.2, part 2.

Tandberg J. 1938 Proc. Phys. Soc. (London) Vol.50, p 87.

van Bavel C.H.M. 1956 Soil Sci., Vol. 82, p 29.

- 1957 Soil Sci.,Soc. Amer., Proc.21,p 588.

- 1959 Soil Sci., Vol. 87, p 50.

Vomocil J.A. 1954 Agr. Engng., Vol. 35, No.9, p 651.

Weinberg A.M. and Wigner E.P. 1958 "The Physical Theory of Neutron Chain Reactors", University of Chicago Press.

Wiechers G. 1958 Thesis, University of Pretoria, South Africa.

Yakhontov K. 1958 D.S.I.R., N.L.L. Boston Spa, Translation RTS 2166.

Yaltakaya E. and Senturk S. 1962 RILEM Bulletin 15, June.

Zhukov V.S. et al. 1958 D.S.I.R., N.L.L. Boston Spa, Translation RTS 2163.

Zytowitsch N.A. and Ferronski W.I. 1960 Hochschule fur Bauwesen, Leipzig, Symposium. See U.S.A.E.C. Translation tr - 5632.

APPENDIX A

NOTATION

A	Atomic weight of an element.
A, B	Functions of ρ or d' (Chapters 2.5.6, 2.9 and 4.7).
E	Energy MeV.
E_o	Source energy.
G_i	Mass fraction of i^{th} element in the concrete $\sum_n G_i = 1.$
I	Intensity of radiation photons/sec or neutrons/sec.
I_o	Source intensity.
I_s	Scattered intensity.
I_u	Unscattered intensity.
N	Number of pulses registered in time interval T.
N_A	Avogadro's number = 0.6025×10^{24} mole $^{-1}$.
R	Nett count rate.
R_o	Count rate with no concrete in the apparatus (Part 3).
R_u	Count rate due to unscattered radiation (Part 3).
T_s	Count rate due to scattered radiation (Part 3).
R_b, R_p, R_s	Defined in Chapter 2.4 for Parts 2 and 4.
S	Sensitivity of apparatus defined in Chapter 2.6.
T	Time interval for detecting N counts.

X — Compton scattering factor = $\sum_{n} \frac{G_i Z_i}{A_i}$.

Z — Atomic number of an element.

a — Distance source to detector.

h, b, d, e — Dimensions from apparatus to edge of specimen.

a, b, c, d — Constants in equation of the gamma ray backscattering system.

h — Height of gamma backscatter apparatus above the concrete surface.

j, k, m, n — Constants in equation of the neutron backscattering system.

p — Probability.

r — Ratio of count on specimen to count on standard.

t — Time.

x — Path length

x — Distance (Chapters 2.5.6, 2.9 and 4.7).

x — Thickness of a concrete specimen (Part 3).

α — Angle of detector (Part 2).

β — Apparent cross section per electron (Part 3).

ε $E/0.511$ E is photon energy in MeV.

ς Average logarithmic energy loss per collision for neutron scattering off an element.

η Ratio of pulses registered to photons or neutrons passing through the detector.

θ Angle of scatter.

λ Decay constant of isotope.

μ Mass attenuation coefficient = Σ/ρ.

μ_a Mass absorption coefficient = Σ_a/ρ.

μ_s Mass scattering coefficient = Σ_s/ρ.

ξ Compton scatter cross section per electron.

ρ Density.

σ Standard error.

Σ Macroscopic cross section.

Σ_a Absorption cross section.

Σ_s Scattering cross section.

$\Sigma_t = \Sigma_s + \Sigma_a$ in Parts 2 and 3.

Σ_{tr} Transport cross section.

Other symbols are explained, where relevant, in the text.

APPENDIX B

CALCULATION OF THE FINAL ENERGY OF A PHOTON WHICH HAS SCATTERED TWICE, THROUGH A GIVEN TOTAL ANGLE, IN A PLANE SYSTEM

Let θ_1 be the angle between the initial direction and the direction after the first scatter, and θ_2 the angle between the directions before and after the second scatter. The changes in direction are not necessarily equal to the angles of scatter but their cosines are always equal. As the system is plane, the total angle θ is given by

$$\theta = \theta_1 + \theta_2 \qquad \text{B.(1)}$$

If E_o is the initial energy in MeV, E_1 the energy after the first scatter and E_2 the final energy, then (Evans 1955)

$$E_1 = \frac{E_o}{1 + \frac{E_o}{0.511}(1 - \cos\theta_1)} \qquad \text{B.(2)}$$

and

$$E_2 = \frac{E_1}{1 + \frac{E_1}{0.511}(1 - \cos\theta_2)} \qquad \text{B.(3)}$$

where 0.511 is the rest energy of the electron in MeV.

Writing $\frac{E_o}{.511} = \varepsilon_o$, and substituting B.(1) and B.(2) in B.(3)

$$E_2 = \frac{E_o}{1 + \varepsilon_o [2 - \cos\theta_1 - \cos(\theta - \theta_2)]} \qquad \text{B.(4)}$$

E_2 was calculated as a function of θ_1 for source energies 0.662 MeV and 1.25 MeV, for various angles θ. The results for $\theta = 75^\circ$ and $\theta = 120^\circ$ are shown in Figure 60.

The maximum and minimum values of E_2 and the angles at which they occur may be found by differentiating B.(4).

Letting $u = 1 + \varepsilon_0 [2 - \cos\theta_1 - \cos(\theta - \theta_1)]$

$$\frac{dE_2}{d\theta_1} = \frac{-E_0\varepsilon_0 [\sin\theta_1 - \sin(\theta - \theta_1)]}{u^2} \qquad \text{B.(5)}$$

$$\frac{d^2E}{d\theta_1^2} = \frac{E_0\varepsilon_0^2}{u^3}\left\{2 [\sin\theta_1 - \sin(\theta - \theta_1)] + u [\cos\theta_1 + \cos(\theta - \theta_1)]\right\} \qquad \text{B.(6)}$$

The solutions to B.(5) for $0 < \theta < \pi$ are

$$\theta_1 = \theta/2$$

$$\text{or } \theta_1 = 180^\circ + \theta/2$$

When $\theta_1 = \theta/2$, $\frac{d^2E_2}{d\theta^2} > 0$, E_2 a maximum

$\theta_1 = 180^\circ + \theta/2$, $\frac{d^2E_2}{d\theta^2} > 0$, E_2 a minimum

Substituting in B.(4),

$$\text{Maximum } E_2 = \frac{E_0}{1 + 2\varepsilon_0(1 - \cos\theta/2)} \qquad \text{B.(7)}$$

$$\text{Minimum } E_2 = \frac{E_0}{1 + 2\varepsilon_0(1 + \cos\theta/2)} \qquad \text{B.(8)}$$

The following results may be noted.

a) The highest value of E_2 is due to two equal scatters, each through $\theta/2$.

b) The lower values of E_2 are due to initial changes of

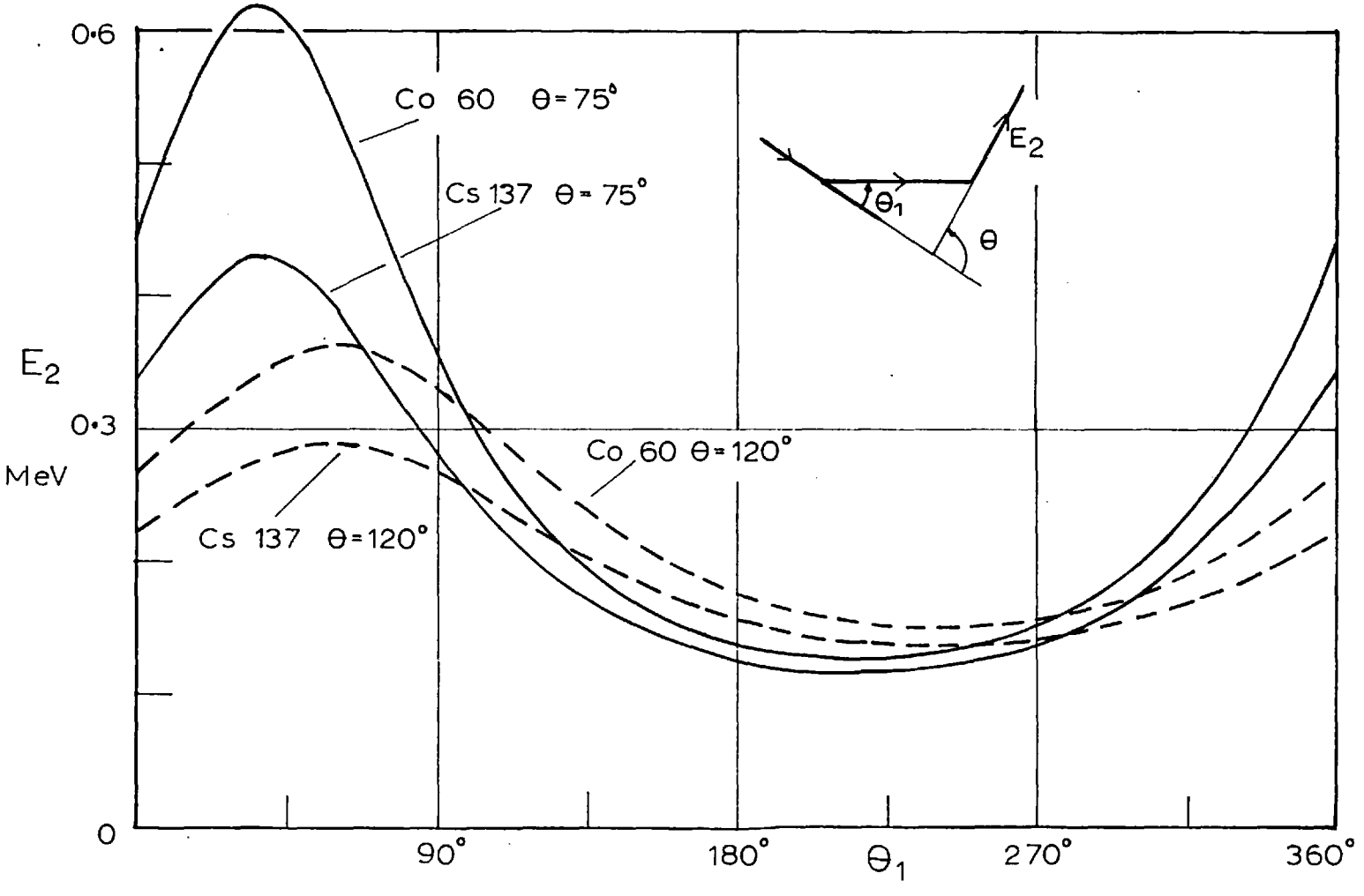

E_2 vs θ_1
0·6
0·3
0
E_2
MeV
Co 60 θ=75°
Cs 137 θ=75°
Co 60 θ=120°
Cs 137 θ=120°
E_2
θ_1
θ
90°
180°
θ_1
270°
360°

Fig.60

direction in the range 180^{o} to $(180^{o} + \theta)$. The magnitudes of the angles of scatter then range from $\theta_1 = 180^{o}$ and $\theta_2 = \theta$, to $\theta_1 = 180^{o} - \theta$ and $\theta_2 = 180^{o}$.

c) The greater θ, the higher the lowest value of E_2. This is because the relevant range of magnitude of the first angle of scatter is from 180^{o} to $180^{o} - \theta$.

Figure 61 illustrates these results.

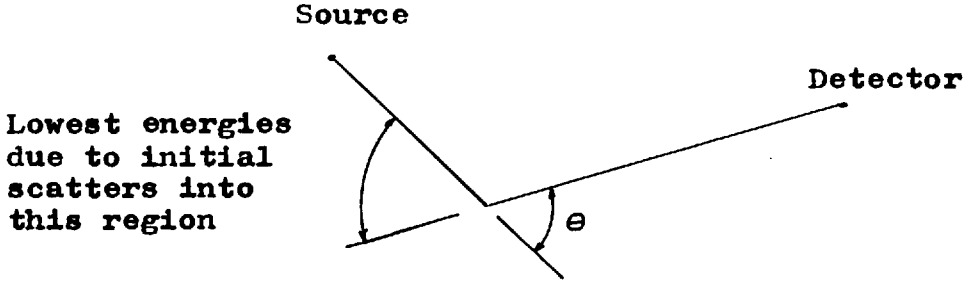


Figure 61

d) The lowest energy is but little dependent on the value of initial energy, and is due to a first scatter into direction $180^{o} + \theta/2$.

TABLE 42

θ	Source	Minimum E_2 MeV	θ_1 at minimum E_2
75^{o}	Cs 137	0.117	217.5
75^{o}	Co 60	0.128	217.5
120^{o}	Cs 137	0.135	240^{o}
120^{o}	Co 60	0.150	240^{o}

APPENDIX C

CALCULATION OF THE RELATIVE COUNT DUE TO ONCE SCATTERED RADIATION IN THE GAMMA RAY TRANSMISSION APPARATUS

Assuming that

a) lead is perfectly opaque to gamma radiation,

b) attenuation of the beam by air is negligible,

c) the detector efficiency η is constant over the detection channel,

d) the apparatus is symmetrical about the centre line,

then, from Figure 37, for a source of 4π photons/second, the flux of radiation at (r_o, α_o) is $\frac{e^{-\Sigma_o x_o}}{r_o^2}$

The intensity leaving the differential volume in the direction of the detector will be $\frac{e^{-\Sigma_o x_o}}{r_o^2} \Sigma(\theta) \Omega \, dV$

where dV is the differential volume and Ω the solid angle at the detector subtended by dV.

$$dV = r_o^2 \, d\alpha_o \, dr_o \, d\varphi \sin\alpha_o$$

where $d\varphi$ is the angle at the differential volume subtended by the source, in the plane normal to the axis of symmetry.

The intensity at the detector due to the differential volume $dI = e^{-\Sigma_o x_o - \Sigma_i x_i} \sin\alpha_o \Sigma(\theta) \Omega \, dr_o \, d\alpha_o \, d\phi$

As shown in Chapter 2.2. $\Sigma = N_A \times \xi \rho$ and, due to symmetry,

$$\int_0^{2\pi} d\varphi = 2\pi$$

The count rate due to all the volume

$$R = \int \eta \, dI$$

$$= 2\pi\eta \int_{0}^{\alpha_{o}\,max} \int_{r_{o}\,min}^{r_{o}\,max} \xi(\theta) N_A \rho X \sin\alpha_o \, \Omega \, e^{-N_A \rho X (\xi_o x_o + \xi_i x_i)} \, dr_o \, d\alpha_o \qquad C.(1)$$

For calculation of the count rate contributed by a ring of square section z x z cm at a given position, where the directions of z are parallel and normal to the axis of symmetry

$$dr_o \doteq \frac{z}{\cos\alpha_o}$$

$$d\alpha_o \doteq \frac{z \cos\alpha_o}{r_o}$$

Assuming that the variation in count rate is small over the dimensions of z, the count rate due to radiation scattered once from the ring will be

$$R = 2\pi\eta \, \xi(\theta) N_A \rho X \sin\alpha_o \, \Omega \, e^{-N_A \rho X (\xi_o x_o + \xi_i x_i)} \frac{z^2}{r_o} \qquad C.(2)$$

A Mercury autocode programme for the numerical integration of equation C.(1) for apparatus as in Figure 37, is shown on the following pages.

The data are in two groups, with the following numbers in group 1 ; b inches, d inches, source energy MeV, g inches, Compton scattering factor X and e inches. The following are numbers in group 2; density g/cc, thickness inches, $\Delta\alpha_o$ radians and Δr_o cm.

The programme will evaluate the uncollided and once scattered intensities normalized to an arbitrary source

intensity and will calculate β assuming no higher modes of scattering. After printing the solution to a case it will read another density, If this is less than 100 g/cc it will continue to read group 2, if greater than 100 g/cc it will read group 1 and continue as the first case. This is illustrated by the typical data and output shown after the programme.

With that data the time required was:

programme feed in .. 1 minute

cases 1 and 3 ... 1 minute each

case 2 ... 2 minutes.

```
TITLE
TRANSMISSION TEST-ONCE SCATTERED INTENSITY-U640

CHAPTER1
F→100
A→7
B→10
E→5
G→3
H→6
X→1

1)NEWLINE
CAPTION
ONCE SCATTERED INTENSITY=
PRINT(10000Bn)1,4
NEWLINE

Bo=xLOG(Bn+Cn)
B1=AA+2AD+DD
B1=xLOG(£GG/B1)                Calculate β
Bo=B1-Bo
Bo=Bo/C
Bo=Bo/Dn

CAPTION
BETA=
PRINT(1.6116Bo/Z)1,5

NEWLINE
ACROSS1/0

xEXP
xSQRT
xSIN
xCOS
xLOG
CLOSE
```

```
CHAPTERo
VARIABLESı

9o)READ(B)                    b inches
B=2.54B
READ(D)                       d inches
D=2.54D
READ(E)                       Initial energy MeV
READ(G)                       g inches
G=2.54G
READ(Z)                       Compton scattering factor X
READ(G2)                      e inches

ı)READ(Dn)                    Density g/cc
→9o,Dn>1oo
READ(C)                       Concrete thickness inches
C=2.54C
READ(Go)                      Δα_o radians
READ(Ho)                      Δr_o cm

NEWLINE
NEWLINE
NEWLINE
CAPTION
PARAMETERS
PRINT(Dn)ı,3                  Density g/cc
PRINT(C)ı,2                   Concrete thickness cm
PRINT(Go)ı,3                  Δα_o radians
PRINT(Ho)ı,2                  Δr_o cm
PRINT(E)ı,3                   Initial energy MeV
NEWLINE

A=B+C+D
An=XTAN(G/D)                  Tan α_1 limit
Eo=ı.95702E
JUMPDOWN3
E2=.ı008BoZDn
Bn=o

Bo=A+D
Bo=BoBo
Bı=XEXP(-CE2)                 Calculate uncollided
Cn=£GGBı/Bo                         intensity
NEWLINE
CAPTION
UNCOLLIDED INTENSITY=
PRINT(ıoooocn)ı,4
NEWLINE

Gı=.5Go                       Initial α_o
2)Ao=XCOS(Gı)
Aı=ı/Ao
H3=BAı                        r_o min.
H2=H3+CAı                     r_o max.
Hı=H3+.5Ho?                   r_o
A2=XSIN(Gı)
Aı=AıA2
```

```
4)H4=XSQRT(H1H1+AA-2H1AAo)?          r1
Xo=XRADIUS(H1A2-BA1,H1Ao-B)          x0
A3=H1A2/H4                           sin α1
Vn=A3A3
Vn=1/Vn-1
Vn=XSQRT(1/Vn)?                      tan α1
→7,Vn>An

X1=XRADIUS(B+C-H1Ao,H1A2-DVn)?       x1
Vn=XARCTAN(1,Vn)                     α1
E5=Vn+G1                             θ1

B5=XCOS(E5)
Bo=B5B5+1
B1=1-B5
B2=1.95702EB1+1                      Calculate ζ (θ)
B4=B2B2
B4=1/B4
B3=3.829927EEB1B1
B2=BoB2
B3=B3/B2+1
Gn=.5BoB4B3?

E4=.047845ZGnDn?                     ζ(θ) Xρ

B2=.510976/E
Bo=B1+B2
E1=1/Bo?
Eo=E1
JUMPDOWN3
E3=.3008BoZDn?

Bo=H1A2                              Coordinates of present volume,
B1=B+C-H1Ao                          ⊥and ∥ axis of symmetry, origin
→5,G>Bo                              at detector

B2=XDIVIDE(Bo+G,2D+B1)
B3=XDIVIDE(Bo-G,B1)
B2=.5B2+.5B3
B6=XDIVIDE(B2B2+1,B2B2)
B2=DB2
B5=GG-B2B2                           Calculate Q
→91,o>B5
B3=XSQRT(GG-B2B2)
B4=XARCTAN(B3,B2)
B5=.5£GG-B2B3-GGB4
B7=Bo-B2
B7=B6B7B7?
B8=Bo+B2
B8=B6B8B8
H=B5/B7+B5/B8?
```

```
6)Bo=XEXP(-E2Xo-E3X1)
Bo=6.28319E4BoGoHoHA2?
Bn=Bn+Bo

92)H1=H1+Ho
→4,H2>H1

7)G1=G1+Go
→2,G2>G1
ACROSS1/1

3)Bo=2Eo+1
B1=XLOG(Bo)
B2=Eo+1
B3=EoEo
B4=XDIVIDE(2B2B2,B3Bo)
B5=XDIVIDE(B3-2B2,2EoB3)
B1=B1B5
B2=XDIVIDE(Eo+Bo,BbBo)
Bo=B1+B4-B2?
RETURN

5)H=2D+B1
H=HH
H=£GG/H
→6

91)H=o
→92

XEXP
XSQRT
XCOS
XARCTAN
XTAN
PSA
CLOSE
→
```

ΔR

Calculate ζ_o and ζ_1

Calculate Ω if coordinate ⊥ axis of symmetry < g

Eliminates imaginary value of Ω due to rounding and truncation errors

Typical data sheet

```
4.35   1   .662   .3125   .5   .185   Apparatus parameters

2.4    4   .02    .5                  Concrete parameters
2.4    4   .01    .25                   2 cases

1111                                  Cue to jump to 90)

2.35   1   .662   .3125   .5   .185   Apparatus parameters

2.4    6   .02    .5                  Concrete parameters

→
```

Output for the above data

```
TRANSMISSION TEST-ONCE SCATTERED INTENSITY-U640
Q
Q
Q
Q
 0   118   794   912
Q
Q


PARAMETERS   2.400   10.16   0.020   0.50   0.662

UNCOLLIDED INTENSITY= 4.3584

ONCE SCATTERED INTENSITY= 0.4717
BETA= 0.23528


PARAMETERS   2.400   10.16   0.010   0.25   0.662

UNCOLLIDED INTENSITY= 4.3584

ONCE SCATTERED INTENSITY= 0.4859
BETA= 0.23489


PARAMETERS   2.400   15.24   0.020   0.50   0.662

UNCOLLIDED INTENSITY= 1.7003

ONCE SCATTERED INTENSITY= 0.2720
BETA= 0.23579
```

APPENDIX D

ANALYSIS OF THE STATISTICAL ERRORS DUE TO A RHODIUM FOIL DETECTOR IN A CONSTANT BACKGROUND

a) Foil Irradiation and Residual Activity

The rhodium may be activated to either the 42 second or 4.4 minute half life states as shown in Figure 41. The longer lived state decays to the shorter lived state, which then decays to Pd 104 with the emission of a detectable β particle.

If suffix a denotes the long lived state and b the short lived state and σ_a and σ_b the activation cross sections for each state

N_o the number of nuclei of Rh 103 originally present

N_a and N_b the number of nuclei in state a or b at time t

φ the activating neutron flux

λ_a and λ_b the decay constants for a and b respectively.

Then, neglecting the decrease in N_o the rate of formation of state a is given by

$$\frac{dN_a}{dt} = \varphi N_o \sigma_a - \lambda_a N_a \qquad \text{D.(1)}$$

and that of b by

$$\frac{dN_b}{dt} = \varphi N_o \sigma_b + \lambda_a N_a - \lambda_b N_b \qquad \text{D.(2)}$$

If $N_a = 0$ at $t = 0$, solving D.(1) gives

$$N_a = \frac{\varphi N_o \sigma_a}{\lambda_a} \left(1 - e^{-\lambda_a t}\right) \qquad \text{D.(3)}$$

Substituting D.(3) in D.(2), solving, and applying the condition $N_b = 0$ at $t = 0$ gives

$$N_b = \frac{\varphi N_o (\sigma_a + \sigma_b)}{\lambda_b} \left(1 - e^{-\lambda_b t}\right) + \frac{\varphi N_o \sigma_a}{\lambda_b - \lambda_a} \left(e^{-\lambda_a t} - e^{-\lambda_b t}\right) \qquad \text{D.(4)}$$

If the contribution due to N_a were neglected in equation D.(2), that is $\sigma_a = 0$, the solution would be

$$N_b = \frac{\varphi N_o \sigma_b}{\lambda_b} \left(1 - e^{-\lambda_b t}\right) \qquad \text{D.(5)}$$

Substituting the values $\lambda_a = 0.1575 \text{ min}^{-1}$

$\lambda_b = 1 \text{ min}^{-1}$

$\sigma_a = 12$ barns

$\sigma_b = 140$ barns

$t = 3$ minutes

From D.(3) $N_a = 29\, \varphi N_o$

From D.(4) $N_b = 135 \varphi N_o$

From D.(5) $N_b = 133 \varphi N_o$

Denoting the number of nuclei activated to states a and b after 3 minutes by N_{ao} and N_{bo}, and choosing this time to be the new datum, the total count N recorded by a detector of efficiency η in a time interval t_1 to t_2 is given by

$$\frac{N}{\eta} = \frac{N_{ao}}{\lambda_b - \lambda_a} \left[\lambda_a \left(e^{-\lambda_b t_2} - e^{-\lambda_b t_1}\right) - \lambda_b \left(e^{-\lambda_a t_2} - e^{-\lambda_a t_1}\right)\right] \qquad \text{D.(6)}$$
$$- N_{bo} \left(e^{-\lambda_b t_2} - e^{-\lambda_b t_1}\right)$$

The first term is due to the decay of state a through state b, the second is due to the decay of the nuclei N_{bo} existing at the end of irradiation. For the first cycle the count was taken in the interval from the 5th to 155th second after irradiation. When the second cycle of irradiation and counting was performed a residual activity occurred in the counting-interval from 365 to 515 seconds, in the next cycle from 725 to 875 seconds, and so on. These counts were calculated from equation D.(6) and shown in Table 43.

TABLE 43

Cycle	Due to N_{ao}	Due to N_{bo}	Total
1	6.5	116.6	123.1
2	4.5	0.3	4.8
3	1.7	7×10^{-4}	1.7
4	0.7	-	0.7
5	0.3	-	0.3
6	0.1	-	0.1

Relative counts are shown. For absolute counts multiply the tabulated numbers by $\eta\varphi N_o$.

b) Statistical Error due to Decay in a Constant Background

For this calculation it was assumed that the foil

decayed with a single half life of 42 seconds.

Consider a foil of decay constant λ decaying for t seconds with an initial rate R_o counts per second in a constant background of R_b counts per second. The total counts registered will be

$$N = N_{FOIL} + N_{BACKGROUND}$$

$$= \frac{R_o}{\lambda}\left(1 - e^{-\lambda t}\right) + R_b t \qquad D.(7)$$

S_N = the variance of N

$$= \frac{R_o}{\lambda}\left(1 - e^{-\lambda t}\right) e^{-\lambda t} + R_b t \qquad D.(8)$$

The optimum counting time will be that for which $\frac{S_N}{N^2_{FOIL}}$ is a minimum and may be shown (Tandberg 1938) to be given by

$$\frac{R_o}{R_b} = e^{\lambda t} - \frac{2\lambda t}{1 - e^{-\lambda t}} \qquad D.(9)$$

Table 44 shows the optimum counting time, in number of mean lives, for various ratios R_o/R_b.

TABLE 44

R_o/R_b	2	5	10	20	50
λt	1.85	2.30	2.75	3.28	4.10

The best achievable coefficient of variation for given values of R_o and R_b is given by

$$\frac{\sqrt{\frac{R_o}{\lambda}\left(1-e^{-\lambda t}\right)e^{-\lambda t}+R_b t}}{\frac{R_o}{\lambda}\left(1-e^{-\lambda t}\right)} \qquad \text{D.(10)}$$

where t is the optimum counting time. This is plotted as a function of R_o for various values of R_b in Figure 62.

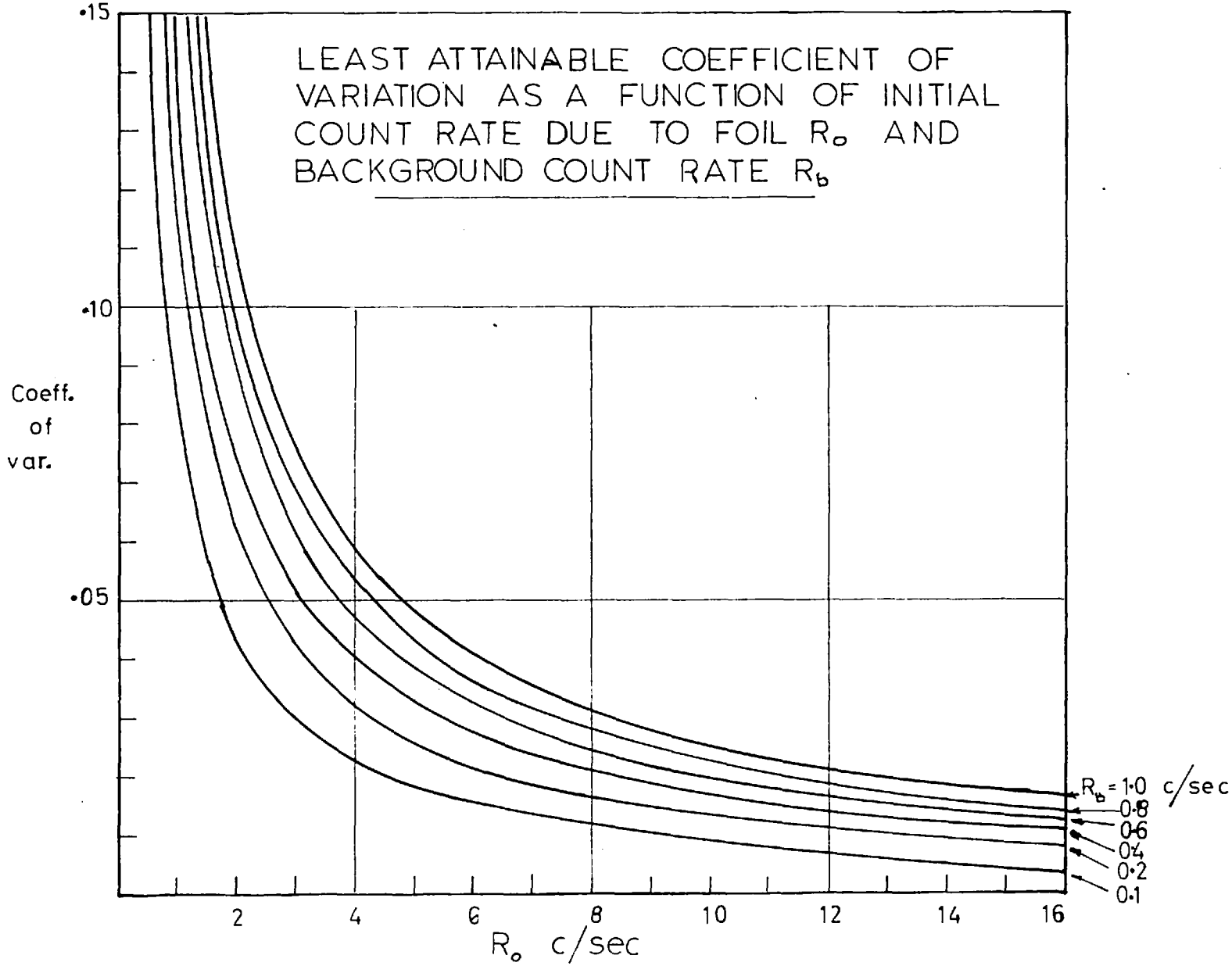

LEAST ATTAINABLE COEFFICIENT OF VARIATION AS A FUNCTION OF INITIAL COUNT RATE DUE TO FOIL R_o AND BACKGROUND COUNT RATE R_b
·15
·10
·05
Coeff. of var.
2
4
6
8
10
12
14
16
R_o c/sec
R_b = 1·0 c/sec
0·8
0·6
0·4
0·2
0·1

Fig. 62